

**Inter-aquifer connectivity:
investigating groundwater
movement through a regional-
scale aquitard using a multi-
scale and multi-tracer approach**

by

Stacey Priestley

*Thesis
Submitted to Flinders University
for the degree of*

Doctor of Philosophy
College of Science and Engineering
9th May 2018

Declaration

I certify that this thesis does not incorporate without acknowledgment any material previously submitted for a degree or diploma in any university; and that to the best of my knowledge and belief it does not contain any material previously published or written by another person except where due reference is made in the text.

Stacey Priestley

August 2017

Co-authorship

Stacey Priestley is the primary author on all chapters in this thesis. Co-authors listed on published chapters provided intellectual supervision and editorial support.

Acknowledgements

I would like to acknowledge funding from the Government of South Australia's Department of Environment, Water and Natural Resources (DEWNR), Australia under its Bioregional Assessment Program on the Arckaringa Basin and AINSE Ltd for providing financial assistance (Award - PGRA). The work undertaken in this thesis would not have been possible without this funding.

I wholeheartedly thank my supervisors, Vincent Post, Andrew Love and Paul Shand, for all of their support and scientific guidance. I sincerely appreciate their passion, knowledge and enthusiasm for hydrochemistry and hydrogeology and value their friendship. It was a pleasure working with them and I will be eternally grateful for their patience and generosity.

In particular, I wish to thank Daniel Wohling, Mark Keppel and Tavis Kleinig from DEWNR, as without their generosity and willingness to collaborate I could not have undertaken this research project. Additionally, I would like to thank Peter Kretschmer for his assistance with fieldwork.

My sincere gratitude goes to Professor Rolf Kipfer, Dr Tim Payne and Professor Martin Stute for hosting me at the Swiss Federal Institute of Technology, Switzerland, the Australian Nuclear Science and Technology Organisation, Australia and the Lamont-Doherty Earth Observatory, USA, respectively. I also wish to thank Linda Baker, Matthias Brennwald, Sangeeth Thiruvoth and Lina Tyroller for being part of this invaluable experience. The times I spent with you all, whilst brief, contributed greatly to my understanding.

I would also like to thank my other co-authors and collaborators, specifically Ilka Wallis and Jennifer Harrison, for their contributions to scientific ideas and editorial comment. In addition, I would like to thank editors and reviewers of manuscripts where feedback has been received.

To my Flinders University colleagues, thank you for making the PhD experience an enjoyable one.

Finally, my heartfelt thanks go to my family, partner and friends for their ongoing support and encouragement.

Summary

Aquitards play an important role in the physical and chemical evolution of groundwater, however, the location and amount of inter-aquifer leakage through the aquitard is often unknown. 'Diffuse inter-aquifer leakage' through aquitard pores can be a significant component of the water balance over large areas. 'Enhanced inter-aquifer leakage' can occur through the aquitard via preferential pathways causing an increased rate of groundwater movement through the aquitard relative to diffuse inter-aquifer leakage. Despite the potential importance of inter-aquifer leakage, it is not generally studied in groundwater investigations, in part because of the inherent difficulty in obtaining the necessary data to determine the magnitude of the groundwater flux. Quantifying inter-aquifer leakage at a regional-scale is complicated by diffuse inter-aquifer leakage rates that are often so small that they are very hard to detect and quantify, although they can be a significant component of the water balance over large areas. Localised enhanced inter-aquifer leakage fluxes can be missed at the spatial resolution of regional surveys. Additionally, there remain issues with incorporating scale and heterogeneity in the few methods that are available to investigate inter-aquifer leakage.

This thesis investigated inter-aquifer leakage at multiple scales in an arid zone regional groundwater basin using environmental tracers in an attempt to account for heterogeneity and the different scales of leakage. Diffuse inter-aquifer leakage of the aquitard pore water and enhanced inter-aquifer leakage through preferential pathways were included in this approach. This thesis focussed on the connectivity between the Great Artesian Basin (GAB) and underlying Arckaringa Basin, located in central Australia. A sparse observation network in central Australia and hence data scarcity is an additional challenge encountered in this study, as well as limited hydrogeological investigations elsewhere.

The first part of this thesis determined inter-aquifer leakage at a regional-scale by the implementation of a comprehensive multidisciplinary approach. Diffuse inter-aquifer leakage direction and flow rates through the aquitard pores were estimated by calculating the aquitard's hydraulic resistance. The locations of enhanced inter-aquifer leakage were identified through the interpretation of hydrological data, and environmental tracers including a range of isotopes. While the exact nature of the enhanced inter-aquifer leakage mechanism remains unknown in detail, the proportion of enhanced inter-aquifer leakage was calculated using strontium isotopes and radiogenic helium. The protocol of well-couplet sampling and analysis methodologies undertaken

in this study provided a comprehensive approach to investigate inter-aquifer leakage on a regional-scale where only limited wells were available.

The second part of this study investigated uranium isotope distributions and the processes that control it in groundwater in the GAB and underlying Arckaringa Basin. Through interpretation of regional groundwater and sequential extraction of mineral phases, it was found that rock weathering, the geochemical environment and α -recoil of daughter products control ^{238}U and ^{234}U isotope distributions within the groundwater basins. The importance of each of these processes is determined by the sample's location within the groundwater flow system, although due to the complexity of uranium isotope systematics it was not possible to conclusively determine at all locations the processes controlling the distribution of uranium isotopes. Nevertheless, interpretation of uranium isotope trends and distributions identified a number of recharge locations and helped to constrain groundwater flow processes, including a location of stagnant flow. However, in this groundwater basin uranium isotopes were not as successful in identifying inter-aquifer leakage as in other studies.

The final part of this study investigated diffuse inter-aquifer leakage using chloride and helium transport through the aquitard pore waters with one-dimensional analytical and numerical models. A core through the GAB and Arckaringa Basin was drilled in March 2015 and samples for noble gases, stable isotopes and major ion analysis of aquitard pore waters were collected. Models of chloride and helium transport showed that both diffusion and slow downward advection through the aquitard pores control solute transport. The concurrent use of chloride and helium constrained the models that would fit the solute profiles to the final model presented, and provided independent information about the hydrological conditions. Helium, being produced in-situ and influenced by groundwater residence time, provided evidence of solute transport rates and processes, and chloride also provided insight into palaeohydrological conditions. An increase in chloride concentration in the upper part of the profile is interpreted as being due to a reduction in recharge for at least 3000 years. Additionally, groundwater extraction from the lower aquifer since 2008, and resultant drawdown in the lower aquifer, has penetrated and moved through the aquitard, although the subsequent increase in chloride and helium concentration has only penetrated into the lower few meters of the aquitard. The aquitard properties and hydraulic head measurements gave an instantaneous picture of potential diffuse inter-aquifer leakage at the time of sampling while environmental tracer profiles provided a long-term perspective and insight into solute transport processes.

The three studies contained in this thesis provided field- and laboratory-focused research on both diffuse inter-aquifer leakage rates and localised enhanced inter-aquifer leakage between the GAB and underlying Arckaringa Basin, supported by modelling. This links inter-aquifer connectivity at the point-scale to whole-basin processes, which is rarely undertaken (Herczeg and Leaney 2011).

Table of contents

Declaration	i
Co-authorship	ii
Acknowledgements.....	iii
Summary	iv
Table of contents	vii
List of figures	xi
List of tables.....	xiv
Chapter 1 Introduction	1
1.1 Research problem	1
1.2 Literature Review.....	2
1.2.1 Point-scale studies	2
1.2.2 Regional-scale studies.....	3
1.2.3 Whole-basin studies.....	5
1.3 Knowledge gaps.....	5
1.4 Thesis aims	6
1.5 Contribution of this PhD.....	7
Chapter 2 Study Area.....	9
2.1 Background.....	9
2.2 Location.....	9
2.3 Climate, topography and land use	11
2.4 Geological setting	13
2.5 Hydrogeology	21
2.6 Site Description.....	27

Chapter 3	Environmental tracers: background and sampling	31
3.1	Sampling.....	31
3.1.1	Groundwater sampling	31
3.1.2	Core sampling	31
3.1.3	Sample analysis.....	32
3.2	Environmental tracers.....	32
3.2.1	Major ions.....	32
3.2.2	$\delta^{18}\text{O}$ and $\delta^2\text{H}$	33
3.2.3	$\delta^{13}\text{C}$	33
3.2.4	$^{87}\text{Sr}/^{86}\text{Sr}$	34
3.2.5	Uranium isotopes.....	34
3.2.6	^{14}C	34
3.2.7	$^{36}\text{Cl}/\text{Cl}$	35
3.2.8	Helium isotopes	35
Chapter 4	Detecting inter-aquifer leakage in areas with limited data using hydraulics and multiple environmental tracers, including ^4He, $^{36}\text{Cl}/\text{Cl}$, ^{14}C and $^{87}\text{Sr}/^{86}\text{Sr}$.....	37
4.1	Abstract.....	37
4.2	Introduction.....	37
4.3	Site description	41
4.4	Methods	45
4.5	Results.....	48
4.5.1	Hydrogeology.....	48
4.5.2	Tracer results	54
4.6	Discussion.....	58
4.6.1	Chemical and physical processes	58
4.6.2	Inter-aquifer leakage	62
4.6.3	Evaluation of method	65
4.7	Conclusions.....	68

Chapter 5	Uranium geochemistry in the south-western margin of the Great Artesian Basin and Arckaringa Basin, central Australia.....	70
5.1	Abstract.....	70
5.2	Introduction.....	71
5.3	Study area	74
5.4	Methods.....	78
5.4.1	Groundwater samples.....	78
5.4.2	Core samples.....	79
5.5	Results.....	80
5.5.1	Uranium isotopes in groundwater.....	80
5.5.2	Sequential extraction results	87
5.6	Discussion.....	90
5.6.1	Geochemistry of uranium isotopes.....	90
5.6.2	Uranium isotopes as an indicator of groundwater flow	93
5.6.3	Environmental health implications	95
5.7	Conclusions.....	95
Chapter 6	Palaeohydrogeology and transport parameters derived from ⁴He and Cl profiles in aquitard pore waters in a large multilayer aquifer system, central Australia	97
6.1	Abstract.....	97
6.2	Introduction.....	97
6.3	Site description	100
6.4	Methods.....	103
6.4.1	Sampling and analytical methods	103
6.4.2	Modelling.....	106
6.5	Results.....	108
6.5.1	Field data	108
6.5.2	Model scenarios.....	117
6.5.3	Model results	119
6.6	Discussion.....	121
6.7	Conclusions.....	124

Chapter 7	Conclusions	127
7.1	Summary of the findings	127
7.2	Future work	129
7.2.1	Site-specific investigations	129
7.2.2	Generally applicable	129
Appendix A:	Environmental tracers in groundwaters and pore waters to understand groundwater movement through an argillaceous aquitard	132
A.1	Abstract.....	132
A.2	Introduction.....	132
A.3	Study area	133
A.4	Methods.....	133
A.5	Results and discussion.....	135
A.6	Conclusions.....	135
Appendix B	Detecting inter-aquifer leakage using multiple environmental tracers	136
Appendix C	Detecting inter-aquifer leakage and recharge using multiple environmental tracers	137
Appendix D	A method to investigate inter-aquifer leakage using hydraulics and multiple environmental tracers.....	138
Appendix E	Inter-aquifer leakage and groundwater flow inferred from environmental tracers especially noble gases	139
Appendix F	Inter-aquifer leakage and groundwater flow inferred from isotopes and noble gases.....	140
References	141

List of figures

Figure 2.1 (a) Extent of the GAB and Arckaringa Basin and (b) GAB and Arckaringa Basin extents, outcrops and well locations	10
Figure 2.2 Annual mean monthly temperatures recorded at Coober Pedy rain gauge station.....	11
Figure 2.3 Annual rainfall recorded at Coober Pedy rain gauge station	11
Figure 2.4 Land surface elevation and ephemeral surface water features	13
Figure 2.5 Simplified Cretaceous to Cambrian Stratigraphy.....	15
Figure 2.6 Extent and thickness of the Bulldog Shale	15
Figure 2.7 (a) Elevation of top of the J aquifer and (b) thickness of the J aquifer.....	16
Figure 2.8 (a) Elevation of top of the Mount Toondina Fm. and (b) thickness of the Mount Toondina Fm	18
Figure 2.9 (a) Elevation of top of the Stuart Range Fm. and (b) thickness of the Stuart Range Fm..	19
Figure 2.10 (a) Elevation of top of the Boorthanna Fm. and (b) thickness of the Boorthanna Fm..	20
Figure 2.11 Elevation of top of the basement	21
Figure 2.12 J aquifer hydraulic head (m AHD) and potentiometric surface contours.....	23
Figure 2.13 Mount Toondina Fm. hydraulic head (m AHD).....	24
Figure 2.14 Boorthanna Fm. hydraulic head (m AHD)	26
Figure 2.15 Basement hydraulic head (m AHD).....	27
Figure 2.16 Potentiometric surface and the generalised groundwater flow paths for (a) the J aquifer and (b) the Boorthanna Fm.....	28
Figure 2.17 Transect through the study area (a) showing lithology and (b) stratigraphy.....	29
Figure 2.18 Hydrogeological transect following Boorthanna Fm. groundwater flow path.....	30
Figure 4.1 (a) Map of the extent and generalised groundwater flow paths of the upper aquifer and lower aquifer and (b) full GAB and underlying Arckaringa basin extents	41
Figure 4.2 Map showing pre-pumping freshwater head potentiometric surface and the generalised groundwater flow paths for (a) the upper aquifer and (b) the lower aquifer.....	43
Figure 4.3 Hydrogeological transect following the generalised groundwater flow path in the lower aquifer.....	44
Figure 4.4 Lower aquitard extent and thickness, interpreted faults, locations of well couplets, calculated leakage rates and hydraulic resistance	49

Figure 4.5 Pre-pumping density corrected freshwater heads of the well couplets	53
Figure 4.6 Depth to water variation over time from pumping wells in the lower aquifer and corresponding upper aquifer wells for well couplets 10 and 18	54
Figure 4.7 (a) chloride concentration, (b) $^{87}\text{Sr}/^{86}\text{Sr}$ ratio, (c) ^{14}C , (d) $^{36}\text{Cl}/\text{Cl}$, (e) radiogenic ^4He concentration and (f) $^3\text{He}/^4\text{He}$ ratio plotted against distance from the discharge area	57
Figure 4.8 (a) $\delta^2\text{H}$ plotted against $\delta^{18}\text{O}$ with the local meteoric water line and amount weighted monthly rainfall volume, (b) ^{14}C plotted against sample depth, (c) $\delta^2\text{H}$ plotted against chloride concentration and (d) Br/Cl mass ratio plotted against chloride concentration	58
Figure 4.9 (a) $^{87}\text{Sr}/^{86}\text{Sr}$ ratio plotted against Sr concentration with the two theoretical end-member mixing lines for well couplet 10 and (b) radiogenic ^4He concentration plotted against distance from the discharge area with the two theoretical end-member mixing lines	64
Figure 5.1 GAB and Arckaringa Basin extents with the location of wells and aquifer outcrop.....	75
Figure 5.2 Potentiometric surface and generalised groundwater flow path for (a) the J aquifer, (b) the Boorthanna Fm. and (c) inter-aquifer leakage and recharge locations and location of sampled wells	77
Figure 5.3 Hydrogeological transect from A to A' through the study area showing stratigraphy and interpreted groundwater flow directions	78
Figure 5.4 (a) Uranium activity concentration, (b) Uranium activity ratios and (c) $^{36}\text{Cl}/\text{Cl}$ ratios in the groundwater samples	84
Figure 5.5 (a) ^{238}U activity concentration plotted against the distance to the discharge area, (b) ^{238}U activity concentration plotted against the depth below the water table, (c) ^{238}U activity concentration plotted against Eh, (d) ^{238}U activity concentration plotted against EC, (e) ^{238}U activity concentration plotted against pH, (f) ^{238}U activity concentration plotted against alkalinity, (g) ^{238}U activity concentration plotted against ^{14}C concentration, (h) ^{238}U activity concentration plotted against $^{36}\text{Cl}/\text{Cl}$, (i) ^{238}U activity concentration plotted against ^{238}U activity concentration and (j) ^{238}U activity concentration plotted against CO_3^{2-} activity	85
Figure 5.6 (a) $^{234}\text{U}/^{238}\text{U}$ activity ratio plotted against ^{238}U activity concentration, (b) $^{234}\text{U}/^{238}\text{U}$ activity ratio plotted against Eh, (c) $^{234}\text{U}/^{238}\text{U}$ activity ratio plotted against the depth below the water table and (d) $^{234}\text{U}/^{238}\text{U}$ activity ratio plotted against ^{14}C concentration.....	86
Figure 5.7 (a) ^{238}U activity concentration and (b) $^{234}\text{U}/^{238}\text{U}$ activity ratios from sequential extractions of core samples plotted against sample depth.....	89

Figure 6.1 (a) Study location in the GAB and Arckaringa Basin in central Australia, also showing main recharge areas, (b) location of core and groundwater potentiometric surfaces and (c) cross section showing stratigraphy and depth of the core.....	102
Figure 6.2 $\delta^{18}\text{O}$ and $\delta^2\text{H}$ in pore water, groundwater and drilling fluid samples and local meteoric water line	113
Figure 6.3 hydraulic head in m AHD by the VWP installed throughout the aquitard and measured in nearby wells in the upper aquifer and lower aquifer	114
Figure 6.4 Profiles of (a) chloride and (b) ^4He concentrations and steady state solute transport analytical models 1–3	116
Figure 6.5 Time taken to reach steady state solute transport in model 4 for (a) chloride and (b) ^4He concentration. Solute transport model 5 profiles for (c) chloride and (d) ^4He concentration	120
Figure 6.6 Steady state solute transport model 6 for (a) chloride and (b) ^4He concentration and transient model 7 profile for (c) chloride and (d) ^4He concentration.....	121
Figure A.1 (a) Map showing aquifer extents and potentiometric surfaces and (b) stratigraphy of hydrogeological cross-section.....	134
Figure A.2. Chloride concentration through the aquitard	135

List of tables

Table 2.1 Aquifer and aquitard hydraulic conductivity and porosity measurements	22
Table 3.1 Well couplet hydraulic head, temperature and total dissolved solids measurements and estimated diffusive inter-aquifer leakage flow rates.....	51
Table 3.2 Table of available hydrochemical results for the well couplets.....	55
Table 3.3 Evaluation of the individual ‘tools’ used to identify enhanced inter-aquifer leakage	65
Table 4.1 Element concentrations and isotope ratios of groundwater sampled as well as the major uranium species in solution	82
Table 4.2 Uranium activity concentrations and $^{234}\text{U}/^{238}\text{U}$ isotope ratios in core sequential extractions and adjacent groundwater samples	88
Table 4.3 Quantitative XRD analysis of bulk, micronized and calcium saturated core samples	89
Table 5.1 Aquitard pore water chemistry, measured aquitard properties, groundwater chemistry, as well as uranium and thorium concentrations in sediment samples.....	110
Table 5.2 Solute transport model boundary conditions and SRMS error	112
Table 5.3 Measured aquitard core properties and Peclet Numbers for ^4He and chloride.....	115

Chapter 1 Introduction

1.1 Research problem

Low permeability geological formations known as aquitards confine and separate aquifers, playing an important role in the physical and chemical evolution of groundwater (Back 1986; Cherry and Parker 2004). In most groundwater systems, the location and quantity of groundwater movement through an aquitard, referred to as inter-aquifer leakage, is unknown. Even in extremely tight aquitards with low hydraulic conductivities ($<10^{-12}$ m/yr) there is a small amount of 'diffuse inter-aquifer leakage' of pore water (Cherry and Parker 2004). The presence of preferential pathways, such as faults, intercalations of higher permeability sediments, or thinner aquitard sections, can increase the rate of water movement through an aquitard causing 'enhanced inter-aquifer leakage' (Bredehoeft et al. 1983; Neuzil 1994; Hendry et al. 2004; Hart et al. 2006; Myers 2012). In areas affected by large-scale groundwater abstraction, e.g. mining, and for safety assessment studies of waste repositories, an understanding of the hydrogeological and hydrochemical role of aquitards is also vital to understand and manage groundwater systems. Furthermore, not taking into account leakage rates in the analysis of large-scale flow systems can lead to underestimation or overestimation of groundwater flow rates in aquifers (Love et al. 1993; Love et al. 1996; Tóth 2009). Despite this, aquitards remain less well studied in comparison with aquifers because of the focus on determining aquifer yields and sustainability, and the inherent difficulty of obtaining the necessary information.

Field-focused research is needed to test potential mechanisms and pathways by which groundwater can be contaminated (Jackson et al. 2013; Rahm and Riha 2014). With the few methods that are available to characterise aquitards and investigate inter-aquifer leakage, described in section 1.2, there are issues of scale and heterogeneity. Studies explicitly designed to link processes at the point-scale to whole-basin processes are rarely undertaken (Herczeg and Leaney 2011). This thesis will investigate inter-aquifer leakage at multiple scales in an arid zone regional groundwater basin using environmental tracers, including isotopes and noble gases, in an attempt to account for heterogeneity and different scales of inter-aquifer leakage.

1.2 Literature Review

1.2.1 Point-scale studies

Measurements within the aquitard itself provide localised and detailed evidence of inter-aquifer leakage through pores. However, due to their low permeability, piezometers installed in aquitards are slow to equilibrate with the aquitard pore water, thus only shallow surficial fractured aquitards have been studied by sampling aquitard pore water using piezometers (Desaulniers et al. 1981; Desaulniers et al. 1986; Keller et al. 1988; Desaulniers and Cherry 1989; Fortin et al. 1991; Rudolph et al. 1991; Remenda et al. 1996; Ortega-Guerrero 2003; Hendry et al. 2004). Instead, aquitard drill core pore water and well fluid pressures can be used to investigate deeper consolidated aquitards.

Aquitard core pore waters can provide insights into the mechanisms, direction and rate of groundwater flow, as well as vertical heterogeneity. Measured hydraulic properties of aquitard core samples and fluid pressures within a piezometer, or in-situ vibrating wire pressure transducers can be used to determine hydraulic properties and their variability in aquitards (Neuzil and Bredehoeft 1980; Macfarlane et al. 1994; Shaw and Hendry 1998; Croisé et al. 2004; Larroque et al. 2013; Smerdon et al. 2014). However, when the hydraulic gradient is less than 1 Darcy's law may no longer be applicable as this threshold gradient represents the minimum hydraulic gradient required to cause flow by exceeding the viscous frictional forces (Law and Lee 1981; Tavenas et al. 1983; Marschall et al. 2004). Alternatively, due to heterogeneity, hydraulic conductivity measurements can increase with the scale of measurement due to incorporation of any preferential flow paths (Neuzil and Bredehoeft 1980; Neuzil 1986; Batlle-Aguilar et al. 2016). To incorporate heterogeneity in aquitard characterisations Neuman and Witherspoon (1972) developed leaky aquifer pumping tests by pumping from a single aquifer with monitoring wells in the aquifer above and/or below the aquitard of interest. These pumping tests require weeks or longer due to the low hydraulic conductivity of aquitards and thus are not commonly applied to characterise aquitards (Batlle-Aguilar et al. 2016). Modelling of aquitard pore water solute concentrations have been used to estimate inter-aquifer leakage flow rates. As the method is also applied to the whole aquitard thickness some preferential flow paths and heterogeneity are incorporated in these flow rate estimates.

Aquitard pore water solute composition has previously been used to evaluate the origin, age, and migration processes of water and solutes, as well as the palaeohydrogeological evolution of

groundwater systems (Konikow and Arevalo 1993; Harrington and Hendry 2005; Hendry et al. 2011). Naturally occurring environmental tracers, such as stable isotopes of water (Hendry and Wassenaar 1999; Kelln et al. 2001; Gimmi et al. 2007; Savoye et al. 2008; Hendry et al. 2011; Hendry et al. 2013; Hendry et al. 2015a) and major elements (Desaulniers et al. 1986; Desaulniers and Cherry 1989; Konikow and Arevalo 1993; Jones et al. 1994; Love et al. 1996; Pucci 1998; Hendry and Wassenaar 1999; Hendry and Wassenaar 2000; Hendry et al. 2000; Harrington et al. 2001; Waber et al. 2001; Hendry and Wassenaar 2004; Bensenouci et al. 2013; Harrington et al. 2013; Sanford et al. 2013; Hendry and Harrington 2014; Al et al. 2015), and noble gases (Osenbrück et al. 1998; Rubel et al. 2002; Sheldon et al. 2003; Mazurek et al. 2007; Ali et al. 2011; Bensenouci et al. 2011; Mazurek et al. 2011; Gardner et al. 2012; Clark et al. 2013), in combination with mathematical models have been used successfully to determine transport processes and to reconstruct past environmental conditions.

1.2.2 Regional-scale studies

The vast majority of aquitard studies have identified diffusion as the dominant solute transport process (for example, Savoye et al. 2008; Bensenouci et al. 2013), supporting assertions that enhanced inter-aquifer leakage occurs along regionally active preferential pathways in the systems studied. Some regional-scale investigations have identified these preferential pathways in aquitards using hydraulic head measurements, environmental tracers and dating tracers in aquifers (for example, Clark et al. 1997; Trabelsi et al. 2009; Arslan et al. 2015). A clear contrast in environmental tracers between aquifers can highlight where there is little inter-aquifer leakage, whereas similar environmental tracer concentrations may be an indication of mixing or enhanced inter-aquifer leakage. A sufficient difference in environmental tracer concentrations for water circulating in the different aquifers is required to compare the aquifers. The similarity in major and trace element concentrations, or stable isotopes of water between aquifers separated by an aquitard have identified locations of enhanced inter-aquifer leakage (Trabelsi et al. 2009; Zilberbrand et al. 2014; Moya et al. 2015). Additionally, some isotopes and environmental tracers, for instance strontium and uranium isotopes, are sensitive to the redox conditions and/or the types of rocks that are in the aquifer, and thus are useful indicators of inter-aquifer mixing (for example, Herczeg et al. 1996; Dogramaci and Herczeg 2002; Brenot et al. 2015). Strontium isotopes especially have been proven to be an excellent mixing tracer if there is sufficient distinction between the aquifers in question and knowledge of the reactivity of strontium within the aquifers (Johnson and DePaolo 1997; Shand et al. 2009).

Uranium isotope distributions in aquifers and aquitards are complex and can be affected by multiple processes resulting in complex behaviours (Osmond and Cowart 1976; Gascoyne 1992; Osmond and Cowart 1992; Osmond and Ivanovich 1992; Porcelli and Swarzenski 2003). Deconstruction of uranium isotope distributions have been used to infer the location of inter-aquifer leakage in the Otway Basin, Australia (Herczeg et al. 1996) and the Continental Intercalaire aquifer, Tunisia (Dhaoui et al. 2016). Additionally, Henderson et al. (1999) measured the rate of pore water leakage through a carbonate platform using uranium isotope distributions.

Dating tracer distributions along groundwater flow paths can be disrupted by the introduction of water from the surface or from aquifers above or below providing evidence of localised recharge and enhanced inter-aquifer leakage through preferential pathways. Age tracers also have been used in combination with environmental tracer concentrations and isotope ratios to provide evidence of enhanced inter-aquifer leakage (for example, Herczeg et al. 1996; Love et al. 1993; Cartwright et al. 2012).

Noble gases, especially helium isotopes, are particularly useful tracers to investigate groundwater mixing and groundwater leakage because they are chemically inert and have multiple origins (Mazor and Bosch 1987; Kipfer et al. 2002; Marty et al. 2003). High ^3He at the surface is an indication of volatiles transported from the mantle and is known to occur in regions that have been tectonically active as found by Hooker et al. (1985a), Hooker et al. (1985b) and Martel et al. (1989). Radiogenic ^4He concentrations increase with groundwater residence time and can be used to calculate groundwater age up to thousands or millions of years (Mazor and Bosch 1987; Osenbrück et al. 1998; Beyerle et al. 2000; Kipfer et al. 2002). Comparison of helium isotopes in combination with environmental tracers, isotope ratios and other dating tracers have provided evidence of recharge and mixing, as well as enhanced inter-aquifer leakage (Clark et al. 1997; Bethke et al. 1999; Larsen et al. 2003; Althaus et al. 2009; Warriar et al. 2013; Arslan et al. 2015; Gumm et al. 2016). Castro et al. (1998a) and Castro et al. (1998b) measured and modelled noble gas concentrations and showed the dominance of vertical transport by advection in fault zones and both advection and diffusion throughout the rest of the Paris Basin.

Noble gases have also been adopted in aquitard core pore water studies to investigate transport processes through an aquitard. They have been used to date pore waters (Osenbrück et al. 1998) and examine solute mass transport (Bethke et al. 1999; Rubel et al. 2002; Althaus et al. 2009; Clark et al. 2013; Trinchero et al. 2014).

1.2.3 Whole-basin studies

To gain a comprehensive picture of inter-aquifer leakage, including diffuse inter-aquifer leakage through the aquitard pores and any enhanced inter-aquifer leakage through preferential pathways, it is desirable to combine both regional-scale and point-scale investigations. Fortin et al. (1991) compared regional aquifer hydrochemistry to shallow till aquitard pore water data from studies by Keller et al. (1986), Keller et al. (1987), Keller et al. (1988) and Keller and van der Kamp (1988), showing that hydrochemical patterns in the aquifer appear to be related to the geochemical conditions within the till aquitard and groundwater flow in the aquifer. A 3-D conceptual model of groundwater flow and hydrochemistry in a fractured aquitard highlighted the importance of transmissive bedding planes (Eaton et al. 2007). Additionally, helium concentrations above those in the aquitard pore waters in the discharge zone provided evidence of transport through preferential pathways in an aquitard in the Great Artesian Basin, Australia (Gardner et al. 2012). While diffusion is often the dominant transport mechanism within an aquitard, secondary permeability features, such as fractures and discontinuities can cause multifarious enhanced inter-aquifer leakage pathways through aquitards.

Numerical models of groundwater basins have also been used to estimate inter-aquifer leakage fluxes (Bredehoeft et al. 1983; Mazurek et al. 1998; Hart et al. 2006). However, these models are often limited by uncertainty in the conceptual models due to the long timescales involved, inadequate data, and hydraulic conductivity measurements available for aquifers only, or if aquitard hydraulic conductivity measurements are available, they are often extrapolated from laboratory scale measurements. Additionally, these models are most likely to be calibrated against hydraulic head only. Consequently, these models could be improved by calibrating against environmental tracers as well as hydraulic head and using scale appropriate, in addition to locational relevant, hydraulic conductivity measurements (Batlle-Aguilar et al. 2016). Therefore, there remains a need for integrated studies of pore water scale and regional-scale measurements using multiple environmental tracers, isotopes and noble gases to gain a better insight into inter-aquifer leakage processes.

1.3 Knowledge gaps

Studies explicitly designed to link inter-aquifer leakage processes at the point-scale to whole-basin are still required as knowledge of both diffuse inter-aquifer leakage and enhanced inter-aquifer leakage is important to improve our understanding of groundwater systems and to improve their

management. As the overview of the existing literature has demonstrated point-scale measurements within the aquitard itself, while providing localised estimates of diffuse discharge, are not often able to incorporate preferential flow paths and heterogeneity in flow rate estimates. And while locations of heterogeneity and enhanced inter-aquifer leakage through an aquitard have been identified in a number of regional-scale investigations through interpretation of hydraulic head measurements, environmental tracers and dating tracers in aquifers, these studies are not generally systematically investigating inter-aquifer leakage. In addition, systematic investigations of inter-aquifer leakage at both the point- and regional-scale are very rarely undertaken within a single area to identify both diffuse and enhanced inter-aquifer leakage. Therefore there remain issues regarding the scale of the study undertaken and incorporation of heterogeneity in the current literature investigating inter-aquifer leakage.

1.4 Thesis aims

There are a multitude of techniques currently available to investigate inter-aquifer leakage; however, there are issues of scale and heterogeneity. Quantifying inter-aquifer leakage at a regional-scale is complicated by diffuse inter-aquifer leakage rates that are often small and very hard to detect and quantify, although they can result in a large volumetric flow. Localised high fluxes of enhanced inter-aquifer leakage can be missed at the spatial resolution of regional surveys. Scarcity of data is an additional challenge encountered in regional hydrogeological investigations in sparsely developed areas, such as central Australia (Melloul 1995; Cudennec et al. 2007; Masoud et al. 2013; Candela et al. 2014).

The broad aim of this thesis is to investigate inter-aquifer leakage at multiple scales in an arid zone regional groundwater basin using multiple environmental tracers and isotopes, including noble gases, addressing issues of scale and heterogeneity. This thesis focusses on the connectivity between the Great Artesian Basin (GAB) and underlying Arckaringa Basin, located in central Australia. This thesis specifically investigates:

- i. Inter-aquifer leakage at a regional-scale in an area with a scarcity of observation points. This study uses a comprehensive multidisciplinary approach to determine if, and which, combinations of methods are best suited to improve the regional-scale understanding of the system.
- ii. Uranium isotope distributions and the processes that control them in groundwater. Identification of the complex processes controlling uranium isotope distributions may

provide insights into groundwater flow, recharge, discharge and inter-aquifer connectivity between the GAB and Arckaringa Basin.

- iii. Vertical groundwater flow and solute transport through aquitard pores using chloride, the stable isotopes of water and helium in conjunction with analytical and numerical modelling.

These specific research aims are the focus of three manuscripts presented in Chapters 4 through to 6. Chapter 1 provides a brief background to the thesis and summarises the research aims of the thesis, Chapter 2 provides the study area background and Chapter 3 provides a summary of the sampling procedures and background on environmental tracers and isotopes used in the study. A summary of the main conclusions from this thesis are given in Chapter 6. Conference proceedings from work contained in this thesis are presented in Appendices A to F.

1.5 Contribution of this PhD

This PhD thesis explores the connectivity between the GAB and underlying Arckaringa Basin in central Australia and makes an important scientific contribution as it presents new information and understanding of groundwater processes in a regional-scale aquifer system in an area of the Australian continent where data are severely lacking. The research is performed through a regional groundwater field investigation and aquitard coring program, and subsequent data analysis and interpretation. The research provides evidence of both diffuse inter-aquifer leakage rates and solute transport as well as localised enhanced inter-aquifer leakage. This is achieved by specifically examining:

- i. Inter-aquifer leakage at a regional-scale using a comprehensive multidisciplinary approach. Interpretation of aquitard hydraulic resistance provided an indication of diffuse leakage direction and flow rates through the aquitard pores. Interpretation of hydrochemistry, specifically the major elements, stable isotopes of water, strontium isotopes, chlorine-36, carbon-14 and radiogenic helium, identified enhanced inter-aquifer leakage through the aquitard in the centre of the basin. While the leakage mechanism remains unknown in detail, the proportion of enhanced inter-aquifer leakage was able to be calculated with strontium isotopes and radiogenic helium. This multi-tracer approach along with groundwater hydraulics provides a tool-set to investigate inter-aquifer leakage in a regional-scale sedimentary basin with a paucity of data.
- ii. Uranium isotope distributions and the processes that control them in groundwater in the

GAB and underlying Arckaringa Basin. The complex processes controlling uranium isotope distributions were identified by interpretation of regional groundwater chemistry and sequential extraction of mineral phases. This indicated a number of recharge locations and highlighted groundwater flow processes, including a region of stagnant flow. However, it was not possible, with the current dataset, to conclusively ascertain the processes resulting in intricate uranium isotope behaviours at all locations or identify enhanced inter-aquifer leakage locations.

- iii. Vertical groundwater flow, and chloride and helium transport through the aquitard pores with analytical and numerical models. The use of both chloride and helium concurrently was useful to estimate groundwater flow and solute transport, and limited the models that fit the data, leading to the final model presented. Transport properties through the aquitard pores were calibrated using the best-fit model, concluding that solute transport is controlled by both diffusion and advection in the study location. Additionally, the chloride profile provided information on the palaeohydrological conditions in the study area with concentration variability in the aquifers a result of high evapotranspiration compared to precipitation concentrating solutes in recharging groundwater.

This investigation provides field- and laboratory-focused research showing inter-aquifer connectivity between the GAB and underlying Arckaringa Basin. The study was explicitly designed to link inter-aquifer connectivity at the point-scale to whole-basin processes, which is rarely undertaken (Herczeg and Leaney 2011). This type of research helps to address water quality issues on a local and regional basis. It provides a better understanding of modern and palaeohydrological conditions necessary to underpin groundwater sustainability and highlights the need for field-testing of potential mechanisms and pathways that groundwater can be contaminated, as well as improve conceptual models and water balance models for groundwater management (Jackson et al. 2013; Rahm and Riha 2014).

Chapter 2 Study Area

2.1 Background

This thesis focusses on the inter-aquifer connectivity between the Great Artesian Basin (GAB) and the underlying Arckaringa Basin located in central Australia (Figure 2.1 a). Extraction of groundwater from the GAB since 1880 has provided water supplies for towns, agriculture and mining industries (Habermehl 1980). Because of its importance as a water resource, there have been numerous studies of the GAB, which focused especially on the eastern artesian and north-western sections of the basin (Habermehl 1980; Herczeg et al. 1991; Love et al. 2000; Mahara et al. 2009; Love et al. 2013; IESC 2014; Moya et al. 2015). Those few studies covering the unconfined south-western part of the GAB have highlighted the potential connectivity between the GAB and the Arckaringa Basin (Smerdon et al. 2012; Keppel et al. 2015). The Arckaringa Basin contains coal and gas deposits and there are currently numerous proposals for exploration and mining of these (Wohling et al. 2013). The Prominent Hill copper and gold mine and water supply well fields, developed in a progressive manner since 2008, is the largest user of water in the Arckaringa Basin and has been extracting groundwater at a rate of up to 26 ML/d (SKM 2010).

2.2 Location

The GAB is one of the world's largest multi-layer aquifer systems underlying Queensland, New South Wales, Northern Territory and South Australia (it underlies 22% of the Australian continent; Figure 2.1 a). The Arckaringa Basin covers an area of approximately 100,000 km² located in South Australia approximately 600 km north-west of Adelaide (Figure 2.1 a; Wohling et al. 2013).

Coober Pedy, located in the centre of the Arckaringa Basin, is the largest town in the area with a population of approximately 3500. A number of smaller towns such as Oodnadatta, Marla and William Creek are situated close to the margin of the Arckaringa Basin (Figure 2.1 b). The Prominent Hill copper and gold mine is located in the south-eastern corner of the Arckaringa Basin (Figure 2.1 b).

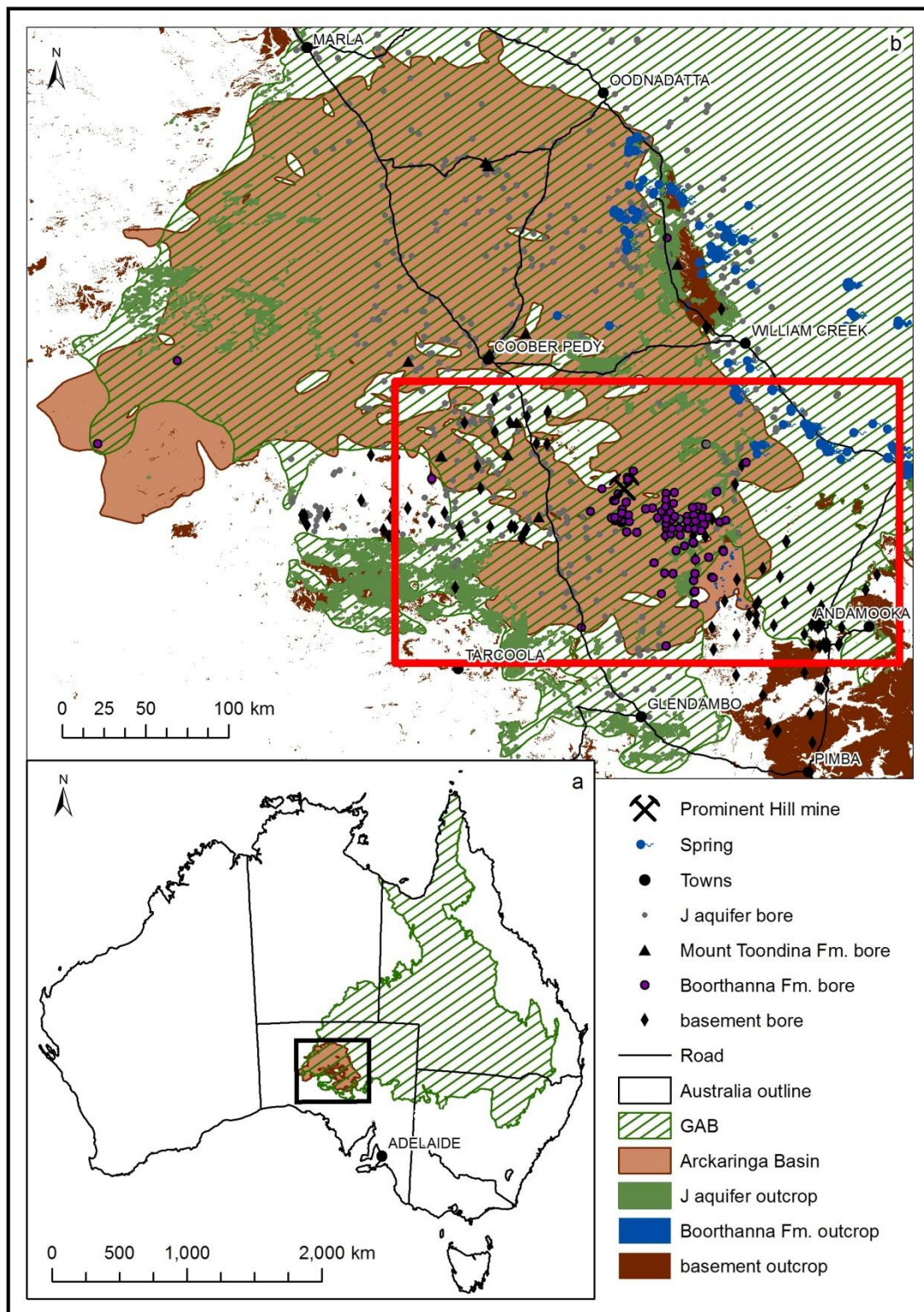


Figure 2.1 (a) Extent of the GAB and Arckaringa Basin and (b) GAB and Arckaringa Basin extents; J aquifer, Boorthanna Formation (Fm.) and basement outcrop, and well locations. The red box surrounds the study area where the majority of groundwater wells have been drilled into the Arckaringa Basin (Boorthanna Fm.).

2.3 Climate, topography and land use

The Arckaringa Basin is located within in the Australian arid zone. The arid zone is characterised by long hot summers with daily maximum temperatures averaging 36°C (January) and cool dry winters with daily maximum temperatures averaging 20°C (July) (minimum temperatures below 10°C; Figure 2.2). Average annual precipitation rates are approximately 120 mm/yr, but precipitation is variable, both temporally (Figure 2.3) and spatially, so vegetation species in the region are adapted for survival in arid climates (Allan 1990; Bureau of Meterology 2017).

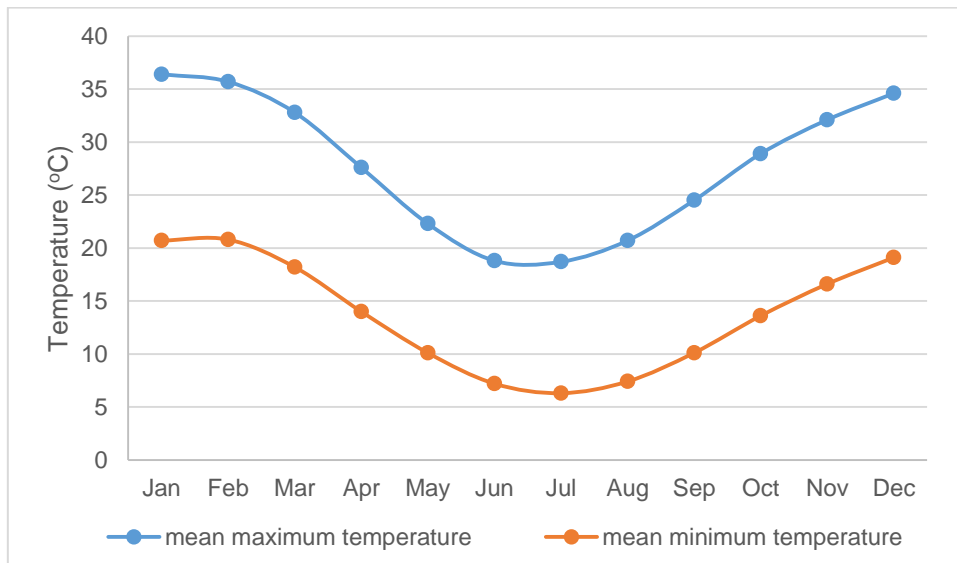


Figure 2.2 Annual mean monthly temperatures recorded at Coober Pedy rain gauge station (Bureau of Meterology 2017).

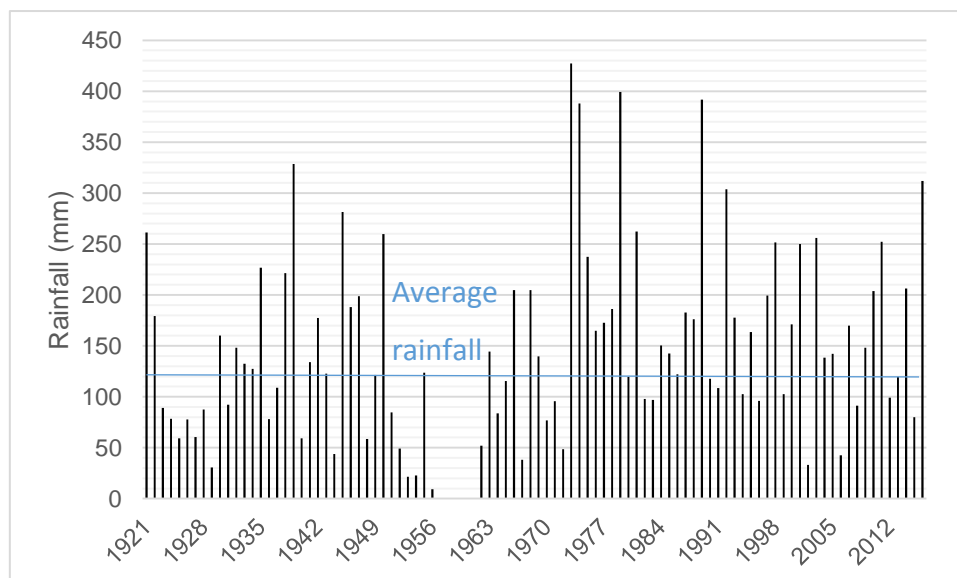


Figure 2.3 Annual rainfall recorded at Coober Pedy rain gauge station, no data available years 1957–1962 (Bureau of Meterology 2017).

Precipitation originates from weak winter cold fronts related to ocean temperatures in the Southern Indian Ocean Precipitation, or less commonly, from intermittent summer monsoons that originate in north-west Australia (Allan 1990; Wohling et al. 2013). Potential evaporation exceeds precipitation with measured evaporation rates between 2.5–3.6 m/yr (Allan 1990; Hamilton et al. 2005; Bunn et al. 2006).

The topography of the Arckaringa Basin region is largely flat, with a mean elevation of 180 m above Australian Height Datum (AHD; 20–180 m AHD), characterised by flat-topped plateaus with sharp escarpments, and lower lying gibber and flood plains created by ephemeral rivers (Figure 2.4). Ephemeral rivers are characterised by extreme variation in discharge and flow duration with extended periods of drought followed by major flood events (Habermehl 1980). The Stuart Range is a low-rising escarpment that transects the Arckaringa Basin from north to south (Figure 2.4). The Arckaringa Basin is bordered by a series of ranges, ridges and plateaus, including the Peake and Denison Inlier to the east consisting of cropping out basement rocks with a maximum elevation between 400–420 m AHD (Figure 2.4; Wopfner & Twidale 1967; Wohling et al. 2013).

Spring wetland environments occur on the eastern margin of the Arckaringa Basin (Figure 2.4). They are often referred to as ‘Mound Springs’ in other publications because of the travertine mound surrounding the spring vent at most springs (Keppel et al. 2013). These important permanent sources of water containing endemic flora and fauna have cultural and spiritual significance for the Indigenous people of the region, the Arrabuna, Dieri, Lower Southern Arrente, Wokangurru and Kuyani peoples (Wohling et al. 2013).

The pastoral industry produces beef-cattle throughout the area, and sheep near Coober Pedy. Unmetered pastoral production and domestic wells within the limits of the Arckaringa Basin primarily extract groundwater from aquifers within the GAB. Mining is another important industry in the region with private opal mining in the vicinity of Coober Pedy. The Prominent Hill copper and gold mine extracts up to 26.6 ML/d from the Boorthanna Formation (Fm.) to sustain its copper and gold mining operations (SKM 2010).

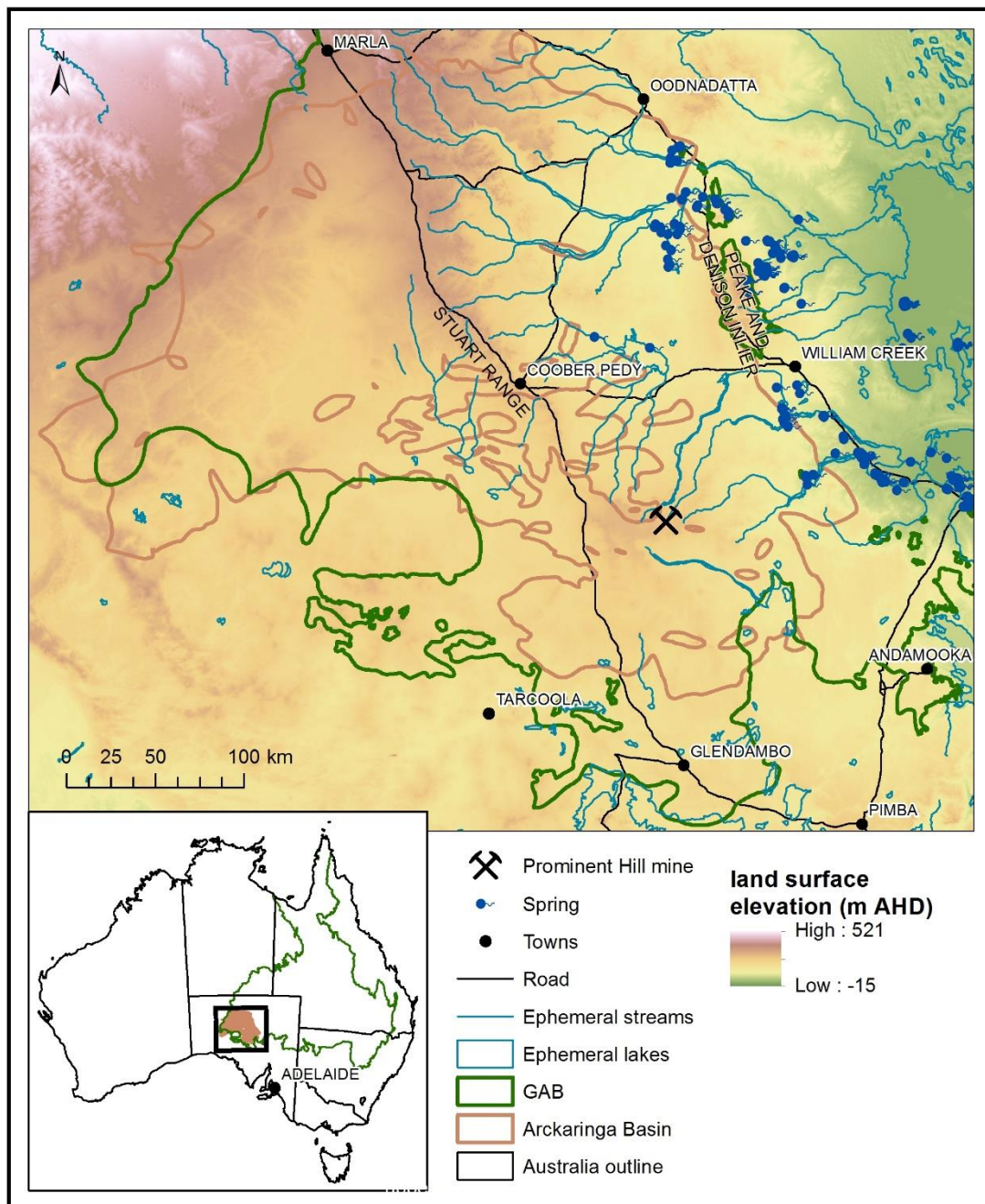


Figure 2.4 Land surface elevation and ephemeral surface water features.

2.4 Geological setting

The GAB is composed of Late Jurassic to Early Cretaceous sedimentary rocks (Senior et al. 1978; Gallagher and Lambeck 1989; Toupin et al. 1997), whereas the underlying Arckaringa Basin comprises Late Carboniferous to Early Permian sedimentary rocks (Ambrose and Flint 1980). Both the Arckaringa Basin and GAB are underlain by Proterozoic-Archean crystalline metasediment, limestone and igneous rocks of the Adelaide Geosyncline and Stuart Shelf to the south and south-east of Cober Pedy. To the north and west, the Arckaringa Basin and GAB are underlain by the

Devonian-Precambrian Warburton Basin and Officer Basin, respectively (Krieg et al. 1990; Kellett et al. 1999; Wohling et al. 2013; Miles et al. 2015). Glacial scouring during the Devonian-Carboniferous and faulting during the Early Permian has resulted in the formation of troughs and sub-basins (Wohling et al. 2013; Keppel et al. 2015). Since formation, the basins have undergone many compression and uplift events (approximately 50 Ma and 15–5 Ma) and erosional phases to today's levels (Toupin et al. 1997; Wohling et al. 2013).

The GAB in the western margin is composed of three formations, the Bulldog Shale, Cadna-Owie Fm. and Algebuckina Sandstone (Ambrose and Flint 1980; Drexel and Preiss 1995; Keppel et al. 2013; Wohling et al. 2013; Figure 2.5). The Bulldog Shale, a marine shaly mudstone and silt aquitard deposited in a low energy marine environment, is on average 30 m thick (1–320 m; Figure 2.6) in the Arckaringa Basin region (Freytag 1966). The Cadna-Owie Fm. is a fine-grained sandstone and siltstone deposited in a marine transitional and terrestrial environment (Wopfner et al. 1970). The Algebuckina Sandstone is a fine to coarse-grained sandstone deposited in a low-gradient fluvial environment during both arid and wet climates (Wopfner et al. 1970). The Cadna-Owie Fm. and Algebuckina Sandstone are hydraulically connected in the western margin of the GAB and are thus treated as one aquifer referred to as the J aquifer (Love et al. 2013), which is on average 60 m thick (1–140 m; Figure 2.7 b) in the Arckaringa Basin region. The J aquifer underlies the Bulldog Shale, which confines the aquifer throughout the eastern and north-western GAB, although the aquifer is unconfined in the south-western portion of the GAB (Love et al. 2013). The J aquifer crops out in multiple locations throughout the western, southern and eastern Arckaringa Basin region (Figure 2.1 b).

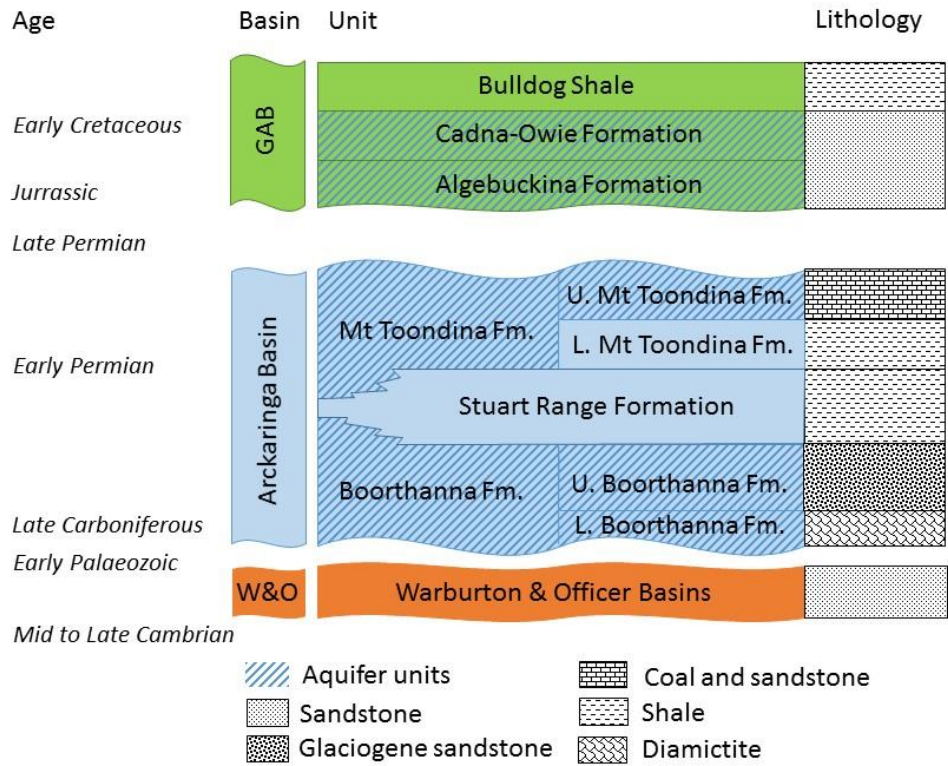


Figure 2.5 Simplified Cretaceous to Cambrian Stratigraphy adapted from Wohling et al. (2013).

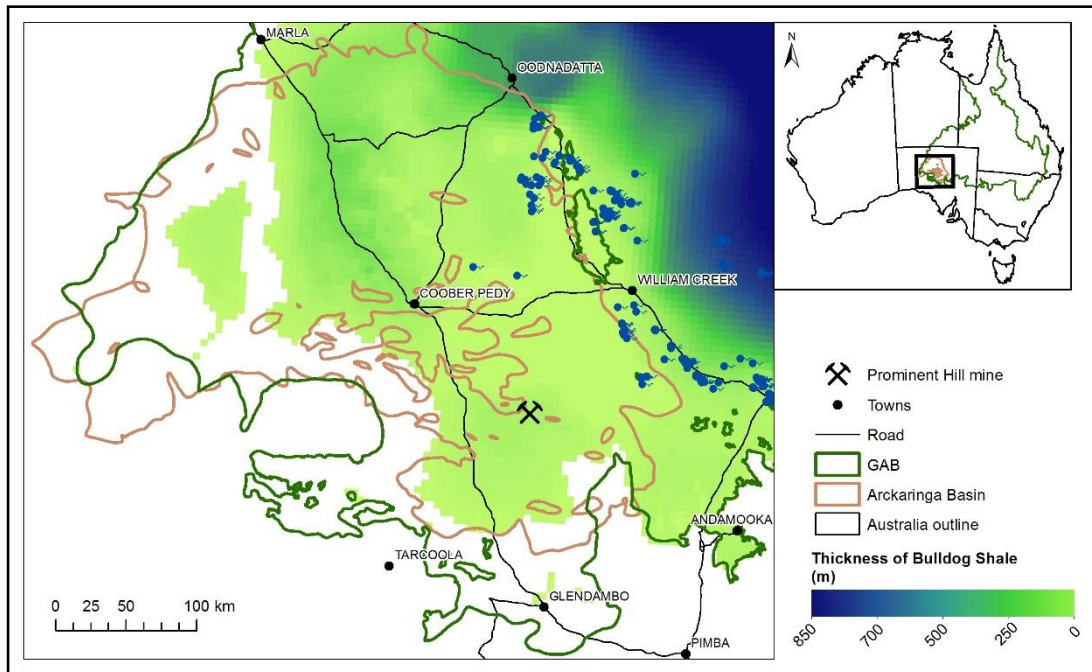


Figure 2.6 Extent and thickness of the Bulldog Shale (Sampson et al. 2012a; Sampson et al. 2012b).

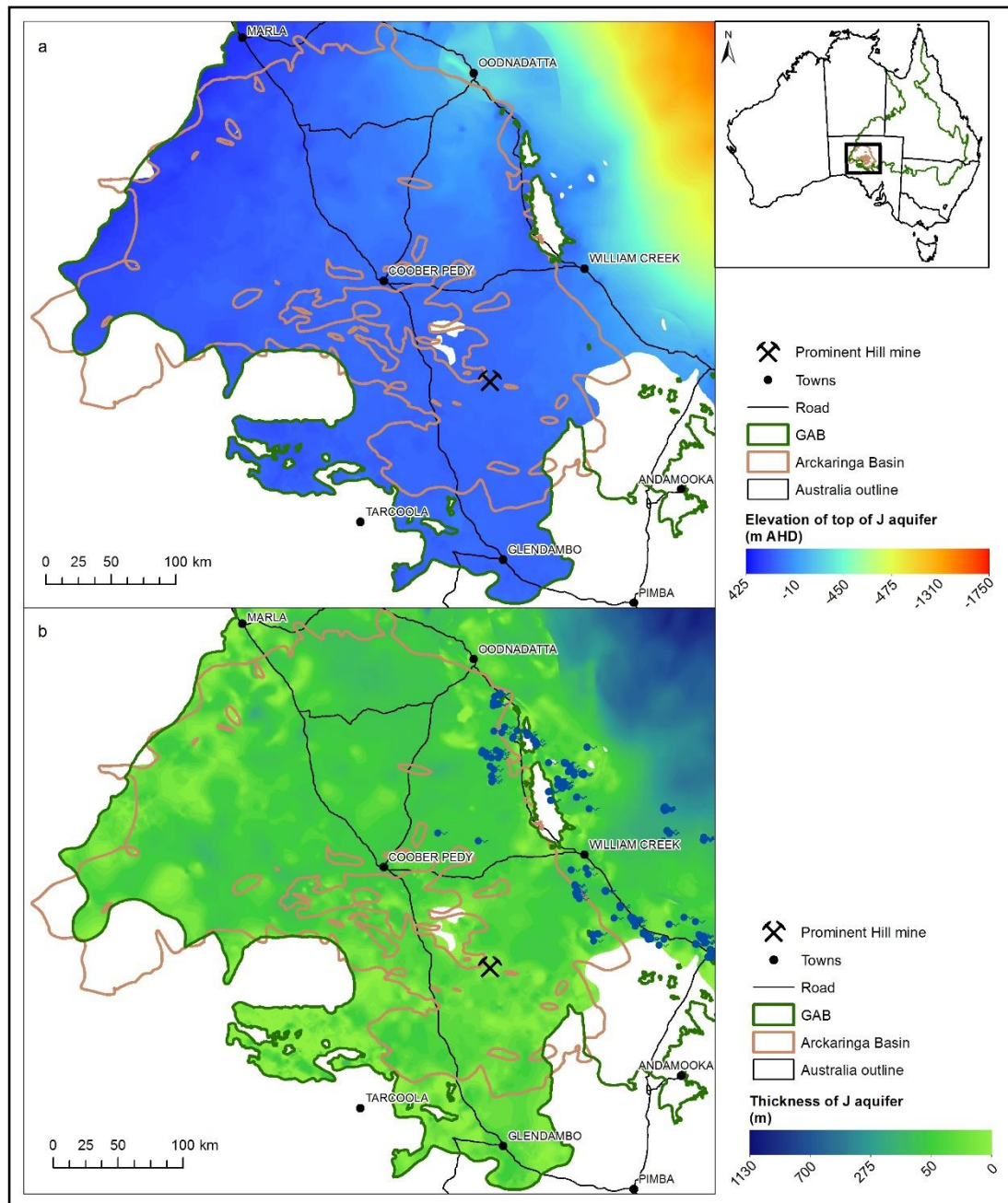


Figure 2.7 (a) Elevation of top of the J aquifer and (b) thickness of the J aquifer (Sampson et al. 2012a; Sampson et al. 2012b).

The Arckaringa Basin sits unconformably below the GAB and is composed of three formations, the Mount Toondina Fm., Stuart Range Fm. and Boorthanna Fm. (Figure 2.5; Townsend and Ludbrook 1975; Ambrose and Flint 1980; Wohling et al. 2013; Keppel et al. 2015). The Mount Toondina Fm. lies directly below the J aquifer but is absent from most of the south-western margin (Figure 2.8 b). The Mount Toondina Fm. comprises grey carbonaceous shales, coals and interbedded grey sandstones, siltstones and sandy shales; the lower section is less carbonaceous and slightly sandier. Non-marine lagoons and swamps with intermittent deposition of fluvial sands formed the

Mount Toondina Fm. (Townsend and Ludbrook 1975). The formation occurs only in the subsurface and is on average 195 m thick (1–830 m; Figure 2.8 b). The Stuart Range Fm., the aquitard of interest in this study, is made up by mudstone, siltstone and shale, deposited in an at times anoxic marine environment, is on average 85 m thick (1–510 m; Figure 2.9 b; Townsend and Ludbrook 1975). The Stuart Range Fm., where present, separates the underlying Boorthanna Fm. from the overlying Mount Toondina Fm. and J aquifer (Figure 2.9). The Boorthanna Fm., a marine and glacial sandstone and diamictite aquifer deposited in marine and glacial environments, is on average 85 m thick (1–510 m; Figure 2.10 b). The Boorthanna Fm. while extensive in the subsurface (Figure 2.10), only crops out in the south-eastern margin where the GAB sediments are absent (Figure 2.1; Townsend and Ludbrook 1975). The Boorthanna Fm. is underlain by Proterozoic-Archean crystalline metasediment, limestone and igneous rocks, which are colloquially referred to as 'basement' (Figure 2.11).

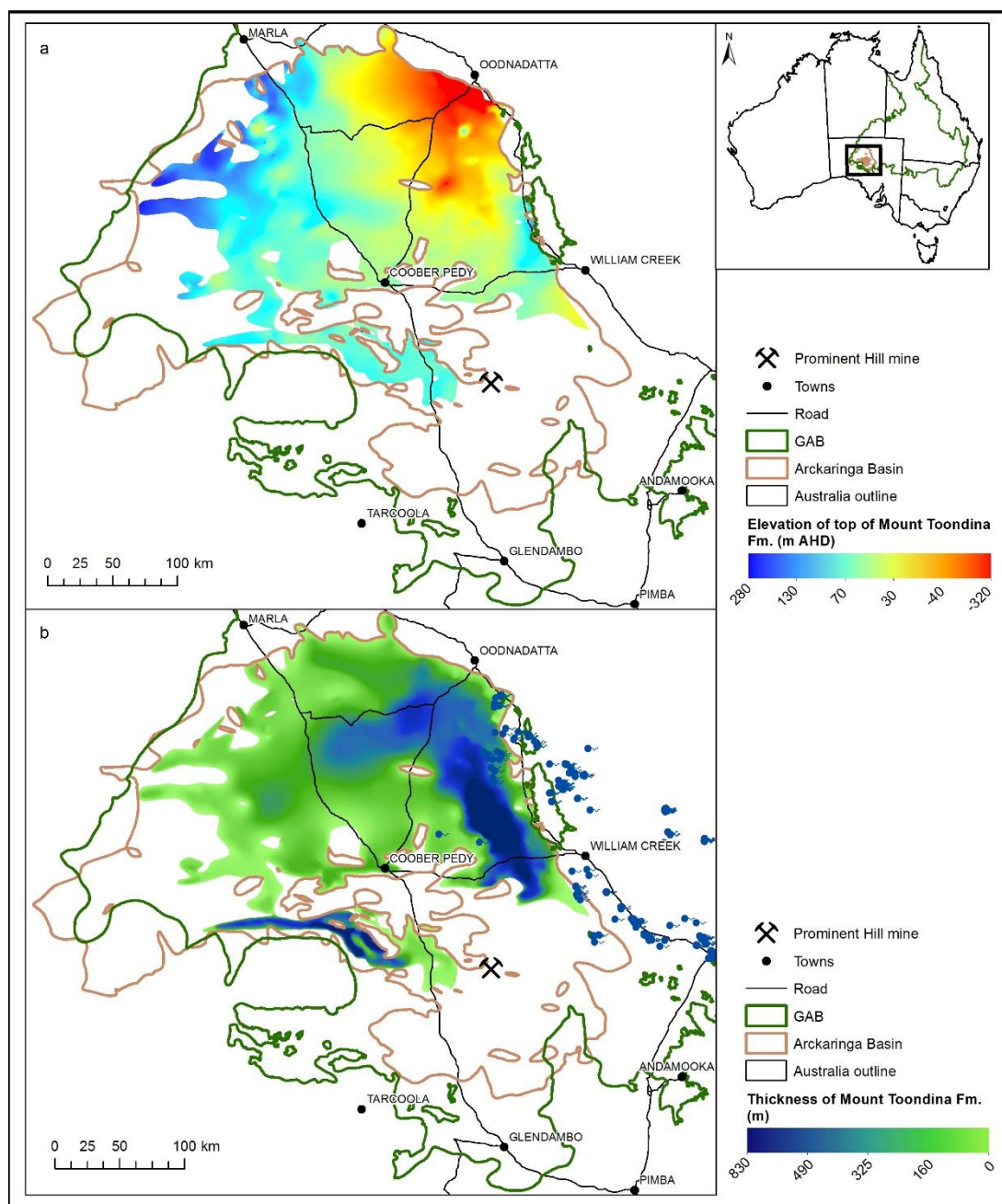


Figure 2.8 (a) Elevation of top of the Mount Toondina Fm. and (b) thickness of the Mount Toondina Fm. (Sampson et al. 2015).

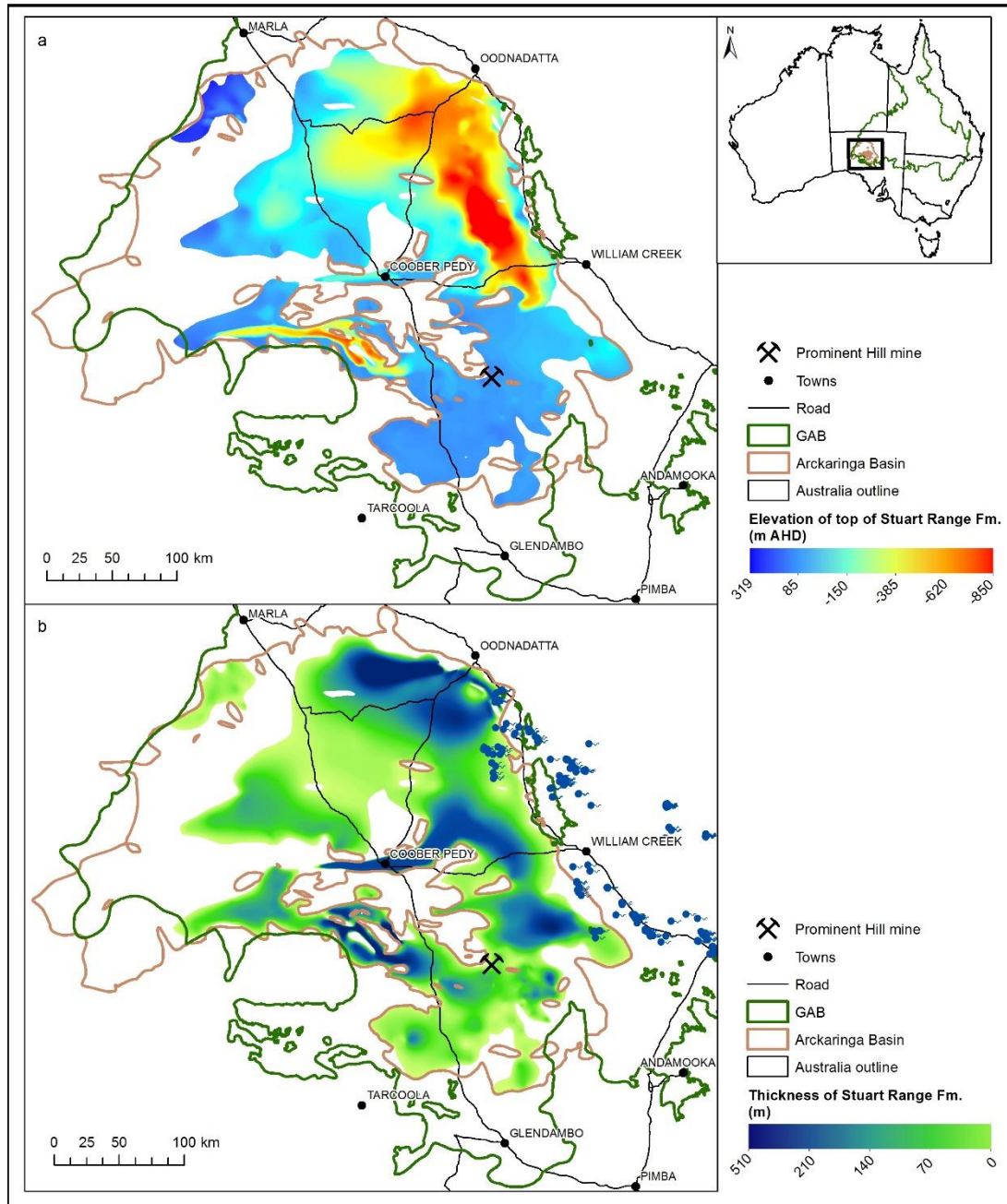


Figure 2.9 (a) Elevation of top of the Stuart Range Fm. and (b) thickness of the Stuart Range Fm. (Sampson et al. 2015).

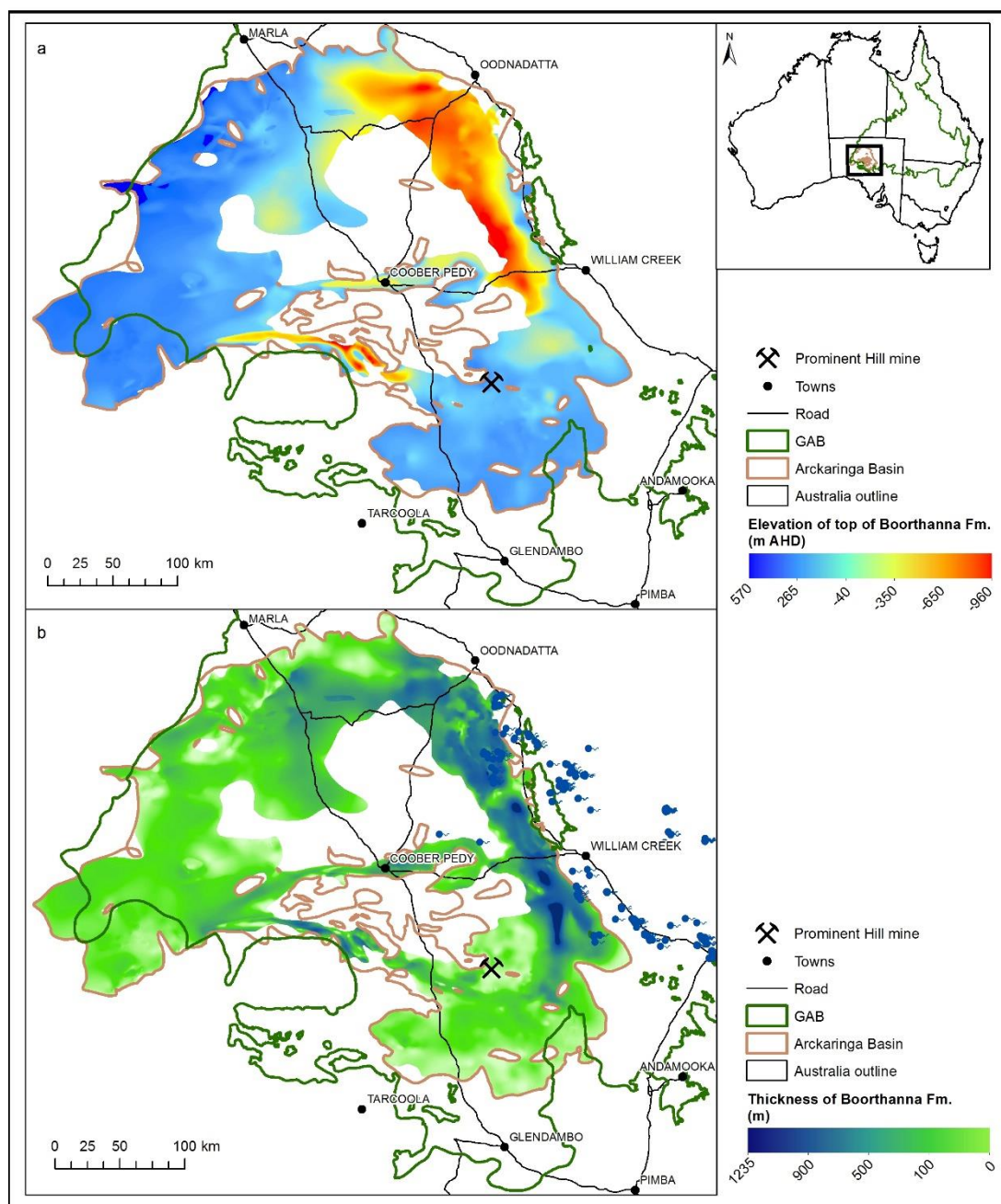


Figure 2.10 (a) Elevation of top of the Boorthanna Fm. and (b) thickness of the Boorthanna Fm. (Sampson et al. 2015).

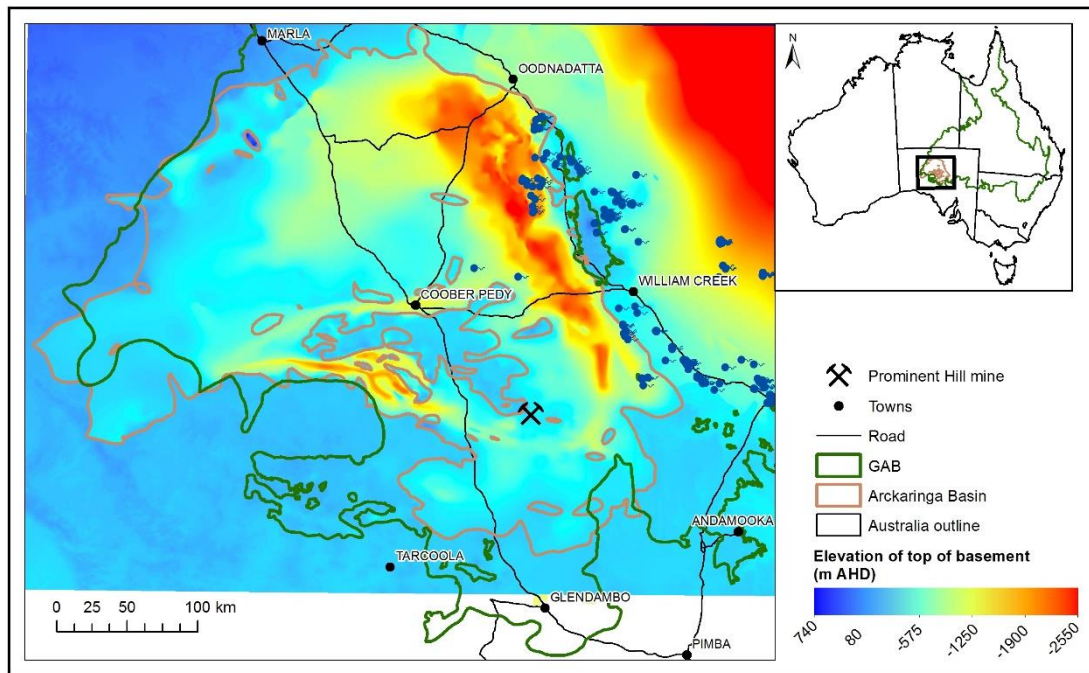


Figure 2.11 Elevation of top of the basement (Sampson et al. 2015).

2.5 Hydrogeology

The Bulldog Shale crops out extensively in the western margin of the GAB and as the vertical hydraulic conductivity is low (4.6×10^{-14} – 3.6×10^{-9} m/s; Table 2.1), it inhibits recharge to the underlying aquifers. Diffuse recharge to the J aquifer through the Bulldog Shale was estimated by Love et al. (2013) to be <0.25 mm/yr. Higher recharge rates occur in areas where the aquifer (sub)crops out along the western and southern margin, as well as focused beneath disconnected ephemeral rivers (Love et al. 2013). The generalised direction of groundwater flow is from the north-west, western and southern margins of the J aquifer towards the Peak and Dennison Inlier and south-eastern margin (Figure 2.12). Hydraulic heads range from 324 m AHD in the north-west margin to 0 m AHD in the south-eastern margin (Figure 2.12). Hydraulic conductivity in the J aquifer is up to 2.6×10^{-4} m/s and porosity is 0.21 (Table 2.1) with well yields between 0.1 to 6 L/s (Kellett et al. 1999).

Table 2.1 Aquifer and aquitard hydraulic conductivity and porosity measurements

Formation	Hydraulic conductivity (m/s)	Porosity	Source
Bulldog Shale	3.6×10^{-9} ^a		Kinhill Stearns (1984)
	4.6×10^{-14} – 4.6×10^{-13} ^a	Mean of 0.4	Love et al. (2013)
J aquifer	2.3×10^{-7} – 9.5×10^{-4}	Mean of 0.21	Audibert (1976)
	1×10^{-5} – 1.5×10^{-4} (mean of 7.3×10^{-5})	—	RUST PPK Consultants (1994)
	1.9×10^{-5} – 2×10^{-4} (mean of 8×10^{-5})	—	Berry and Armstrong (1995)
	5.8×10^{-6} – 2.6×10^{-4} (mean of 8×10^{-5})	—	Armstrong and Berry (1997)
	1×10^{-6} – 2.3×10^{-4}	—	Welsh (2007)
Mount Toondina Fm.	1×10^{-9} – 1×10^{-5}	—	Coffey and Partners (1983)
	—	0.04–0.08	Allchurch and Wopfner (1967)
	—	0.22–0.37	Linc Energy (2010a); Linc Energy (2010b)
Stuart Range Fm.	—	0.06–0.09	DMITRE (2011)
	1×10^{-9} ^a	—	Howe et al. (2008)
	1×10^{-10} ^a	—	SKM (2009a)
Boorthanna Fm.	4.6×10^{-13} – 3.5×10^{-10} ^a	—	Kleinig et al. (2015)
	—	0.04–0.23	CRAE (1987)
	—	0.20–0.25	Tucker (1997)
	—	0.14	DMITRE (2011)
Basement	1×10^{-5} – 5.8×10^{-5}	—	Howe et al. (2008)
	—	—	—

^a Vertical hydraulic conductivity

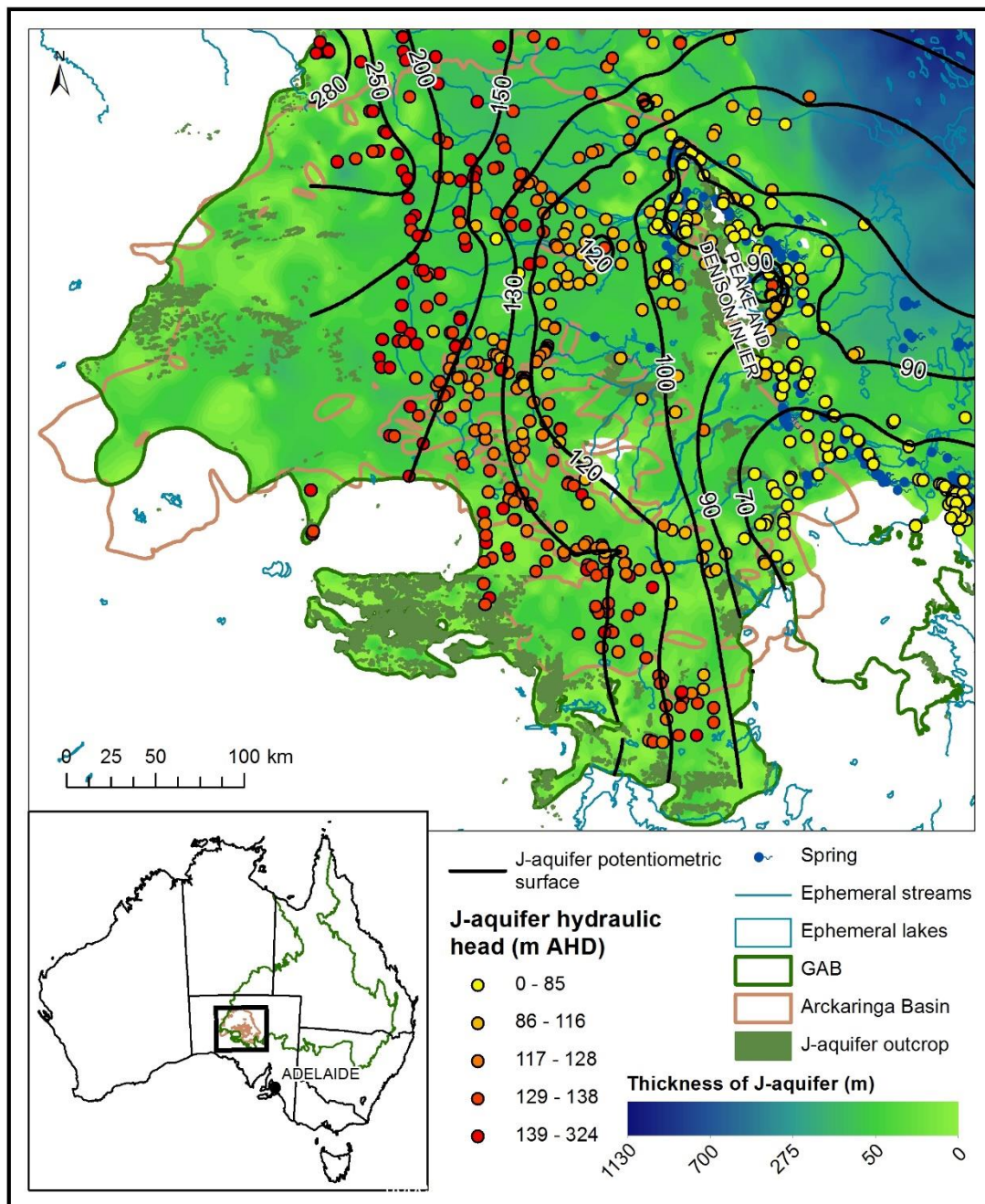


Figure 2.12 J aquifer hydraulic head (m AHD) and potentiometric surface contours (Love et al. 2013).

The Mount Toondina Fm. sits unconformably below the J aquifer and has hydraulic heads similar to those in the J aquifer at the same locations (Figure 2.12 and Figure 2.13). There are insufficient wells completed in the Mount Toondina Fm. to determine the potentiometric surface and groundwater flow directions; however, Wohling et al. (2013) found that it probably forms a single hydrogeologic unit with the J aquifer. Hydraulic heads range from 138 m AHD near the Peake and Dennison Inlier to 38 m AHD along the centre of the eastern margin (Figure 2.13). Hydraulic conductivity and porosity values for the Mount Toondina Fm. are 1×10^{-5} – 1×10^{-9} m/s and

0.04–0.37, respectively (Table 2.1). The higher measurements are from the coal beds due to greater permeability from fracturing (Coffey and Partners 1983; Wohling et al. 2013).

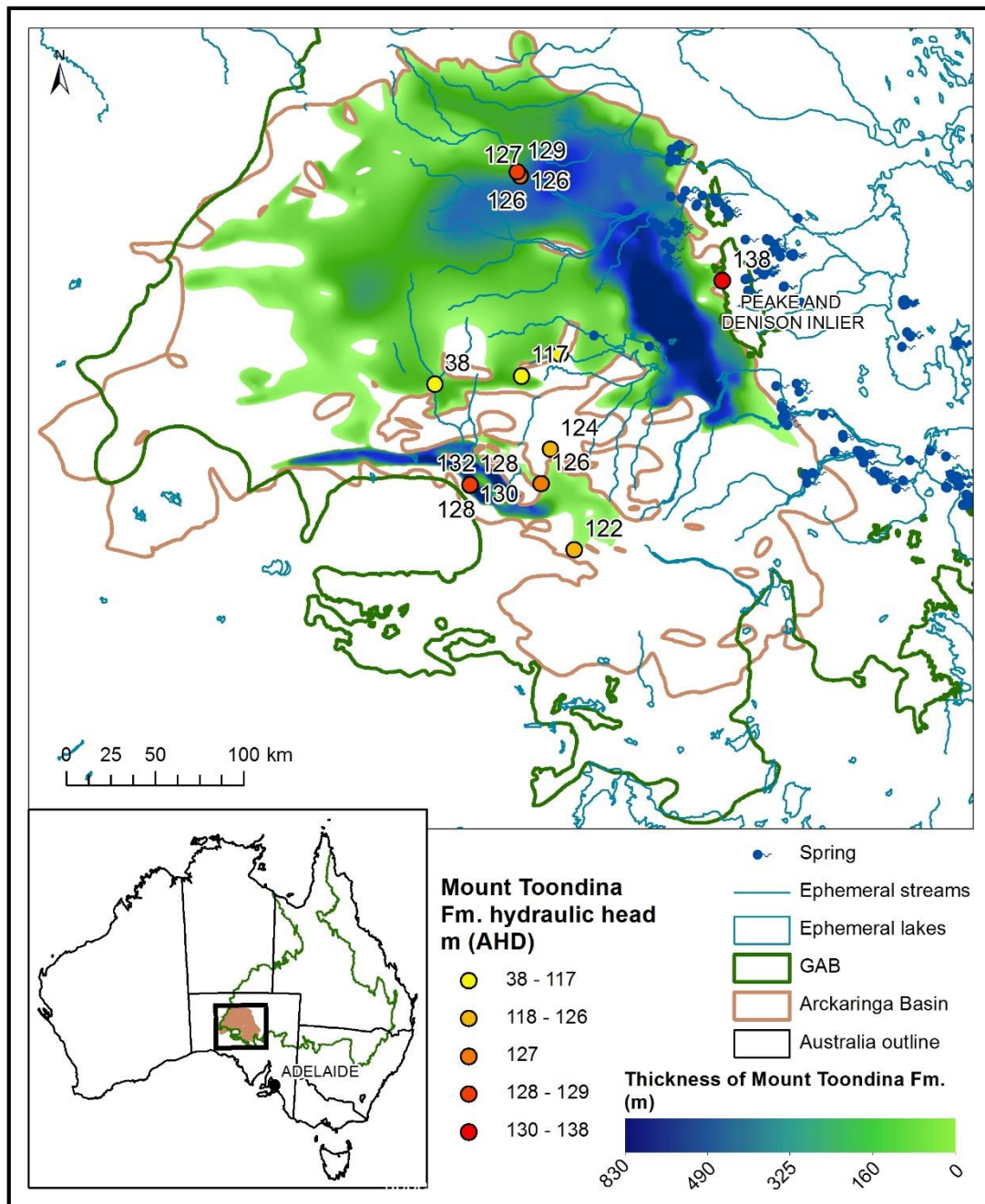


Figure 2.13 Mount Toondina Fm. hydraulic head (m AHD).

The Stuart Range Fm., which is the aquitard of interest in this thesis, has been referred to as a leaky aquitard (Kellett et al. 1999; Belperio 2005) because it lessens groundwater drawdown in the production wells in the underlying Boorthanna Fm. due to leakage (Aquaterra 2009; SKM 2009b). In other studies however, the Stuart Range Fm. has been interpreted as an effective barrier to inter-aquifer leakage between the Boorthanna Fm. and unconfined J aquifer (Aquaterra REM

2005; SKM 2009b; Lyons and Hulmes 2010). Vertical hydraulic conductivity measurements in the Stuart Range Fm. are between 1×10^{-9} – 4.6×10^{-13} m/s (Table 2.1).

The extent of areas where the Boorthanna Fm. crops out are limited, thus recharge to the Boorthanna Fm. most likely occurs via diffuse discharge from the J aquifer where the Stuart Range Fm. is thin or absent (Keppel et al. 2015). Using the chloride mass balance approach Wohling et al. (2013) estimated diffuse recharge to range between 0.05 mm/y and 0.22 mm/y, whereas using the same method Kellett et al. (1999) calculated diffuse recharge rates up to 0.5 mm/y. In the southern margin, recharge can occur where the aquifer crops out and beneath ephemeral rivers (Figure 2.14; Keppel et al. 2015). The majority of groundwater wells in the Boorthanna Fm. have been drilled for the Prominent Hill mine for their mining activities and drinking water supply (Figure 2.14; Wohling et al. 2013). Present day hydraulic head measurements in the Prominent Hill well-field show drawdowns of up to 40 m (Figure 2.14; SKM 2009 b). Hydraulic heads range from 130 m AHD in the north-west margin to 50 m AHD in the south-eastern margin and there are two wells on the western margin with hydraulic heads of 172 and 193 m AHD (Figure 2.14). Hydraulic conductivity and porosity measurements in the Boorthanna Fm. are between 1×10^{-5} – 5.8×10^{-5} m/s and 0.04–0.25, respectively (Table 2.1), with groundwater yields between 0.01–31 L/s (Wohling et al. 2013).

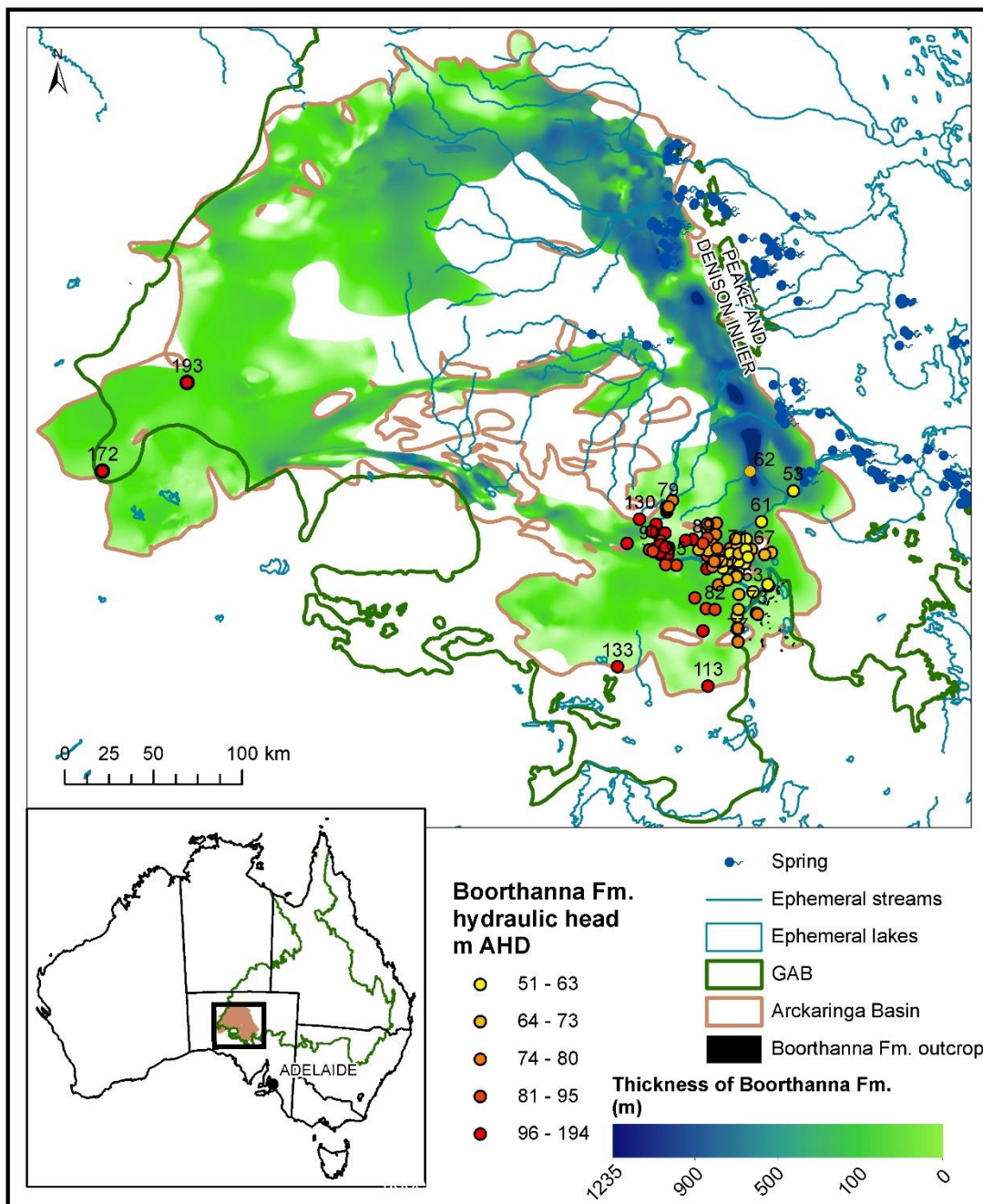


Figure 2.14 Boorthanna Fm. hydraulic head (m AHD).

Very few wells are completed in the basement, but the wells that are have hydraulic head measurements very similar to those in the Boorthanna Fm. in similar locations (Figure 2.14 and Figure 2.15).

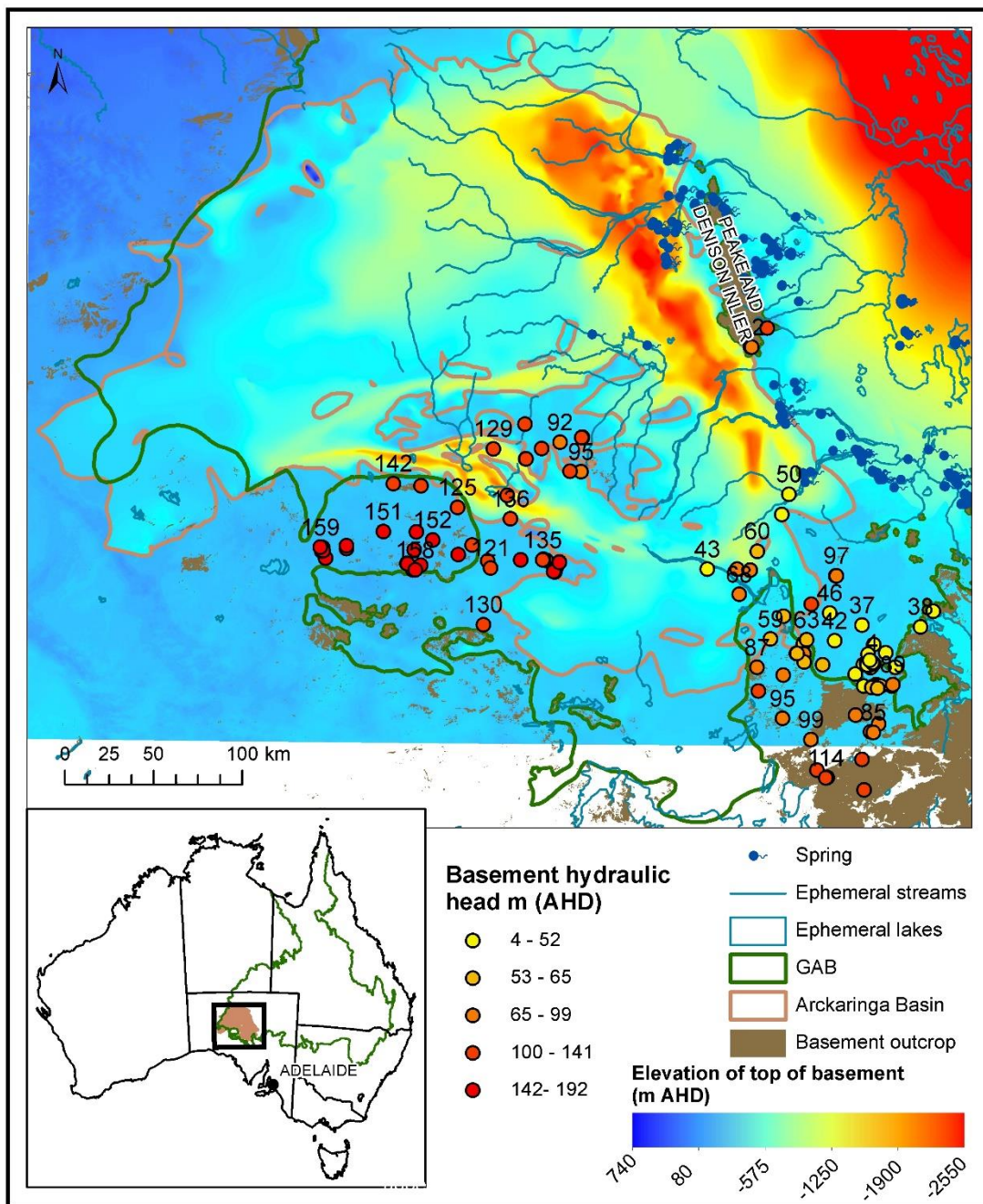


Figure 2.15 Basement hydraulic head (m AHD).

2.6 Site Description

There is substantially more hydrogeological information in the GAB than the Arckaringa Basin. This thesis focuses on the eastern portion of the Arckaringa Basin where the majority of groundwater wells have been drilled into the Boorthanna Fm. by the Prominent Hill mine for their mining and drinking water supplies (Figure 2.1 b; Wohling et al. 2013).

In the study area, groundwater flow in the J aquifer and Boorthanna Fm., and to a certain extent the basement, is from the west towards the east with some flow from the north-west in the

J aquifer and basement (Figure 2.15 and Figure 2.16). Basement highs from glacial scouring and faulting (during Devonian-Permian) possibly interrupt groundwater flow in the Boorthanna Fm. and J aquifer (Figure 2.17). Higher hydraulic heads in the J aquifer around some of these basement highs (Figure 2.17) highlight that these could be localised recharge areas.

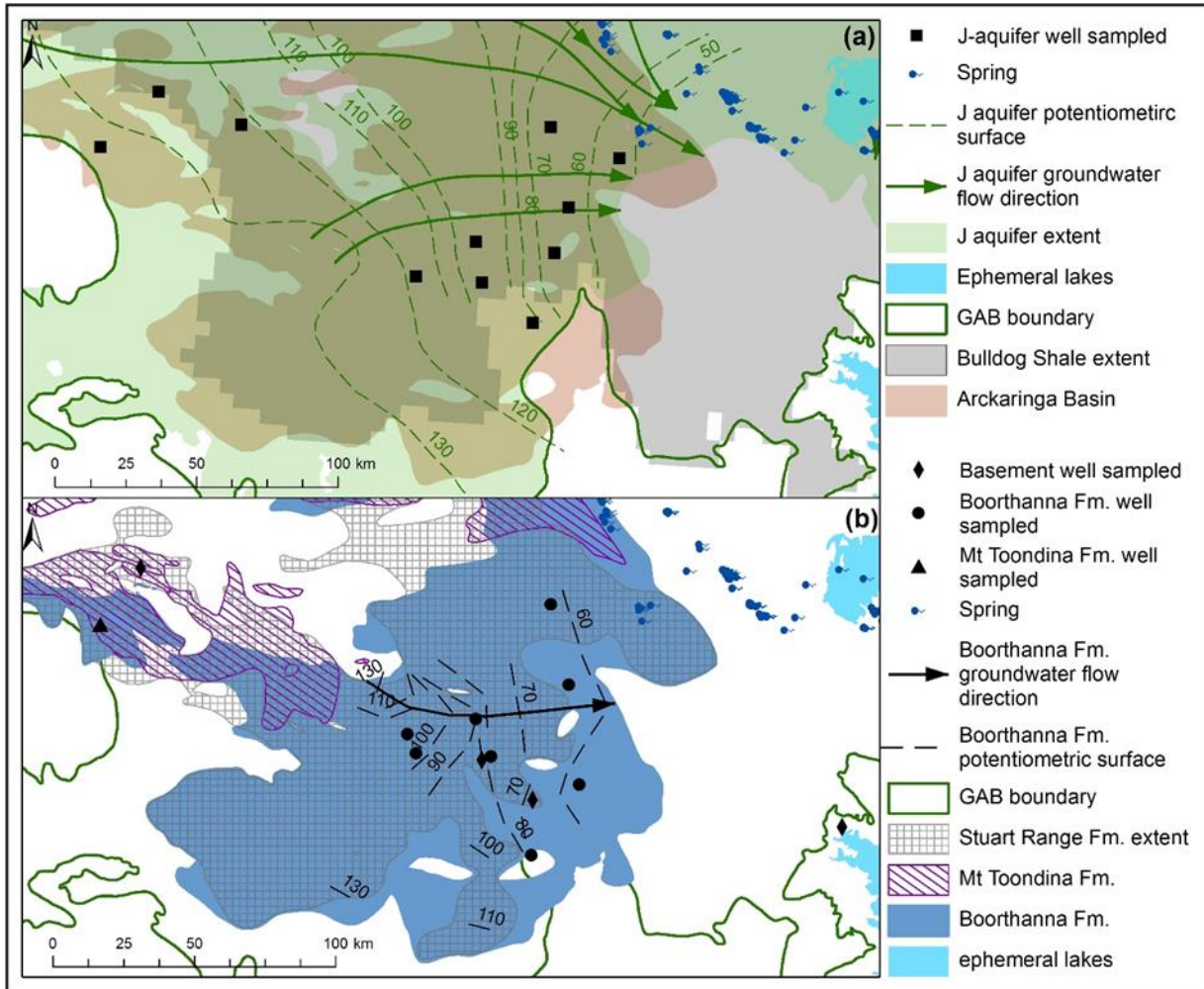


Figure 2.16 Pre-pumping freshwater head potentiometric surface and the generalised groundwater flow paths for (a) the J aquifer and (b) the Boorthanna Fm. including sampled wells.

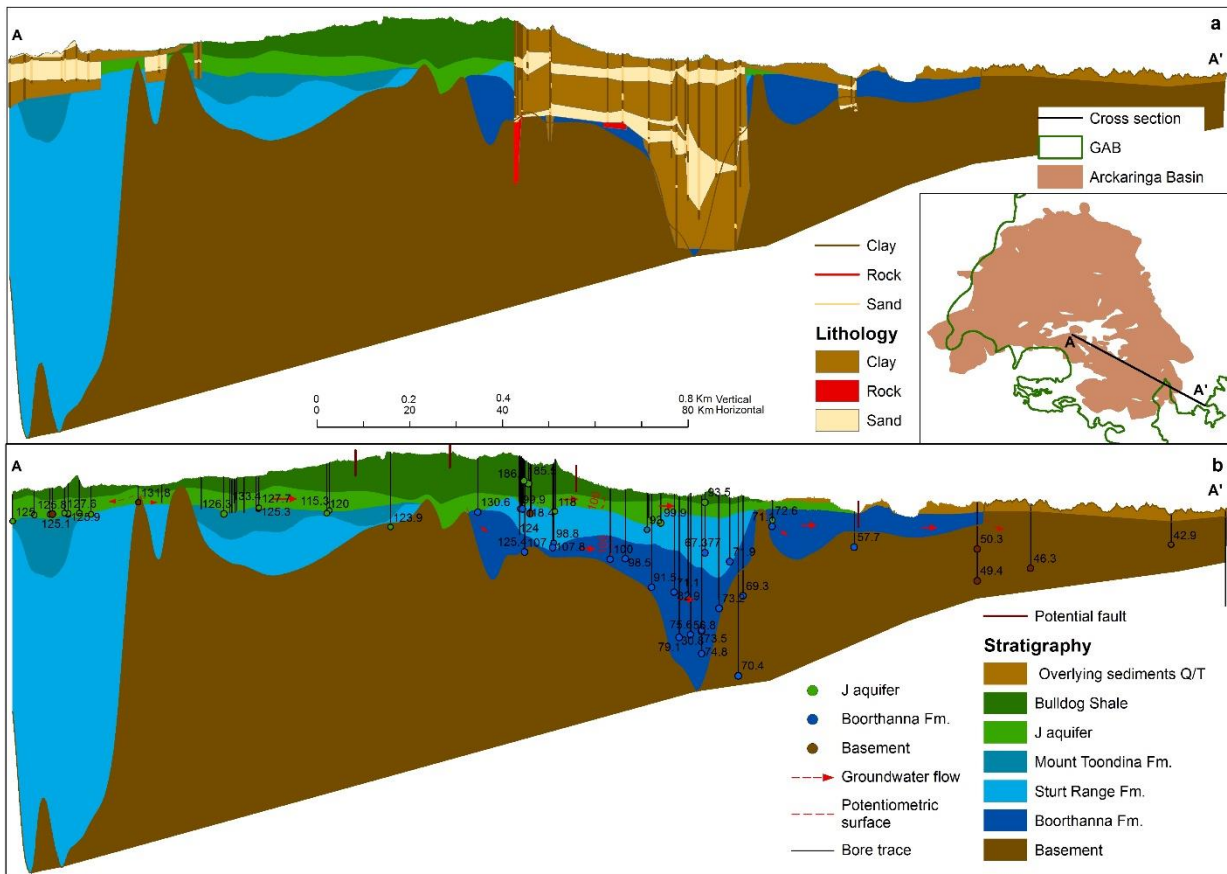


Figure 2.17 Transect A to A' through the study area with (a) showing lithology and (b) showing stratigraphy, well depths, density corrected freshwater hydraulic head and interpreted groundwater flow directions.

The Boorthanna Fm. is absent from the north-west part of the study area, where only the Mt Toondina Fm. and J aquifer are in contact (Figure 2.16 and Figure 2.17). The Mt Toondina Fm. is absent throughout the majority of the study area, and the J aquifer and Boorthanna Fm. are separated by the Sturt Range Fm. aquitard (Figure 2.16, Figure 2.17 and Figure 2.18). Generally, there appears to be potential for downward flow from the J aquifer to the Mount Toondina Fm. (where present), or to the Boorthanna Fm. and basement aquifers (Figure 2.17 and Figure 2.18). Smerdon et al. (2012) and Keppel et al. (2015) also noted the potential connectivity between the GAB and the Arckaringa Basin. However, high groundwater fluxes through the Stuart Range Fm. are probably dependent on any secondary permeability, heterogeneity or hydraulically active faults that are present.

The Stuart Range Fm. pinches out or is missing at a number of locations throughout the study area (Figure 2.17 and Figure 2.18) increasing the likelihood of inter-aquifer connectivity between the Boorthanna Fm. and the J aquifer. Where the Stuart Range Fm. is absent along the eastern margin

both the J aquifer and Boorthanna Fm. converge so groundwater potentially discharges from the J aquifer into the Boorthanna Fm., and there is potentially discharge into the basement (Figure 2.17 and Figure 2.18). In the north-eastern section of the study area hydraulic heads in the Boorthanna Fm. are higher than those in the J aquifer so there is potential for upward inter-aquifer leakage and groundwater discharge to the springs (Figure 2.16). This is examined in more detail in Chapter 4.

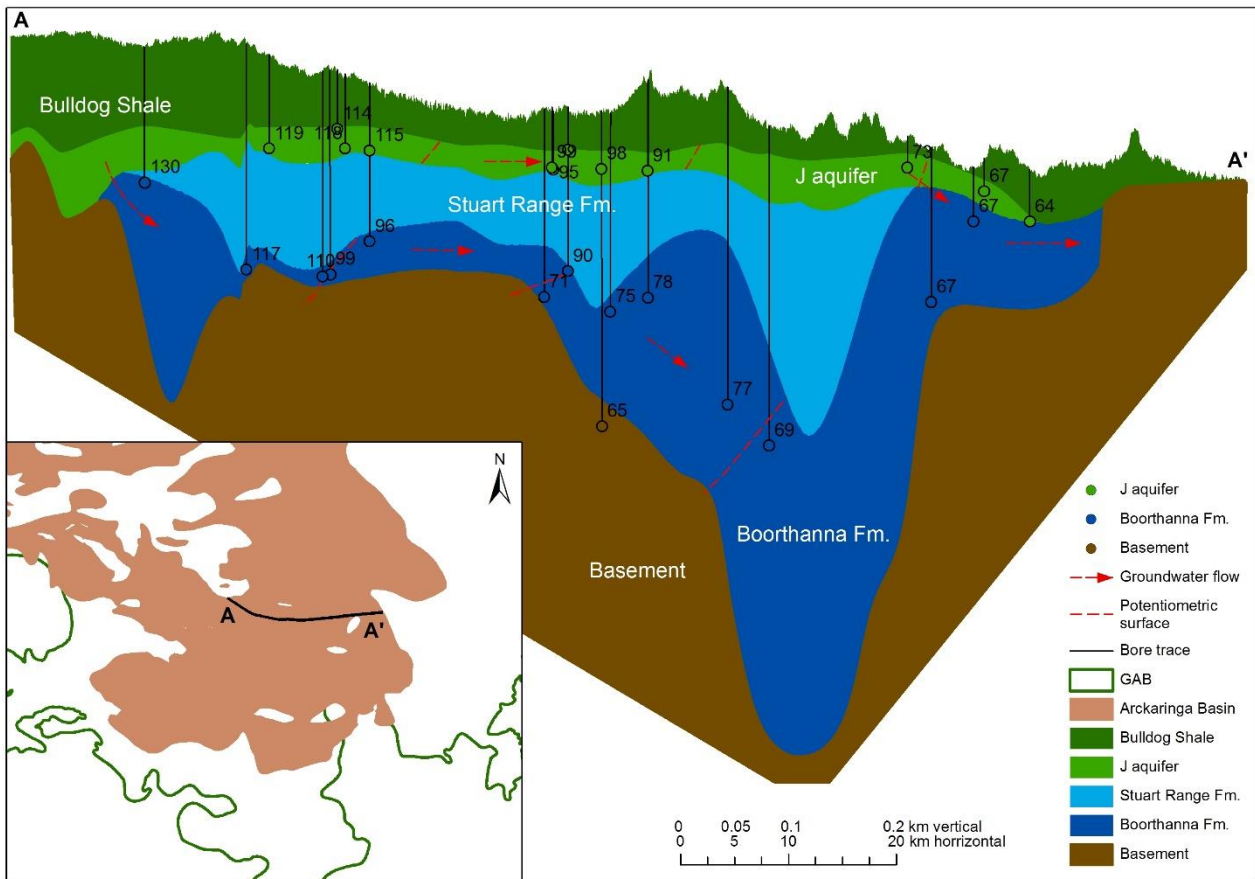


Figure 2.18 Hydrogeological transect from A to A' following the Boorthanna Fm. groundwater flow path shown in Figure 2.16.

Chapter 3 Environmental tracers: sampling and background

3.1 Sampling

3.1.1 Groundwater sampling

A total of 26 groundwater samples were collected from pastoral production wells as well as mining monitoring and production wells within the Arckaringa Basin between November 2013 and May 2014. Samples were obtained from the south-eastern part of the Arckaringa Basin, where Boorthanna wells are located within approximately 5 km of GAB wells, and with a particular bias along a north-west to south-east transect along a groundwater flow-path interpreted from potentiometric contours (Figure 2.16).

All investigation and observation wells were pumped using a Grundfos® SQE1-140 electric spooled submersible pump (74 mm) and production wells were pumped using the pump already in place. Prior to pumping, depth to water and where possible, depth of well measurements were taken and recorded. Water samples were only taken after each well had at least three well volumes purged and the pH and electrical conductivity (EC) of the discharging water did not vary by more than 5%. The pH, EC, Temperature and Oxidation-Reduction Potential (ORP) were continuously monitored at the discharge pipe using a YSI® 556MPS. In addition to the parameters above, the alkalinity of groundwater samples were determined in the field using a Hach® field titration kit.

Groundwater samples were collected for a variety of chemical and isotope analyses including: anions (125 mL HDPE bottle, 0.45µm filtered), cations (125 mL HDPE bottle, 0.45µm filtered, acidified to pH <2 with HNO₃), δ¹⁸O and δ²H (McCartney vial, unfiltered), ¹⁴C and δ¹³C (1 L HDPE bottle, unfiltered), ³⁶Cl/Cl (500 mL HDPE bottle, unfiltered), ⁸⁷Sr/⁸⁶Sr (1 L HDPE bottle, 0.45µm filtered), uranium isotopes (5 L HDPE bottle, acidified to pH <1 with HCl) and noble gases samples were collected in copper tubes using stainless steel pinch-off clamps (Weiss 1968; Beyerle et al. 2000). All bottles were rinsed several times prior to collecting the final sample to avoid contamination.

3.1.2 Core sampling

A continuous core through the GAB, the Stuart Range Fm. and into the Boorthanna Fm. was drilled in March 2015. The aquitard core was drilled using wireline diamond core drilling and recovered in 3 m lengths. Core samples were collected for physical and chemical analysis by first shaving and

discarding the outer core (approximately 2 mm) to avoid drilling fluid contamination. To confirm contamination of the pore water by the drilling fluid had not occurred the drilling fluid was spiked with heavy water (D_2O), this is discussed further in section 6.5.1.

Samples for pore water major ions and stable isotopes of pore water analysis were taken at approximately 2 m intervals. Samples for uranium and thorium isotopes in sediment analysis were collected at 5 m intervals. The major ion and, uranium and thorium isotopes samples were vacuum-sealed in two Food Saver® bags then placed in a large Ziploc® bag. The stable isotope samples were sealed in a small Ziploc® bag with all the air squeezed out then placed in a second large Ziploc® bag using the method outlined by Wassenaar et al. (2008). Permeability, porosity and XRD samples were taken at approximately 10 m intervals, or at any lithological change. The permeability and porosity samples were wrapped in thin plastic wrap and labelled with the depth interval and an arrow to indicate direction to top of core, then placed in PVC pipe for protection and vacuum sealed in a Food Saver® bag. Core samples for XRD analysis were vacuum-sealed in two Food Saver® bags. All samples were stored in insulated coolers. 4He samples were sub-cored every 5 m using a handheld electric drill and transferred into stainless steel canisters for storage, following the sub-core degassing method developed by Osenbrück et al. (1998).

3.1.3 Sample analysis

The relevant analysis methods and procedures are explained in detail in chapters 4, 5 and 6, in sections 4.4, 5.4 and 6.4, respectively.

3.2 Environmental tracers

3.2.1 Major ions

Major solutes in groundwater are derived from atmospheric sources, weathering processes, water-rock interactions, mixing with formation waters or diffusion from adjacent formations (Gibb 1970; Appelo and Postma 2005). In groundwater the positively charged cations: sodium (Na^+), potassium (K^+), calcium (Ca^{2+}) and magnesium (Mg^{2+}), and the four negatively charged anions: chloride (Cl^-), sulphate (SO_4^{2-}), bicarbonate plus carbonate ($HCO_3^- + CO_3^{2-}$) and nitrate (NO_3^-) represent the majority of ions in solution (Cook and Herczeg 2000; Appelo and Postma 2005).

In this study chloride concentrations are used as physical tracers to indicate potential groundwater movement and mixing. The chloride ion has a similar mobility as water and is considered to be

conservative in groundwaters as it is not involved in the common geochemical reactions that occur in aquifers. Therefore, changes in chloride concentrations are a result of physical processes such as changes in evapotranspiration rate during recharge or mixing with another groundwater body of different chloride concentration (Love et al. 1993; Cook and Herczeg 2000; Appelo and Postma 2005). Chloride concentrations in Australian groundwaters can vary considerably. For example, chloride concentrations in the Murray Basin can range from <300 mg/L in fresh groundwater to ~300,000 mg/L in hypersaline brines (Herczeg et al. 2001).

3.2.2 $\delta^{18}\text{O}$ and $\delta^2\text{H}$

Stable isotopes of water ^{18}O and ^2H , reported as $\delta^{18}\text{O}$ and $\delta^2\text{H}$, are naturally occurring components of the water molecule. Due to differences in mass, stable isotopes behave slightly differently in physical, chemical and biological processes leading to fractionation of the isotopes. The resulting small variations in isotopic concentrations due to fractionation and their inclusion in the water molecule means that ^{18}O and ^2H are particularly good tracers of hydrologic cycle processes (Gat et al. 1969; Love et al. 1993; Cook and Herczeg 2000).

Groundwater $\delta^{18}\text{O}$ and $\delta^2\text{H}$ composition in semi-arid environments are a record of the source of precipitation and the amount of evapotranspiration that occurred prior to recharge. Therefore, $\delta^{18}\text{O}$ and $\delta^2\text{H}$ can be used to determine sources and mechanisms of recharge, evapotranspiration, palaeoclimate and palaeorecharge, surface water-groundwater interactions as well as mixing and differentiation between meteoric and connate water (Love et al. 1993; Cook and Herczeg 2000; Appelo and Postma 2005). Groundwater bodies commonly have stable isotope compositions between standard seawater ($\delta^{18}\text{O} = 0$, $\delta^2\text{H} = 0$) and waters depleted in ^{18}O and ^2H ($\delta^{18}\text{O} = -20$, $\delta^2\text{H} = -120$) depending on the strength of the 'continental rainout' effect on rainfall stable isotopes of water and other fractionation mechanisms.

3.2.3 $\delta^{13}\text{C}$

Two stable isotopes of carbon occur in nature, ^{12}C and ^{13}C , and the ^{13}C of dissolved carbon species in groundwater, reported as $\delta^{13}\text{C}$, is a function of the pH, Pco_2 , the manner in which minerals are dissolved or precipitated, fractionation among the carbonate species in the solution, as well as, the ^{13}C content of the ground water recharge and carbonate rock (Deines et al. 1974; Appelo and Postma 2005). An understanding of geochemical reactions including information about the recharge conditions, the type of mineralisation of the groundwater, the proportion of the biogenic

carbon and the origin and the area of pollution of water can be determined from $\delta^{13}\text{C}$ of the dissolved inorganic carbon (DIC) in groundwater (Deines et al. 1974; Aggarwal et al. 2005; Appelo and Postma 2005). The $\delta^{13}\text{C}$ values of DIC in groundwater are typically in the range of 0 to -20 ‰.

3.2.4 $^{87}\text{Sr}/^{86}\text{Sr}$

Strontium isotopes ($^{87}\text{Sr}/^{86}\text{Sr}$) in groundwaters are controlled by variations in initial inputs (atmospheric), differences in mineralogy, mineral dissolution along flow paths, groundwater residence time and groundwater mixing (Johnson and DePaolo 1997; Shand et al. 2009). $^{87}\text{Sr}/^{86}\text{Sr}$ ratios are particularly useful in determining weathering processes and sources, as well as, identifying and quantifying end-member mixing processes using an isotopic mass balance (Johnson and DePaolo 1997; Dogramaci and Herczeg 2002; Shand et al. 2009). In rocks $^{87}\text{Sr}/^{86}\text{Sr}$ ratios up to 1.10 can be found, however groundwater $^{87}\text{Sr}/^{86}\text{Sr}$ ratios generally range between 0.700 to 0.720.

3.2.5 Uranium isotopes

Aqueous uranium isotope distributions (^{238}U and ^{234}U) are complex and affected by many processes including: weathering; solution geochemistry; solution/precipitation of more/less soluble daughter products; sorption/desorption from surfaces; alpha recoil; as well as production from parent atoms in solution or radioactive decay (Osmond and Cowart 1976; Gascoyne 1992; Osmond and Cowart 1992). Under favourable conditions the uranium isotope distributions can provide insights into groundwater flow processes including: recharge, discharge and mixing (Porcelli and Swarzenski 2003). Uranium concentrations in oxidised groundwaters can reach up to 100 $\mu\text{g}/\text{L}$ (Osmond and Cowart 1992). $^{234}\text{U}/^{238}\text{U}$ activity ratios in groundwater are generally ≥ 1 because of dissolution of uranium isotopes in secular equilibrium from minerals ($^{234}\text{U}/^{238}\text{U}$ activity ratio = 1; Osmond and Ivanovich 1992) and build-up of ^{234}U released by alpha recoil from aquifer minerals along the groundwater flow path.

3.2.6 ^{14}C

Radiocarbon (^{14}C) is naturally formed in the upper atmosphere through the interaction of cosmic rays with ^{14}N atoms. It is oxidised to CO_2 and is incorporated in groundwater during recharge by interaction of infiltrating water with unsaturated zone CO_2 (Plummer and Glynn 2013). Following recharge, the dissolved inorganic carbon (DIC) becomes isolated and ^{14}C decays with time (modern half-life 5730 years). The amount of ^{14}C decay can be estimated to determine a groundwater 'age' assuming piston flow conditions (Münnich 1957; Godwin 1962; Plummer and Glynn 2013). In

addition to radioactive decay, physical and chemical processes can affect the $^{14}\text{C}_{\text{DIC}}$ in groundwater. In order to interpret groundwater ^{14}C 'ages' and their uncertainties the processes in the unsaturated zone, geochemical reactions that occur within the aquifer, mixing and hydrodynamic dispersion along flow paths and historical variations in atmospheric ^{14}C need to be considered (Plummer and Glynn 2013). The Vogel (Vogel and Ehalt 1963; Vogel 1970), Tamers (Tamers 1967) Pearson (Ingerson and Pearson 1964) and Fontes and Garnier (Fontes and Garnier 1979; Fontes 1992) geochemical adjustment models have been developed to correct ^{14}C groundwater 'ages' for geochemical reactions affecting groundwater ^{14}C activities. These corrected ^{14}C groundwater 'ages' can be used to investigate groundwater residence time, groundwater recharge, regional flow characteristics, mixing and inter-aquifer leakage (Vogel 1967; Love et al. 1993; Harrington et al. 2002). ^{14}C activities in groundwater are reported as a percentage of a standards activity in percent modern carbon (pMC) with modern, pre-nuclear detonation atmospheric ^{14}C activity being 100 pMC. Groundwater can therefore have ^{14}C activities between 100 to 0 pMC and ^{14}C model ages can be used to estimate groundwater ages up to approximately 30–40 ka.

3.2.7 $^{36}\text{Cl}/\text{Cl}$

^{36}Cl is produced in the atmosphere through the interaction of cosmic rays with ^{40}Ar atoms. ^{36}Cl is then deposited on the land surface dissolved in precipitation and as dry deposition and incorporated in groundwater recharge (Andrews et al. 1986; Phillips 2013). ^{36}Cl groundwater 'ages' can be estimated from the decay of ^{36}Cl (half-life 301,000 years); although, this can be complicated by variations in the chloride concentration of groundwater and the need to estimate the initial ^{36}Cl input (Bentley et al. 1986; Phillips 2013). Nevertheless, the ^{36}Cl age calculation can be corrected to account for these processes if the causes of chloride concentration variations are understood. The ^{36}Cl activities are reported as $^{36}\text{Cl}/\text{Cl}$ with $^{36}\text{Cl}/\text{Cl}$ inputs up to 100×10^{-15} – 1000×10^{-15} in continental interior settings, and groundwater $^{36}\text{Cl}/\text{Cl}$ ratios between 5×10^{-15} to 50×10^{-15} . ^{36}Cl dating is generally applicable to groundwater in 'old' groundwater systems in the age range 100 ka–1 Ma (Phillips 2013).

3.2.8 Helium isotopes

^4He is the alpha decay product from the radioactive decay of U–Th series elements (Torgersen and Stute 2013). ^4He concentrations in groundwater are controlled by dissolution of atmospheric noble gases, inclusion of 'excess air', radiogenic ^4He production, as well as, crustal and mantle

fluxes (Kipfer et al. 2002; Torgersen and Stute 2013). Radiogenic ^4He concentrations increase with groundwater residence time due to the decay of U–Th series elements in aquifer rocks and can be used to calculate groundwater ‘age’ if the various other sources can be accounted for (Mazor and Bosch 1987; Osenbrück et al. 1998; Beyerle et al. 2000; Kipfer et al. 2002). The radiogenic ^4He component can be determined from reported He concentrations (ccSTP/g) by estimating and removing the atmospheric helium and ‘excess air’ components (Ballentine et al. 2002). Additionally, the crustal and mantle fluxes can be estimated by comparison with other dating tracers and ^3He isotopes, as well as, modelling. Radiogenic ^4He concentrations in groundwater systems can be found up to 1×10^{-2} ccSTP/g. Where the ^4He sources can be accounted for and assuming a constant accumulation rate of radiogenic ^4He groundwater ‘ages’ up to thousands or millions of years can be calculated.

^3He is produced by the decay of ^3H and can be used to date young groundwater with a residence time of up to 50 years, or examine volatiles transported from the mantle. $^3\text{He}/^4\text{He}$ isotope ratios are $>10^{-7}$ in recharge areas and $<10^{-7}$ elsewhere, and $^3\text{He}/^4\text{He}$ isotope ratios $<10^{-5}$ are indicative of ^3He that has migrated from volatiles transported from the mantle in regions that have been tectonically active (Kipfer et al. 2002).

Radiogenic ^4He concentrations and $^3\text{He}/^4\text{He}$ isotope ratios can both be used to investigate groundwater residence time, groundwater recharge, regional flow characteristics, mixing and inter-aquifer leakage, especially through faults.

Chapter 4 Detecting inter-aquifer leakage in areas with limited data using hydraulics and multiple environmental tracers, including ^4He , $^{36}\text{Cl}/\text{Cl}$, ^{14}C and $^{87}\text{Sr}/^{86}\text{Sr}$

Published in *Hydrogeology Journal*: Stacey C. Priestley, Daniel L. Wohling, Mark N. Keppel, Vincent E. A. Post, Andrew J. Love, Paul Shand, Lina Tyroller, Rolf Kipfer (2017) Detecting inter-aquifer leakage in areas with limited data using hydraulics and multiple environmental tracers, including ^4He , $^{36}\text{Cl}/\text{Cl}$, ^{14}C and $^{87}\text{Sr}/^{86}\text{Sr}$, *Hydrogeology Journal*, doi: 10.1007/s10040-017-1609-x

4.1 Abstract

The investigation of regionally extensive groundwater systems in remote areas is hindered by a shortage of data due to a sparse observation network, which limits our understanding of the hydrogeological processes in arid regions. The study used a multidisciplinary approach to determine hydraulic connectivity between the Great Artesian Basin (GAB) and the underlying Arckaringa Basin in the desert region of Central Australia. In order to manage the impacts of groundwater abstraction from the Arckaringa Basin, it is vital to understand its connectivity with the GAB (upper aquifer), as the latter supports local pastoral stations and groundwater-dependent springs with unique endemic flora and fauna. The study is based on the collation of available geological information, a detailed analysis of hydraulic data, and data on environmental tracers. Enhanced inter-aquifer leakage in the centre of the study area was identified, as well as recharge to the GAB from ephemeral rivers and waterholes. Throughout the rest of the study area, inter-aquifer leakage is likely controlled by diffuse inter-aquifer leakage, but the coarse spatial resolution means that the presence of additional enhanced inter-aquifer leakage sites can not be excluded. This study makes the case that a multi-tracer approach along with groundwater hydraulics and geology provides a tool-set to investigate enhanced inter-aquifer leakage even in a groundwater basin with a paucity of data. A particular problem encountered in this study was the ambiguous interpretation of different age tracers, which is attributed to diffusive transport across flow paths caused by low recharge rates.

4.2 Introduction

The sustainable management of groundwater resources requires understanding of the water flows between aquifers (Alley et al. 2002; Hiscock et al. 2002). Failing to take into account inter-aquifer leakage in the analysis of regional-scale flow systems can lead to significant errors in the

estimation of flow rates in aquifers (Freeze and Witherspoon 1967; Love et al. 1996; Tóth 2009). There has been increased interest in inter-aquifer leakage mechanisms in recent times because of the exploration for and development of coal seam and shale gas resources and the associated risk of groundwater contamination (Myers 2012; Vidic et al. 2013; Brantley et al. 2014; Field et al. 2014).

Laterally-extensive aquitards that have no preferential flow pathways are the major control to separate aquifers (Cherry and Parker 2004). But even in tight aquitards there is always a small amount of diffuse leakage through the aquitard pores (Cherry and Parker 2004). The volumetric flow across the aquitard from diffuse leakage can be a significant component of the water balance over large areas (Cherry and Parker 2004; Konikow and Neuzil 2007). The presence of preferential pathways enhances the rate of water movement through an aquitard causing enhanced inter-aquifer leakage (Neuzil 1994; Hendry et al. 2004; Hart et al. 2006; Myers 2012). Such preferential pathways can be faults, intercalations of higher permeability sediments, or thinner aquitard sections (Cherry and Parker 2004). Zones of enhanced inter-aquifer leakage can have a disproportional contribution to the water balance relative to their size. Bredehoeft et al. (1983) found that 25% of groundwater discharged from the Dakota groundwater system is enhanced inter-aquifer leakage through faults from the aquifer below. The difficulty to quantify inter-aquifer leakage at a regional-scale is that diffuse inter-aquifer leakage rates are often so small that they are very hard to detect and quantify, although they can result in a large volumetric flow. Localised enhanced inter-aquifer leakage with high fluxes can easily be missed at the spatial resolution of regional surveys.

The direction of inter-aquifer leakage can be determined by hydraulic head differences between aquifers (Dogramaci et al. 2001; Arslan et al. 2015), but this can be complicated when groundwater flow is affected by variations in water density (Post et al. 2007). The rates of diffuse leakage through aquitards can in principle be calculated if an appropriate vertical hydraulic conductivity is known (K_v). Generally K_v values measured from aquitard core samples are used, although they have been found to be consistently lower than regional-scale K_v values, as the latter incorporate both diffuse and preferential leakage (van der Kamp 2001; Smerdon et al. 2014; Batlle-Aguilar et al. 2016).

Environmental tracers can be used as indicators for enhanced inter-aquifer leakage and mixing in regional groundwater investigations (Glynn and Plummer 2005; Sanford et al. 2011). Clear

contrasts in the environmental tracer concentrations, (or ratios expressing the relative abundance of isotopes) between aquifers indicate where there is little vertical flow, whereas similar environmental tracer concentrations may be an indication of mixing or enhanced inter-aquifer leakage. For example, major and trace element concentration data were used to demonstrate enhanced inter-aquifer leakage within the Galilee Basin, Australia (Moya et al. 2015) and the Yarkon-Taninim basin, Israel (Zilberbrand et al. 2014). Vertical leakage between the Continental and Djeffara aquifer system in Tunisia through a fault was identified and quantified using stable isotopes of water (Trabelsi et al. 2009). Additionally, groundwater mixing and locations of enhanced inter-aquifer leakage have been identified by $^{87}\text{Sr}/^{86}\text{Sr}$ ratios and other tracers such as $\delta^{34}\text{S}$ and $\delta^{18}\text{O}$ values of SO_4 or $\delta^{13}\text{C}$ in the Murray Basin, Australia (Dogramaci et al. 2001; Dogramaci and Herczeg 2002) and Adour-Garonne district, France (Brenot et al. 2015).

For simple flow systems with little mixing, decaying age tracers, such as ^{14}C and $^{36}\text{Cl}/\text{Cl}$, decrease along the flow path, and accumulating tracers, such as ^4He , increase along the flow path. Such regular patterns can be disrupted by the localised introduction of different age water. Age tracers used in combination with major and trace elements (Herczeg et al. 1996), stable isotopes of water (Love et al. 1993), as well as $^{87}\text{Sr}/^{86}\text{Sr}$ ratios and $\delta^{13}\text{C}$ (Cartwright et al. 2012) have provided evidence for locations of inter-aquifer leakage and hydrochemical evolution within the Otway Basin and the Murray Basin, Australia.

Due to their conservative nature, noble gases are also useful tracers to analyse for inter-aquifer leakage (Kipfer et al. 2002). Measurements of noble gases, stable isotopes of water, Cl and ^{14}C provided evidence for localised downward leakage of shallow groundwater in the Upper Floridan aquifer system, USA (Clark et al. 1997). $^3\text{H}/^3\text{He}$ ratios in combination with major ion geochemical reaction modelling were used to determine downward leakage into the Memphis aquifer, USA (Larsen et al. 2003). Upward inter-aquifer leakage in the vicinity of faults has been identified by radiogenic ^4He in the Lower Rhine Embayment, Germany (Gumm et al. 2016) and by $^3\text{He}/^4\text{He}$ ratios in the Kazan Basin, Turkey (Arslan et al. 2015). For the Paris Basin, Marty et al. (2003) demonstrated with ^3He concentrations that diffusive mass transfer across a major aquitard was negligible, implying that groundwater moves along a major fault.

This study focusses on the connectivity between the Great Artesian Basin (GAB) and underlying Arckaringa Basin, located in central Australia (Figure 4.1 b). The GAB is one of the largest aquifer systems in the world, and has been the subject of numerous investigations, which focused largely

on the eastern artesian and north-western sections of the basin (Habermehl 1980; Herczeg et al. 1991; Love et al. 2000; Mahara et al. 2009; Love et al. 2013; IESC 2014; Moya et al. 2015). Few studies focused on the unconfined south-western part of the GAB, but some have highlighted the potential connectivity between the GAB and the Arckaringa Basin (Smerdon et al. 2012; Keppel et al. 2015). There are currently numerous proposals for exploration and mining of coal and gas in the Arckaringa Basin (Wohling et al. 2013). Because of the associated risk of groundwater contamination from coal seam and shale gas extraction via fracking, it is vital to investigate potential inter-aquifer leakage mechanisms (Myers 2012; Vidic et al. 2013). However, the scarcity of observation points hampers an understanding of inter-aquifer leakage processes, and the groundwater system more generally.

A major challenge encountered in hydrogeological investigations in sparsely-developed areas such as the Arckaringa Basin is the scarcity of data (Melloul 1995; Cudennec et al. 2007; Masoud et al. 2013; Candela et al. 2014). Whilst drilling additional observation wells is the only real solution to this problem, prohibitive costs, as well as access and time constraints, often render this intractable. Accepting that the number of observation points is fixed, increasing the information content at each location may address the problem to some extent (Melloul 1995). The present study therefore adopted a comprehensive multidisciplinary approach based on the aforementioned techniques and had the objective to assess if, and which, combinations of methods are best suited to improve the regional-scale understanding of the system when the spatial data density is low. The usefulness of each of the individual investigation methods, and combinations thereof, will be assessed and evaluated.

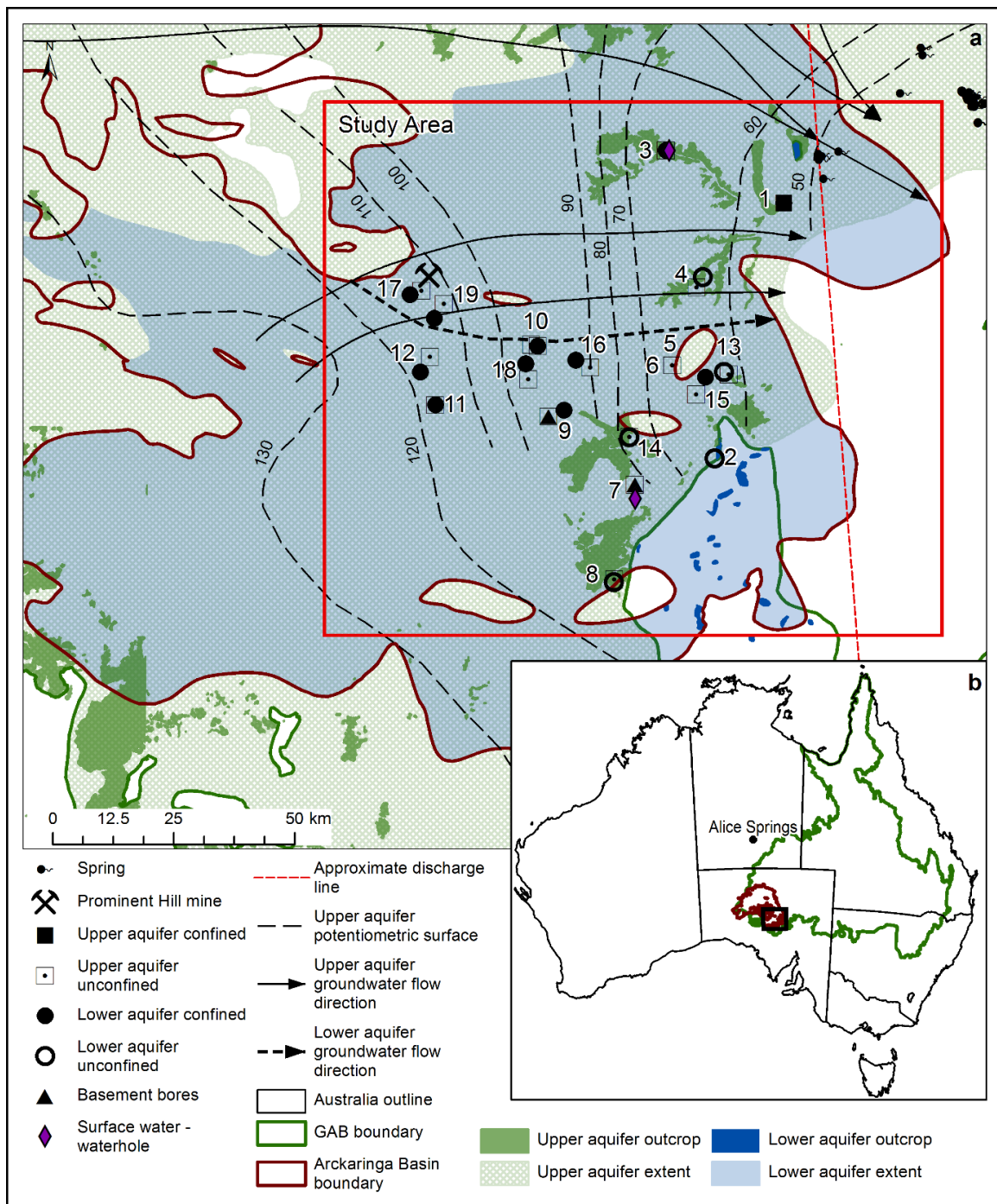


Figure 4.1 (a) Map of the extent and generalised groundwater flow paths of the upper aquifer and lower aquifer. The upper aquifer density-corrected freshwater potentiometric surface is also included. An approximate ‘discharge line’ is shown by a red dashed line for both upper and lower aquifers. The study area shown by the red box includes the majority of the wells completed in the lower aquifer and is ~14,000 km² in area. (b) Full GAB and underlying Arckaringa basin extents.

4.3 Site description

The GAB and Arckaringa Basin are underlain by Proterozoic-Archean crystalline metasediment, limestone and igneous rocks, which are colloquially referred to as ‘basement’ (Ambrose and Flint

1980). The GAB contains Jurassic-Cretaceous sedimentary rocks, whereas the Arckaringa Basin comprises older Carboniferous-Permian sedimentary rocks. Glacial scouring during the Devonian-Carboniferous and faulting during the Early Permian has resulted in the formation of troughs and sub-basins (Wohling et al. 2013). Compression and uplift events at approximately 50 Ma and 15–5 Ma have caused further deformation of Carboniferous-Permian sediments (Wohling et al. 2013).

The main GAB aquifer units within the study area (Figure 4.1 a) are the Cadna-Owie Fm. and Algebuckina Sandstone which are hydraulically connected in the western margin of the GAB and are thus treated as one aquifer (Love et al. 2013), which will be referred to as the ‘upper aquifer’ in this chapter. The upper aquifer is approximately 20 m thick in the study area with measured hydraulic conductivity measurements >10 m/day (Keppel et al. 2013) and hydraulic heads ranging from 150 to 30 m AHD (Figure 4.2 a). The upper aquifer is confined by the Bulldog Shale, except near the south-western and eastern margin of the Arckaringa Basin, where the aquifer crops out and is unconfined (Figure 4.1 a). The Bulldog Shale, referred to as the ‘upper aquitard’, is a marine mudstone aquitard with vertical conductivity measurements of 10^{-14} to 10^{-13} m/s hence it is inferred that any significant inter-aquifer leakage is via preferential flow paths (Keppel et al. 2013). The main aquifer in the Arckaringa Basin in the study area is the Boorthanna Fm., a marine and glacial sandstone and diamictite, which will be referred to as the ‘lower aquifer’. The lower aquifer average thickness is 50 m in the study area with measured hydraulic conductivity measurements from 1–5 m/day (Wohling et al. 2013) and hydraulic heads range from 100 to 60 m AHD (Figure 4.2 b). The lower aquifer only crops out along the south-eastern margin of the Arckaringa Basin (Figure 4.1 a). The upper and lower aquifers are separated by an aquitard formed by mudstones, siltstones and shales of the Stuart Range Fm. throughout most of the basin; it is here referred to as the ‘lower aquitard’ (Figure 4.3). In the study area the lower aquitard average thickness is 70 m with aquitard core hydraulic conductivity measurements between 10^{-10} to 10^{-13} m/s (Kleinig et al. 2015).

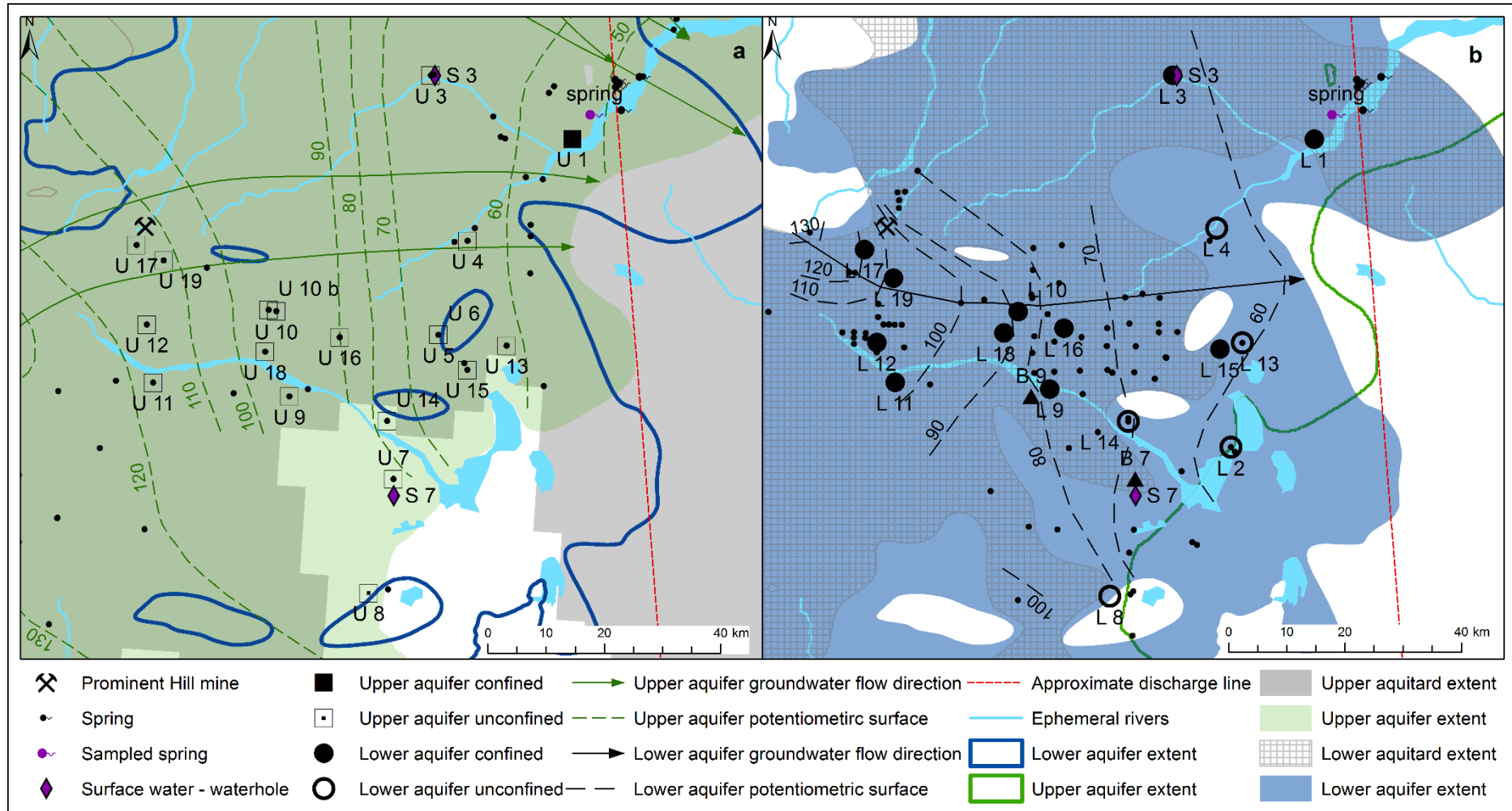


Figure 4.2 Map showing pre-pumping freshwater head potentiometric surface and the generalised groundwater flow paths for (a) the upper aquifer and (b) the lower aquifer. An approximate 'discharge line' is shown by a red dashed line for both upper and lower aquifers, and wells that have not been sampled are indicated by black dots.

The climate of the study area is arid; precipitation is extremely variable, both temporally and spatially. The long-term average annual precipitation rate is estimated to be 120 mm/yr (Allan 1990; McMahon et al. 2005). The upper aquitard inhibits recharge to the underlying aquifers, which is estimated by Love et al. (2013) to be <0.25 mm/yr. Higher recharge rates occur in areas with ephemeral rivers where the aquifer crops out or is close to the surface (Love et al. 2013). Within the study area groundwater flow in the upper aquifer is from the west towards the east (Love et al. 2013). In the eastern margin where the upper and lower aquifers come into contact (i.e. the lower aquitard is absent; Figure 4.3), groundwater potentially discharges into the lower aquifer and then into the basement (Figure 4.1 a). In the north-eastern section of the study area the Arckaringa Basin groundwater discharges upward to the springs (Figure 4.1 a).

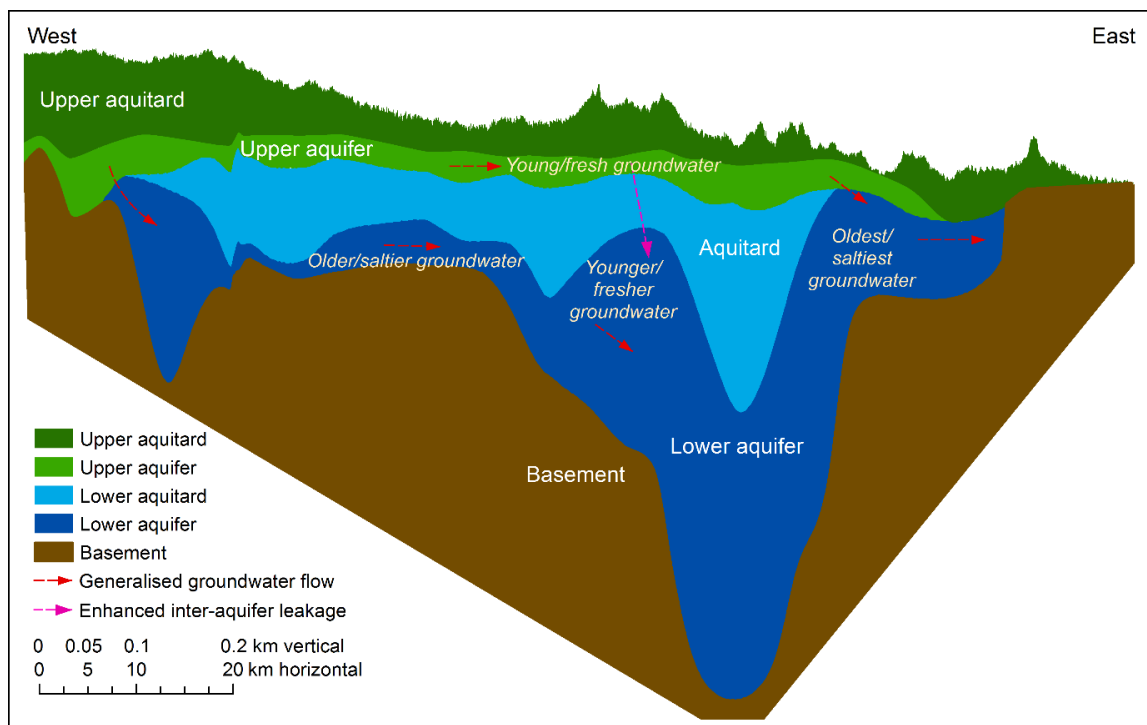


Figure 4.3 Hydrogeological transect following the generalised groundwater flow path in the lower aquifer (Figure 4.1 a). Schematic depiction of variation in environmental tracers in the lower aquifer from enhanced inter-aquifer leakage of upper aquifer water as described in conceptual model 2.

The lower aquifer outcrop extent is limited so recharge is most likely to occur from the upper aquifer. Vertical flow from the upper to the lower aquifer is estimated to be between 0.05 and 0.5 mm/y and likely to be an important component of the water balance (Keppel et al. 2015). In the southern margin recharge could occur where the aquifer crops out or is close to the surface below ephemeral rivers (Keppel et al. 2015). Given the lack of wells completed in the lower aquifer, this study focused on the area with the most wells available (Figure 4.1 a). The Prominent

Hill mine has been extracting groundwater from the lower aquifer from these wells since 2008 (SKM 2010).

4.4 Methods

Published geological information, including interpreted elevation top of aquifers and aquitards, as well as aquifer isopachs (Sampson et al. 2012a; Sampson et al. 2012b; Sampson et al. 2015) and fault locations (Ambrose and Flint 1980; Cowley and Martin 1991; Drexel and Preiss 1995), were used to identify zones that may potentially be associated with enhanced vertical permeability. Where the thickness of the aquitard is lower, resistance to vertical flow is also reduced. This effect is expressed by the hydraulic resistance (3.1)

$$c = \frac{b}{K_v} \quad (3.1)$$

where c is the hydraulic resistance [T], b the aquitard thickness where present, or vertical distance ($z_2 - z_1$) where the aquitard is absent [L] and K_v the vertical hydraulic conductivity of the aquitard [L/T]. K_v values in the study area were measured on core samples obtained from a borehole drilled alongside well couplet 11 in March 2015 (Kleinig et al. 2015). The upper aquifer samples comprise medium to coarse-grained sand sequences that had an average measured K_v of 2×10^{-7} m/s from two samples (6×10^{-6} – 1×10^{-8} m/s). The lower aquitard samples are variable grey and brown consolidated claystone samples with thin (<50 mm) sandstone interbeds and gradational sequences that had an average measured K_v of 5×10^{-12} m/s from eight samples (4×10^{-10} – 4×10^{-13} m/s). A lower aquifer sample grey sandstone with poorly sorted sand and moderate percentage of clay had a measured K_v of 5×10^{-11} m/s (Kleinig et al. 2015), although other K_v estimates between 1×10^{-5} – 5×10^{-5} m/s are more representative of the lower aquifer (Wohling et al. 2013).

The second step involved a detailed analysis of the hydraulics within the two aquifers. This included preparation of pre-exploitation freshwater head contour maps (Bachu 1995) and vertical head gradients across the aquitard to determine potential vertical flow direction. No multi-level observation wells were present in the study area, so well couplets were selected by matching wells in the upper and lower aquifers that are located within 4 km of each other. Additionally, time series of hydraulic head in the upper aquifer were analysed to detect a response to Prominent Hill mine groundwater extraction from the lower aquifer, which would indicate enhanced inter-aquifer connectivity (Neuman and Witherspoon 1972).

If hydraulic resistance (c) is known, the rate of diffuse inter-aquifer leakage can be estimated. The analysis needs to take into account the difference in groundwater density due to variations in salinity or temperature of the groundwater (Post et al. 2007). Using a freshwater head formulation (Post et al. 2007), the vertical Darcy flux q_z can be calculated using:

$$q_z = -\frac{1}{c} \left[\Delta h_f + b \left(\frac{\rho_a - \rho_f}{\rho_f} \right) \right] = -K_v \left[\frac{\Delta h_f}{b} + \left(\frac{\rho_a - \rho_f}{\rho_f} \right) \right] \quad (3.2)$$

where K_v is the vertical hydraulic conductivity [L/T], $\Delta h_f = h_{f,u} - h_{f,l}$, with $h_{f,u}$ and $h_{f,l}$ [L] being the freshwater head in the upper aquifer and lower aquifer, respectively, b the aquitard thickness where present, or vertical distance ($z_2 - z_1$) where the aquitard is absent [L] and $(\rho_a - \rho_f)/\rho_f$ the term that represents the relative density contrast, which accounts for the buoyancy effect on vertical flow, in which ρ_f is the freshwater density and ρ_a the average density of groundwater across the aquitard [M/L^3] calculated using functions in McCutcheon et al. (1993).

It follows from equation 3.2 that a high Δh_f only indicates high flow when c is low. In other words, a large hydraulic head difference between the aquifers can indicate that there is an effective barrier against diffuse flow between aquifers (c is high), and small head gradients can reflect high rates of diffuse inter-aquifer leakage when c is low. In essence, hydraulics provides the direction of inter-aquifer leakage and estimates of diffuse inter-aquifer leakage, but to ascertain if enhanced inter-aquifer leakage is occurring it is necessary to consider environmental tracers. Here, major and trace elements, stable isotopes of water, $\delta^{13}C$ and $^{87}Sr/^{86}Sr$ ratios were considered. These tracers have been found to be useful to determine the location and proportion of mixing and inter-aquifer leakage in previous studies (Dogramaci and Herczeg 2002; Trabelsi et al. 2009; Zilberbrand et al. 2014). In addition, the age tracers ^{14}C , $^{36}Cl/Cl$ and radiogenic 4He were analysed. The latter was interpreted in combination with $^3He/^4He$ ratios.

Approximately 130 wells are recorded as being completed in the lower aquifer with the majority (>90%) concentrated in the south-eastern Arckaringa Basin clustered in the Prominent Hill mine well fields (Figure 4.2 b). There are only approximately 40 wells completed in the upper aquifer in the same location (Figure 4.2 a). Well couplets were preferentially selected for sampling along a north-west to south-east transect along the regional groundwater flow direction. Groundwater samples were collected from pastoral production and monitoring wells within the upper aquifer as well as mining monitoring wells within the lower aquifer in November 2013 and May 2014. A total of 26 groundwater samples were collected.

Groundwater was sampled from well couplets throughout the south-eastern part of the Arckaringa Basin, central Australia. Not all of the well couplets identified were able to be sampled because the submersible pump was too large for a number of wells, some historic wells were not able to be located, and mining production wells were in use. All wells that could be sampled were pumped and groundwater samples taken after a minimum of three well volumes had been purged and pH, electrical conductivity and temperature measurements had stabilised. All bottles were rinsed with the sample several times prior to collecting the final sample to avoid contamination. Groundwater samples were collected for a variety of chemical and isotope analyses including: anions (125 mL HDPE bottle, 0.45µm filtered), cations (125 mL HDPE bottle, 0.45µm filtered, acidified to pH <2 with HNO₃), ¹⁸O and ²H (McCartney vial, unfiltered), ¹⁴C and δ¹³C (1 L HDPE bottle, unfiltered), ³⁶Cl/Cl (500 mL HDPE bottle, unfiltered), ⁸⁷Sr/⁸⁶Sr (1 L HDPE bottle, 0.45µm filtered). Two waterholes located adjacent to sampled wells and a groundwater spring were also sampled for major ions and some isotopes.

Anion analysis was undertaken by The Analytical Services Unit, Commonwealth Scientific and Industrial Research Organisation (CSIRO). Chloride concentration was measured by ion chromatography using a Dionex ICS-2500 system (APHA 1998). The coefficient of variance for these methods is <2%. ¹⁸O and ²H were analysed simultaneously by laser spectroscopy using a Laser Water Isotope Analyser V2 (Los Gatos Research Instruments) by the University of California Davis Stable Isotope Facility. Sample isotope ratios are standardised against IAEA standard reference materials (VSMOW, GISP, and SLAP). δ¹⁸O and δ²H values are reported relative to VSMOW with a precision of ≤0.3 per mil for δ¹⁸O and ≤2.0 per mil for δ²H. ¹⁴C and δ¹³C analysis was undertaken by Rafter Radiocarbon Laboratory. ¹⁴C and δ¹³C isotope ratios of dissolved inorganic carbon (DIC) were analysed by accelerator mass spectrometry (AMS) and isotope-ratio mass spectrometry (IRMS), respectively (Stuiver and Polach 1977). Uncertainties are primarily based on ¹⁴C counting statistics and precision is reported at 1 standard deviation of the mean. ⁸⁷Sr/⁸⁶Sr ratio analysis was undertaken by the School of Earth and Environmental Sciences, The University of Adelaide, using a Finnigan MAT262 thermal ionization mass spectrometer (TIMS) following the method described in Cartwright et al. (2007). The mass spectrometer measurement precision is 2 standard error of the mean after a 2 standard deviation rejection test. ³⁶Cl/Cl analysis was undertaken by the Department of Nuclear Physics at The Australian National University (ANU). Analysis was completed using a combination of a high efficiency ion source,

tandem acceleration and heavy-ion detection and identification techniques with a precision of $\leq 3\%$ (Fifield et al. 2010).

He isotope samples were collected in copper tubes (Beyerle et al. 2000) and analysed by mass spectrometry (MS) in the noble gas laboratory of the Swiss Federal Institute of Technology (ETH) according to the methods discussed by Beyerle et al. (2000). Measurement precision is between 0.2% and 1.0% for He isotopes.

Two possible conceptual groundwater flow models were developed for the study area: In the first model (model 1), there is no enhanced inter-aquifer leakage (e.g. the extremely tight aquitard only allows diffuse inter-aquifer leakage at low flow rates). In the second model (model 2) there is concentrated enhanced inter-aquifer leakage via localised secondary features having higher permeabilities.

Model 1 represents an idealised case where radiogenic ^4He concentrations increase and the ^{14}C and $^{36}\text{Cl}/\text{Cl}$ decrease along the inferred flow paths. Moreover, provided that $^{87}\text{Sr}/^{86}\text{Sr}$ ratios, $\delta^{13}\text{C}$ values and other environmental tracer concentrations, or isotope ratios, are distinctly different in both aquifers, environmental tracer concentrations, or isotope ratios, are likely to remain different in this model. When water-rock-gas interactions also affect environmental tracers, they need to be taken in to consideration. In model 2 mixing and enhanced inter-aquifer leakage cause variation in groundwater residence time from the idealised system with increasing groundwater residence time along groundwater flow paths (Goode 1996; Bethke and Johnson 2008). Therefore, spatially irregular variations in age tracers (radiogenic ^4He , ^{14}C and $^{36}\text{Cl}/\text{Cl}$) and overlap in environmental tracer concentrations, or isotope ratios, due to enhanced inter-aquifer leakage is expected. This is shown schematically in Figure 4.3.

4.5 Results

4.5.1 Hydrogeology

The map of lower aquitard thickness and interpreted tectonic features (Figure 4.4) shows that the lower aquitard can be up to 300 m thick. It becomes thinner toward the margins of the aquitard, where it pinches out, and has an average thickness of 70 m. The hydraulic resistance (c ; equation 3.1) is included in Figure 4.4, and is highest (10^{+4} – 10^{+6} years) wherever the aquitard is present, highlighting areas of reduced diffuse inter-aquifer leakage through the aquitard. The hydraulic resistance reduces considerably (<25 years) where the aquifers are in contact.

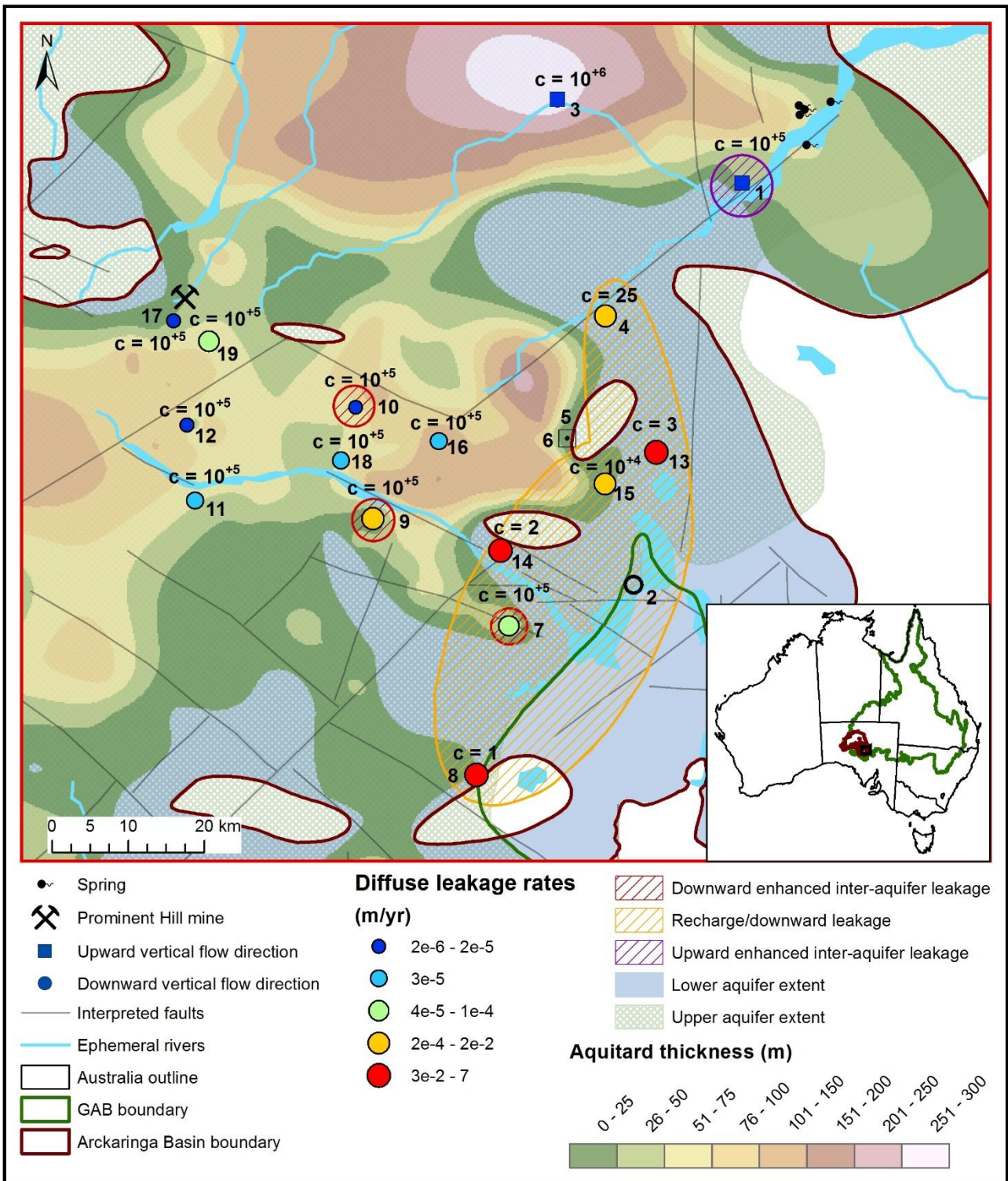


Figure 4.4 Lower aquitard extent and thickness highlighted with colour variations, interpreted faults and the locations of well couplets with hydraulic data. The leakage rates (m/yr) are calculated using $K_v = 5 \times 10^{-12}$ m/s for the lower aquitard and $K_v = 2 \times 10^{-7}$ m/s for the upper aquifer (Kleinig et al. 2015) and pre-pumping density-corrected freshwater heads. The range of leakage rates are indicated by colour variations. The hydraulic resistance (c) are labelled in years above the well couplets with the well couplet number also labelled.

The pre-pumping freshwater head contour map of the lower aquifer indicates groundwater flows from the north-west towards the eastern margin of the study area (Figure 4.1 a and Figure 4.2 b). A clear recharge area for the lower aquifer could not be delineated due to the limited number and distribution of observation wells outside the Prominent Hill well fields in the Arckaringa Basin (Figure 4.2 b). Groundwater flow directions in the upper and lower aquifers are similar, with discharge to the basement where the aquifers terminate indicated on Figure 4.1 a, and Figure 4.2, near the eastern margin of the lower aquifer.

The well couplet hydraulic head measurements were corrected to freshwater hydraulic heads using measured temperature and total dissolved solid (TDS) concentrations (Table 4.1). The freshwater heads of the well couplets are plotted along the regional head gradient to determine the direction of inter-aquifer leakage (Figure 4.5). The density correction can be significant, especially where there are high salinities in the lower aquifer (up to 46 g/L leading to head correction terms of up to 2.5 m; Table 4.1). The range in groundwater density (ρ_a) across the aquitard and measured K_v were used to calculate diffuse inter-aquifer leakage flow rates (equation 3.2; Post et al. 2007). The buoyancy term in equation 3.2 was about an order of magnitude less than the freshwater hydraulic gradient, so the latter can be taken as an indicator of the flow direction. The majority of the well couplets showed downward leakage from the upper aquifer to the lower aquifer. However, there is evidence for upward leakage at well couplet locations 1 and 3; shown with slightly higher density corrected freshwater heads in the lower aquifer compared to the upper aquifer (Figure 4.5). The calculated diffuse leakage rates through the lower aquitard were <1 mm/year, but higher rates were calculated where the aquitard is thin or absent (up to 7 m/year) (Figure 4.4).

Table 4.1 Well couplet hydraulic head (h_i), temperature and total dissolved solids (TDS) measurements and corrected freshwater hydraulic heads (h_f). The range of groundwater density across the aquitard (ρ_a) used in the freshwater head formulation (equation 3.2; Post et al. 2007) along with the range of measured K_v were used to calculate diffuse inter-aquifer leakage flow rates.

Well couplet number	Name	Source	Distance to discharge line (km)	Temperature (°C)	TDS (mg/L)	h_i (m AHD)	h_f (m AHD)	Δz or b (m)	Hydraulic resistance (years)	ρ_a^c	Diffusive inter-aquifer leakage flow rate (m/yr)
1	U 1	upper aquifer	10.0	26.2	9243	51.88	52.15	25.00	10^{+5} (10^{+2} – 10^{+6})	1006–1007	-2×10^{-5} (-7×10^{-4} – -7×10^{-7})
	L 1	lower aquifer	10.0	25.6	15738	52.52	53.33				
3	U 3	upper aquifer	32.7	27.1	1112	60.82	60.83	277.00	10^{+6} (10^{+4} – 10^{+7})	1000–1002	-6×10^{-6} (-3×10^{-4} – -2×10^{-7})
	L 3	lower aquifer	32.7	36.2	12623	64.66	65.77				
4	U 4	upper aquifer	29.8	24.5	8589	62.67	62.71	189.50	25 (1 – 10^{+2})	1004	2×10^{-2} (6×10^{-1} – 7×10^{-4})
	L 4	lower aquifer	29.8	24.0	9700	61.14	62.24				
7	U 7	upper aquifer	48.1	24.7	665	93.88	93.89	58.00	10^{+2} (10^{+3} – 10^{+6})	1002–1003	1×10^{-4} (7×10^{-3} – 7×10^{-6})
	L 7	lower aquifer	48.0	27.8 ^a	12511	66.37	66.51				
	B 7	basement	48.1	27.0	11909	63.28	63.35				
8	U 8	upper aquifer	50.2	20.9 ^a	6760	80.22	80.27	5.00	1 (10^{-2} – 10^{+2})	999–1003	6 (2×10^{-1} – $1 \times 10^{+2}$)
	L 8	lower aquifer	49.7	24.6	5079	77.29	77.32				
9	U 9	upper aquifer	63.6	25.6	16386	98.24	98.23	29.33	10^{+5} (10^{+3} – 10^{+6})	1004–1007	2×10^{-4} (9×10^{-3} – 9×10^{-6})
	L 9	lower aquifer	60.3	30.0	14461	77.12	76.99				
	B 9	basement	60.3	29.3	7240	76.98	77.13				
10	U 10	upper aquifer	64.2	23.8	8047	94.64	94.66	64.33	10^{+5} (10^{+3} – 10^{+6})	1003–1006	2×10^{-5} (1×10^{-3} – 1×10^{-6})
	U 10b	upper aquifer	62.2	26.6	10231	95.04	95.05				
	L 10	lower aquifer	64.2	31.6	19000	89.21	89.86				
11	U 11	upper aquifer	86.8	25.2	11229	114.91	114.96	57.00	10^{+5} (10^{+3} – 10^{+6})	1008–1017	3×10^{-5} (1×10^{-3} – 1×10^{-6})
	L 11	lower aquifer	86.8	23.0	40600	106.52	108.09				
12	U 12	upper aquifer	86.8	26.3	20703	113.54	113.53	84.00	10^{+5} (10^{+3} – 10^{+6})	1014–1019	4×10^{-6} (1×10^{-4} – 2×10^{-7})
	L 12	lower aquifer	89.2	28.0	34967	108.81	110.89				
13	U 13	upper aquifer	25.1	20.9 ^a	4251	79.59	79.61	19.50	31 (10^{-1} – 10^{+2})	1000–1001	7 ($2 \times 10^{+2}$ – 3×10^{-1})
	L 13	lower aquifer	26.1	23.9 ^a	4693	67.03	67.05				
14	U 14	upper aquifer	47.2	20.3 ^a	2216	72.72	72.71	13.75	2 (10^{-1} – 10^{+2})	999–1000	9×10^{-1} (4×10^{-2} – $2 \times 10^{+1}$)
	L 14	lower aquifer	47.2	26.0	2784	71.11	71.11				
15	U 15	upper aquifer	33.1	20.7 ^a	1332 ^b	91.11	91.11	6.00	10^{+4} (10^{+2} – 10^{+5})	1003–1006	1×10^{-3} (5×10^{-2} – 5×10^{-5})
	L 15	lower aquifer	33.1	23.9	13099	66.85	67.00				
16	U 16	upper aquifer	53.7	26.7	12542	90.86	90.87	106.50	10^{+5} (10^{+3} – 10^{+6})	1003–1005	3×10^{-5} (1×10^{-3} – 1×10^{-6})

	L 16	lower aquifer	56.3	30.4	11993	79.7	80.15				
17	U 17	upper aquifer	87.1	21.9 ^a	6320	118.54	118.56	25.00	10^{+5} (10^{+3} – 10^{+6})	999–1003	2×10^{-6} (1×10^{-4} – 6×10^{-8})
	L 17	lower aquifer	89.6	27.0 ^a	6960	118.39	118.36				
18	U 18	upper aquifer	66.9	26.9	12790	98.84	98.84	54.00	10^{+5} (10^{+3} – 10^{+6})	1006–1008	3×10^{-5} (1×10^{-3} – 1×10^{-6})
	L 18	lower aquifer	67.1	31.6 ^a	19000	91.47	92.15				
19	U 19	upper aquifer	82.7	21.7 ^a	20200 ^b	117.98	118.16	76.00	10^{+5} (10^{+3} – 10^{+5})	1001 -1010	7×10^{-5} (3×10^{-3} – 3×10^{-6})
	L 19	lower aquifer	85.1	27.0 ^a	11000	98.8	99.26				

^a temperature estimated from nearby well at similar depth

^b TDS estimated from nearby well at similar depth

^c groundwater density distribution across the aquitard (ρ_a) has been estimated assuming minimum and maximum vertical density distributions (Post et al. 2007)

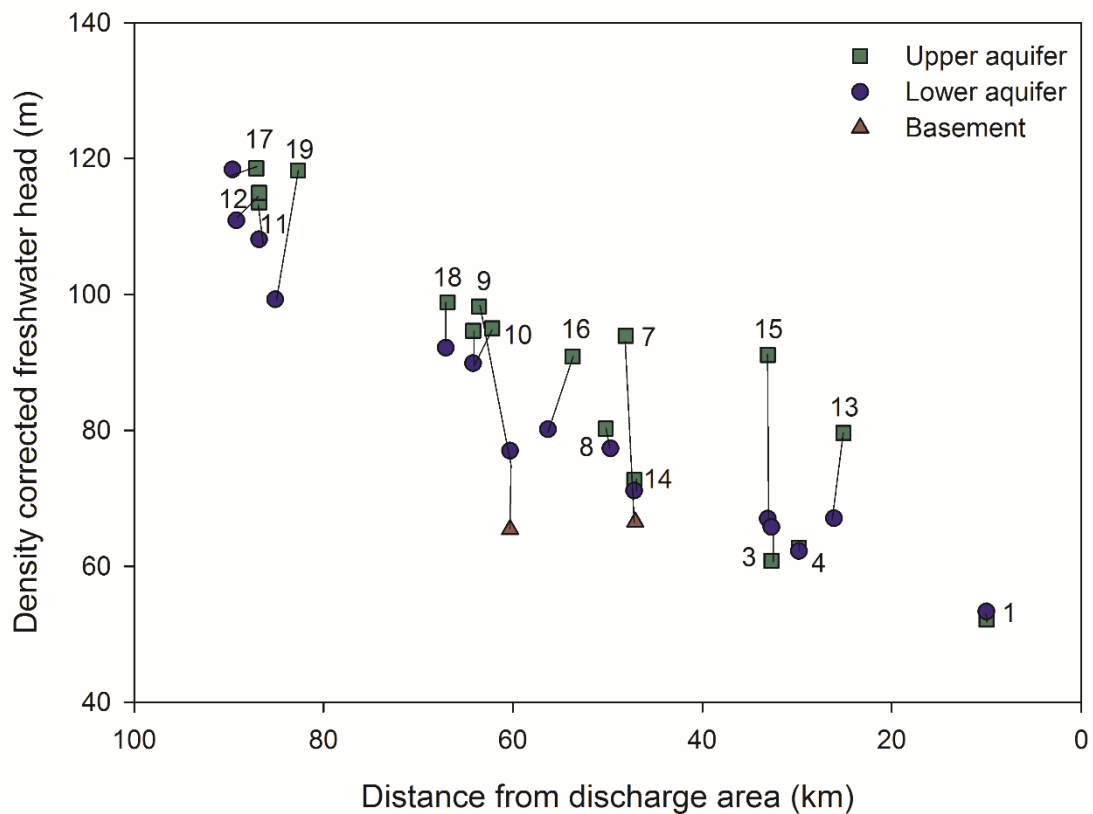


Figure 4.5 Pre-pumping density corrected freshwater heads of the well couplets transposed onto a transect from the approximate discharge line, where zero represents the discharge line shown in Figure 4.1 a and numbers represent the well couplets.

Pumping in the lower aquifer since 2008 has caused drawdowns of up to 30 m in the lower aquifer (Figure 4.6; Richards, 2013). Time series well couplet hydraulic head data in the upper and lower aquifers were compared to locate enhanced inter-aquifer connectivity, with well couplet 10 and 18 time series data plotted in Figure 4.6. There are no drawdowns observed in the upper aquifer except for well U 10b in the upper aquifer that recorded a drawdown of approximately 2 m (Figure 4.6). The 2 m drawdown in the upper aquifer, as a consequence of pumping in the lower aquifer, could be indicative of enhanced inter-aquifer leakage to the lower aquifer at this location.

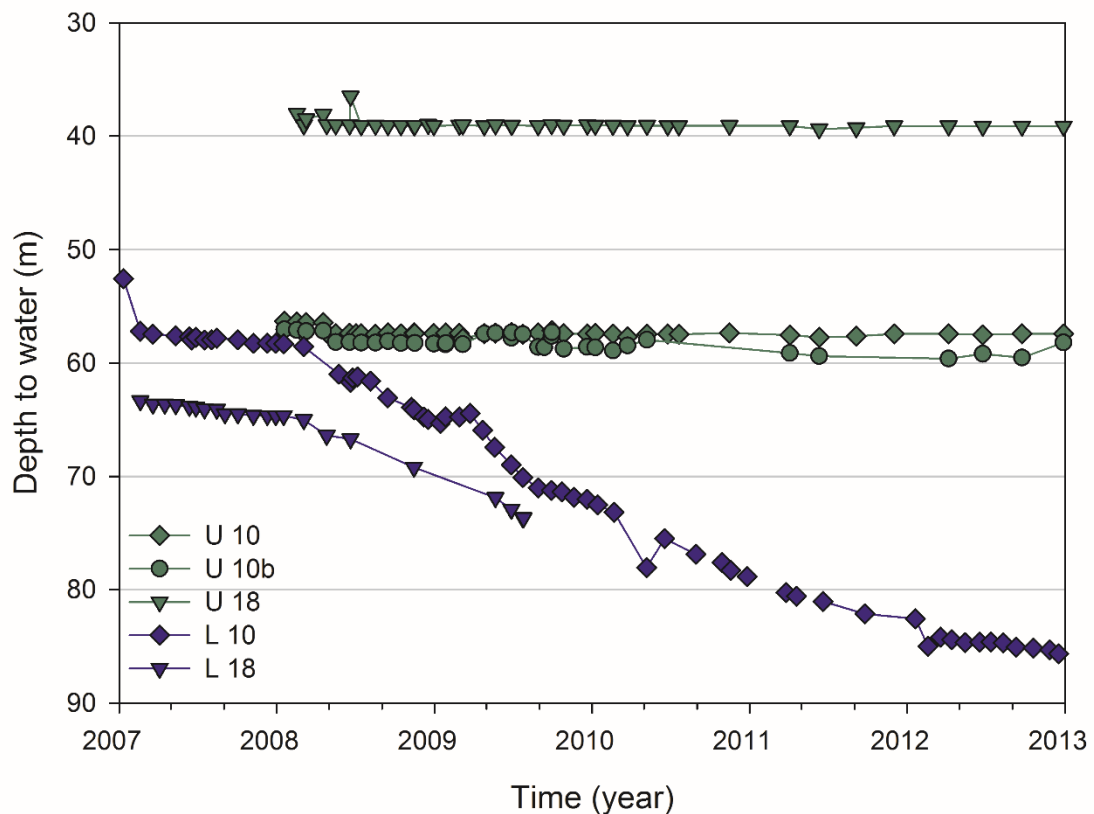


Figure 4.6 Depth to water variation over time from pumping wells in the lower aquifer and corresponding upper aquifer wells for well couplets 10 and 18 (Richards 2013). For well locations, see Figure 4.2.

4.5.2 Tracer results

Hydrochemical results for well couplet groundwater samples, as well as two waterholes and a spring, are presented in Table 4.2.

Chloride concentrations are generally below 7,600 mg/L, except in the lower aquifer at two locations in the western part of the study area, which have concentrations between 21,500–22,800 mg/L (Figure 4.7 a). At the well couplets, chloride concentrations in the upper aquifer (79–7600 mg/L) are significantly different (T-test gave a p-value <0.1; Table 4.2) compared to the lower aquifer (1800–22800 mg/L), although some well couplets have similar concentrations (well couplets 4 and 10; Figure 4.7 a). In addition, the samples from waterholes S 3 and S 7 and nearby upper aquifer wells U 3 and U 7, respectively, have chloride concentrations <500 m/L (Table 4.2).

Table 4.2 Table of available hydrochemical results for the well couples including chloride and strontium concentrations, stable isotopes of water, $^{87}\text{Sr}/^{86}\text{Sr}$ ratios, $\delta^{13}\text{C}$, ^{14}C , $^{36}\text{Cl}/\text{Cl}$ and He isotopes.

Well couplet number	Name	source	Distance to discharge line (km)	Cl (mg/L)	Sr (mg/L)	$\delta^2\text{H}$ (‰ VSMOW)	$\delta^{18}\text{O}$ (‰ VSMOW)	$^{87}\text{Sr}/^{86}\text{Sr}$	$\delta^{13}\text{C}$ (‰)	pMC (‰)	$^{36}\text{Cl}/\text{Cl}$ ($\times 10^{-15}$)	^{36}Cl (atoms/L)	$^3\text{He}/^4\text{He}$	Radiogenic ^4He (ccSTP/g)
1	U 1	upper aquifer	10.0	4100	7.45	-32.1	-4.08	0.71944	-12.24	9.7	11.8	$8.2 \times 10^{+8}$	$2.7 \times 10^{+8}$	$5 \times 10^{+5}$
2	L 2	lower aquifer	29.7	3400	4.21	-43.5	-5.34	0.71379	-8.55	10.99	44.5	$2.6 \times 10^{+9}$	$1.5 \times 10^{+8}$	$2 \times 10^{+5}$
3	U 3	upper aquifer	32.7	458	0.47	-39.3	-5.43	0.71364	-9.35	71.55	66.4	$5.2 \times 10^{+8}$	$1.3 \times 10^{+7}$	$6 \times 10^{+7}$
	L 3	lower aquifer	32.7	7480	15.10	-39.3	-5.14	0.71899	-15.86	23.44	9.9	$1.3 \times 10^{+9}$	$2.6 \times 10^{+8}$	$3 \times 10^{+4}$
4	U 4	upper aquifer	29.8	3500	4.04	-25.9	-1.72	0.71304	-14.21	45.75	55.5	$3.3 \times 10^{+9}$	$1.0 \times 10^{+6}$	$7 \times 10^{+8}$
	L 4	lower aquifer	29.8	4500	11.10	-32.9	-3.72	0.71514	-10.25	5.51	26.5	$2.0 \times 10^{+9}$	$1.9 \times 10^{+8}$	$2 \times 10^{+5}$
5	U 5	upper aquifer	36.4	660	2.44	-39	-5.63	0.71198	-5.37	5.58	78.4	$8.8 \times 10^{+8}$	$4.0 \times 10^{+8}$	$1 \times 10^{+6}$
6	U 6	upper aquifer	36.4	640	1.24	-40.8	-5.95	0.71208	-6.63	10.02	74.0	$8.0 \times 10^{+8}$	$5.5 \times 10^{+8}$	$5 \times 10^{+6}$
7	U 7	upper aquifer	48.1	79	0.50	-14.3	-1.93	0.71259	-13.75	89.19	82.9	$1.1 \times 10^{+8}$	$1.1 \times 10^{+6}$	$8 \times 10^{+7}$
	B 7	basement	48.1	5400	6.23	-35.1	-4.03	0.71418	-11.08	13.13	44.1	$4.0 \times 10^{+9}$	$4.2 \times 10^{+8}$	$1 \times 10^{+4}$
8	L 8	lower aquifer	49.7	1800	2.20	-42.3	-5.52	0.71411	-8.22	44.99	45.3	$1.4 \times 10^{+9}$	$5.3 \times 10^{+8}$	$4 \times 10^{+6}$
9	U 9	upper aquifer	63.6	7600	9.96	-24.5	-1.15	0.71251	-3.72	40	78.8	$1.0 \times 10^{+10}$	$6.2 \times 10^{+7}$	$2 \times 10^{+8}$
	L 9	lower aquifer	60.3	2800	2.69	-35.1	-3.88	0.71315	-7.27	2.58	37.9	$1.8 \times 10^{+9}$	$2.7 \times 10^{+8}$	$3 \times 10^{+5}$
	B 9	basement	60.3	6900	7.04	-33.1	-3.44	0.71383	-9.62	3.1	23.2	$2.7 \times 10^{+9}$	$2.7 \times 10^{+8}$	$1 \times 10^{+4}$
10	U 10	upper aquifer	64.2	4330	3.92	-31.1	-2.19	0.71281	-9.93	7.08	53.4	$3.9 \times 10^{+9}$	$7.9 \times 10^{+7}$	$2 \times 10^{+8}$
	L 10	lower aquifer	64.2	5030	4.50	-31.1	-2.14	0.71298	-10.78	0.92	49.5	$4.2 \times 10^{+9}$	$3.9 \times 10^{+8}$	$3 \times 10^{+6}$
11	U 11	upper aquifer	86.8	6390	7.23	-32.2	-2.67	0.71271	-6.91	7.4	50.4	$5.5 \times 10^{+9}$	$7.4 \times 10^{+7}$	$4 \times 10^{+8}$
	L 11	lower aquifer	86.8	21500	13.20	-35.8	-3.70	0.71563	-20.64	5.53	8.4	$3.1 \times 10^{+9}$	$1.7 \times 10^{+8}$	$8 \times 10^{+5}$
12	U 12	upper aquifer	86.8	6500	4.89	-31.6	-2.65	0.71317	-10.84	15.77	44.6	$4.9 \times 10^{+9}$	—	—
	L 12	lower aquifer	89.2	22800	11.40	-33.7	-3.60	0.71624	-13.51	0.58	4.8	$1.9 \times 10^{+9}$	$5.9 \times 10^{+9}$	$4 \times 10^{+5}$
-	spring	spring	5.5	7300	8.72	-27.1	-1.50	0.71358	—	—	52.7	$6.5 \times 10^{+9}$	—	—
-	S 3	surface water – waterhole	32.4	14.8	0.05	-13.0	-1.35	0.71241	—	—	—	—	—	—
-	S 7	surface water – waterhole	47.4	12	0.19	—	—	—	—	—	—	—	—	—
T-test (two-tailed unequal variance) p-value				0.0807 ^b	0.0606 ^b	0.0894 ^b	0.2901	0.1334	0.1995	0.0855 ^b	0.0027 ^a	0.5795	0.0032 ^a	0.0391 ^a

^a significant difference between upper and lower aquifer samples at $p < 0.05$

^b significant difference between upper and lower aquifer samples at $p < 0.10$

Most of the data points of the stable isotopes plot along a linear trend (Figure 4.8 a). The line of best fit from the data in all aquifers ($\delta^2\text{H} = 3.3 \times \delta^{18}\text{O} - 22$), excluding the outliers S 3 and U 7, intersects the Alice Springs local meteoric water line (LMWL) close to that of the intense rainfall events at $\delta^2\text{H} = -46.7$ and $\delta^{18}\text{O} = -7.3$ (Figure 4.8 a).

$\delta^{13}\text{C}$ values of the upper aquifer (-3.7– -14.2 ‰), as well as the lower aquifer and basement samples (-7.3– -20.6 ‰) have a similar range with no significant difference (Table 4.2). This limits their application in tracing leakage in this particular study.

The lower aquifer has a relatively large range in $^{87}\text{Sr}/^{86}\text{Sr}$ ratios (0.713–0.719); and the basement samples fall within this range (0.714; Figure 4.7 b). The $^{87}\text{Sr}/^{86}\text{Sr}$ ratios are <0.715 in the lower aquifer samples L 2, 4, 8, 9 and 10, as well as basement samples B 7 and B 9 (Figure 4.7 b). There is a tendency for less radiogenic $^{87}\text{Sr}/^{86}\text{Sr}$ ratios in the upper aquifer samples (0.712–0.714), but with no significant difference from the lower aquifer (Table 4.2). The waterhole sample S 3 $^{87}\text{Sr}/^{86}\text{Sr}$ ratio is 0.712 and sample U 1 closest to the discharge zone has the highest $^{87}\text{Sr}/^{86}\text{Sr}$ ratio in the dataset (0.719).

Generally the lower aquifer and basement samples have higher radiogenic ^4He (3×10^{-6} – 3×10^{-4} ccSTP/g), as well as lower $^{36}\text{Cl}/\text{Cl}$ (5×10^{-15} – 50×10^{-15}) ratios and ^{14}C activities (0.6–45 pMC) that are significantly different (p-value <0.10; Table 4.2) compared to the upper aquifer (Figure 4.7 c, d and e). They also have lower $^3\text{He}/^4\text{He}$ ratios (6×10^{-9} to 5×10^{-8}) compared to the upper aquifer samples (p-value <0.05; Table 4.2; Figure 4.7 f). The majority of the lower aquifer and basement samples have ^{14}C ranging between 0.6–11 pMC, except for wells L 3, B 7 and L 8 which have ^{14}C activities of 23 pMC, 13 pMC and 45 pMC, respectively. The upper aquifer samples show a large variation in ^{14}C activity (7–89 pMC), with the highest values at U 3 and U 7 (72 and 89 pMC).

There is a distinction between the $^{36}\text{Cl}/\text{Cl}$ ratios of the basement/lower aquifers and the upper aquifer (Figure 4.7 d). The majority of the lower aquifer and basement samples have $^{36}\text{Cl}/\text{Cl}$ ratios varying from 8×10^{-15} – 50×10^{-15} (Figure 4.7 d). $^{36}\text{Cl}/\text{Cl}$ ratios are generally higher in the upper aquifer (45×10^{-15} – 83×10^{-15}), except U 1 that has $^{36}\text{Cl}/\text{Cl} = 12 \times 10^{-15}$. The $^{36}\text{Cl}/\text{Cl}$ ratio from a spring in the groundwater discharge area is 52×10^{-15} (Figure 4.7 d).

There is a clear distinction between the basement/lower aquifers and the upper aquifer for the radiogenic ^4He concentrations and $^3\text{He}/^4\text{He}$ ratios (Figure 4.7 e and f). The radiogenic ^4He concentrations are lower for the upper aquifer samples (2×10^{-8} – 5×10^{-6} ccSTP/g) than in the

lower aquifer and basement samples (3×10^{-6} – 3×10^{-4} ccSTP/g), except for U 1 (5×10^{-5} ccSTP/g). Samples L 10 (3×10^{-6} ccSTP/g), L 8 (4×10^{-6} ccSTP/g), L 4 (2×10^{-5} ccSTP/g) and L 2 (2×10^{-5} ccSTP/g) have lower radiogenic ^4He concentrations compared to the other lower aquifer wells (Figure 4.7 e). There appears to be an increase in radiogenic ^4He concentrations in some of the upper aquifer wells, and to a smaller extent the lower aquifer wells with decreasing distance to the discharge area. The $^3\text{He}/^4\text{He}$ ratios of the lower aquifer and basement samples vary within a band of values between 6×10^{-9} to 5×10^{-8} (Figure 4.7 f). The $^3\text{He}/^4\text{He}$ ratios of the upper aquifer samples are commonly higher (9×10^{-7}), but the ratios of the samples U 1, U 3, U 5 and U 6 are markedly lower (Figure 4.7 f).

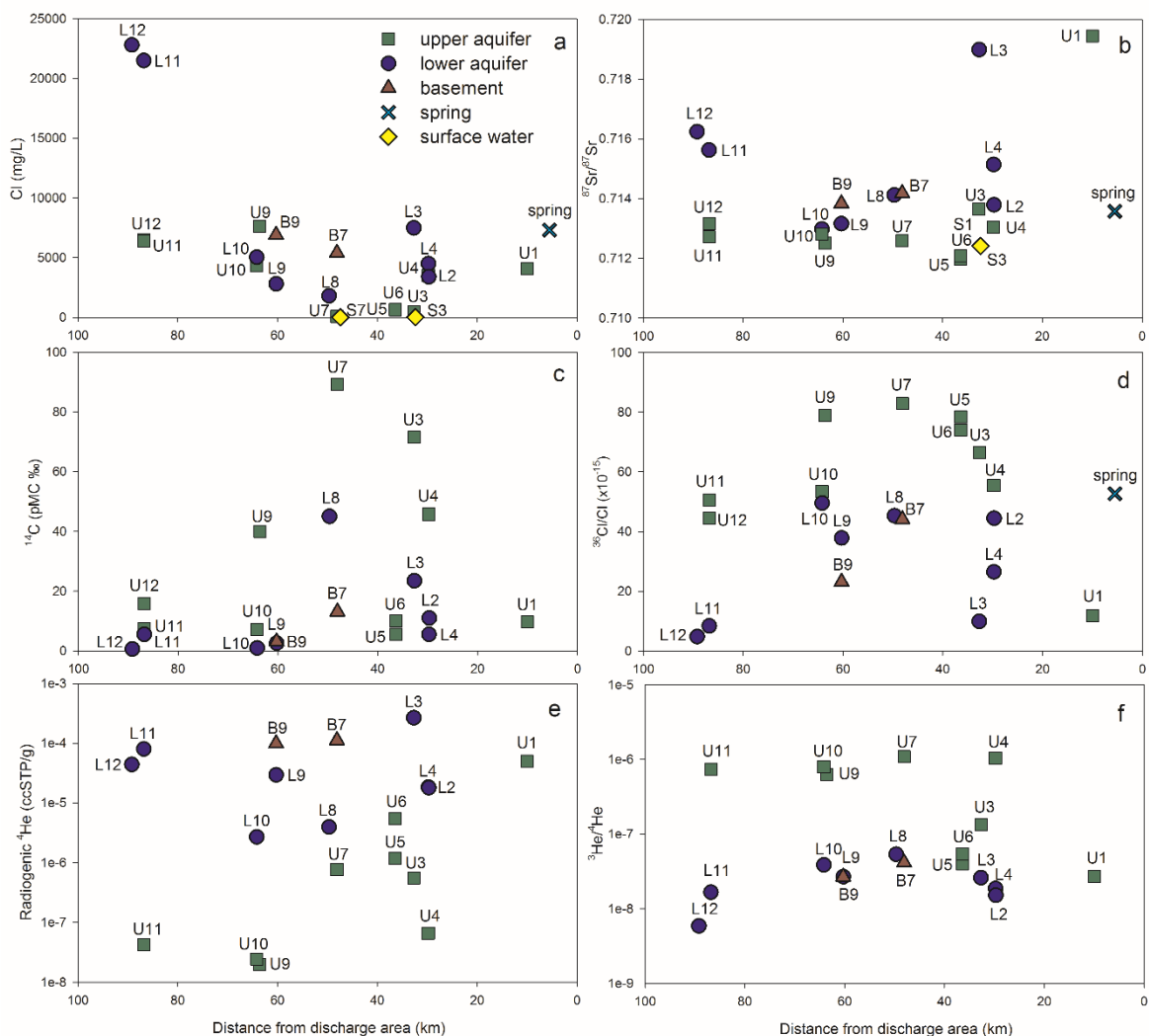


Figure 4.7 Environmental tracers plotted against distance from the discharge area for (a) chloride concentration, (b) $^{87}\text{Sr}/^{86}\text{Sr}$ ratio, (c) ^{14}C , (d) $^{36}\text{Cl}/\text{Cl}$, (e) radiogenic ^4He concentration and (f) $^3\text{He}/^4\text{He}$ ratio.

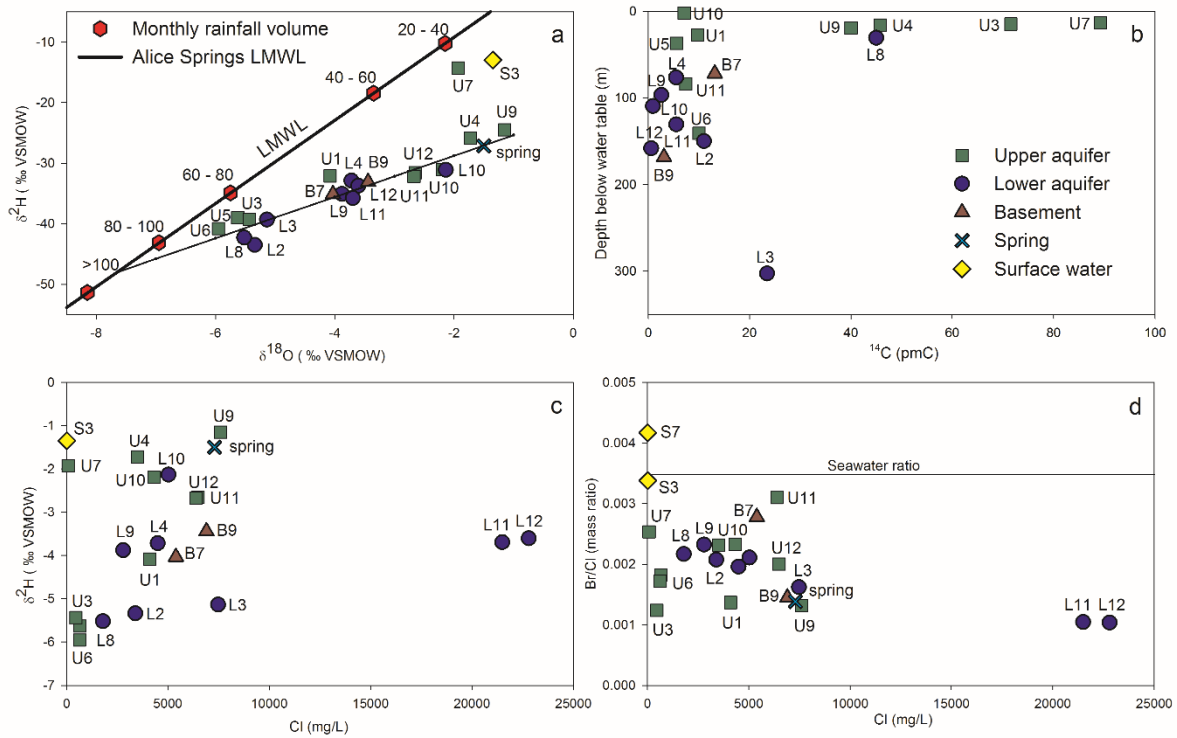


Figure 4.8 (a) $\delta^2\text{H}$ plotted against $\delta^{18}\text{O}$ with the local meteoric water line (LMWL) $\delta^2\text{H} = 7.2\delta^{18}\text{O} + 5.7$ from Alice Springs (Figure 4.1 b) and amount weighted monthly rainfall volume included (Kretschmer and Wohling 2014). (b) ^{14}C plotted against sample depth, which is taken as the mid-point of the well screen interval. (c) $\delta^2\text{H}$ plotted against chloride concentration and (d) Br/Cl mass ratio plotted against chloride concentration.

4.6 Discussion

4.6.1 Chemical and physical processes

Regional groundwater flow

All groundwater samples, except L 10 and L 12, with ^{14}C above background (>1 pMC) are likely to contain $^{14}\text{C}_{\text{DIC}}$ with a residence time of <30 ka due to decay of ^{14}C ($t_{1/2} = 5730$ years; Plummer and Glynn 2013). In fact, groundwater samples with $^{14}\text{C} >40$ pMC (U 3, U 4, U 7, U 9 and L 8) are likely to contain $^{14}\text{C}_{\text{DIC}}$ with a residence time of <6 ka. Groundwater samples of which there has been substantial decay of ^{36}Cl ($^{36}\text{Cl}/\text{Cl} <45 \times 10^{-15}$; U 1, L 2, L 3, L 4, L 9, L 11, L 12, B 7 and B 9) have residence times of several 10s to 100s ka (Love et al. 2000). Groundwater residence times could be greater than 500 ka in those areas where groundwater samples (U 1, L 2, L 3, L 4, L 9, L 11, B 7 and B 9) have radiogenic $^4\text{He} >1 \times 10^{-5}$ ccSTP/g, assuming 1×10^{-12} – 10×10^{-12} ccSTP/g/yr radiogenic ^4He input (Torgersen and Clarke 1985; Bethke et al. 1999; Gardner et al. 2012).

Measureable ^{14}C points to a maximum residence time of 30 ka (Plummer and Glynn 2013). For a residence time of 30 ka the ^{36}Cl would have decayed by no more than 7% (based on $C = C_0 e^{-\lambda t}$, with $t = 30,000$ years), and radiogenic ^4He should not exceed 3×10^{-8} – 30×10^{-8} ccSTP/g/yr (assuming 1×10^{-12} – 10×10^{-12} ccSTP/g/yr input for 30 ka). However, throughout this study area the age tracers were beyond these theoretical limits emphasising the importance of mixing of different ‘age’ groundwater, and possibly the influx of tracers by diffusion (Walker and Cook 1991). Because of the low groundwater flow velocities, diffusion of age and other tracers could be more relevant here than in areas with higher flow rates. For example, ^{14}C could diffuse in from above and radiogenic ^4He could diffuse from below.

The ^{14}C value of 23 pMC at L 3 is inconsistent with the hydraulic data and the other age tracers ($^{36}\text{Cl}/\text{Cl}$ ratio $<45 \times 10^{-15}$ and radiogenic ^4He $>1 \times 10^{-5}$ ccSTP/g), as well as the depth of the well (300 m; Figure 4.8 b). The reason for this inconsistency is unknown, but it is unlikely to be representative for the groundwater in the lower aquifer at that location.

The upper aquifer samples in the westernmost part of the study area (U 10, U 11 and U 12) with radiogenic ^4He $<1 \times 10^{-7}$ ccSTP/g and $^{36}\text{Cl}/\text{Cl}$ values $>45 \times 10^{-15}$, have groundwater residence times less than several 10s ka. Groundwater samples further to the east (U 5, U 6 and U 1) have low ^{14}C values ^{14}C (<10 pMC) and higher radiogenic ^4He concentrations ($>1 \times 10^{-6}$ ccSTP/g), indicating groundwater residence times of several 100s ka. The inconsistency between ^{14}C , radiogenic ^4He and $^{36}\text{Cl}/\text{Cl}$ in a number of samples, for example L 3, L 11 and U 3, is possibly due to mixing and diffusion. However, the general pattern of increasing groundwater residence times is consistent with the west-east directed groundwater flow in the upper aquifer, as inferred from the hydraulic head distribution (Figure 4.2 a). The lower aquifer and basement groundwater residence times are generally older (several 10s to 100s ka) than the upper aquifer, with the highest radiogenic ^4He concentrations (2×10^{-4} ccSTP/g), and, hence oldest groundwater, toward the end of the inferred groundwater flow path at L 3 (Figure 4.2 b).

Recharge

Love et al. (2013) contended that recharge to the upper aquifer would occur at ephemeral rivers where the aquifer sub-crops or the upper aquitard is absent. Groundwater samples in the upper aquifer close to ephemeral rivers (samples U 3, U 4 and U 9) and waterholes (also samples U 3 and U 7) with $^{14}\text{C}_{\text{DIC}}$ residence times of <6 ka support this interpretation. Additionally, the chloride

concentrations in the upper aquifer samples U 3 and U 7 (<500 mg/L) are significantly lower than the surrounding upper aquifer (~3500 mg/L), and comparable to the surface water samples (<100 mg/L; Figure 4.7 a). However, radiogenic ^4He groundwater residence time estimates greater than several 10s ka at some of these locations (U 3 and U 7; Figure 4.7 d and e) indicate that modern water mixes with older water. Therefore, where ephemeral surface water features exist, even where the upper aquitard is present (Figure 4.2 a), the distribution of age tracers represents pulses of younger water punctuating the increasing age of groundwater along the flow paths. Whilst this was apparent for samples U 3, U 4, U 7 and U 9 ($^{14}\text{C}_{\text{DIC}}$ residence times of <6 ka) near surface water features, the spatial resolution of the dataset was insufficient to identify areas of recharge more precisely.

Groundwater samples further to the east and away from the ephemeral rivers (U 1, U 5, U 6 and U 10; Figure 4.4) have low ^{14}C values (<10 pMC) indicating little to no addition of modern water at these locations. Therefore, there is no evidence for preferential recharge in those upper aquifer samples located away from ephemeral rivers.

The stable water isotope data plot along a straight line with a low slope of 3.3 that is indicative of waters that have undergone evaporation as well as mixing (Figure 4.8 a). Considering that groundwater residence time can be >500 ka (radiogenic ^4He >1 x 10⁻⁵ ccSTP/g in U 1, L 2, L 3, L 4, L 9, L 11, B 7 and B 9), some of the groundwater would have been recharged during wetter climatic periods, consistent with previous work in the adjacent GAB (Love et al. 2013). Nevertheless, extrapolating the line to the LMWL suggests that recharge is predominantly from intense rainfall events with volumes between 80–100 mm/month (Keppel et al. 2015) being consistent with other areas in Central Australia (Harrington et al. 2002). S 3 (a water hole sample) and U 7, sitting off this common trend line are most likely explained by recent evaporated rainfall derived from smaller volume rainfall events.

Chemical processes

The data point of the stable water isotopes delta values plotted against chloride (Figure 4.8 c) do not show a straight-line relationship highlighting that processes other than simple evapotranspiration have been important. Groundwater mixing affects these tracers as well as recharge from evaporated surface water features. Preferential recharge from surface water features along the groundwater flow path allows mixing of modern, fresh groundwater with older,

saltier groundwater leading to groundwater in the centre of the study area with decreased residence times and chloride concentrations. The origin of the high salinity is most probably a fallout of marine and continentally derived salts from the atmosphere and a subsequent evaporative enrichment as has been described for other sedimentary basins of Australia (Herczeg et al. 2001) as well as dissolution of halite. Complete evaporation of all rainwater during some years, and the precipitation of the salts contained in it, followed by recharge, and re-dissolution of salts during wetter years could contribute to the halite signature. Chloride/bromide mass ratios consistently below the seawater dilution line (Figure 4.8 d) are evidence of halite dissolution, in addition to evaporation and mixing, control on chloride concentrations.

Upper and lower aquifers $\delta^{13}\text{C}$ ratios have a similar range representing similar origin $\delta^{13}\text{C}$; with $\delta^{13}\text{C}$ soil input and carbonate dissolution with no significant difference between the aquifers (Table 4.2). Because the $\delta^{13}\text{C}$ values between the aquifers are similar, it is not possible to distinguish mixing or enhanced inter-aquifer leakage using this tracer.

The upper aquifer $^{87}\text{Sr}/^{86}\text{Sr}$ ratios (0.712–0.714, excluding U 1) only show a small variation from the recharging groundwater (S 3 with $^{87}\text{Sr}/^{86}\text{Sr} = 0.712$), so weathering exchange in the upper aquifer may occur between atmospheric Sr (ca. 0.709) and aquifer minerals with an $^{87}\text{Sr}/^{86}\text{Sr}$ ratio of approximately 0.714. The lower aquifer and basement groundwater samples show slightly higher variability with $^{87}\text{Sr}/^{86}\text{Sr}$ ratios up to 0.719. Therefore, there may be more radiogenic ^{87}Sr in the minerals undergoing weathering in the lower aquifers. Mixing and enhanced inter-aquifer leakage from the upper aquifer may cause the large variability in $^{87}\text{Sr}/^{86}\text{Sr}$ ratios in the lower aquifer and basement samples, and this is examined further in section 3.6.2 below. However, it cannot be ruled out that weathering-derived $^{87}\text{Sr}/^{86}\text{Sr}$ may not be uniform across the aquifers.

Stagnant zones

The high salinity of the groundwater in the lower aquifer (L 11 and L 12, with 21,500 and 22,800 mg/L Cl, respectively; Figure 4.7 a) is seemingly at odds with its position in the upstream part of the lower aquifer flow field. While L 11 has ^{14}C above background (5.5 pMC; $^{14}\text{C}_{\text{DIC}}$ with a residence time of <30 ka), both L 11 and L 12 show substantial decay of ^{36}Cl , and high radiogenic ^4He concentrations indicating groundwater residence times up to several 100s ka (Figure 4.7 c, d and e). In these two locations, there could be mixing of old and a small amount of young water, or diffusion of ^{14}C , in the stagnant zones. Indeed the lower aquifer seems not to form a continuous

unit everywhere in the Arckaringa Basin as regions of low-permeability are known to occur (Howe et al. 2008; SKM 2009b). Suckow et al. (2016) reported similar findings for the Surat Basin. The origin of the high salinity is most likely evaporative enrichment of atmospherically-derived salts, as has been found for groundwater in sedimentary basins elsewhere in Australia (Herczeg et al. 2001). The relatively high salt concentration must indicate that the evaporative solute enrichment process acted with greater intensity on groundwater in this part of the aquifer than in other parts, which may be linked to much dryer climatic conditions in the past. This would mean that these saline groundwaters are no longer formed under the current hydrological conditions, and have been replaced by fresher groundwater in areas where there is active flow.

4.6.2 Inter-aquifer leakage

Diffuse inter-aquifer leakage

Density corrected freshwater heads at the well couplets show that downward leakage is possible throughout the majority of the study area. Where the lower aquitard is present, diffuse leakage is estimated to be $q_v < 1$ mm/yr.

Density corrected freshwater heads at well couplets located near the north-eastern spring discharge area (well couplets 1 and 3) indicate upward groundwater flow. Indeed, the age tracer values and $^{87}\text{Sr}/^{86}\text{Sr}$ ratio of sample U 1 are similar to the distribution in the lower but not to the upper aquifer: e.g. most radiogenic $^{87}\text{Sr}/^{86}\text{Sr}$ ratio, residence time of several 10s to 100s ka (high radiogenic ^4He concentration, low $^{36}\text{Cl}/\text{Cl}$ ratio and low ^{14}C value) and $^3\text{He}/^4\text{He}$ ratio $< 1 \times 10^{-7}$ (Figure 4.7 b, c, d, e and f). The interpretation of sample U 3 is less straightforward because it has high ^{14}C values with a $^{14}\text{C}_{\text{DIC}}$ residence time of < 30 ka in combination with a high ^4He concentration with a residence time of > 500 ka, and $^3\text{He}/^4\text{He}$ ratio $< 1 \times 10^{-7}$. Samples consisting of waters of different age are known to yield conflicting age tracer values (Bethke and Johnson 2008; Suckow 2013).

Enhanced inter-aquifer leakage

Where the lower aquitard is absent the hydraulic resistance is reduced and leakage between the aquifers increases up to $q_v = 7$ m/yr (Figure 4.4). The increased rate is consistent with the age tracer values suggesting mixing or addition of younger water in the lower aquifer where the aquitard is absent. This mixing is evident from lower radiogenic ^4He concentrations (L 8, L 4 and L

2), as well as higher ^{14}C values (L 8) and $^{36}\text{Cl}/\text{Cl}$ ratios (L 8 and L 2) if compared to surrounding groundwater samples from the lower aquifer and basement (Figure 4.7 c, d and e).

The areas where the lower aquitard is thin (<25 m) and with a higher incidence of tectonic features have been interpreted as areas where enhanced inter-aquifer leakage is most likely (Figure 4.4). It was hypothesised that zones of enhanced downward inter-aquifer leakage would be apparent from anomalies in age tracer values in the lower aquifer, and overlap in environmental tracer concentrations, or isotope ratios, between the upper aquifer and the lower aquitard. This seems to be the case at well couplet 10, and possibly at well couplets 7 and 9, because the age tracers indicate the addition of younger water to the lower aquifer and basement at L 10 and L 9 (indicated by $^{36}\text{Cl}/\text{Cl}$ and ^4He) and B 7 (indicated by $^{36}\text{Cl}/\text{Cl}$ and ^{14}C). The $^{87}\text{Sr}/^{86}\text{Sr}$ ratios are less radiogenic and more similar to the upper aquifer (L 9, L 10, B 7 and B 9), and furthermore, there is overlap in chloride concentration, $\delta^2\text{H}$ and $\delta^{18}\text{O}$ in the upper and lower aquifers at well couplet 10. At well couplets 7 and 9 the freshwater head difference is similar to most of the other couplets, but at site 10 the difference is less than 5 m. Moreover, a hydraulic connection between the aquifers at well couplet 10 may be indicated by a slight drawdown at U 10b, which was recorded during the pumping of groundwater from the lower aquifer (Figure 4.6). This could also explain why the pre-pumping head difference was small at this location. The reason for the inferred hydraulic connection at couplet 10 is unclear. Well couplet 10 is less than 3 km from an interpreted fault zone but without more detailed data on the structural geology the hydrogeological role of faults can not be ascertained. Well couplets 7 and 9 are also similar distances from interpreted fault zones, but at these locations the thinning and pinching out of the aquitard may also cause greater aquifer connectivity, because these couplets are located within 5 km from the inferred extent of the aquitard. Figure 4.4 summarises the locations of enhanced inter-aquifer leakage through the lower aquitard and downward leakage being identified by hydraulics and tracers.

Previous studies have used end member mixing mass balance models using $^{87}\text{Sr}/^{86}\text{Sr}$ ratios to estimate the proportion of inter-aquifer mixing (Dogramaci and Herczeg 2002; Shand et al. 2009). Attempts to use this model to quantify the mixing ratio between upper and lower aquifer groundwater for sample L 10, the site with the strongest indications for inter-aquifer leakage, are hampered by the difficulty of selecting appropriate $^{87}\text{Sr}/^{86}\text{Sr}$ ratio weathering end members. Clearer distinction between radiogenic ^4He concentrations in the upper and lower aquifer and less spatial variation within each aquifer make selecting radiogenic ^4He end members relatively easier.

This is also due to order of magnitude differences in the radiogenic ^4He concentrations compared to the Sr isotopes. As such, either L 12 or B 9 could be representative of the lower aquifer and U 10 for the upper aquifer. Following the mixing calculations in Faure (1986) using both $^{87}\text{Sr}/^{86}\text{Sr}$ ratios and radiogenic ^4He concentrations up to 80–95% of groundwater in L 10 could originate from the upper aquifer (Figure 4.9 a and b).

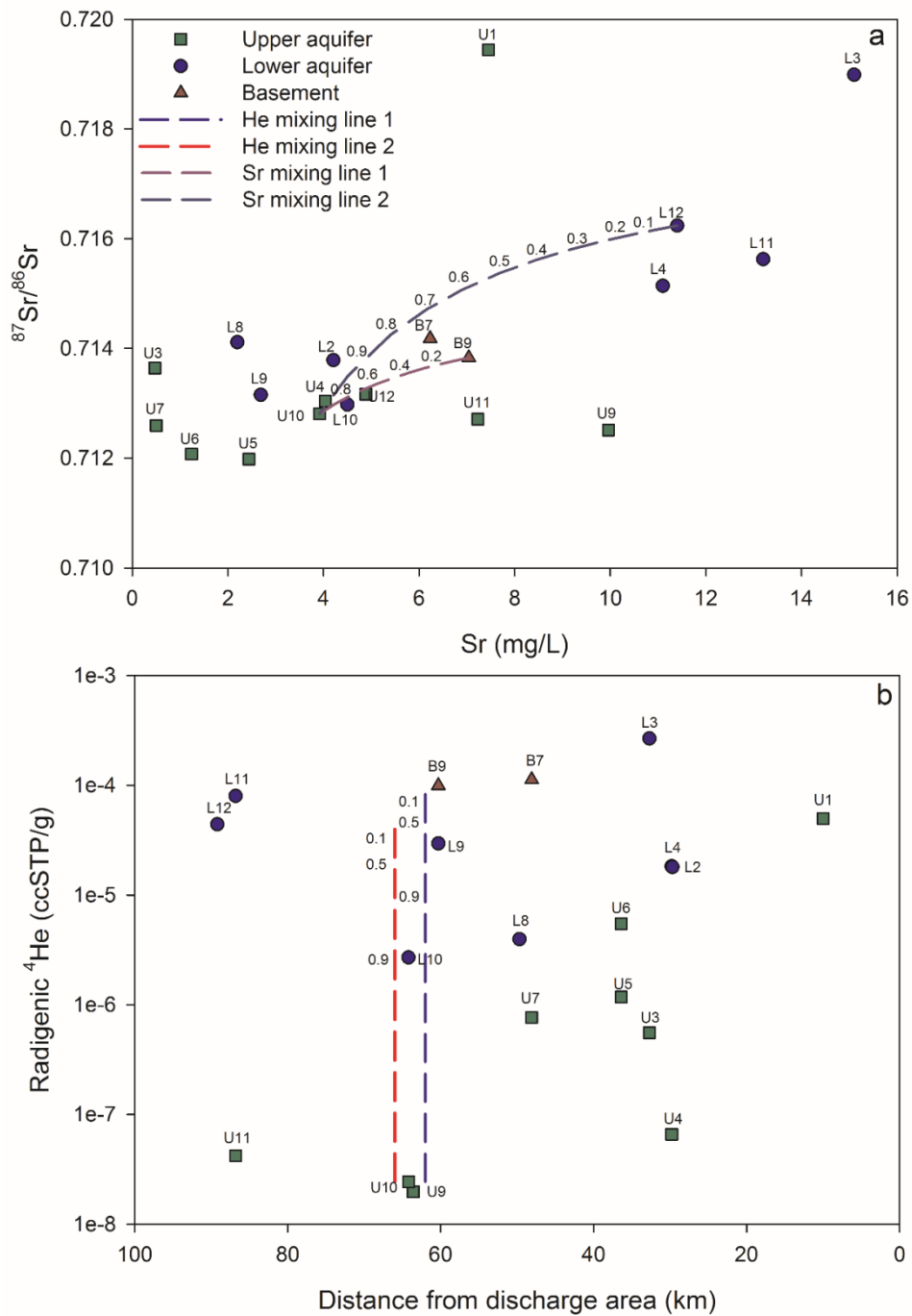


Figure 4.9 (a) $^{87}\text{Sr}/^{86}\text{Sr}$ ratio plotted against Sr concentration. The two theoretical end-member mixing lines for well couplet 10 are shown with U 10 representing the upper aquifer end member and L 12 (dark blue dashed line) or B 9

(purple dashed line) representing the lower aquifer end member. Mixing lines labelled with fraction of upper aquifer sample. (b) Radiogenic ^4He concentration plotted against distance from the discharge area. Given that L 12 (red dashed line) or B 9 (blue dashed line) may be representative of the lower aquifer and U 10 represents the upper aquifer, the two theoretical end-member mixing lines have been calculated for well couplet 10. The two mixing lines have been arbitrarily placed on the x-axis alongside well couplet 10. Mixing lines labelled with fraction of upper aquifer sample.

4.6.3 Evaluation of method

This study evaluated a comprehensive approach to investigate inter-aquifer leakage on a regional-scale where only limited wells are available. However, it is noted that the collection and analyses of multiple environmental tracers is costly and may prohibit the use of this method elsewhere. The usefulness of each of the investigation methods, or combinations thereof, is therefore summarised in Table 4.3 and discussed below.

Table 4.3 Evaluation of the individual ‘tools’ used in the method to identify enhanced inter-aquifer leakage

Method component	Beneficial in this study to identify enhanced inter-aquifer leakage?		Enhanced inter-aquifer leakage sites identified	Recharge and other groundwater flow trends identified
	Yes/no	Reason		
Interpreted fault collation	No	Not all identified faults are hydraulically active. Possibly useful to explain leakage mechanism but need to establish which formations are intersected.	—	—
Aquitard thickness	No	Useful to calculate hydraulic resistance and highlights where potential recharge and inter-aquifer mixing could occur.	—	Low hydraulic resistance at well couplets 4, 8, 11 and 13.
Well couplet density corrected heads	Yes	Useful to indicate direction of inter-aquifer leakage. Small density-corrected freshwater head differences indicated locations of possible inter-aquifer leakage.	Similar density-corrected freshwater hydraulic heads where the lower aquitard is present at well couplets 1, 10 and 17.	Similar density-corrected freshwater hydraulic heads at well couplets 4, 8 and 14.
Hydraulic head changes with pumping (pumping test equivalent)	Yes	Useful to identify head response in an adjacent aquifer to the pumped aquifer when adjacent aquifer not being exploited.	Identified head difference in the upper aquifer in well couplet 10 (U 10b).	—
Major solutes (Cl concentration)	No	Not very useful in this location because generally there is overlap in major solute concentrations in the aquifers.	Similar Cl concentrations at well couplets 4 and 10.	—

Stable isotopes of water	No	Not useful in this location because generally overlap in the stable isotopes of water in the aquifers.	Similar $\delta^2\text{H}$ and $\delta^{18}\text{O}$ in the upper and lower aquifers at well couplet location 3 and 10.	Recharge from high intensity rainfall events.
$\delta^{13}\text{C}$	No	Not useful in this location because generally there is overlap in $\delta^{13}\text{C}$ in the aquifers and possibly organic matter in the aquifer sediment.	Similar $\delta^{13}\text{C}$ in the upper and lower aquifers at well couplet location 10.	—
$^{87}\text{Sr}/^{86}\text{Sr}$	Yes	Useful to identify upper and lower aquifer $^{87}\text{Sr}/^{86}\text{Sr}$ ratios with overlap indicative of inter-aquifer leakage and calculate mixing proportions.	Similar $^{87}\text{Sr}/^{86}\text{Sr}$ ratios to upper aquifer in lower aquifer at well couplets 7, 9 and 10. U 1 has the most radiogenic $^{87}\text{Sr}/^{86}\text{Sr}$ ratio consistent with lower aquifer.	Identified similar $^{87}\text{Sr}/^{86}\text{Sr}$ ratio at well couplets 2, 4 and 8.
^{14}C	Yes	Useful to identify addition of different age groundwater along flow paths (applicable from few hundred years to ~30 ka).	Identified lower ^{14}C concentration groundwater at U 1, L 11 and L 12. Identified higher ^{14}C concentration groundwater at B 7.	Identified higher ^{14}C concentration groundwater at U 3, U 4, U 7 and U 9.
$^{36}\text{Cl}/\text{Cl}$	Yes	Useful to identify addition of different age groundwater along flow paths (applicable from ~50 ka to 1 Ma).	Identified higher $^{36}\text{Cl}/\text{Cl}$ concentration groundwater at B 7 and L 10. Identified lower $^{36}\text{Cl}/\text{Cl}$ concentration groundwater at U 1.	Identified higher $^{36}\text{Cl}/\text{Cl}$ concentration groundwater at L 8, U 3, U 4, U 7, U 9 and L 8.
Radiogenic ^4He	Yes	Useful to identify addition of different age groundwater along flow paths (applicable from ~10 years).	Identified lower radiogenic ^4He concentrations at L 10. Identified higher radiogenic ^4He concentrations at U 1.	Identified lower radiogenic ^4He concentrations at L 2, L 4 and L 8.
$^3\text{He}/^4\text{He}$	Yes	Useful to identify separation of aquifers and addition of older groundwater (lower $^3\text{He}/^4\text{He}$ ratio).	Identified lower $^3\text{He}/^4\text{He}$ ratios at U 1 and U 3.	—
All data combined	Yes	Extremely useful to identify where multiple methods highlighted inter-aquifer leakage.	Identified enhanced inter-aquifer leakage into the lower aquifer at well couplet 10 and possibly at well couplets 7 and 9. Identified enhanced inter-aquifer leakage from the lower aquifer into the upper aquifer at well couplet 1.	—

The availability of well couplets was an essential prerequisite for the successful detection of inter-aquifer leakage. Based on the hydraulics and multiple environmental tracers enhanced inter-aquifer leakage could be identified at these sites. The similarities between environmental tracer

concentrations, or isotope ratios, in the upper and lower aquifer show that enhanced inter-aquifer leakage may be occurring where freshwater hydraulic heads are similar in both aquifers, such as exemplified by well couplet 10. Small head differences may thus be indicators of the presence of windows of enhanced permeability within the aquitard. Pumping from the lower aquifer and a respective drawdown in the upper aquifer supported the assertion of enhanced inter-aquifer leakage at well couplet 10. It requires, however, that no or minimal aquifer abstraction is occurring in one of the aquifers of interest (Neuman and Witherspoon 1972) which is not always the case.

Regional overviews of the hydraulic resistance of the lower aquitard and locations of interpreted faults were not useful to identify locations of enhanced inter-aquifer leakage. However, the hydraulic resistance and vertical Darcy flux provides an indication of diffuse inter-aquifer leakage direction and flow rate through the aquitard pores which can be extremely useful for regional-scale water balance models.

Some studies have been able to quantify mixing with other environmental tracers, such as Cl, $\delta^{13}\text{C}$ and the stable isotopes of water (Dogramaci and Herczeg 2002; Trabelsi et al. 2009; Wang et al. 2013); however, this was not possible in this study area as there was a range of values and no significant differentiation between the aquifers for those tracers. Radiogenic ^4He concentrations and $^{87}\text{Sr}/^{86}\text{Sr}$ ratios made it possible to quantify the proportion of enhanced inter-aquifer leakage at one site, but the difficulty in the identification of a suitable end member restricted the broad use of Sr.

In contrast, the clearest evidence came from the tracers that are transient in time. The use of three age tracers was found to be helpful for the purpose of this study. The different age tracers are applicable over different timescales which allows identification of enhanced inter-aquifer leakage of groundwater of different residence times. For example, addition of older groundwater to the upper aquifer at well location 1 was evidenced by a large variation in ^{14}C and $^{36}\text{Cl}/\text{Cl}$ but less obvious with regards to the respective radiogenic ^4He concentration. Alternatively, addition of younger groundwater to the lower aquifer at L 2, L 4, L 8 and L 10 was most obvious in the radiogenic ^4He concentration. Radiogenic ^4He is the most sensitive to these changes as it varied over five orders of magnitude, compared to just two orders of magnitude for ^{14}C and $^{36}\text{Cl}/\text{Cl}$. The use of transient tracers is especially important in large groundwater basins with groundwater residence times that can vary considerably. ^{14}C and $^{36}\text{Cl}/\text{Cl}$ values were found useful to identify

localised surface water recharge locations. The range of residence time tracers can give inconsistent results as in this study, but this provides a powerful tool to evaluate mixing of groundwater e.g. the presence of ^{14}C in very old waters suggest a younger component is likely to be present in the groundwater. Similar findings have been reported for other basins (Suckow et al. 2013), as well as theoretically (McCallum et al. 2017). Additionally, because of the low groundwater flow rates the vertical diffusion of age and other tracers may be more pertinent compared to areas with higher flow rates.

The protocol of well couplet hydrochemistry sampling and analysis methodologies proposed could be applied elsewhere to investigate inter-aquifer leakage at a regional-scale. A multi-tracer approach along with groundwater hydraulics provides a tool-set to investigate enhanced inter-aquifer leakage in a regional-scale sedimentary basin with a paucity of data. While the usefulness of individual environmental tracers as tools to identify enhanced inter-aquifer leakage is dependent on climatic, geological, hydrogeological and hydrochemical conditions, and just as in this study, it is possible that only some of the tracers would be useful, the authors strongly recommend the use of multiple environmental tracers, and especially multiple age tracers.

4.7 Conclusions

Inter-aquifer leakage between the GAB and Arckaringa Basin was analysed with sparse observation points using geological, hydrological and tracer information. An upper aquifer (GAB) and lower aquifer (Arckaringa Basin) are separated by an aquitard that can reach a thickness of up to 300 m but pinching out toward the western and eastern parts of the study area. The diffuse inter-aquifer leakage rates are estimated to be <1 mm/yr where the lower aquitard is thick and continuous. Inter-aquifer leakage rates are higher where the lower aquitard is absent, such as in the south-eastern part of the study area.

Recharge into the upper aquifer (GAB) from ephemeral streams and waterholes is recognised at several locations. Stable water isotope values indicate that recharge is derived mainly from high-intensity rainfall events. There is evidence for downward enhanced inter-aquifer leakage, in one region, where the lower aquitard is continuous. Moreover, there may be downward enhanced inter-aquifer leakage near the margin of the aquitard as well as upward enhanced inter-aquifer leakage in the spring discharge area. This spatial distribution could be the result of thinning of the aquitard or focused leakage surrounding fault zones. There is no evidence for enhanced inter-aquifer leakage in other areas of the groundwater system where the aquitard is present.

Considering there is evidence that preferential flow exists at some locations, it is possible that enhanced inter-aquifer leakage could occur at other locations across the basin, but the monitoring infrastructure lacks the resolution to establish this with certainty. Nevertheless it is an important outcome, especially from a management point of view. Any future development should be accompanied by a local-scale assessment of the nature of the leakage, supported by commensurate data, such as seismics to verify the continuity of layers.

A scarcity of wells can be a major obstacle when investigating inter-aquifer leakage locations and even the most comprehensive set of tracers can't solve that problem. However, this study provides baseline information at a regional-scale that can be used prior to increased groundwater abstraction for mining or other activities in the groundwater basin.

Chapter 5 Uranium geochemistry in the south-western margin of the Great Artesian Basin and Arckaringa Basin, central Australia

Submitted for publication consideration in Applied Geochemistry: Stacey C. Priestley, Vincent E. A. Post, Paul Shand, Andrew J. Love, Timothy E. Payne, Jennifer J. Harrison, Daniel L. Wohling (under review) Uranium geochemistry in the south-western margin of the Great Artesian Basin and Arckaringa Basin, central Australia

5.1 Abstract

The distribution of uranium isotopes (^{238}U and ^{234}U) in groundwaters of the south-western margin of the Great Artesian Basin (GAB), Australia, and underlying Arckaringa Basin were examined using groundwater samples and a sequential extraction of aquifer sediments. Rock weathering, the geochemical environment and α -recoil of daughter products control the ^{238}U and ^{234}U isotope distributions giving rise to large spatial variations. Generally, the shallowest aquifer (J aquifer) contains groundwater with higher ^{238}U activity concentrations and $^{234}\text{U}/^{238}\text{U}$ activity ratios close to secular equilibrium. However, the source input of uranium is spatially variable as intermittent recharge from ephemeral rivers passes through rocks that have already undergone extensive weathering and contain low ^{238}U activity concentrations. Other locations in the J aquifer that receive little or no recharge contain higher ^{238}U activity concentrations because localised uranium-rich rocks have been leached into solution and the geochemical environment allows the uranium to be kept in solution. The geochemical conditions of the deeper aquifers generally result in lower ^{238}U activity concentrations in the groundwater accompanied by higher $^{234}\text{U}/^{238}\text{U}$ activity ratios. The sequential extraction of aquifer sediments showed that α -recoil of ^{234}U from the resistate solid phase into the groundwater, rather than dissolution and/or exchange with the groundwater accessible minerals in the aquifer, caused enrichment of groundwater $^{234}\text{U}/^{238}\text{U}$ activity ratios in the lower aquifer. Decay of ^{238}U in uranium-rich coatings on J aquifer sediments caused resistant phase $^{234}\text{U}/^{238}\text{U}$ activity ratio enrichment. The groundwater $^{234}\text{U}/^{238}\text{U}$ activity ratio magnitude is dependent on groundwater residence time or flow rate, depending on the flow path trajectory. Thus, uranium isotope variations confirmed earlier groundwater flow interpretations based on other tracers; however, spatial heterogeneity, and the lack of clear regional correlations, made it difficult to identify recharge and inter-aquifer leakage.

5.2 Introduction

Uranium is a naturally occurring trace element, which if present in high concentrations can be of environmental health concern (Sidle and Lee 1996; Welch and Lico 1998; Sheppard et al. 2005; Vesterbacka et al. 2005; Atkins et al. 2016). The distributions of naturally occurring uranium isotopes in groundwater are complex and affected by many processes, providing analogues of anthropogenic nuclide migration, information on water-rock interactions as well as potentially tracing groundwater flow (Porcelli and Swarzenski 2003).

Aqueous uranium isotope distributions (^{238}U and ^{234}U) are controlled by a range of geochemical processes, including: inputs from weathering; addition or removal due to Eh-pH variations; solution and precipitation of more or less soluble daughter products; sorption or desorption from surfaces; alpha recoil (direct alpha-decay recoil of daughter products); recoil and vulnerability (leaching from weakened lattices due to alpha-decay); as well as production from parent atoms in solution or loss due to radioactive decay (Osmond and Cowart 1976; Gascoyne 1992; Osmond and Cowart 1992; Osmond and Ivanovich 1992; Porcelli and Swarzenski 2003). While clear interpretations of uranium isotope compositions and quantification of the processes responsible for change remain difficult (Porcelli and Swarzenski 2003), under favourable conditions these complex processes can provide insights into groundwater flow, recharge, discharge and inter-aquifer connectivity within groundwater systems.

In general, groundwater passing through the recharge zone where oxidising conditions prevail contains uranium mobilised in the 6+ state as uranyl ion (UO_2^{2+}). Where a change towards reducing conditions takes place, uranium concentrations rapidly decrease as uranium is deposited because the 4+ state forms relatively insoluble uranous phases (Gascoyne 1992; Osmond and Ivanovich 1992). Therefore, Eh-pH variations cause large variations in uranium concentrations. Uranium solubility can be enhanced by formation of carbonate, sulfate, chloride and other complexes, and uranium can be transported as colloids (Langmuir 1978). Uranium precipitated on grain surfaces as reducing conditions are encountered can be readily redissolved and transported forward if oxidising waters advance.

In a rock matrix undisturbed since 1–1.5 Ma the isotopes ^{238}U (half-life 4.47×10^9 years) and ^{234}U (half-life 2.45×10^5 years) are often in secular equilibrium ($^{234}\text{U}/^{238}\text{U}$ activity ratio = 1; Osmond and Ivanovich 1992). The $^{234}\text{U}/^{238}\text{U}$ activity ratio can decrease ($^{234}\text{U}/^{238}\text{U}$ activity ratio <1) due to dissolution of uranium bearing precipitates that have had ^{234}U preferentially removed, but this is

much rarer than a ^{234}U excess (Yanase et al. 1995; Porcelli and Swarzenski 2003; Payne and Airey 2006). Cherdyntsev et al. (1955) have shown that groundwater $^{234}\text{U}/^{238}\text{U}$ activity ratios are generally greater than secular equilibrium due to alpha decay of ^{238}U . Alpha decay of ^{238}U recoils the radiogenic progeny (^{234}Th) over a distance of 10–55 nm through crystalline media with a fraction ejected from the mineral grain into the pore water. The insoluble ^{234}Th is rapidly adsorbed on the grain surface and then promptly decays to ^{234}Pa (half-lives of 24.1 days and 6.69 hours, respectively), and then ^{234}U . The daughter ^{234}U , now residing on grain surfaces or in weakened crystal lattice sites, is more readily transferred into the pore water with these processes, which for simplicity are referred to as ‘ α -recoil’ (Andrews et al. 1982; Gascoyne 1992; Osmond and Ivanovich 1992; Porcelli and Swarzenski 2003; Méjean et al. 2016). It has also been suggested that ^{234}U oxidised during the recoil process remains in solution more readily compared to ^{238}U (Suksi et al. 2006). The addition of ^{234}U will not significantly increase the mass of uranium in solution but can greatly increase the $^{234}\text{U}/^{238}\text{U}$ activity ratio. Therefore, the $^{234}\text{U}/^{238}\text{U}$ activity depends upon the composition of the groundwater and numerous aquifer parameters including aquifer composition, water-rock ratio, fracture surfaces, as well as the duration of the recoil solution process (Andrews et al. 1982; Gascoyne 1992; Osmond and Ivanovich 1992; Porcelli and Swarzenski 2003).

A number of studies have used uranium activity concentrations and $^{234}\text{U}/^{238}\text{U}$ activity ratios to ‘finger print’ groundwater bodies and track groundwater flow paths. Where the uranium activity concentrations (or more commonly $^{234}\text{U}/^{238}\text{U}$ activity ratios) behave conservatively along groundwater flow paths any variability can potentially identify inter-aquifer mixing, identify source waters and determine proportion contributions of source waters. $^{234}\text{U}/^{238}\text{U}$ activity ratios and uranium activity concentrations have been used to determine mixing and spring source waters in carbonate aquifers in the Floridan aquifer, USA (Osmond et al. 1974), Judea Group aquifer, Israel (Rosenthal and Kronfeld 1982), and the Nubian aquifer, Egypt (Dabous and Osmond 2001). In Pahranaagat Valley, USA, two- or three-component mixing models of $^{234}\text{U}/^{238}\text{U}$ activity ratios and $^{87}\text{Sr}/^{86}\text{Sr}$ identified spring source waters (Paces and Wurster 2014). The conservative behaviour of $^{234}\text{U}/^{238}\text{U}$ activity ratios and other tracers helped identify groundwater flow paths in the vicinity of Yucca Mountain, USA (Paces et al. 2002) as well as groundwater mixing in the Otway Basin, Australia (Herczeg et al. 1996).

Uranium isotope variations have also been used to determine groundwater flow rates by either the ^{234}U excess decay model or alternatively, by determining the progressive augmentation by aquifer processes to constant values (Kronfeld et al. 1975; Ivanovich et al. 1991; Porcelli 2008).

Kronfeld and Rosenthal (1981) and Guttman and Kronfeld (1982) correlated the excess ^{234}U with aquifer thickness and residence time in the Bet Shean-Harod Valleys and Kefar Uriuua-Agur region, Israel, and similarly, Henderson et al. (1999) used the increase in excess ^{234}U due to α -recoil to determine pore water flow rates in the Great Bahama Bank pore waters. Ivanovich et al. (1991) determined groundwater flow rates using the decrease of excess ^{234}U in the Milk River aquifer, Canada. A one-dimensional reactive transport model that considered dissolution, precipitation and α -recoil was used to estimate the water residence time in the granitic Ringelbach catchment, France (Schaffhauser et al. 2014). Other studies found that excess ^{234}U depended more upon the radioelement distribution, extent of water-rock interaction and stabilisation of uranium complexes rather than groundwater residence time (Osmond et al. 1974; Andrews et al. 1982; Andrews and Kay 1983).

The groundwater redox conditions exert a major control on the distribution of uranium isotopes in the majority of groundwater basins, as found by Andrews and Kay (1982) in the Lincolnshire Limestone, England. Complexation with groundwater ligands can increase uranium concentration in groundwater, such as in the Delaware Basin, USA (Herczeg et al. 1988) and Central Valley, California, USA (Jurgens et al. 2010). Additionally, uranium distributions in some aquifers are a reflection of diverse vadose zone inputs that are preserved within the aquifer along different flow lines (Tricca et al. 2001), or predominantly influenced by weathering conditions rather than aquifer lithology (Kronfeld et al. 2004). Méjean et al. (2016) concluded that increased addition of excess ^{234}U (and the ^4He decay product) was locally controlled by stress-induced rock fracturing. Dhaoui et al. (2016) found groundwater uranium concentration to be controlled by mixing, α -recoil of ^{234}U and water-rock interactions in the Continental Intercalaire aquifer, Tunisia. Post et al. (2017) found that evapo-concentration of mobilised uranium caused high dissolved uranium concentrations in northern Burundi.

Multiple processes, which result in convoluted behaviours, generally affect the uranium isotopes. Nevertheless, the respective ^{234}U and ^{238}U activities can contain useful information about the flow system behaviour (Suksi et al. 2006; Chkir et al. 2009; Dhaoui et al. 2016) if the water-rock interactions can be determined. The sequential extraction procedure developed by Yanase et al. (1991) can be used to determine the distribution of uranium isotopes in operationally defined mineral phases. Payne et al. (2001) found that uranium lightly adsorbed to the aquifer sediments extracted during the Tamm's ammonium oxalate solution extraction step had a similar $^{234}\text{U}/^{238}\text{U}$ activity ratio to the associated groundwater. Dabous et al. (2002) using an analogous method for a

granite aquifer reported a similar result, with uranium lightly adsorbed to the aquifer sediments having a similar $^{234}\text{U}/^{238}\text{U}$ activity ratio to the associated groundwater.

Thus, by employing sequential extraction to study uranium distributions and isotope ratios in defined solid phases, there is the potential for significant new insights into uranium distributions and mobilisation mechanisms. In particular, the mild leaching step may enable the more mobile (accessible) phases to be estimated which are in relatively short-term exchange with the groundwater. In contrast, the more resistate phases are unlikely to be accessible to the groundwater, and the net loss or enrichment of uranium in these phases is more likely to be influenced by recoil fluxes of uranium isotopes. The present work explores the applicability of sequential extraction techniques in studying these exchange and recoil processes.

The Great Artesian Basin (GAB) and Arckaringa basin are regional groundwater resources in semi-arid central Australia used for agriculture, towns and mining (Habermehl 1980; Wohling et al. 2013; Keppel et al. 2015). It is important to understand connectivity between these groundwater basins and surface water catchments to determine potential risks to the system and to understand the processes affecting groundwater quantity and quality (Gleeson et al. 2012; Currell 2014). The objective of the study was to investigate uranium isotope distributions and the processes that control them in groundwater in the south-western margin of the GAB and underlying Arckaringa Basin. As well as collecting and analysing water samples, a sequential extraction of mineral phases containing uranium isotopes was undertaken on sediments from a geological sequence that intersects two of the key aquifers of interest in order to characterise water-rock interactions concerning uranium isotope distributions in groundwater. It is hypothesised that α -recoil, radioactive decay, addition or removal due to changes in redox conditions affect uranium activity concentrations and ratios. Their identification will help to support the interpretation of the groundwater flow, recharge, discharge and inter-aquifer connectivity based on groundwater uranium data.

5.3 Study area

The GAB is one of the world's largest aquifer systems underlying 22% of the Australian continent (Figure 5.1 inset). The GAB is composed of Jurassic-Cretaceous sediments and the main aquifer, the J aquifer, comprises fluvial and marine sandstones (Wopfner et al. 1970; Senior et al. 1978; Gallagher and Lambeck 1989; Toupin et al. 1997; Love et al. 2013). The J aquifer underlies the

Bulldog Shale, being confined throughout the eastern and north-western GAB, but unconfined in the south-western portion of the GAB (Freytag 1966; Love et al. 2013).

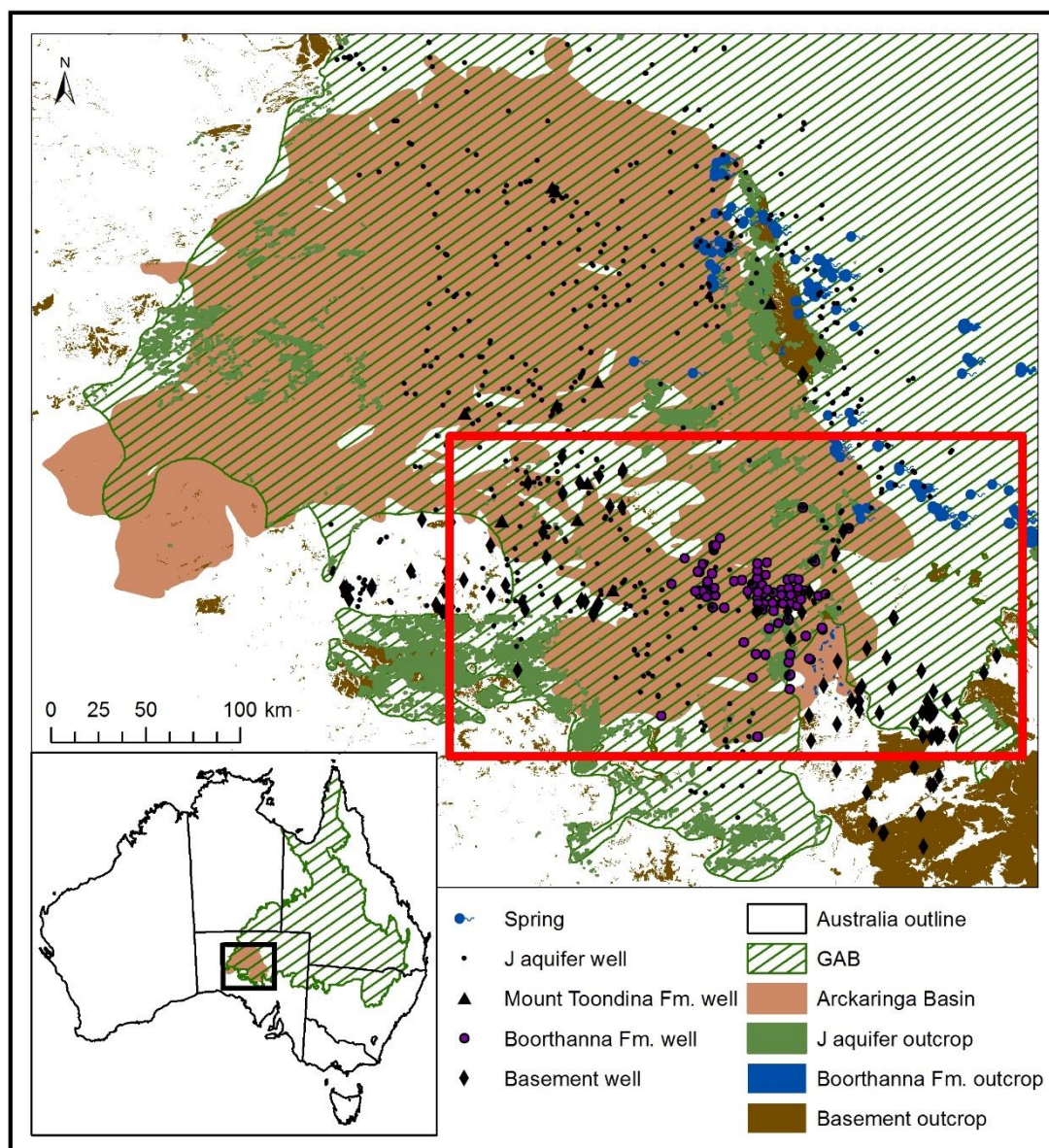


Figure 5.1 GAB and Arckaringa Basin extents with the location of wells in the J aquifer, Mt Toondina Fm., Boorthanna Fm. and basement, as well as J aquifer outcrop, Boorthanna Fm. outcrop and basement outcrop. The red rectangle is the study region (see Figure 5.2).

The Arckaringa Basin sits unconformably below the GAB and both are underlain by ‘basement’ that comprises Proterozoic-Archean crystalline metasedimentary and igneous rocks (Townsend and Ludbrook 1975; Ambrose and Flint 1980; Wohling et al. 2013; Keppel et al. 2015). Sub-basins and troughs have been formed within the Arckaringa Basin by glacial scouring during the Devonian-Carboniferous periods and faulting during the Early Permian (Toupin et al. 1997; Wohling et al. 2013; Keppel et al. 2015). The Arckaringa Basin consists of Carboniferous-Permian

sediments with the Boorthanna Fm., a marine and glacial sandstone, forming the main aquifer in the study area (Figure 5.2 b). The Mt Toondina Fm., a heterogeneous layered shale and sandstone formation lies directly below the J aquifer but is absent from most of the study area (Figure 5.2 b and Figure 5.3). The Stuart Range Fm., a mudstone/siltstone/shale aquitard, separates the J aquifer and Boorthanna Fm. throughout the majority of the study area (Figure 5.2 b and Figure 5.3).

There is substantially more hydrogeological information about the GAB than the Arckaringa Basin. This study focuses on the eastern portion of the Arckaringa Basin where the majority of groundwater wells have been drilled into the Boorthanna Fm. by the Prominent Hill mine for their operational and drinking water supplies (Figure 5.1; Wohling et al. 2013).

The potentiometric surface inferred from the available groundwater wells shows that groundwater flow in the Boorthanna Fm. is from the north-west toward the eastern margin of the basin (Figure 5.2 b). There is also some flow from the southern edge of the Arckaringa Basin north-east toward the regional discharge area. Groundwater flow in the J aquifer in the unconfined south-western margin of the GAB is from the west and south-west towards the groundwater springs and eastern margin of the Arckaringa Basin (Figure 5.2 a).

In this semi-arid part of central Australia, precipitation varies temporally and spatially; the average annual precipitation rate is estimated to be 120 mm/yr and surface waters are ephemeral (Allan 1990; McMahon et al. 2005). Recharge occurs to the J aquifer via diffuse recharge through the Bulldog Shale (<0.25mm/yr) and from ephemeral rivers (Love et al. 2013; Priestley et al. 2017). Recharge to the Boorthanna Fm. is most likely via diffuse discharge from the J aquifer where the Stuart Range Fm. is thin or absent as there are few locations where the aquifer crops out (Keppel et al. 2015). Both the J aquifer and Boorthanna Fm. converge in the discharge zone so groundwater discharges from the J aquifer into the Boorthanna Fm., and there is potentially discharge into the basement (Figure 5.2 c and Figure 5.3; Priestley et al. 2017). Additionally, there is evidence for inter-aquifer leakage from the J aquifer to the Boorthanna Fm. through the Stuart Range Fm. in the centre of the study area, as well as upward inter-aquifer leakage near the springs (Figure 5.2 c; Priestley et al. 2017).

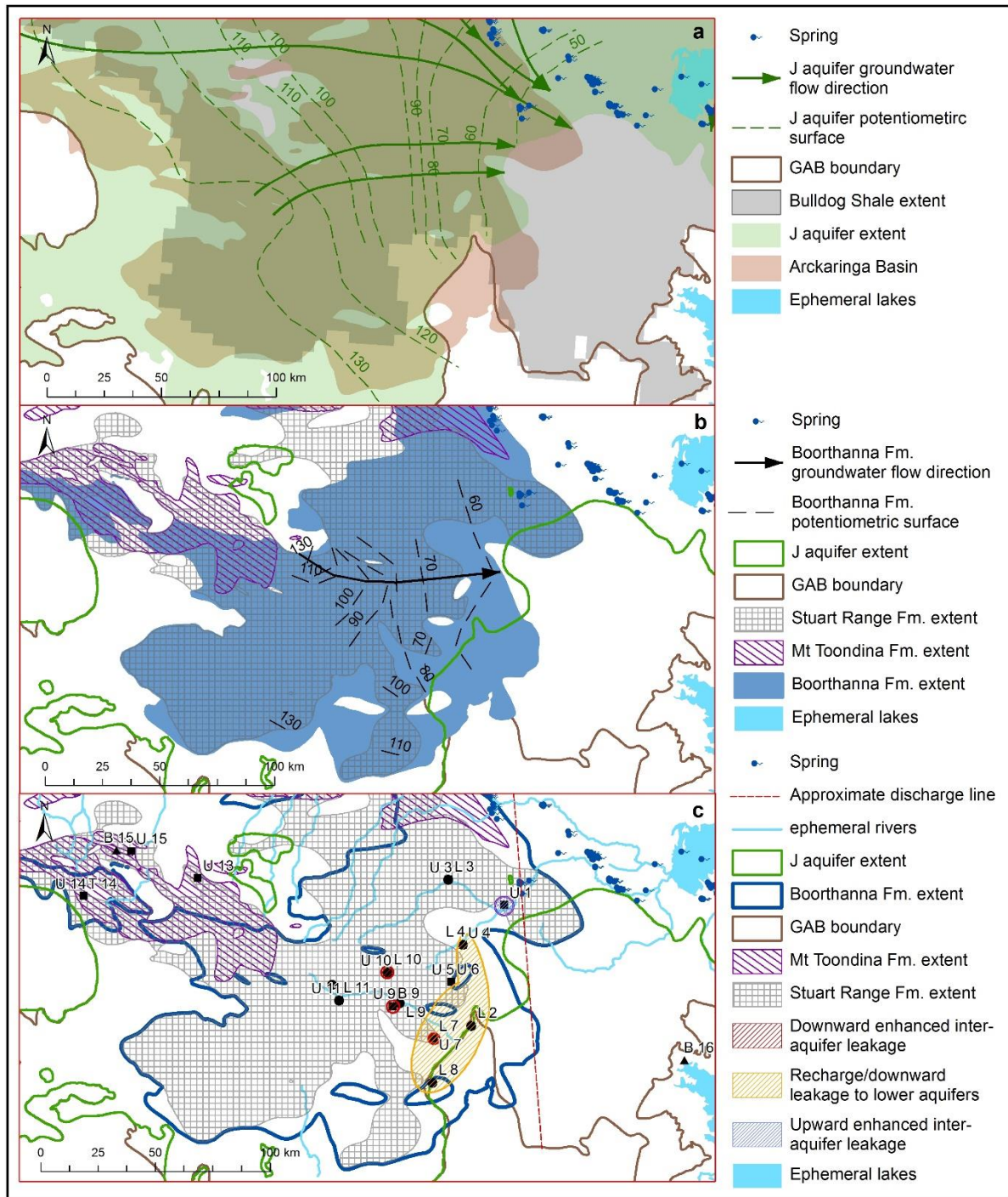


Figure 5.2 Potentiometric surface and generalised groundwater flow path for (a) the J aquifer, (b) the Boorthanna Fm. and (c) inter-aquifer leakage and recharge locations, and approximate discharge line from Priestley et al. (2017). Sampled wells are labelled U from the J aquifer, L from the Boorthanna Fm. and B from the basement.

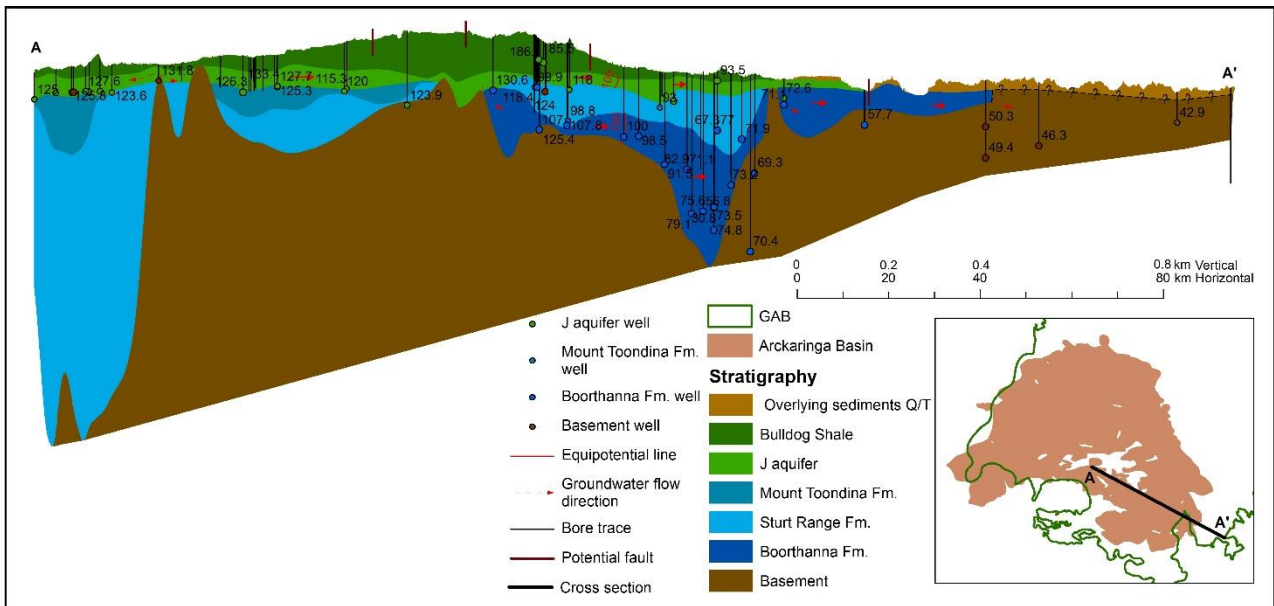


Figure 5.3 Hydrogeological transect from A to A' through the study area showing stratigraphy, well depths labelled with density corrected freshwater hydraulic head and interpreted groundwater flow directions.

5.4 Methods

5.4.1 Groundwater samples

Groundwater samples were collected from pastoral production wells as well as mining, monitoring and production wells within the GAB and Arkaringa Basin between November 2013 and May 2014. Wells were selected along a north-west to south-east transect along a groundwater flow path interpreted from potentiometric contours. Some targeted wells were excluded from sampling because the submersible pump was too large or the water recovery during pumping was too slow. The locations of the samples are shown in Figure 5.2 c and samples labelled U are from the J aquifer, L are from the Boorthanna Fm. and B are from the basement aquifers (Table 5.1). Water samples were collected in rinsed containers after a minimum of three well volumes had been purged and when the field measured parameters (pH, electrical conductivity (EC), Reduction Potential (Eh) and temperature) had stabilised. Field parameters were measured using a calibrated YSI Professional Plus handheld multiparameter meter with ORP readings converted into Eh corrected to SHE (Standard Hydrogen Electrode). The samples were collected for a variety of chemical and isotope analyses including: anions (125 mL HDPE Bottle, 0.45µm filtered), ¹⁴C (1 L HDPE Bottle, unfiltered), ³⁶Cl/Cl (500 mL HDPE bottle, unfiltered), as well as uranium isotopes (5 L HDPE bottle, acidified to pH <1 with HCl).

Anion concentrations were measured by ion chromatography using method 4110 in APHA (1998) by the Analytical Services Unit, Commonwealth Scientific and Industrial Research Organisation (CSIRO). The coefficient of variance for these methods is <5%. ^{14}C isotope ratios of Dissolved Inorganic Carbon (DIC) were analysed by accelerator mass spectrometry (AMS) by Rafter Radiocarbon Laboratory and precision is reported at 1 standard deviation of the mean (Stuiver and Polach 1977). $^{36}\text{Cl}/\text{Cl}$ analysis was completed using a combination of a high efficiency ion source, tandem acceleration and heavy-ion detection and identification techniques with a precision of $\leq 3\%$ (Fifield et al. 2010) by the Department of Nuclear Physics at The Australian National University (ANU).

^{234}U and ^{238}U were analysed by alpha spectrometry in the Radioanalytical Chemistry Laboratory, Australian Nuclear Science and Technology Organisation (ANSTO). The procedures were based on standard radiochemical techniques described in Harrison et al. (2011). After addition of a ^{232}U radiotracer spike to each groundwater sample, Fe (III) solution was added to the solution, then the pH was adjusted to pH = 8 to precipitate iron hydroxide. The iron hydroxide precipitate was separated from the solution, then redissolved in 3M HNO_3 and loaded onto stacked TEVA[®] and TRU[®] prepacked ion exchange chromatography resins. Uranium was retained on TRU[®] Resin and was eluted using 0.1 M ammonium bioxalate. The separated uranium solutions had cerium carrier and HF added to produce cerium fluoride micro-precipitate alpha sources for measurement using alpha spectrometry with uncertainties reported in Table 5.1. Similarly to Carvalho and Oliveira (2009) uranium concentrations were calculated from the alpha spectrometry results using the specific activity of ^{238}U and corrected for the presence of ^{235}U . For verification purposes, uranium concentrations were also measured by ICP-MS in the ANSTO Analytical Chemistry Laboratory using Method VI 2809 with quantification limits between 1 to 10 ppb.

5.4.2 Core samples

A core through the basins located next to wells U 11 and L 11 (Figure 5.2 c) was drilled using HQ diamond (60 mm inner diameter, 95 mm outer diameter) and mud rotary methods to 110.4 m below ground surface in March 2015 (Kleinig et al. 2015). This core was selected for this study because the top section traverses the J aquifer, and the bottom section intersects the Boorthanna Fm. The intervening section traverses the Stuart Range Fm. aquitard that separates the two key aquifers of interest to our study.

The top section of the core samples (0–17.8 m) comprise dark grey-brown, silty clay with trace sand sequences of the Bulldog Shale aquitard, the subsequent samples comprised medium-to-coarse-grained sand sequences of the J aquifer (17.8–46.6 m). The succeeding samples comprise variable grey and brown consolidated claystone samples with thin (<50 mm) sandstone interbeds and gradational sequences of the Stuart Range Fm. aquitard (46.6–104.0 m) and the bottom samples (104–110.4 m) intersected the Boorthanna Fm. which comprised grey sandstone with poorly sorted sand with a moderate percentage of clay.

Core samples for sequential extraction and XRD analysis were vacuum-sealed in two Food Saver® bags in the field during drilling. Quantitative XRD analysis of milled core samples for mineral phase identification was undertaken by the Mineralogical Services laboratory at CSIRO Land and Water using Method AS 1289.6.7.3-1999 (Standards Australia 1999).

The sequential extraction procedure was used to determine the distribution of uranium in three operationally defined phases of core samples (Yanase et al. 1991): adsorbed elements, carbonate minerals and amorphous iron minerals were extracted using Tamm's ammonium oxalate solution; then crystalline iron minerals, clay and some refractory minerals were extracted using 6M HCl; finally all remaining resistate minerals were extracted by fusion. Yanase et al. (1991) outlined the extraction specifications for both the Tamm's ammonium oxalate solution and 6M HCl. The fusion extraction procedure is outlined in IAEA (2009). Once the extraction solution was separated from remaining sediment, the separation and measurement of ^{234}U and ^{238}U was the same as for groundwater samples.

5.5 Results

5.5.1 Uranium isotopes in groundwater

There are large variations in solute uranium concentrations and element ratios in the groundwater sampled throughout the western margin of the GAB (Table 5.1). Total uranium concentrations ranged from 0.02 to 19.08 $\mu\text{g}/\text{kg}$, ^{238}U activity concentrations ranged from 0.2 mBq/kg to 236 mBq/kg, and ^{234}U activity concentrations range from 0.6 mBq/kg to 462 mBq/kg (Table 5.1). The $^{234}\text{U}/^{238}\text{U}$ activity ratios range from almost secular equilibrium (1.09) up to 26.6 (Table 5.1). These values do not display any regional trend. Both high and low ^{238}U activity concentrations and $^{234}\text{U}/^{238}\text{U}$ activity ratios occur throughout the groundwater basins (Figure 5.4 a and b). There is no

obvious relationship between ^{238}U activity concentration and distance along the generalised groundwater flow path (Figure 5.5 a).

Measured ^{14}C concentrations varied from 0.58 (background) to 89.2 pMC and measured $^{36}\text{Cl}/\text{Cl}$ ratios range from 4.8×10^{-15} to 82.9×10^{-15} (Table 5.1). As the half-life of ^{14}C is 5730 years (Godwin 1962; Plummer and Glynn 2013) those samples with $^{14}\text{C} > 40$ pMC (U 3, U 4, U 7, U 9 and L 8) are likely to contain ^{14}C with a residence time of < 6 ka and remaining samples with ^{14}C above 1 pMC are likely to contain ^{14}C with a residence time of < 30 ka (Priestley et al. 2017). The half-life of ^{36}Cl is 3.01×10^5 years (Bentley et al. 1986; Phillips 2013), so where there has been substantial decay of ^{36}Cl ($^{36}\text{Cl}/\text{Cl} < 45 \times 10^{-15}$; U 1, L 2, L 3, L 4, L 9, L 11, L 12, B 7 and B 9) groundwater residence times could be up to 100s ka. Differing groundwater age tracer values ($^{36}\text{Cl}/\text{Cl}$; Figure 5.4 c) highlight the importance of mixing of different 'age' groundwater in the study area (Priestley et al. 2017).

There is a relationship between ^{238}U activity concentration and depth (Figure 5.5 b). All of the wells with an average depth > 60 m below the water table, or top of potentiometric surface where confined have low ^{238}U activity concentrations (less than 2.5 mBq/kg), whereas the wells with shallower depth below water table (< 60 m) have ^{238}U activity concentrations ranging from 0.2 mBq/kg up to 235 mBq/kg (Figure 5.5 b). Some of the higher total uranium activity concentrations (U 5 and U 7; Table 5.1) exceed the Australian drinking water regulations of 17 $\mu\text{g}/\text{L}$ (NHMRC and NRMCC 2011).

There is no correlation between ^{238}U activity concentration with Eh, EC, pH, alkalinity, ^{14}C and $^{36}\text{Cl}/\text{Cl}$ ratios (Figure 5.5 c – f). There are both low and high ^{238}U activity concentrations across the range of Eh (-79–412 mV), pH (5.7–8.2 pH), alkalinity (0.5–6.2 mmol/L), ^{14}C (0.58–89.19 pMC) and $^{36}\text{Cl}/\text{Cl}$ (4.8×10^{-15} – 82.9×10^{-15}) measurements (Figure 5.5 c – f; Table 5.1), although the high ^{238}U activity concentrations are generally in those samples with ^{14}C concentrations less than 11 pMC (Figure 5.5 g). The EC measurements range from 1–120 mS/cm, so the groundwater in the region ranges from fresh to brine. The highest ^{238}U activity concentrations (8–235 mBq/kg) are generally in the brackish to fresh groundwater samples (EC between 1–34 mS/cm); except for B 16, which is classified as brine (EC of 78 mS/cm) (Figure 5.5 d).

Table 5.1 Element concentrations and isotope ratios of groundwater sampled throughout the study area as well as the major uranium species in solution

Well Name	Aquifer	Total U (µg/L)	²³⁸ U (mBq/kg)	²³⁴ U (mBq/kg)	²³⁴ U/ ²³⁸ U activity ratio	Specific EC (mS/cm)	pH	Eh (mV)	Cl (mmol/L)	Total alkalinity as HCO ₃ (mmol/L)	³⁶ Cl/Cl (x10 ⁻¹⁵)	¹⁴ C (pMC)	Major species in solution ^a	CO ₃ ²⁻ activity ^b
U 1	J aquifer	0.04	0.5 ± 0.1	2.1 ± 0.2	4.32 ± 0.6	13.8	7.4	110	115.5	1.6	11.8 ± 1.1	9.70 ± 0.10	UO ₂ (CO ₃) ₃ ⁴⁻	1.5 × 10 ⁻⁶
U 3	J aquifer	0.07	0.9 ± 0.1	1.5 ± 0.1	1.65 ± 0.2	1.7	5.7	412	12.9	0.8	66.4 ± 3.2	71.6 ± 0.19	UO ₂ (CO ₃) ₂ ²⁻	1.8 × 10 ⁻⁸
U 4	J aquifer	0.70	8.6 ± 0.5	10.7 ± 0.6	1.25 ± 0.05	12.8	6.2	239	98.6	0.5	55.5 ± 2.7	45.8 ± 0.18	UO ₂ (CO ₃) ₃ ⁴⁻ , UO ₂ (CO ₃) ₂ ²⁻	3.5 × 10 ⁻⁸
U 5	J aquifer	17.30	214 ± 11.4	284 ± 15.1	1.33 ± 0.02	3.0	7.0	133	18.6	3.5	78.4 ± 3.5	5.58 ± 0.09	UO ₂ (CO ₃) ₃ ⁴⁻ , UO ₂ (CO ₃) ₂ ²⁻	1.4 × 10 ⁻⁶
U 6	J aquifer	0.02	0.2 ± 0.05	0.7 ± 0.1	3.63 ± 1.0	2.7	7.6	-79	18.0	2.2	74.0 ± 3.4	10.02 ± 0.10	UO ₂ (CO ₃) ₃ ⁴⁻ , U(OH) ₄	1.6 × 10 ⁻⁵
U 7	J aquifer	19.08	236 ± 12.6	462 ± 24.4	1.96 ± 0.02	1.0	7.7	130	2.2	5.3	82.9 ± 4.9	89.2 ± 0.28	UO ₂ (CO ₃) ₃ ⁴⁻	1.1 × 10 ⁻⁵
U 9	J aquifer	1.83	22.6 ± 1.4	57.2 ± 3.2	2.53 ± 0.1	24.5	7.0	239	214.1	1.2	78.8 ± 3.6	40.0 ± 0.17	UO ₂ (CO ₃) ₃ ⁴⁻ , UO ₂ (CO ₃) ₂ ²⁻	4.2 × 10 ⁻⁷
U 10	J aquifer	0.46	5.7 ± 0.5	9.9 ± 0.7	1.76 ± 0.1	11.9	6.3	389	122.0	1.7	53.4 ± 2.7	7.08 ± 0.10	UO ₂ (CO ₃) ₂ ²⁻ , UO ₂ (CO ₃) ₃ ⁴⁻	1.3 × 10 ⁻⁷
U 11	J aquifer	12.97	160 ± 8.7	184 ± 9.9	1.15 ± 0.02	16.8	6.5	381	180.0	2.0	50.4 ± 2.6	7.40 ± 0.10	UO ₂ (CO ₃) ₃ ⁴⁻ , UO ₂ (CO ₃) ₂ ²⁻	2.2 × 10 ⁻⁷
U 13	J aquifer	11.52	142 ± 7.8	156 ± 8.5	1.09 ± 0.02	34.6	7.8	346	298.6	2.0	38.6 ± 2.2	1.83 ± 0.09	UO ₂ (CO ₃) ₃ ⁴⁻	3.3 × 10 ⁻⁶
U 14	J aquifer	0.09	1.1 ± 0.1	2.1 ± 0.2	1.87 ± 0.2	70.4	6.0	311	701.4	1.4	49.0 ± 2.5	4.98 ± 0.09	UO ₂ (CO ₃) ₃ ⁴⁻ , UO ₂ (CO ₃) ₂ ²⁻	5.2 × 10 ⁻⁸
U 15	J aquifer	0.28	3.4 ± 0.2	4.7 ± 0.3	1.36 ± 0.1	66.5	7.3	329	650.7	1.5	29.8 ± 1.9	10.53 ± 0.10	UO ₂ (CO ₃) ₃ ⁴⁻	7.5 × 10 ⁻⁷
T 14	Mt Toondina Fm.	0.02	0.3 ± 0.04	0.6 ± 0.1	2.20 ± 0.4	119.7	6.0	310	1371.8	1.7	37.3 ± 2.3	1.40 ± 0.09	UO ₂ (CO ₃) ₃ ⁴⁻ , UO ₂ (CO ₃) ₂ ²⁻	5.2 × 10 ⁻⁸
L 2	Boorthanna Fm.	3.77	46.6 ± 2.5	145 ± 7.5	3.10 ± 0.1	12.2	7.2	61	95.8	3.9	44.5 ± 2.7	10.99 ± 0.10	UO ₂ (CO ₃) ₃ ⁴⁻	2.3 × 10 ⁻⁶
L 3	Boorthanna Fm.	0.02	0.3 ± 0.1	0.7 ± 0.1	2.02 ± 0.4	18.8	7.0	331	210.7	2.6	9.9 ± 1.0	23.44 ± 0.12	UO ₂ (CO ₃) ₃ ⁴⁻	1.0 × 10 ⁻⁶
L 4	Boorthanna Fm.	0.04	0.5 ± 0.1	2.6 ± 0.2	5.03 ± 0.6	16.1	7.2	-28	126.8	3.0	26.5 ± 1.7	5.51 ± 0.09	UO ₂ (CO ₃) ₃ ⁴⁻	1.6 × 10 ⁻⁶
L 8	Boorthanna Fm.	3.25	40.2 ± 2.4	109.3 ± 6.0	2.72 ± 0.1	7.6	7.0	108	50.7	5.9	45.3 ± 2.4	44.99 ± 0.14	UO ₂ (CO ₃) ₃ ⁴⁻	1.9 × 10 ⁻⁶
L 9	Boorthanna Fm.	0.20	2.5 ± 0.2	16.9 ± 0.9	6.87 ± 0.4	10.8	7.1	11	78.9	3.3	37.9 ± 2.3	2.58 ± 0.07	UO ₂ (CO ₃) ₃ ⁴⁻	1.7 × 10 ⁻⁶
L 10	Boorthanna Fm.	0.07	0.8 ± 0.1	10.0 ± 0.6	12.2 ± 1.3	13.9	7.0	368	141.7	4.9	49.5 ± 2.5	0.92 ± 0.09	UO ₂ (CO ₃) ₃ ⁴⁻	1.7 × 10 ⁻⁶
L 11	Boorthanna Fm.	0.03	0.4 ± 0.2	2.0 ± 0.4	4.84 ± 2.2	47.8	8.2	-32	605.6	6.2	8.4 ± 0.9	5.53 ± 0.10	UO ₂ (CO ₃) ₃ ⁴⁻	2.1 × 10 ⁻⁵

L 12	Boorthanna Fm.	0.09	1.1 ± 0.1	15.0 ± 0.8	13.6 ± 1.3	52.2	7.2	342	642.3	2.5	4.8 ± 0.9	0.58 ± 0.09	UO ₂ (CO ₃) ₃ ⁴⁻	9.8 × 10 ⁻⁷
B 7	Basement	0.11	1.4 ± 0.1	37.1 ± 2.0	26.6 ± 1.9	18.7	7.0	-17	152.1	4.1	44.1 ± 2.3	13.13 ± 0.10	UO ₂ (CO ₃) ₃ ⁴⁻	1.3 × 10 ⁻⁶
B 9	Basement	0.12	1.5 ± 0.1	14.2 ± 0.8	9.64 ± 0.7	21.6	6.9	41	194.4	3.6	23.2 ± 1.7	3.10 ± 0.08	UO ₂ (CO ₃) ₃ ⁴⁻	9.7 × 10 ⁻⁷
B 15	Basement	0.19	2.3 ± 0.2	3.8 ± 0.3	1.63 ± 0.1	59.2	6.6	316	574.6	0.8	35.8 ± 2.1	32.2 ± 0.14	UO ₂ (CO ₃) ₃ ⁴⁻ , UO ₂ (CO ₃) ₂ ²⁻	9.2 × 10 ⁻⁸
B 16	Basement	5.96	73.6 ± 4.1	254 ± 13.5	3.45 ± 0.1	78.6	6.6	126	816.9	4.2	40.3 ± 2.2	1.06 ± 0.08	UO ₂ (CO ₃) ₃ ⁴⁻	4.7 × 10 ⁻⁷

^a Speciation calculated using PHREEQC speciation model and SIT (Specific ion Interaction Theory) aqueous model. Species making up >80% of species in solution given.

^b Activity of CO₃²⁻ in solution given by the PHREEQC speciation model.

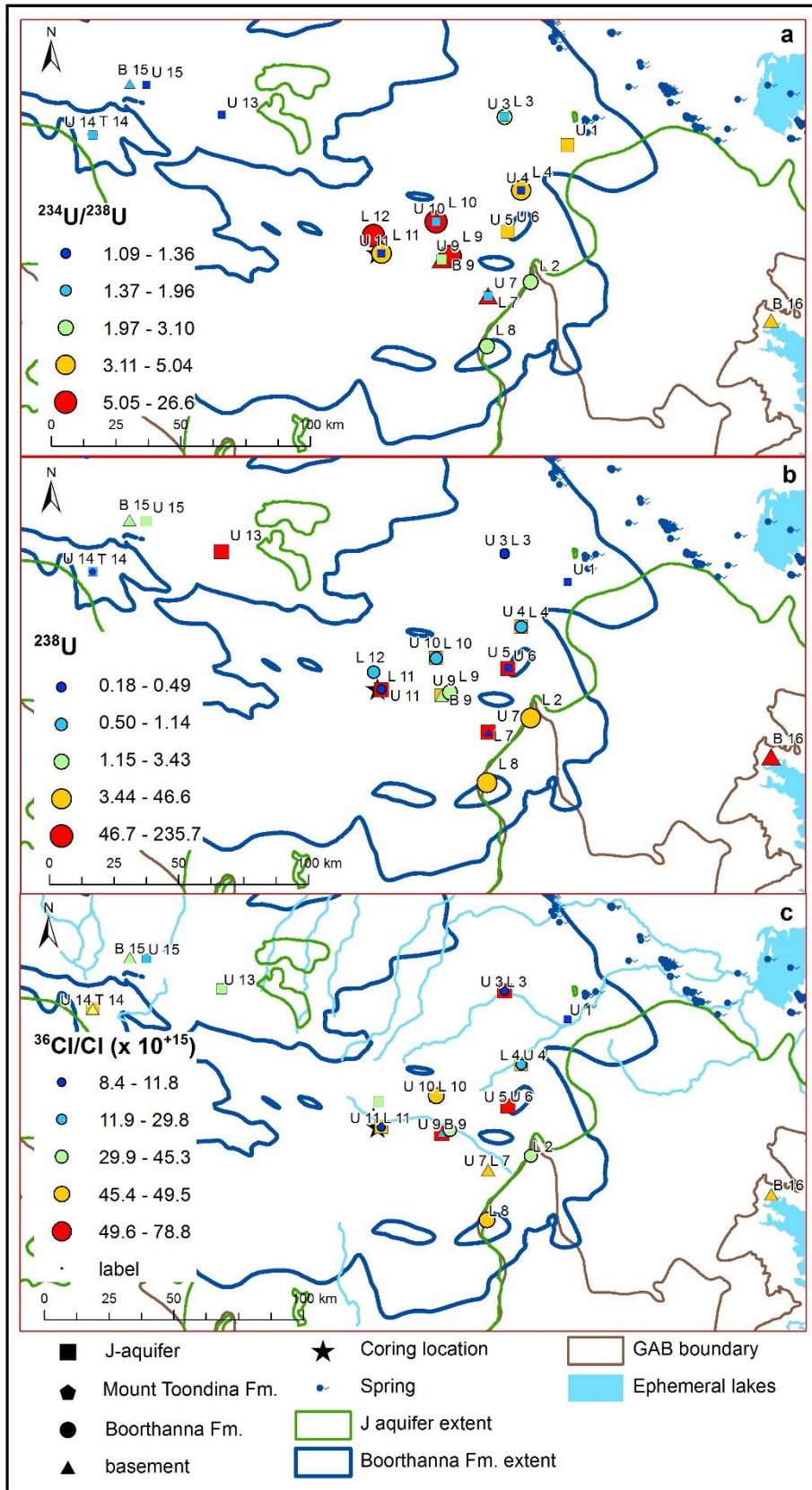


Figure 5.4 (a) Uranium activity concentration, (b) Uranium activity ratios and (c) $^{36}\text{Cl}/\text{Cl}$ ratios in the groundwater samples

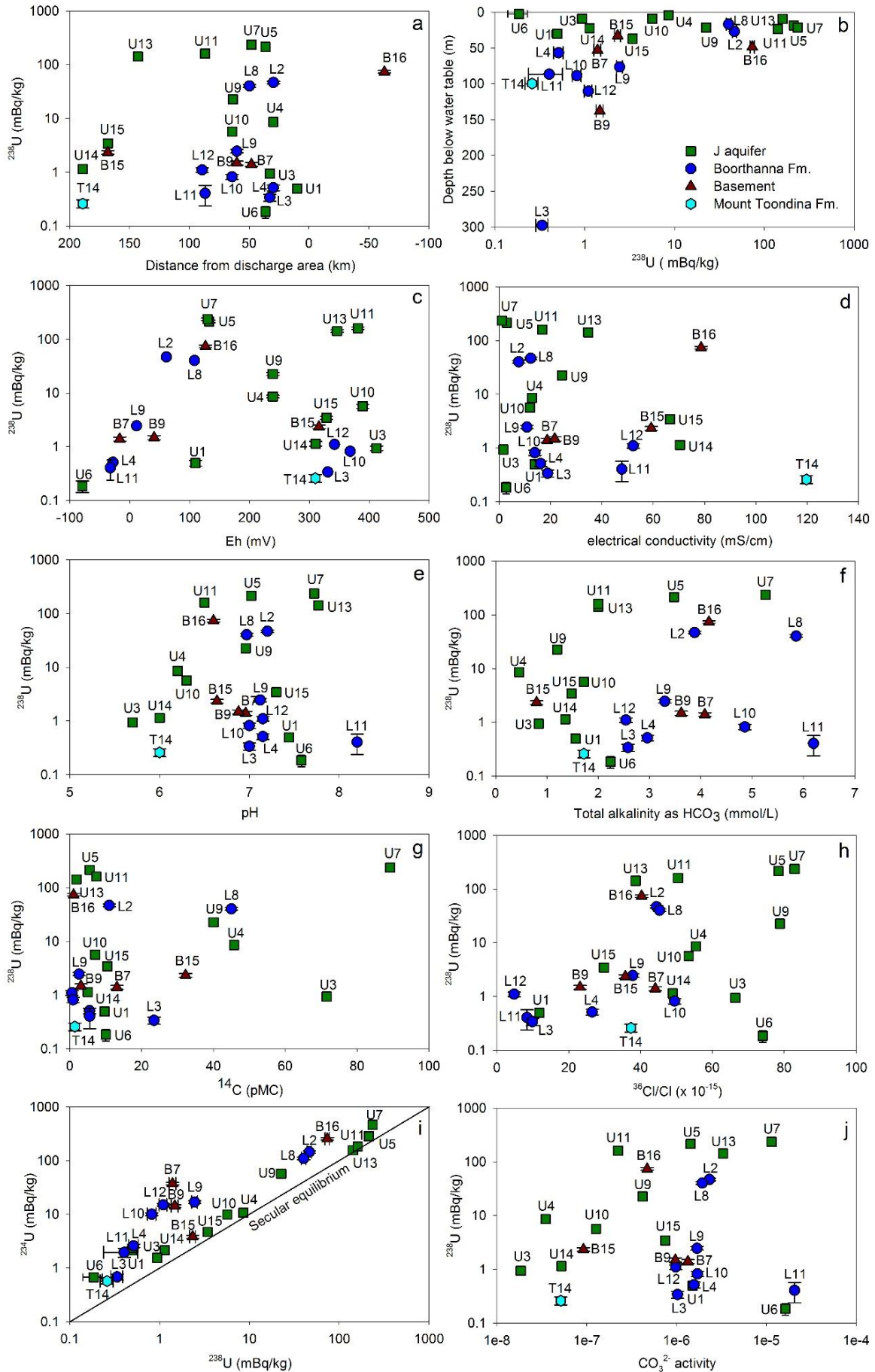


Figure 5.5 (a) ^{238}U activity concentration plotted on log scale against the distance to the discharge area (Figure 5.2 c), (b) ^{238}U activity concentration plotted on log scale against the depth below the water table, (c) ^{238}U activity concentration plotted on log scale against Eh, (d) ^{238}U activity concentration plotted on log scale against EC, (e) ^{238}U activity concentration plotted on log scale against pH, (f) ^{238}U activity concentration plotted on log scale against alkalinity, (g) ^{238}U activity concentration plotted on log scale against ^{14}C concentration, (h) ^{238}U activity concentration plotted on log scale against $^{36}\text{Cl}/\text{Cl}$, (i) ^{234}U activity concentration plotted against ^{238}U activity concentration on log scales and (j) ^{238}U activity concentration plotted on log scale against CO_3^{2-} activity. Error bars show analytical uncertainties.

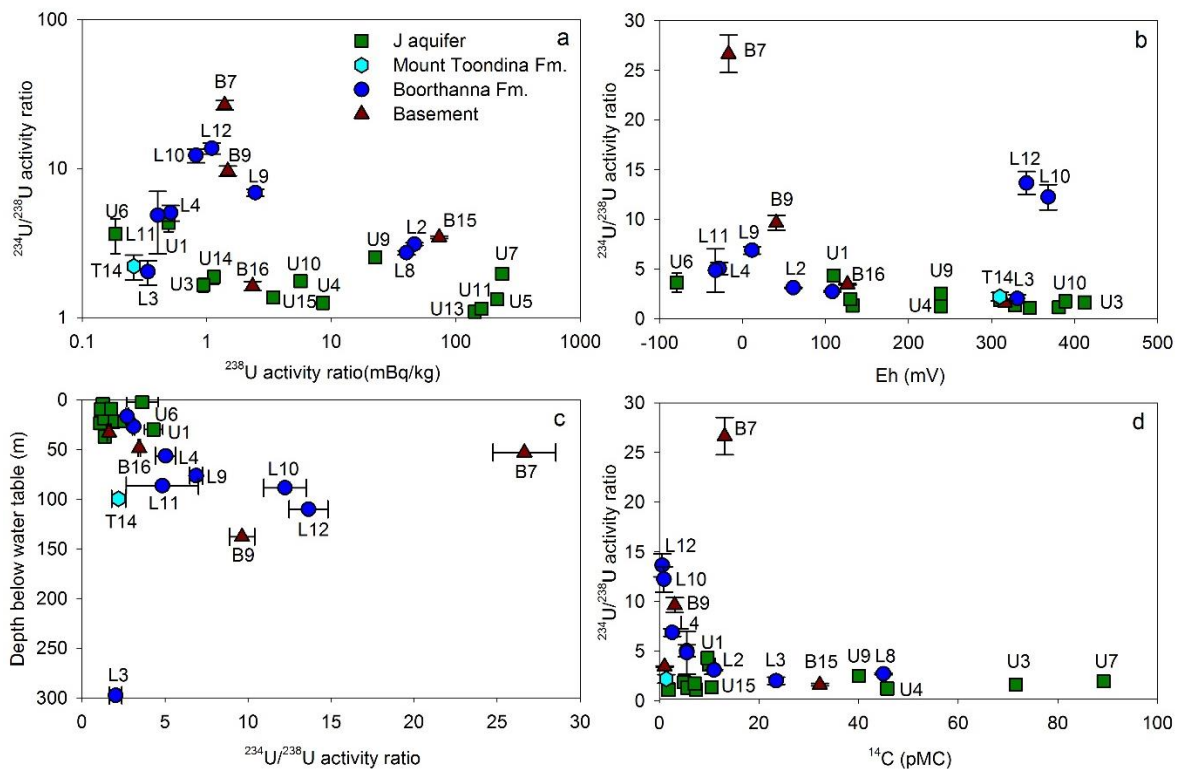


Figure 5.6 (a) $^{234}\text{U}/^{238}\text{U}$ activity ratio plotted against ^{238}U activity concentration on log scales, (b) $^{234}\text{U}/^{238}\text{U}$ activity ratio plotted against Eh, (c) $^{234}\text{U}/^{238}\text{U}$ activity ratio plotted against the depth below the water table and (d) $^{234}\text{U}/^{238}\text{U}$ activity ratio plotted against ^{14}C concentration. Error bars show analytical uncertainties.

The $^{234}\text{U}/^{238}\text{U}$ activity ratios are all above secular equilibrium (Figure 5.5 i). The $^{234}\text{U}/^{238}\text{U}$ activity ratios were most elevated (>5) in groundwater samples with low ^{238}U activity concentrations (<3 mBq/kg), whilst those with higher ^{238}U activity concentrations had $^{234}\text{U}/^{238}\text{U}$ activity ratios <4 (Figure 5.6 a). The J aquifer has more variable ^{238}U activity concentrations and the majority of the $^{234}\text{U}/^{238}\text{U}$ activity ratios are close to secular equilibrium with $^{234}\text{U}/^{238}\text{U}$ activity ratios <2 , except for U 1 and U 6, which have slightly higher $^{234}\text{U}/^{238}\text{U}$ activity ratios of 4.3 and 3.6, respectively (Figure 5.6 a). $^{234}\text{U}/^{238}\text{U}$ activity ratios are generally higher (>2) in the Boorthanna Fm. and basement samples, even in those samples that have higher ^{238}U activity concentrations (L 2, L 8 and B 16)

(Figure 5.6 a). Most of the higher $^{234}\text{U}/^{238}\text{U}$ activity ratios are in the more reducing waters (Eh <100 mV), except for L 10 and L 12 which have $^{234}\text{U}/^{238}\text{U}$ activity ratios between 12–13.6 but are also more oxidising (Eh measurements of 368 mV and 342 mV, respectively) (Figure 5.6 b). Generally, the $^{234}\text{U}/^{238}\text{U}$ activity ratios increase in deeper samples, although the deepest sample L 3 has a relatively small $^{234}\text{U}/^{238}\text{U}$ activity ratio of 2 (Figure 5.6 c) that is unlikely to be representative for the groundwater in the lower aquifer at this location, also noted in Priestley et al. (2017).

5.5.2 Sequential extraction results

The uranium results from the sequential extraction procedure are presented in Table 5.2 and Figure 5.7. The ^{238}U activity concentration in the sequential extractions ranged from 2.7–25 Bq/kg (Figure 5.7 a). The activity concentration in the Tamm's ammonium oxalate extraction (operationally defined as adsorbed trace material, carbonate minerals and amorphous iron minerals) and the 6M HCl extraction (crystalline iron minerals, clay and some refractory minerals) contained slightly less ^{238}U compared to the fusion extraction (remaining resistive minerals), although there is some scatter and overlap (Figure 5.7 a). The resistate ^{238}U activity concentrations are relatively constant with an average value of 14 Bq/kg (6.0–19 Bq/kg; Table 5.2). The Tamm's ammonium oxalate extraction and 6M HCl extractions have average values of 9.4 Bq/kg (3.3–25 Bq/kg) and 8 Bq/kg (2.7–15 Bq/kg), respectively (Table 5.2).

The $^{234}\text{U}/^{238}\text{U}$ activity ratios range from 0.65–2.46 and a number of samples were close to equilibrium for all extractions (Table 5.2). At shallower depths (35–47 m) the Tamm's ammonium oxalate extraction $^{234}\text{U}/^{238}\text{U}$ activity ratios are less than 1, whereas the fusion extraction $^{234}\text{U}/^{238}\text{U}$ activity ratios are greater than 1 (Figure 5.7 b). Throughout the rest of the profile the fusion extraction and 6M HCl extraction $^{234}\text{U}/^{238}\text{U}$ activity ratios are less than 1, and the Tamm's ammonium oxalate extraction $^{234}\text{U}/^{238}\text{U}$ activity ratios are greater than 1 (Figure 5.7 b). Deeper in the profile (>99 m) there is an increase in the $^{234}\text{U}/^{238}\text{U}$ activity ratios in the Tamm's ammonium oxalate extraction (1.3–2.5; Table 5.2).

Quantitative XRD analysis results of a sample from each of the J aquifer, Stuart Range Fm. and Boorthanna Fm. are presented in Table 5.3 for the micronised, calcium saturated bulk sample.

Table 5.2 Uranium activity concentrations and $^{234}\text{U}/^{238}\text{U}$ isotope ratios in core sequential extractions and adjacent groundwater samples

Average Depth (m)	groundwater sample		TAO ^a Extraction		6 M HCl Extraction		Fusion Digestion	
	^{238}U (mBq/kg)	$^{234}\text{U}/^{238}\text{U}$ activity ratio	^{238}U (Bq/kg)	$^{234}\text{U}/^{238}\text{U}$ Activity ratio	^{238}U (Bq/kg)	$^{234}\text{U}/^{238}\text{U}$ activity ratio	^{238}U (Bq/kg)	$^{234}\text{U}/^{238}\text{U}$ activity ratio
17.8	Beginning of J aquifer							
36.6			22.9 ± 1.6	0.81 ± 0.06	15.2 ± 1.1	0.70 ± 0.06	14.8 ± 1.1	1.51 ± 0.10
40.8			3.4 ± 0.4	0.92 ± 0.12	2.7 ± 0.4	0.93 ± 0.18	6.0 ± 0.6	1.05 ± 0.13
39–46.6 ^b	160.3 ± 8.7	1.15 ± 0.02						
46.6	Beginning of Stuart Range Fm.							
47.2			25.4 ± 1.6	0.65 ± 0.04	12.2 ± 1.0	0.68 ± 0.06	14.7 ± 1.1	1.49 ± 0.11
48.7			10.7 ± 0.8	1.12 ± 0.08	7.5 ± 1.2	0.94 ± 0.20	13.3 ± 1.0	1.01 ± 0.08
50.7			7.0 ± 0.6	1.33 ± 0.13	5.1 ± 0.5	0.90 ± 0.12	14.3 ± 1.1	0.77 ± 0.06
52.2			5.7 ± 0.6	1.29 ± 0.16	5.4 ± 0.6	1.05 ± 0.12	13.7 ± 1.1	0.88 ± 0.08
55.6			9.8 ± 0.8	1.06 ± 0.10	9.1 ± 0.8	1.05 ± 0.10	16.6 ± 1.2	0.93 ± 0.07
61.1			10.1 ± 0.9	1.19 ± 0.11	7.5 ± 0.7	0.70 ± 0.08	15.2 ± 1.1	0.92 ± 0.07
71.3			5.3 ± 0.6	1.30 ± 0.13	9.0 ± 0.8	0.81 ± 0.10	14.5 ± 1.1	0.82 ± 0.07
80.7			7.6 ± 0.7	1.38 ± 0.16	6.3 ± 0.6	0.93 ± 0.09	13.2 ± 1.0	1.00 ± 0.09
90.6			14.1 ± 1.1	0.97 ± 0.09	11.4 ± 0.9	0.97 ± 0.08	17.5 ± 1.3	1.04 ± 0.07
97.3			14.4 ± 1.1	0.90 ± 0.09	7.9 ± 0.7	1.28 ± 0.10	11.3 ± 0.9	1.04 ± 0.09
99.7			4.0 ± 0.5	1.81 ± 0.27	6.2 ± 0.6	0.84 ± 0.11	14.4 ± 1.1	0.80 ± 0.07
102.1			4.2 ± 0.5	2.46 ± 0.35	7.2 ± 0.7	0.83 ± 0.10	15.9 ± 1.2	0.93 ± 0.07
103.9			3.3 ± 0.3	1.94 ± 0.22	10.0 ± 0.9	0.89 ± 0.10	12.3 ± 1.0	0.85 ± 0.08
104.0	Beginning of Boorthanna Fm.							
104.5			8.6 ± 0.6	1.29 ± 0.09	10.9 ± 1.0	0.79 ± 0.09	19.1 ± 1.4	0.84 ± 0.06
106.7			3.7 ± 0.4	1.70 ± 0.18	7.3 ± 0.7	0.66 ± 0.09	12.1 ± 1.0	0.82 ± 0.08
108–123 ^c	0.4 ± 0.2	4.84 ± 2.2						

^a Tamm's ammonium oxalate solution

^b U 11

^c L 11

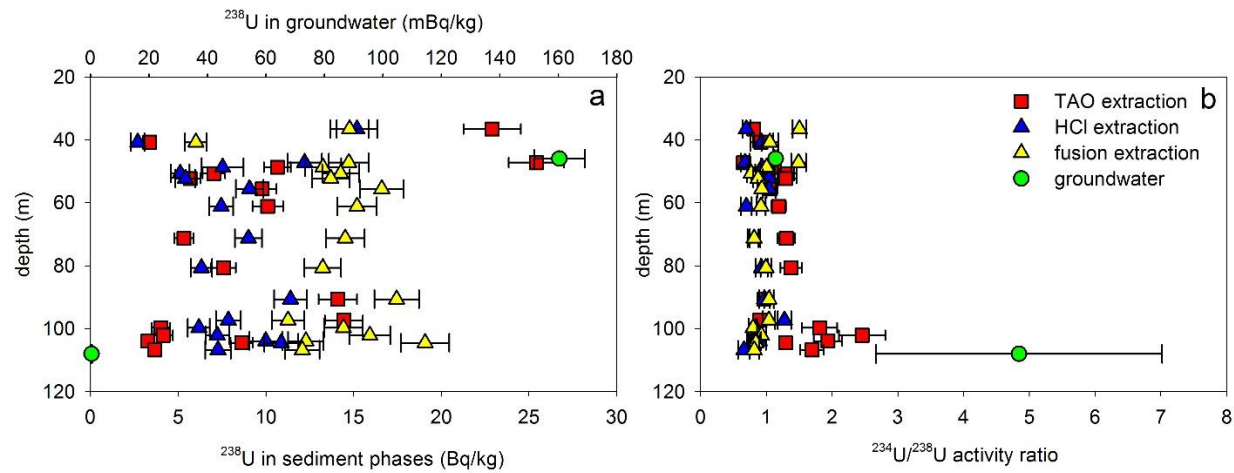


Figure 5.7 (a) ^{238}U activity concentration and (b) $^{234}\text{U}/^{238}\text{U}$ activity ratios from sequential extractions of core samples plotted against sample depth. Error bars show analytical uncertainties.

68

Table 5.3 Quantitative XRD analysis (wt.%) of bulk, micronized and calcium saturated core samples

Sample	Quartz	Kaolinite	Montmorillonite	Illite/ Mica 2M1	Chlorite	Calcite	Dolomite	Siderite	Microcline/ Orthoclase	Albite	Pyrite
J aquifer	56	10	8	11	2	—	—	—	13	—	<1
Stuart Range Fm.	50	5	14	9	2	1		1	14	4	<1
Boorthanna Fm.	64	1	10	6	2	<1	<1	—	10	6	<1

5.6 Discussion

5.6.1 Geochemistry of uranium isotopes

Osmond et al. (1974), Andrews and Kay (1982) and others associated high ^{238}U and $^{234}\text{U}/^{238}\text{U}$ activity ratios near secular equilibrium with groundwater passing through the recharge zone where oxidising conditions prevail. The shallower groundwater samples (depth below water table <50 m) generally have higher ^{238}U activity concentrations (>20 mBq/kg) and the $^{234}\text{U}/^{238}\text{U}$ activity ratios are <4 (Figure 5.6 a). However, there is no correlation between high ^{238}U activity concentration with high Eh (Figure 5.5 c), nor are the 'young' groundwater, estimated with $^{14}\text{C}_{\text{DIC}} >40$ pMC, correlated with high ^{238}U activity concentrations (Figure 5.5 g). Therefore, recharging oxidised groundwater leaching uranium isotopes from minerals in secular equilibrium cannot be the only process controlling the higher uranium activity concentrations and $^{234}\text{U}/^{238}\text{U}$ activity ratios.

Osmond et al. (1974) and Andrews and Kay (1982) also noted that as groundwater moves through the aquifer and becomes reducing the uranium concentrations decrease abruptly and the $^{234}\text{U}/^{238}\text{U}$ activity ratios begin to increase. There is a slight trend of higher $^{234}\text{U}/^{238}\text{U}$ activity ratios (>3) being higher in the more reducing groundwater (Figure 5.6 b). Additionally, the $^{234}\text{U}/^{238}\text{U}$ activity ratios are higher (>5) in the deeper groundwater samples (depth below water table >50 m; Figure 5.6 c). However, there is no correlation between lower ^{238}U activity concentrations with decreasing Eh; both high and low ^{238}U activity concentrations are found throughout the range of Eh measurements (Figure 5.5 c).

Other studies have identified that uranium solubility can be enhanced by the formation of complexes (Langmuir 1978; Gascoyne 1992), most commonly with carbonate (Andrews and Kay 1982) or chloride (Herczeg et al. 1988). The highest ^{238}U activity concentrations (8–235 mBq/kg) are generally in the brackish to fresh groundwater samples (EC between 1–34 mS/cm; chloride concentration between 3–300 mmol/L; Table 5.1); except for B 16 (EC of 78.6 mS/cm; chloride concentration of 817 mmol/L; Table 5.1). While there is chloride available to complex with the uranium in solution, the lack of a relationship between higher chloride concentration and increased ^{238}U activity concentration indicates chloride complexation is not controlling uranium availability. This is confirmed by PHREEQC speciation modelling showing that uranium is predominantly complexed with CO_3 in solution as $\text{UO}_2(\text{CO}_3)_3^{4-}$ and $\text{UO}_2(\text{CO}_3)_2^2$ (Table 5.1).

However, there is not a strong relationship between the ^{238}U activity concentration and alkalinity, or CO_3^{2-} activity from PHREEQC speciation modelling (Table 5.1), as the low ^{238}U activity concentration samples are also spread along all total alkalinity HCO_3^- concentrations and CO_3^{2-} activities (Figure 5.5 f and j). Nevertheless, those samples with high ^{238}U activity concentrations appear to be in the groundwaters with higher alkalinity (as HCO_3^- ; Figure 5.5 f). High alkalinity can limit the adsorption of uranium (Jurgens et al. 2010), therefore, where the uranium is available to be dissolved in groundwater, the carbonate species are complexing with it and helping keep it in solution.

Considering leaching of uranium isotopes from minerals in the vadose zone by recharging oxidised groundwater is not controlling the uranium concentrations, it is possible that there is not a uniform uranium source throughout the vadose zone. Tricca et al. (2001) and Kronfeld et al. (2004) found that uranium distributions are predominantly influenced by weathering conditions which form diverse vadose zone inputs. Varying recharge rates and hence movement of groundwater through the vadose zone in the study area may cause different weathering conditions and uranium availability. Sample U 7 with the highest uranium concentration (236 mBq/kg) and the 'youngest' groundwater age ($^{14}\text{C} >40$ pMC and $^{36}\text{Cl}/\text{Cl} >45 \times 10^{-15}$) probably recharged from a nearby waterhole (Priestley et al. 2017) is discussed further below. Samples U 3 and U 4 also have young groundwater ages ($^{14}\text{C} >40$ pMC) but have low uranium concentrations (<10 mBq/kg) possibly due to recharge through rocks that have been extensively weathered or contain low uranium. Samples U 5, U 11 and U 13 which have high uranium concentrations (>100 mBq/kg) are 'older' indicating little to no recharge at these well locations ($^{14}\text{C} <10$ pMC). It is probable that these waters being slightly oxidising (Eh >100 mV) and containing bicarbonate has allowed previously dissolved uranium to remain in solution, or possibly even leached uranium from nearby rocks with elevated uranium. Some of the unconfined deeper aquifer samples have elevated uranium concentrations (L 8, L 2 and B 16; between 45–73 mBq/kg). These samples also have slightly elevated $^{234}\text{U}/^{238}\text{U}$ activity ratios (3–3.5) so it is likely that these locations receive some recharge that weathers available uranium from the rocks that then mixes with older groundwater with higher $^{234}\text{U}/^{238}\text{U}$ activity ratios. Priestley et al. (2017) found evidence for mixing at these locations based on other environmental tracers.

$^{234}\text{U}/^{238}\text{U}$ activity ratios generally increase with depth (Figure 5.6 c) and this can be due to addition of ^{234}U relative to ^{238}U due to α -recoil (Osmond and Cowart 1976; Gascoyne 1992; Osmond and Cowart 1992; Porcelli and Swarzenski 2003). However, dissolution of uranium bearing precipitates

or desorption from mineral surfaces with high $^{234}\text{U}/^{238}\text{U}$ activity ratios can also cause high $^{234}\text{U}/^{238}\text{U}$ activity ratios in groundwater. Dabous et al. (2002) found that uranium lightly adsorbed to a granite aquifer had a similar $^{234}\text{U}/^{238}\text{U}$ activity ratio to the local groundwater and was, therefore, the source of uranium to the associated groundwater. The Tamm's ammonium oxalate extraction of adsorbed elements, carbonate minerals and amorphous iron minerals operationally defined by Yanase et al. (1991) should indicate the uranium isotopes that are more accessible to groundwater (Payne et al, 2001), although the availability will depend on the geochemical environment and degree of saturation of different minerals in this extraction.

The relatively constant resistate ^{238}U activity concentrations (Figure 5.7 a) may indicate that the aquifers contain a fairly uniform controlling mineralogy. The ^{238}U activity concentrations in the Tamm's ammonium oxalate extractable phase are much higher in the shallow samples (Figure 5.7 a), and it is likely that the uranium is associated with coating phases, such as the fine-grained clay phases (Table 5.3). The physical position of the ^{238}U parent in the coating phases makes it as likely for the ^{234}U daughter to be recoiled into the resistate phase which being isolated from groundwater leads to enrichment of ^{234}U (Rosholt 1983; Sheng and Kuroda 1984; Yanase et al. 1991). Therefore, it is plausible that the decay of ^{238}U in these uranium-rich coatings and recoil of ^{234}U into adjacent relatively uranium-poor resistant phases causes the low $^{234}\text{U}/^{238}\text{U}$ ratios (<1) in the Tamm's ammonium oxalate extractable phase and $^{234}\text{U}/^{238}\text{U}$ activity ratios greater than 1 in the resistate phase at the top of the profile (Figure 5.7 b). The $^{234}\text{U}/^{238}\text{U}$ activity ratio is depleted in the resistate at greater depths with $^{234}\text{U}/^{238}\text{U}$ activity ratios of 0.8 (Table 5.2) most likely due to a loss of ^{234}U from the resistate phase. At these depths, there is less ^{238}U in groundwater and coating phases (Figure 5.7 a), thus it appears that the relative recoil flux of ^{234}U is in the opposite direction i.e. out of the resistate into the coating phases and possibly the groundwater.

The increase in the $^{234}\text{U}/^{238}\text{U}$ activity ratio in the deeper samples of the Tamm's acid oxalate extraction phases follows the higher ratio in groundwater from the Boorthanna Fm. compared with the J aquifer (Figure 5.7 b). Both aquifers exhibit groundwater $^{234}\text{U}/^{238}\text{U}$ activity ratios that are higher than that of the sediments they are passing through. Therefore, it is not possible that dissolution and/or exchange with the groundwater accessible minerals in the aquifer alone can be the source of the high $^{234}\text{U}/^{238}\text{U}$ activity ratios. Therefore, it is considered more likely that the higher $^{234}\text{U}/^{238}\text{U}$ activity ratios in the groundwater are controlled by α -recoil of ^{234}U into solution consistent with conclusions from previous studies (Guttman and Kronfeld 1982; Henderson et al. 1999; Suksi et al. 2006). It is interesting to note that the $^{234}\text{U}/^{238}\text{U}$ activity ratios in the Tamm's acid

oxalate extraction for Boorthanna Fm. core samples are slightly higher than the remaining samples (Figure 5.7 b). It is possible that these groundwater accessible minerals $^{234}\text{U}/^{238}\text{U}$ activity ratios are increasing due to precipitation or exchange with the high $^{234}\text{U}/^{238}\text{U}$ activity ratio of uranium in the groundwater. However, individual groundwater accessible phases could exert a larger effect than others in certain geochemical conditions not discernible from the Tamm's acid oxalate extraction alone. Additionally, not enough aquifer sediment samples have been analysed throughout the area to conclusively demonstrate that there are not high $^{234}\text{U}/^{238}\text{U}$ activity ratios in the groundwater accessible minerals in other parts of the deeper aquifers.

Where $^{234}\text{U}/^{238}\text{U}$ activity ratios in groundwaters are solely due to α -recoil, the degree of excess ^{234}U changes with residence time (Kronfeld and Rosenthal 1981; Guttman and Kronfeld 1982; Henderson et al. 1999). There is a general relationship between the uranium isotope variations and ^{14}C , as the $^{234}\text{U}/^{238}\text{U}$ activity ratios are relatively low (>3) in the younger groundwaters ($^{14}\text{C} >40$ pMC) and higher $^{234}\text{U}/^{238}\text{U}$ activity ratios up to 27, in older groundwater ($^{14}\text{C} <40$ pMC; Figure 5.6 d). However, there is not a distinct trend in increasing $^{234}\text{U}/^{238}\text{U}$ activity ratios with decreasing ^{14}C concentrations, thus there appears to be variable addition of uranium isotopes along the groundwater flow path in addition to α -recoil of ^{234}U . Suksi et al. (2006) also found that groundwater turnover, i.e. flow rate, has a marked effect on the resulting $^{234}\text{U}/^{238}\text{U}$ activity ratio; direct α -recoil of ^{234}U into strongly flowing groundwater water is insignificant with respect to $^{234}\text{U}/^{238}\text{U}$ activity ratio variation. Therefore, the higher $^{234}\text{U}/^{238}\text{U}$ activity ratios in some locations in the Boorthanna Fm. and basement may indicate that the groundwater flow rates are slow.

5.6.2 Uranium isotopes as an indicator of groundwater flow

Uranium isotope distributions in the groundwater basins are dependent on uranium availability, mobility and the geochemical environment, all of which appear to be spatially variable across the study area. Dhaoui et al. (2016) found uranium isotope distributions to be controlled by groundwater mixing as well as α -recoil of ^{234}U and water-rock interactions in the Continental Intercalaire aquifer, Tunisia. Priestley et al. (2017) identified groundwater leakage from the J aquifer into the Boorthanna Fm. at a number of locations throughout the basin and it is likely that this, as well as recharge to the system from ephemeral rivers and waterholes, would also affect the uranium isotope distributions.

Intermittent recharge over long time periods from ephemeral rivers at sites U 3 and U 4 (Priestley et al. 2017) are likely to occur through rocks that have already undergone extensive weathering

and contain low ^{238}U activity concentrations and $^{234}\text{U}/^{238}\text{U}$ activity ratios. Recharge to U 7 from a nearby waterhole (Priestley et al. 2017) contains high ^{238}U activity concentrations and low $^{234}\text{U}/^{238}\text{U}$ activity ratios due to leaching of uranium in secular equilibrium from rocks. The majority of the upper aquifer samples with low ^{238}U activity concentrations and low $^{234}\text{U}/^{238}\text{U}$ activity ratios (U 14, U 6, U 15, U 1, U 10) receive little to no recharge. Groundwater residence times are not long enough for increased $^{234}\text{U}/^{238}\text{U}$ activity ratios because of α -recoil of ^{234}U and if uranium concentrations were elevated up stream this uranium must already have been sorbed or deposited on aquifer sediments. Sites U 1 and U 6 toward the end of the regional groundwater flow path have low uranium activity concentrations and slightly elevated $^{234}\text{U}/^{238}\text{U}$ activity ratios possibly because of α -recoil of ^{234}U . Priestley et al. (2017) determined U 1 is a location of upward leakage from the aquifer below, which often contains elevated $^{234}\text{U}/^{238}\text{U}$ activity ratios, therefore the slightly elevated $^{234}\text{U}/^{238}\text{U}$ activity ratios in U 1 could also highlight upward leakage occurring at this location.

The ^{238}U activity concentrations and $^{234}\text{U}/^{238}\text{U}$ activity ratios in the remaining upper aquifer groundwater samples are a result of their geochemical environment. Samples containing high ^{238}U activity concentrations (U 5, U 11, U 13) receive little or no recharge (Priestley et al. 2017); thus are not due to recharging groundwater containing uranium leached from minerals in the vadose zone. The slightly oxidising groundwaters at these locations contain carbonate that complex with and stabilise uranium keeping it in solution. Additionally, this geochemical environment would allow uranium to be leached from localised rocks with high uranium concentrations near secular equilibrium. Sample U 9 contains slightly elevated ^{238}U activity concentrations and $^{234}\text{U}/^{238}\text{U}$ activity ratios and Priestley et al. (2017) identified this as a location that receives some recharge from ephemeral rivers. Mixing of recharging groundwater with elevated ^{238}U activity concentrations and groundwater in the aquifer with elevated $^{234}\text{U}/^{238}\text{U}$ activity ratios from α -recoil of ^{234}U could result in the uranium isotope distribution at this location.

Generally, the lower aquifers contain low ^{238}U activity concentrations because the uranium has been precipitated as groundwater moves through the aquifer (Osmond et al. 1974; Andrews and Kay 1982), except samples L 2, L 8 and B 16. Samples L 2, L 8 and B 16, located in the unconfined sections of the lower aquifer, receive small amounts of recharge ($^{36}\text{Cl}/\text{Cl}$ between 45×10^{-15} – 40×10^{-15} ; Priestley et al. 2017). The recharging groundwater weathers available uranium from rocks, then mixes with older groundwater with higher $^{234}\text{U}/^{238}\text{U}$ activity ratios. Priestley et al. (2017) also identified leakage of younger groundwater from the upper aquifer to the Boorthanna

Fm. at L 10; however, the low ^{238}U activity concentration in the upper aquifer at this location (U 10) does not appear to have diluted the high $^{234}\text{U}/^{238}\text{U}$ activity ratio (12) in L 10.

The $^{234}\text{U}/^{238}\text{U}$ activity ratios vary throughout the lower aquifers as a result of α -recoil of ^{234}U from the aquifer sediments into the groundwater. The magnitude of the $^{234}\text{U}/^{238}\text{U}$ activity ratios can be dependent on residence time i.e. position in the groundwater flow path (Henderson et al. 1999), or due to the rate of groundwater flow (Suksi et al. 2006). Priestley et al. (2017) identified sites L 11 and L 12 as areas of semi-stagnant groundwater flow allowing the $^{234}\text{U}/^{238}\text{U}$ activity ratios to increase because the α -recoil added ^{234}U is not moved on by the groundwater. The $^{234}\text{U}/^{238}\text{U}$ activity ratio is largest in B 7 ($^{234}\text{U}/^{238}\text{U}$ activity ratio = 27). This the final sample along the Boorthanna Fm. and basement groundwater flow path before the Stuart Range Fm. aquitard pinches out and ^{234}U has been continuously added by α -recoil along the confined groundwater flow path increasing the groundwater $^{234}\text{U}/^{238}\text{U}$ activity ratio.

5.6.3 Environmental health implications

Sites U 5, U 7, U 11 and U 13 with high ^{238}U activity concentrations have total uranium concentrations that approach or exceed Australian drinking water regulations of 17 $\mu\text{g}/\text{L}$ (NHMRC and NRMCC 2011), as well as the 15 $\mu\text{g}/\text{L}$ limit recommended by the World Health Organization (WHO 2004). These basins are within pastoral lands and the J aquifer is a source of drinking water for cattle (Habermehl 1980). These samples are from the J aquifer and are spread throughout the basin which makes it more difficult to track high uranium activity concentrations which could contaminate the groundwater. The groundwater from the Boorthanna Fm. is used for drinking water and mine processing, though the high TDS means that the water is treated before being used as a drinking supply (Oz Minerals 2013). As Priestley et al. (2017) did not definitively detect inter-aquifer leakage via preferential flow paths from the J aquifer to the Boorthanna Fm. at these locations it would thus appear there is minimal risk of contaminating the Boorthanna Fm. groundwater, but these locations should continue to be monitored.

5.7 Conclusions

The objective of this study was to understand the processes that control uranium isotope distributions in groundwater in the south-western margin of the GAB and underlying Arckaringa Basin. Generally, groundwater samples from the J aquifer have higher ^{238}U activity concentrations

and $^{234}\text{U}/^{238}\text{U}$ activity ratios close to secular equilibrium. The deeper Boorthanna Fm. and basement aquifers have lower ^{238}U activity concentrations and higher $^{234}\text{U}/^{238}\text{U}$ activity ratios.

The source of ^{238}U to the aquifers is spatially variable. Reoccurring recharge from ephemeral rivers passes through rocks and sediments that have been weathered extensively as the recharging groundwater contains low ^{238}U activity concentrations. Other locations in the J aquifer contain high ^{238}U activity concentrations but currently receive no recharge. Aquifer minerals with locally high concentrations of uranium are the most likely source; with the uranium being leached into, and remaining in, solution due to the geochemical environment.

The sequential extractions of mineral phases that make up the aquifer sediment have highlighted that α -recoil processes resulted in high $^{234}\text{U}/^{238}\text{U}$ activity ratios in different mineral phases and groundwater. Decay of ^{238}U in uranium-rich coatings on the J aquifer sediments and recoil of ^{234}U into the relatively uranium-poor neighbouring resistant phases causes $^{234}\text{U}/^{238}\text{U}$ ratios beyond secular equilibrium in the resistant phase, as well as some enrichment in the groundwater. The $^{234}\text{U}/^{238}\text{U}$ activity ratio is depleted in the resistate phase in the Boorthanna Fm. as the flux of ^{234}U is from the resistate into the coating phases and groundwater. In both the J aquifer and the Boorthanna Fm., α -recoil processes have resulted in high $^{234}\text{U}/^{238}\text{U}$ activity ratios in the groundwater. Though α -recoil is the process resulting in the $^{234}\text{U}/^{238}\text{U}$ activity ratios, their magnitude is dependent on groundwater residence time or the rate of groundwater flow. Further collection and analysis of sediment samples to determine spatial variability would elucidate the mechanisms which contribute to the high groundwater $^{234}\text{U}/^{238}\text{U}$ activity ratios.

The uranium isotope distributions are due to rock weathering, the geochemical environment and α -recoil of daughter products, giving rise to a large spatial variability. The high spatial heterogeneity, and the lack of clear correlations, made it difficult to use uranium isotopes to conclusively identify recharge and inter-aquifer leakage locations. Although overall, the uranium isotope distributions confirmed earlier interpretations based on other tracers in Priestley et al. (2017).

Chapter 6 Palaeohydrogeology and transport parameters derived from ^4He and Cl profiles in aquitard pore waters in a large multilayer aquifer system, central Australia

Published in *Geofluids*: Stacey C. Priestley, Tavis Kleinig, Andrew J. Love, Vincent E. A. Post, Paul Shand, Martin Stute, Ilka Wallis and Daniel L. Wohling (2017) Palaeohydrogeology and transport parameters derived from ^4He and Cl profiles in aquitard pore waters in a large multilayer aquifer system, central Australia, *Geofluids*, doi: 10.1155/2017/9839861

6.1 Abstract

A study of chloride and ^4He profiles through an aquitard which separates the Great Artesian Basin from the underlying Arckaringa Basin in central Australia is presented. The aquitard separates two aquifers with long water residence times, due to low recharge rates in the arid climate. One-dimensional solute transport models were used to determine the advective flux of groundwater across the aquitard, as well as establish any major changes in past hydrological conditions recorded by variations of the pore water composition. This in situ study showed that both diffusion and slow downward advection ($v_z = 0.7 \text{ mm/yr}$) control solute transport. Numerical simulations show that an increase in chloride concentration in the upper part of the profile is due to a reduction in recharge in the upper aquifer for at least 3000 years. Groundwater extraction since 2008 has probably increased chloride and ^4He concentrations in the lower aquifer by pulling up water from deeper layers; however, there has been insufficient time for upward solute transport into the pore water profile by diffusion against downward advection. The transport model of ^4He and chloride provides insight into how the two aquifers interact through the aquitard and that climate change and pumping rates are being recorded in the aquitard profile.

6.2 Introduction

Aquitards, i.e. low permeability geological formations, play an important role in the physical and chemical evolution of groundwater. They control the response of aquifers to forcing such as pumping, and impede the movement of water between aquifers (Back 1986; Cherry and Parker 2004). They also exert a strong influence on solute migration and can sequester solutes, with important implications for contaminant migration as well as for isotope tracer studies (Sanford 1997; Park et al. 2002; Hendry et al. 2015b). An understanding of the hydrological role of aquitards is vital in areas impacted by large-scale groundwater abstraction, e.g. mining activities, and for

safety assessment studies of waste repositories. Despite this, aquitards remain less well studied in comparison to aquifers because of the inherent difficulty of obtaining water samples and reliable hydraulic data.

Aquitard properties, such as hydraulic conductivity, and their variability, can be determined by fluid pressure measurements within the aquitard using in-situ vibrating wire pressure transducers (Larroque et al. 2013; Smerdon et al. 2014), although hydraulic conductivity measurements can increase with the scale of measurement (Neuzil and Bredehoeft 1980; Batlle-Aguilar et al. 2016). When combined with the gradient of fluid pressure using Darcy's law, the vertical flow direction and rate can be determined.

Since groundwater flow velocities in aquitards can be low, mass transport in these layers tends to be dominated by molecular diffusion (Cherry and Parker 2004). Spatial variations of the pore water composition have been used to evaluate the origin, age, and migration processes of water and solutes. Complexity is introduced by climatic and hydrological changes, which are unknown with certainty at the timescales relevant to transport in aquitards, which are of the order of centuries to millions of years. Naturally occurring environmental tracers, such as chloride and stable isotopes of water, have been used in combination with mathematical models to study transport processes in aquitards and to reconstruct past environmental conditions (Mazurek et al. 2011).

Chloride, helium and stable isotopes of water are considered chemically inert under a wide range of conditions. In the absence of chemical reactions, chloride is concentrated at the surface and in the unsaturated zone by evapotranspiration of rainwater. Its concentration is hence a proxy for climate and recharge rates. Similarly, stable isotopes of water form a record of climate conditions at the time of recharge as the abundance of light over heavy isotopes depends on evaporation and temperature (Herczeg et al. 2001). Noble gases are good tracers of hydrogeological processes because of their inert nature, and have been applied to study aquitard processes (Kipfer et al. 2002; Trinchero et al. 2014). Pore water noble gas compositions have been used to determine fluid sources (Norman and Musgrave 1994), to date pore waters (Osenbrück et al. 1998), to determine solute diffusion coefficients (Rubel et al. 2002; Ali et al. 2011) and to determine rates of water and solute mass transport (Rubel et al. 2002; Sheldon et al. 2003; Mazurek et al. 2007; Bensenouci et al. 2011; Mazurek et al. 2011; Clark et al. 2013; Trinchero et al. 2014). Helium dissolves in the water in the unsaturated zone in equilibrium with the soil air, and its

concentration in groundwater increases with age due to subsurface production, as well as upward migration of deeper crustal and mantle helium (Torgersen and Clarke 1985; Torgersen and Stute 2013). Thus, whilst chloride and stable isotope variations can reflect changes in recharge conditions, concentrations of radiogenic helium are influenced by groundwater residence time.

Most aquitard studies have been undertaken in temperate climates, such as in Canada and Europe, where the importance of glaciation is reflected by the stable water isotopes (Mazurek et al. 2011; Harrington et al. 2013). Stable isotopes of water and major element pore water profiles in shallow clay aquitards showed that solute transport is dominated by diffusion in Ontario, Canada (Desaulniers et al. 1981) and Montreal, Canada (Desaulniers and Cherry 1989). Solute transport in surficial clay aquitards in Saskatchewan, Canada was investigated by $\delta^{18}\text{O}$ (Remenda et al. 1996), $\delta^2\text{H}$ (Hendry and Wassenaar 1999; Hendry et al. 2011) or both (Hendry et al. 2004; Hendry et al. 2013). $\delta^{18}\text{O}$ data constrained hydraulic conductivities in these aquitards and showed diffusion to be the dominant solute transport mechanism even during glaciations (Remenda et al. 1996; Hendry et al. 2013). $\delta^2\text{H}$ profiles provided the timing of climate change during the Holocene (Hendry and Wassenaar 1999; Hendry et al. 2011). Stable isotopes and solute pore water distributions were used to determine transport and geochemical processes controlling pore water composition in the Battleford Fm. in Saskatchewan, Canada (Hendry and Wassenaar 2000) and Michigan Basin in Ontario, Canada (Al et al. 2015).

In south-western Spain, Konikow and Arevalo (1993) were able to determine that an 80 m thick clay aquitard is in steady state with upward flow between 1 mm/yr to 1 cm /yr. Mazurek et al. (2011) compiled stable isotopes of water and solute pore water profiles for nine sites in central Europe from a number of published studies (Falck et al. 1990; Rubel et al. 2002; Patriarche et al. 2004a; Patriarche et al. 2004b; Gimmi et al. 2007; Mazurek et al. 2009; Koroleva et al. 2011). A selection of anion concentration data, stable isotopes of water as well as noble gases comprised the dataset at each site. As found in previous studies (Savoye et al. 2008; Bensenouci et al. 2013), model scenarios confirmed that diffusion is the dominant solute transport process. A study undertaken in the Otway Basin, located in a temperate climate zone of Australia, used stable isotopes of water and major ion concentration profiles to investigate diffusive transport through an aquitard (Love et al. 1996; Harrington et al. 2001). Here, geochemical processes were found to complicate interpretations based on non-conservative major ions (Harrington et al. 2001).

All the above studies have been undertaken in cold or temperate climates. In arid regions the residence times of water in aquifers, not just aquitards, tends to be large ($>10^4$ years) due to low recharge rates (Herczeg and Leaney 2011). Harrington et al. (2013) undertook one of the few studies in arid central Australia and used both chloride and stable isotopes of water to determine the paleohydrogeology of the western Great Artesian Basin (GAB). The chloride profile showed a complex history of climate variations. It was found that pore water isotope contents were not as well suited to identify climate influences. This is because in arid regions and at low latitudes, their interpretation is complicated because the effects of ice volume, temperature, precipitation amount, and moisture transport on isotopic abundances in recharge are all important, whereas in study areas at higher latitudes the temperature effect due to glaciations dominates (Desaulniers et al. 1981; Remenda et al. 1996; Hendry and Wassenaar 1999; Hendry et al. 2004; Hendry et al. 2011; Hendry et al. 2013). Gardner et al. (2012) used ^4He concentrations in the same aquitard profiles, augmented with regional groundwater samples, to estimate vertical fluid flux through the aquitard. Hasegawa et al. (2016) also characterised solute transport in the main confining layer of the GAB using chloride and chlorine isotopes (^{36}Cl , ^{37}Cl) finding that Cl is of meteoric origin and is transported by diffusion. Jones et al. (1994) concluded, based on vertical profiles of salinity and stable water isotopes across the Geera Clay in the Murray River Basin, that the major part of dissolved salts in the pore water was derived from aerosols.

In this study, the vertical groundwater flow and solute transport through an aquitard separating the GAB and the underlying Arckaringa Basin was examined. The aquitard of interest is situated between two aquifers with long residence times of water, due to the low recharge rates in the arid climate (Priestley et al. 2017). Chloride, ^4He and stable isotopes of water in conjunction with numerical and analytical modelling were used to quantify flow velocities and establish the connectivity between the two basins at the site studied.

6.3 Site description

The Arckaringa Basin is a Late Carboniferous to Early Permian sedimentary basin. Glacial scouring during the Devonian-Carboniferous and faulting during the Early Permian resulted in the formation of troughs and sub-basins (Wohling et al. 2013). The Boorthanna Fm., which forms the deeper aquifer (called lower aquifer in this chapter) is a marine and glacial sandstone and diamictite aquifer that overlies Proterozoic basement rock (Figure 6.1 c; Ambrose and Flint 1980). The aquitard is formed by the Stuart Range Fm. that consists of mudstone, siltstone and shale, and

separates the Boorthanna Fm. from the overlying GAB (Figure 6.1 c). The GAB sediments were deposited from the Late Jurassic to the Early Cretaceous (Senior et al. 1978; Gallagher and Lambeck 1989; Toupin et al. 1997). The J aquifer of the GAB (called the upper aquifer in this chapter) comprises the hydraulically connected Jurassic Cadna-Owie Fm. and Algebuckina Sandstone. These are confined by the outcropping Cretaceous Bulldog Shale (Love et al. 2013), a marine mudstone and silt aquitard, which formed due to sea level rise at the start of the Late Cretaceous (Gallagher and Lambeck 1989). Since their formation, the basins have undergone many phases of compression, uplift and erosion to today's levels (Toupin et al. 1997).

The thickness of the Boorthanna Fm., the Stuart Range Fm. and the J aquifer where the core is located are 131 m, 57 m and 29 m, respectively. The Arckaringa Basin is bordered by a series of ranges, ridges and plateaus including the Peake and Denison Inlier to the east consisting of outcropping basement rocks with an elevation between 400–420 m AHD (Wopfner and Twidale 1967). For this study, a continuous core was drilled through the Stuart Range Fm. in central South Australia (Figure 6.1 b). The topography of the region where the aquitard core was taken is relatively flat with an elevation of approximately 150 m AHD. It is characterised by wide flat-topped plateaus with sharp escarpments, and lower lying gibber and flood plains associated with ephemeral rivers.

The climate is arid with an average annual precipitation rate of 120 mm/yr (Allan 1990; McMahon et al. 2005). However, precipitation is variable, both temporally and spatially. Recharge from rainfall is via diffuse infiltration into outcropping and subcropping aquifer sediments (Figure 6.1 a), as well as focused along disconnected ephemeral rivers (Love et al. 2013; Keppel et al. 2015). Vertical groundwater flow from the upper aquifer to the lower aquifer is likely to be the main form of recharge to the latter because it crops out only in a small area (Keppel et al. 2015). The regional groundwater flow direction in both aquifers near the coring location of this study is approximately from west to east (Figure 6.1 b), although the spatial coverage of wells completed in the lower aquifer is limited. Hydraulic heads in the Boorthanna Fm. range from 110 to 60 m AHD, and in the J aquifer range from 150 to 25 m AHD (Figure 6.1b). Groundwater is being extracted from the upper aquifer for stock and domestic use. The Prominent Hill mine (Figure 6.1 b) has been extracting groundwater at a rate of up to 26 ML/d from the lower aquifer from wells surrounding and to the north-east of the coring location since 2008 to sustain its mining operations, which has caused drawdowns of up to 50 m (SKM 2010).

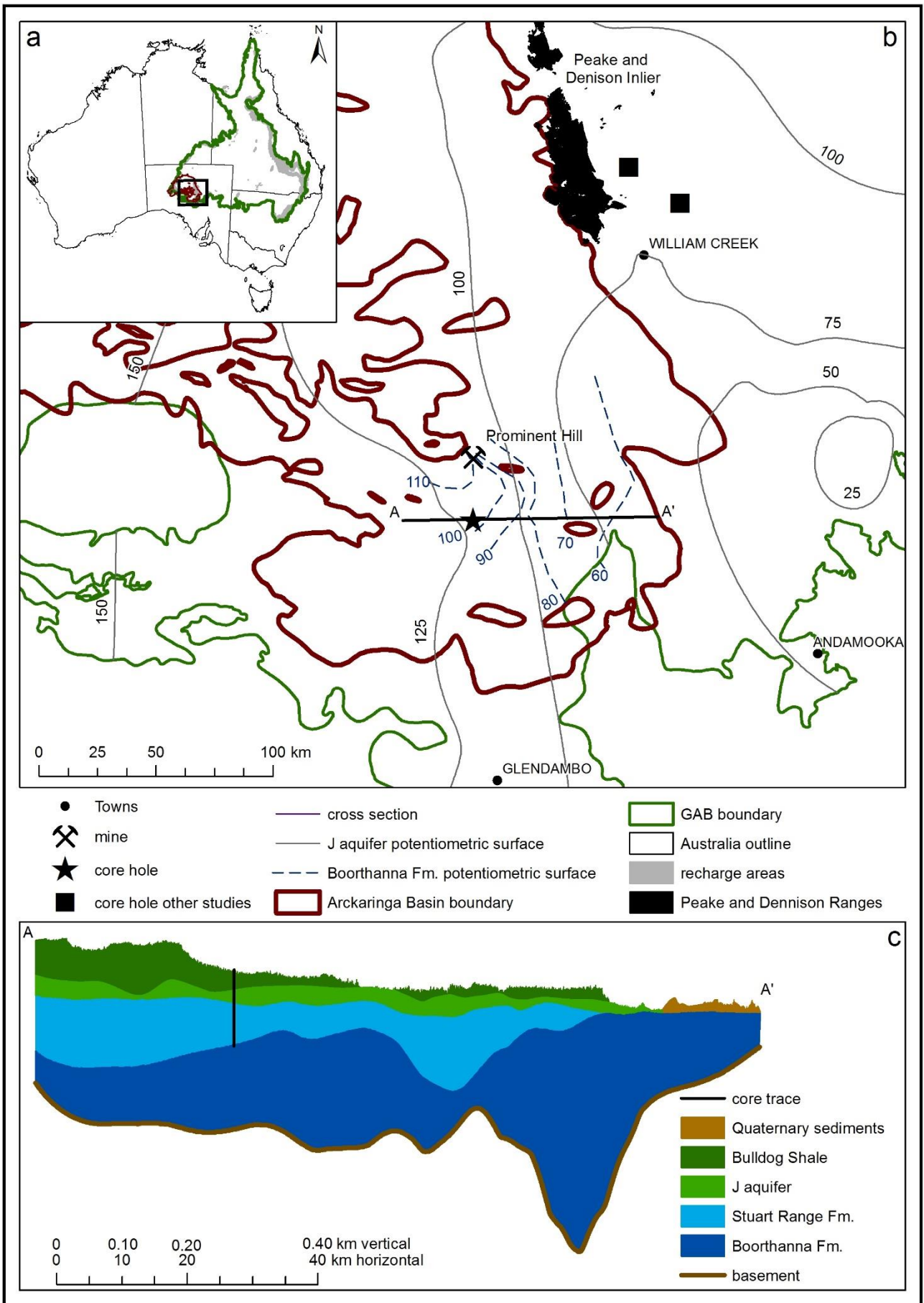


Figure 6.1 (a) Study location in the GAB and Arckaringa Basin in central Australia, also showing main recharge areas, (b) location of core from this study as well as those from Gardner et al. (2012) and Harrington et al. (2013). Groundwater potentiometric surfaces included with hydraulic head in m AHD and (c) cross section showing stratigraphy and depth of the core.

6.4 Methods

6.4.1 Sampling and analytical methods

The core through the GAB, the Stuart Range Fm. and into the lower aquifer was drilled in March 2015. The core was drilled 30 m from existing groundwater wells completed in the J aquifer in the GAB above the aquitard and the Boorthanna Fm. in the Arckaringa Basin below (Kleinig et al. 2015). Upon completion of the borehole, Vibrating Wire Piezometers (VWP) were grouted into the borehole spaced 13 m apart from 50.8 to 102.8 m through the aquitard (Kleinig et al. 2015). VWP pore pressure readings were used to determine the vertical fluid pressure gradient (Smerdon et al. 2014).

Core samples were collected for physical and chemical analysis by first shaving off and discarding the outer core (approximately 2 mm) to avoid drilling fluid contamination. The drilling fluid had been spiked with heavy water (D_2O) to be able to confirm this. Samples for chloride and uranium/thorium analysis were collected at 2 and 5 m intervals, respectively. The 20 cm length shaved samples were vacuum-sealed in two Food Saver® bags. The $\delta^{18}O$ and δ^2H 5 cm length samples collected every 2 m were sealed in a small Ziploc® bag with all the air squeezed out then placed in a second large Ziploc® bag following the method outlined by Wassenaar et al. (2008). Undisturbed 25 cm length samples for permeability and porosity determination were collected every 10 m, and where there was a lithological change. Samples were wrapped in plastic and labelled with the depth interval and an arrow to indicate direction to top of core, then placed in a PVC pipe for protection and vacuum sealed in a Food Saver® bag.

Samples for noble gas analysis were sub-cored every 5 m using a 35 mm diameter handheld electric drill, to avoid sampling the outer core that may have already degassed or been contaminated. The sub-cores were immediately transferred into stainless steel canisters for storage, following the sub-core degassing method developed by Osenbrück et al. (1998). After the sub-cores were transferred, the canisters were flushed with ultra-high purity nitrogen and subsequently evacuated three times to remove any atmospheric gases (Ali et al. 2011), and the

samples were then allowed to degas for 6 months before analysis to ensure total degassing of the noble gases.

The nearby groundwater monitoring wells screened in the upper and lower aquifers were sampled for major elements and noble gases. Major element samples were filtered with a 0.45 µm filter and collected in a rinsed HDPE bottle. Noble gas water samples were collected in copper tubes using stainless steel pinch-off clamps (Weiss 1968; Beyerle et al. 2000).

Groundwater chloride concentrations were measured by ion chromatography by CSIRO, Adelaide, Australia, using APHA method 4110 that has a coefficient of variation <2% (APHA 1998). Uranium and thorium concentrations in the sediment samples were analysed by hydrofluoric acid digestion of the dried sediment and then analysed by mass spectrometry at the same laboratory. Noble gas groundwater concentrations were analysed by mass spectrometry in the noble gas laboratory of ETH Zurich, Switzerland, according to the methods discussed by Beyerle et al. (2000). Measurement precision is <1.0% for helium concentration.

Analysis of chloride, as well as $\delta^{18}\text{O}$ and $\delta^2\text{H}$ in the core pore waters and drilling fluid were undertaken at Flinders University, Australia. It was not possible to obtain a large enough pore water sample from the core by squeezing or centrifuging. Instead, for chloride analysis, pore waters were extracted using the 1:5 dilution method outlined by Sacchi et al. (2001). The extracted water was filtered using a 0.45 µm filter and chloride was then analysed on a Metrohm 883 Basic IC plus Ion Chromatograph (IC) using in-house standard solutions to generate calibration graphs following standard analytical techniques (APHA 1998). Precision for anion analysis is $\leq 2.5\%$. $\delta^{18}\text{O}$ and $\delta^2\text{H}$ were analysed on a Picarro L21302-i using the vapour equilibration method outlined in Wassenaar et al. (2008). The difference between repeated measurements for $\delta^{18}\text{O}$ and $\delta^2\text{H}$ was $\leq 5\%$.

Conversion of the chloride concentrations obtained with the 1:5 dilution method into the in-situ chloride concentration per litre of pore water is based on the so-called geochemical porosity (Horseman et al. 1996; Pearson 1999; Waber and Smellie 2008). The geochemical porosity (also referred to as effective porosity n_e) is less than the total porosity (n), especially for anions, which are repelled from the double layer that occupies the pore space near negatively-charged minerals (Pearson 1999; Van Loon et al. 2007; Waber and Smellie 2008). Typical experimentally derived n_e/n values range between 0.3–0.6, but at high ionic strength ($I \geq 1$ mol/kg) n_e can approach n as

the double layer collapses (Van Loon et al. 2007). The measured concentrations of solutes in the 1:5 dilution extract aqueous leach solution was converted to the pore water concentration (C_{geochem}) according to:

$$C_R = C_L \frac{V_L}{M_R} \quad (6.1)$$

and

$$C_{\text{geochem}} = C_R \rho \frac{1}{n_e} \quad (6.2)$$

where C_R is the mass of chloride per mass of bulk rock sample [M/M], C_L is the mass of chloride per volume of leach solution [M/L³], V_L is the volume of leach solution [L³], M_R mass of bulk sample leached [M], ρ is the bulk density [M/L³] and n_e is the geochemical porosity (Waber and Smellie 2008; Hendry and Harrington 2014). For chloride, n_e is estimated from n by assuming an n_e/n value of 0.7 because of the ionic strength (up to 0.7 mol/kg) of the pore waters (Van Loon et al. 2007).

Permeability, porosity and moisture content measurements were undertaken by the Ground Science Engineering testing laboratory, in Victoria, Australia. The permeability of the sample was measured using a tri-axial cell at the in-situ pressure of the sample, following the method AS 1289.6.7.1-2000 (Standards Australia 2000). The porosity of the samples were measured using both the specific gravity and bulk density (method AS 1289.5.1.1-2000) as well as the moisture content (method AS 1289.2.1.1-2000) methods (Standards Australia 2000). The specific gravity test determines the density of the particles making up the sample, while the bulk density gives the volume and mass of the material. From these it is possible to determine the porosity of the sample using the method AS 1289.6.7.3-1999 (Standards Australia 1999).

The noble gases of the aquitard pore waters were determined by mass spectrometry using standard procedures (Stute et al. 1995; Ali et al. 2011) in the facilities at Lamont Doherty Earth Observatory, New York, US. Measurement precision is between 1.0–3.0% for noble gas concentrations. Some core samples were re-analysed after two weeks to ensure total degassing of the core pore fluids. Pore water concentrations were calculated using an n_e/n ratio of 1.0 since noble gases are chemically neutral and should not be affected by clay mineral double-diffusive layer charge repulsion (Gardner et al. 2012).

To remove the atmospheric helium component, the concentration of neon in water in equilibrium with the atmosphere at 25°C and elevation of 150 m AHD was removed from the measured helium concentrations (Ballentine et al. 2002; Torgersen and Stute 2013). This assumes that helium and neon are in equilibrium with the atmosphere, which is an underestimate, as it does not account for the unknown excess air component. The excess air component could not be calculated because of gas loss during sampling (Osenbrück et al. 1998).

6.4.2 Modelling

Modelling was aimed at evaluating the effective ⁴He and chloride diffusion coefficients, the internal ⁴He release rate from solids and the advective vertical flow component at the site. A steady state analytical solution to the one-dimensional advection-dispersion equation developed by Solomon et al. (1996) and a one-dimensional transient numerical model using MT3DMS (Zheng and Wang 1999) were employed to simulate the observed helium and chloride concentrations at the site.

The 1D advection-dispersion equation (also referred to as 1D advection-diffusion equation) is:

$$n_e \frac{\partial C}{\partial t} = \frac{\partial}{\partial z} \left(n_e D \frac{\partial C}{\partial z} \right) - \frac{\partial}{\partial z} (v_z n_e C) + n_e \rho G \quad (6.3)$$

where v_z is linear pore water velocity [L/T], C is the concentration of chloride [M/L³] or helium [L³/L³] in pore water; z is the vertical spatial coordinate (positive downward) [L]; D is the coefficient of hydrodynamic dispersion [L²T⁻¹], n_e is the effective porosity, i.e. the porosity accessible to the solute, G is accumulation rate per mass of pore water due to zero-order production, i.e. radiogenic ⁴He accumulation rate per volume of pore water [L³/L³T] ($G = 0$ for Cl), ρ is water density [M/L³] and t is time [T].

Under steady state conditions, the transport of a solute that is being produced in the subsurface at a constant rate is described by the following equation:

$$v_z \frac{\partial C}{\partial z} = D \frac{\partial^2 C}{\partial z^2} + \frac{G^*}{n_e} \quad (6.4)$$

where G^* is the release rate per volume of sediment due to zero-order production, i.e. radiogenic ⁴He accumulation rate per volume of sediment [L³/L³T] ($G^* = 0$ for Cl).

The analytical solution of eq. 5.4, subject to boundary conditions, is given by Solomon et al. (1996) as:

$$C(z) = \frac{C_L - \frac{G^*L}{v_z n_e}}{1 - \exp\left(\frac{v_z L}{D}\right)} \left\{ 1 - \exp\left(\frac{v_z z}{D}\right) \right\} + \frac{G^* z}{v_z n_e} \quad (6.5)$$

where L is the depth from the top of the aquitard to the bottom of the aquitard [L] and G^* is the release rate per volume of rock [L^3/L^3T].

For low advection velocities, the coefficient of hydrodynamic dispersion (D) simplifies to the effective diffusion coefficient (D_e) as the contribution of hydrodynamic dispersion to D becomes insignificant. The effective diffusion coefficient can be estimated using an Archie's Law relationship (Grathwohl 1958):

$$D_e = D_o n_e^m \quad (6.6)$$

where D_o is the free solution aqueous diffusion coefficient ($D_o = 6.40 \times 10^{-2} \text{ m}^2/\text{yr}$ for chloride at 25°C and $D_o = 2.30 \times 10^{-1} \text{ m}^2/\text{yr}$ for ^4He at 25°C); (Yuan-Hui and Gregory 1974; Jähne et al. 1987; Cook and Herczeg 2000) and m is an empirical exponent known as the cementation factor. For anions, $m = 2-2.5$ based on laboratory measurements, so a value of 2.3 was used for chloride, as per Harrington et al. (2013). As helium has access to the same pore volume as water $m = 2$ was selected for ^4He to obtain the maximum expected diffusion coefficient (Mazurek et al. 2011; Gardner et al. 2012). An average measured in-situ temperature of 25.4°C (range 24.9–26.0 °C; Table 6.1) measured via the VWP thermistors meant that D_e values did not need to be temperature corrected.

The radiogenic ^4He release rate from solids in $\text{cm}^3 \text{STP}/\text{m}^3_{\text{rock}}/\text{yr}$ (G^*) can be calculated with:

$$G^* = 0.2355 \times 10^{-12} \left([U] \left(1 + 0.123 \left(\frac{[Th]}{[U]} - 4 \right) \right) \right) (\rho \Lambda_{\text{He}}) \quad (6.7)$$

And the radiogenic ^4He accumulation rate per volume of pore water in $\text{cm}^3 \text{STP}/\text{m}^3_{\text{H}_2\text{O}}/\text{yr}$ (G), assuming water density = $10^6 \text{ g}/\text{m}^3$, can be calculated with:

$$G = G^* \left(\frac{1-n}{n} \right) \quad (6.8)$$

where $\Lambda_{\text{He}} = 1$ (Torgersen and Clarke 1985), ρ is the density of the sediment and water filled pore spaces [M/L^3], and [U] and [Th] are concentration of uranium and thorium expressed in parts per million (Torgersen 1980; Torgersen and Stute 2013).

The relative importance of advection and diffusion in an aquitard of thickness L can be characterised by the Peclet number (Pe). Neglecting dispersion and accounting for the effective porosity (n_e) under steady state boundary conditions, Pe is defined as (Huysmans and Dassargues 2005):

$$Pe = \frac{v_z L}{n_e D_e} \quad (6.9)$$

Values of $Pe < 1$ indicate that transport over distance L is dominated by diffusion, whereas if $Pe > 1$ then advection will be dominant over diffusion.

Model parameters and boundary conditions are listed in Table 6.2. The same boundary conditions were used in both the analytical solution and the MT3DMS numerical model. The solute profiles were simulated over the entire aquitard sequence, i.e. extending from 46.6 metres below the surface at the top boundary and 104 metres below the surface at the base. The vertical linear pore water velocity (v_z) was fixed, and hydraulic parameters such as hydraulic conductivity (K_v) and porosity (n), were held constant in all simulations assuming steady state flow conditions in the aquitard. Upper and lower boundary concentrations were fixed in the models (Dirichlet type), but the solute concentrations could be variable in time in the transient MT3DMS numerical model. The radiogenic ^4He accumulation rate (G) was also fixed as this was calculated from U and Th concentrations measured in four aquitard samples (Table 6.1).

6.5 Results

6.5.1 Field data

The measured groundwater and pore water compositional data, and hydraulic properties are given in Table 6.1. The $\delta^2\text{H}$ values of the pore waters (-20 to -33 ‰ VSMOW) are higher compared to the groundwater samples (-32 to -36 ‰ VSMOW; Figure 6.2). Likewise, the $\delta^{18}\text{O}$ values of the pore waters (-1.1 to -2.9 ‰ VSMOW) are higher than the groundwater samples (-2.7 to -3.7 ‰ VSMOW; Figure 6.2). Even though the samples had more than 5% moisture content (Table 6.1) required for the applied method (Wassenaar et al. 2008), it is possible that there was insufficient sample collected to equilibrate with the Ziploc® bag headspace. Hendry et al. (2015a) determined

that samples with less than 3 g of water appear more enriched due to isotope fractionation by water loss to the bag headspace. Contamination by the deuterium spiked drilling fluid would cause an enrichment in $\delta^2\text{H}$ composition only. The slight enrichment of both $\delta^2\text{H}$ and $\delta^{18}\text{O}$ in the pore water compared to the groundwater samples is therefore believed to be due to insufficient pore water in the bag rather than drilling fluid contamination during sampling (Figure 6.2). Because of the suspected analytical problems and the large relative errors (Figure 6.2), the pore water isotopes results were not further considered for modelling.

Table 6.1 Aquitard pore water chemistry, measured aquitard properties, groundwater chemistry in italics, as well as uranium and thorium concentrations in sediment samples.

Formation	Depth (m)	Elevation (m AHD)	Hydraulic head (m AHD)	Temperature (°C)	K_v ($\frac{m}{yr}$)	ρ ($\frac{g}{cm^2}$)	n (%VOL)	Moisture Content (%)	Th ($\frac{mg}{kg}$)	U ($\frac{mg}{kg}$)	4He ($\frac{ccSTP}{H_2O}$)	Ne ($\frac{ccSTP}{H_2O}$)	Ar ($\frac{ccSTP}{H_2O}$)	Cl ($\frac{mg}{L}$)	δ^2H (‰ VSMOW)	$\delta^{18}O$ (‰ VSMOW)
Bulldog Shale - aquitard	0.00	154.00	—	—	—	—	—	—	—	—	—	—	—	—	—	—
	10.80	143.20	—	—	6.31×10^{-3}	1.65	58.10	48	—	—	—	—	—	—	—	—
Upper aquifer (J aquifer)	17.80	136.20	—	—	—	—	—	—	—	—	—	—	—	—	—	—
	34.55	119.45	—	—	$1.89 \times 10^{+1}$	1.80	42.80	19	2.32	0.96	—	—	—	—	—	—
	39.00	115.00	114.96	25.2	—	—	—	—	1.12	1.08	8.70×10^{-8}	1.87×10^{-7}	2.61×10^{-4}	6390	-32.2	-2.7
	46.60	107.40			3.15×10^{-1}	2.40	13.30	5	—	—						
Stuart Range Fm. - aquitard	46.60	107.40	—	—	—	—	—	—	—	—	—	—	—	—	—	—
	47.23	106.78	—	—	—	—	—	—	1.12	1.08	—	—	—	6302	-28.7	-1.9
	48.33	105.68	—	—	3.15×10^{-4}	2.21	26.00	11	—	—	—	—	—	—	-23.9	-1.7
	48.68	105.33	—	—	—	—	—	—	—	—	—	—	—	6053	—	—
	50.68	103.33	109.65	24.89	—	—	—	—	—	—	1.17×10^{-6}	1.16×10^{-7}	2.02×10^{-4}	5532	-21.5	-1.8
	52.23	101.78	—	—	—	—	—	—	—	—	—	—	—	6029	-21.3	-2.1
	53.70	100.30	—	—	2.52×10^{-4}	2.26	25.00	11	—	—	—	—	—	—	—	—
	55.58	98.43	—	—	—	—	—	—	—	—	3.08×10^{-6}	1.34×10^{-7}	2.09×10^{-4}	5416	-25.0	-2.1
	56.73	97.28	—	—	—	—	—	—	—	—	—	—	—	5222	—	—
	58.60	95.40	—	—	6.31×10^{-5}	2.26	24.70	11	1.21	1.23	—	—	—	—	—	—
	59.73	94.28	—	—	—	—	—	—	—	—	—	—	—	5466	-23.9	-2.3
	61.13	92.88	—	—	—	—	—	—	—	—	5.73×10^{-6}	1.28×10^{-7}	2.11×10^{-4}	5472	-28.1	-1.7
	62.63	91.38	108.73	24.92	—	—	—	—	—	—	—	—	—	5237	-20.5	-2.2
	66.38	87.63	—	—	—	—	—	—	—	—	—	—	—	4518	-28.2	-2.5
	68.00	86.00	—	—	—	—	—	—	—	—	—	—	—	5226	-24.6	-2.2
68.30	85.70	—	—	—	1.26×10^{-2}	2.31	21.90	10	—	—	—	—	—	—	—	

	69.73	84.28	—	—	—	—	—	—	—	—	9.38 x 10 ⁻⁶	1.24 x 10 ⁻⁷	2.09 x 10 ⁻⁴	—	—	—
	71.25	82.75	—	—	—	—	—	—	—	—	—	—	—	6909	-32.8	-2.5
	73.15	80.85	—	—	—	—	—	—	—	—	9.65 x 10 ⁻⁶	1.70 x 10 ⁻⁶	1.02 x 10 ⁻³	5658	-26.6	-2.4
	76.15	77.85	106.44	25.36	—	—	—	—	—	—	—	—	—	5955	-24.7	-1.1
	77.30	76.70	—	—	1.89 x 10 ⁻⁵	2.32	20.70	9	—	—	—	—	—	—	—	—
	78.20	75.80	—	—	—	—	—	—	—	—	1.20 x 10 ⁻⁵	1.59 x 10 ⁻⁷	2.00 x 10 ⁻⁴	6142	-28.0	-2.2
	80.65	73.35	—	—	—	—	—	—	—	—	—	—	—	6192	-29.0	-2.3
	83.15	70.85	—	—	—	—	—	—	—	—	—	—	—	6886	-20.5	-2.3
	84.20	69.80	—	—	1.26 x 10 ⁻⁵	2.33	20.40	8	—	—	1.75 x 10 ⁻⁵	1.13 x 10 ⁻⁷	1.97 x 10 ⁻⁴	—	—	—
	85.45	68.55	—	—	—	—	—	—	—	—	—	—	—	8008	-23.7	-2.9
	87.08	66.93	—	—	—	—	—	—	0.79	2.31	—	—	—	9173	-25.8	-2.8
	90.48	63.53	105.01	25.7	—	—	—	—	—	—	—	—	—	—	—	—
	90.60	63.40	—	—	—	—	—	—	—	—	1.81 x 10 ⁻⁵	4.29 x 10 ⁻⁶	1.68 x 10 ⁻³	14439	-25.4	-2.5
	91.78	62.23	—	—	6.31 x 10 ⁻⁵	2.49	12.10	4	—	—	—	—	—	—	—	—
	93.15	60.85	—	—	—	—	—	—	—	—	—	—	—	10548	-22.5	-2.6
	95.23	58.78	—	—	—	—	—	—	—	—	—	—	—	12001	-23.3	-2.9
	97.30	56.70	—	—	—	—	—	—	—	—	2.10 x 10 ⁻⁵	1.17 x 10 ⁻⁷	1.83 x 10 ⁻⁴	15087	-21.2	-2.0
	99.25	54.75	—	—	2.21 x 10 ⁻⁴	2.27	22.30	11	—	—	—	—	—	—	—	—
	99.73	54.28	—	—	—	—	—	—	—	—	—	—	—	14469	-25.9	-2.9
	102.08	51.93	103.33	25.96	—	—	—	—	—	—	—	—	—	14347	-22.7	-2.2
	103.73	50.28	—	—	—	—	—	—	—	—	2.94 x 10 ⁻⁵	1.11 x 10 ⁻⁷	1.95 x 10 ⁻⁴	—	—	—
	103.88	50.13	—	—	—	—	—	—	2.07	1.68	—	—	—	16564	—	—
Lower aquifer (Boorthanna Fm.)	104.00	50.00	—	—	—	—	—	—	—	—	—	—	—	—	—	—
	106.73	47.28	—	—	—	—	—	—	2.64	1.76	—	—	—	—	—	—
	108.00	46.00	107.74	27.44	1.58 x 10 ⁻⁴	2.31	20.10	8.1	—	—	7.99 x 10 ⁻⁵	1.98 x 10 ⁻⁷	2.64 x 10 ⁻⁴	21500	-35.8	-3.7
	138.00	16.00			—	—	—	—	—	—						

Table 6.2 Solute transport model boundary conditions and SRMS error. The model parameters determined from the aquitard core samples are bolded, whereas the model parameters unbolded were allowed to vary from those calculated and estimated from the aquitard core measurements to improve model fit with measured pore water concentrations.

							upper boundary			lower boundary			
	K_v (m/yr)	v_z (m/yr)	G (ccSTP/m ³ _{H₂O} /yr) ^a	solute	D_e (m ² /yr) ^b	n_e	C_i ^c	C t = 0 yrs	C t > 417,000 yrs	C_i ^c	C t = 3000 yrs	SRMS ⁴ He	SRMS Cl
model 1 (diffusion only) ^d	0	0	2.1 x 10⁻⁶	Cl	1.9 x 10⁻³	0.182	5200			21500		37	38
				⁴ He	1.1 x 10⁻²	0.216	8.7 x 10 ⁻⁸			8.0 x 10 ⁻⁵			
model 2 (calculated boundary conditions)	4.6 x 10⁻⁵	2.3 x 10⁻⁵	2.1 x 10⁻⁶	Cl	1.9 x 10⁻³	0.182	5000			21500		36	27
				⁴ He	1.1 x 10⁻²	0.216	8.7 x 10 ⁻⁸			8.0 x 10 ⁻⁵			
model 3 (optimised boundary conditions)	4.3 x 10 ⁻⁴	3.5 x 10 ⁻⁴	2.1 x 10⁻⁶	Cl	7.8 x 10 ⁻⁴	0.182	5000			21500		20	12
				⁴ He	1.2 x 10 ⁻³	0.216	8.7 x 10 ⁻⁸			8.0 x 10 ⁻⁵			
model 4 (model 3-time to steady state)	4.5 x 10 ⁻⁴	3.5 x 10 ⁻⁴	2.1 x 10⁻⁶	Cl	7.8 x 10 ⁻⁴	0.182	21500 ^e	5000 ^f	—	21500	—	20	12
				⁴ He	1.2 x 10 ⁻³	0.216	8.0 x 10 ^{-5e}	8.7 x 10 ^{-8f}	—	8.0 x 10 ⁻⁵	—		
model 5 (model 3 with chloride increase)	4.5 x 10 ⁻⁴	3.5 x 10 ⁻⁴	2.1 x 10⁻⁶	Cl	7.8 x 10 ⁻⁴	0.182	21500 ^e	5000 ^f	6390 ^g	21500	—	20	10
				⁴ He	1.2 x 10 ⁻³	0.216	8.0 x 10 ^{-5e}	8.7 x 10 ^{-8f}	—	8.0 x 10 ⁻⁵	—		
model 6 (reduced concentrations)	8.6 x 10 ⁻⁴	7.0 x 10 ⁻⁴	2.1 x 10⁻⁶	Cl	1.9 x 10⁻³	0.182	5000			16600 ^h		18	12
				⁴ He	1.1 x 10⁻²	0.216	8.7 x 10 ⁻⁸			3.0 x 10 ^{-5h}			
model 7 (model 6 with groundwater extraction)	8.6 x 10 ⁻⁴	7.0 x 10 ⁻⁴	2.1 x 10⁻⁶	Cl	1.9 x 10⁻³	0.182	5000	6390	—	16600	21500 ⁱ	6	10
				⁴ He	1.1 x 10⁻²	0.216	8.7 x 10 ⁻⁸	—	—	3.0 x 10 ⁻⁵	8.0 x 10 ⁻⁵ⁱ		

^a $G = G^* \left(\frac{1-n}{n} \right)$, so $G^* = 5.5 \times 10^{-7}$ ccSTP/m³_{aq}/yr

^b Closer inspection of the equations used in MT3DMS (Zheng and Wang 1999; Harrington et al. 2013) and the steady state solution (Solomon et al. 1996; Sheldon et al. 2003) reveals the effective diffusion coefficient input parameter is actually equivalent to D_p , where $D_p = D_e/n_e$

^c Chloride concentration units are mg/L and helium concentration units are ccSTP/g_{H₂O}

^d Model 1 run in MT3DMS as v_z cannot equal zero in the steady state solute transport analytical solution due to the development of the solution

^e High initial concentration to represent possible initial conditions

^f Instantaneous reduction (freshwater flushing) to estimate minimum time required to reach steady state solute transport

^g Instantaneous chloride concentration increase (increased evapotranspiration) to give the minimum time required to match upper profile

^h Reduced chloride and helium concentrations in the lower boundary to give best steady state solute transport profile fit

ⁱ Instantaneous increase in lower boundary concentrations as a result of groundwater extraction

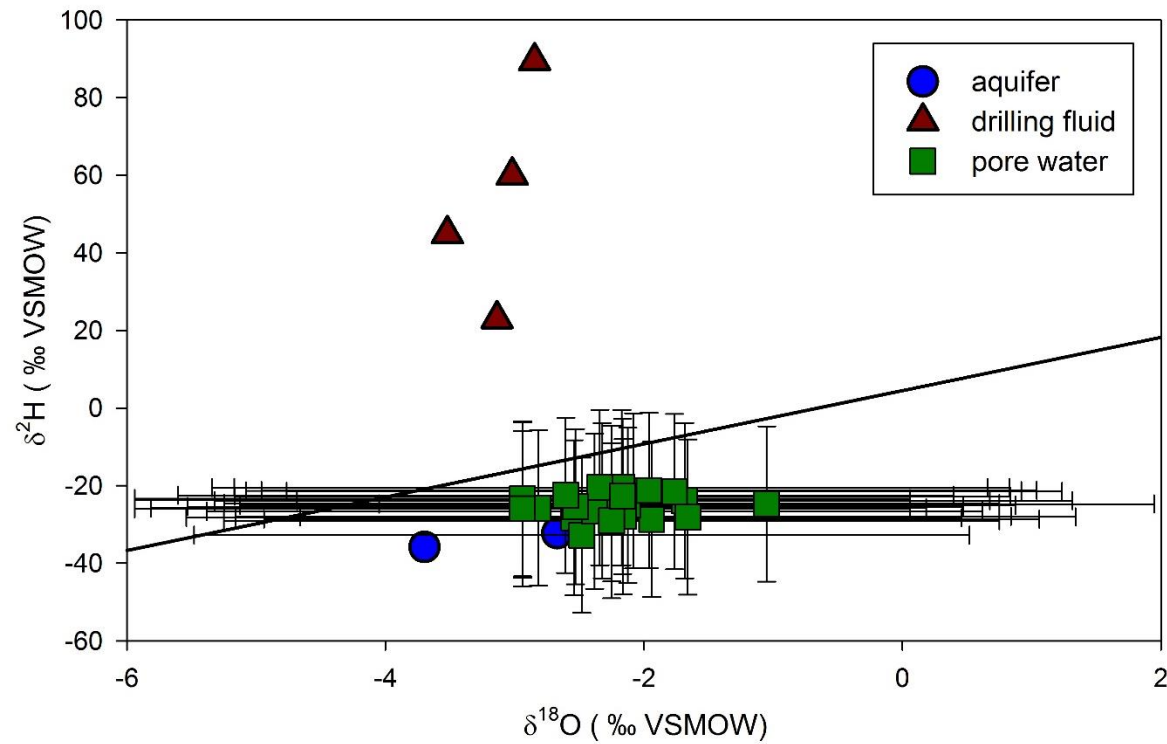


Figure 6.2 $\delta^{18}\text{O}$ and $\delta^2\text{H}$ in pore water, groundwater and drilling fluid samples. Error bars represent the possible isotopic equilibrium fractionation difference for samples with less than 3 g water, adapted from Hendry et al. (2015a). The black line represents the local meteoric water line (LMWL) $\delta^2\text{H} = 7.2\delta^{18}\text{O} + 5.7$ from Alice Springs.

The measured vertical hydraulic conductivity (K_V) of the aquitard ranges from 1.3×10^{-5} to 1.3×10^{-2} m/yr while porosity ranges from 0.12 to 0.26 with no discernible pattern with depth (Table 6.1). The VWP data and hydraulic head measurements in the aquifer piezometers indicate downward flow (Figure 6.3). Pumping from the lower aquifer since 2008 has affected the current flow system by increasing the hydraulic head difference between the upper aquifer and lower aquifer (Figure 6.3). Calculation of the vertical groundwater flow rate using Darcy's law and the harmonic mean K_V of 4.6×10^{-5} m/year and porosity of 0.216 (Table 6.3; Kleinig et al. 2015) and pre-pumping freshwater heads give a vertical linear pore water velocity (v_z) of 2.0×10^{-4} m/yr (range of 6.0×10^{-6} – 6.5×10^{-3} m/yr; Table 6.3). Thus, Pe could range from 0.1–160 for ^4He and 1–1082 for chloride (Table 6.3). The range of Pe values indicate that solute transport in the system could be driven by diffusion, advection or both depending on which K_V measurement is representative of the aquitard as a whole.

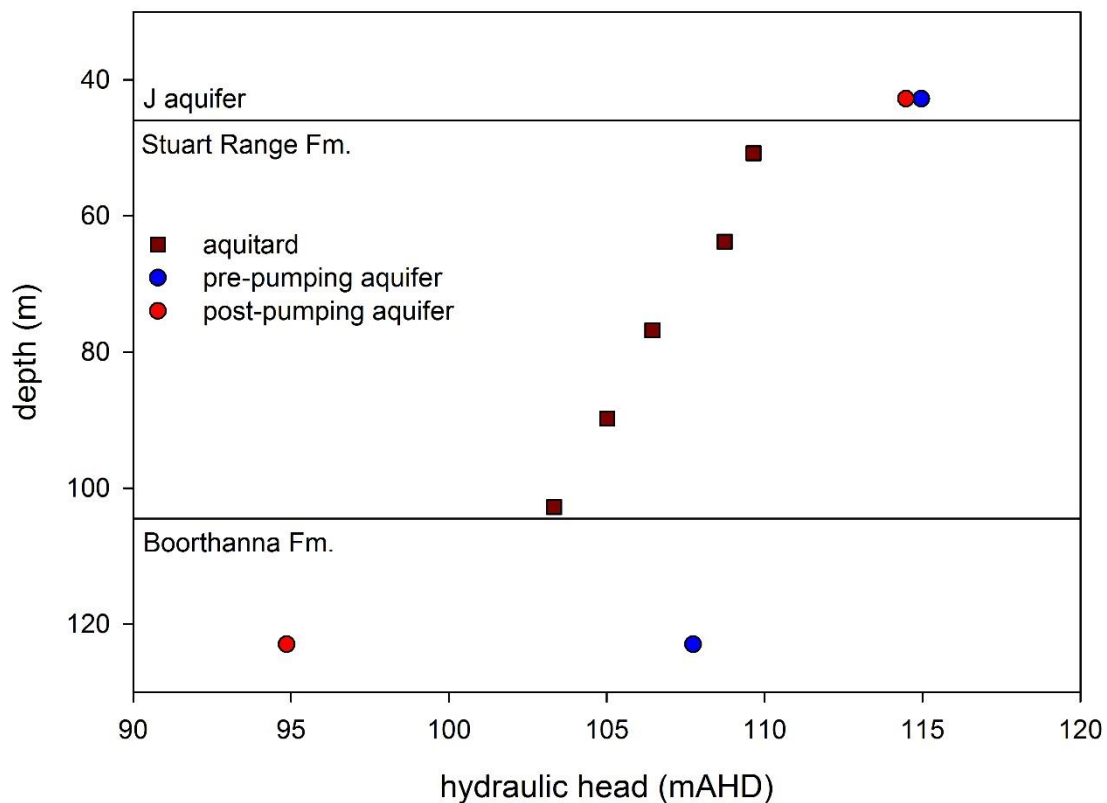


Figure 6.3 hydraulic head in m AHD by the VWP installed throughout the aquitard and measured in nearby wells in the upper aquifer and lower aquifer.

Table 6.3 Measured aquitard core properties bolded (Kleinig et al. 2015) and calculated vertical flow velocities, diffusion coefficients, geochemical porosity and Peclet Numbers for ⁴He and in brackets for chloride

	Min K_V	Max K_V	Mean K_V
K_V (m/yr)	1.3×10^{-5}	1.3×10^{-2}	4.6×10^{-5}
v_z (m/yr)	6.0×10^{-6}	6.5×10^{-3}	2.3×10^{-5}
n_e	0.216 (0.182) ^a		
D_e (m ² /yr)	1.1×10^{-2} (1.9×10^{-3}) ^b		
thickness of aquitard (m)	57.4		
Peclet Numbers	0.1 (1)^c	160 (1082)^c	1 (4)^c

^a lower effective porosity for chloride in brackets

^b smaller effective diffusion coefficient for chloride in brackets

^c Peclet number for chloride in brackets

Pore water chloride and helium profiles are presented in Figure 6.4. Chloride pore water concentrations range from 4518 to 16,564 mg/L (Table 6.1; Van Loon et al. 2007). The lowest chloride concentrations occur around a depth of 65 m. The increase in chloride concentration at the top of the profile suggests there has been a change in the upper boundary condition.

The ⁴He pore water concentrations with the atmospheric component removed using the concentration of neon in water in equilibrium with the atmosphere at 25°C and elevation of 150 m AHD range from 1.2×10^{-6} to 2.9×10^{-5} ccSTP/g (Table 6.1). Neon concentrations in all but two pore water samples are approximately 14–39% less than the values expected for atmospheric equilibrium. This is consistent with Osenbrück et al. (1998) who estimated the gas loss during vacuum extraction to be approximately 30% of the total gas in the pore water. This has been incorporated in the ⁴He concentration uncertainty range, indicated by the bars in Figure 6.4 b. The remaining two pore water samples showed a neon excess greater than 30%, with Ar/Ne ratios between $4 \times 10^{+2}$ – $6 \times 10^{+2}$ showing that the excess is caused by atmospheric air contamination (Ar/Ne = $5 \times 10^{+2}$). The amount of air contamination required to explain the neon and argon concentration was calculated (Ballentine et al. 2002) and removed from the helium pore water concentrations to obtain the terrigenic and in-situ helium production components (Table 6.1). The above corrections and the assumptions therein make very little difference as the pore water ⁴He concentrations are >2500% of the atmospheric ⁴He concentrations. The ⁴He pore water concentrations follow a linear trend with depth. The groundwater sample from the lower aquifer has an almost three times larger concentration than the deepest pore water sample (Figure 6.4 b), and is thus clearly offset from the linear trend within the aquitard.

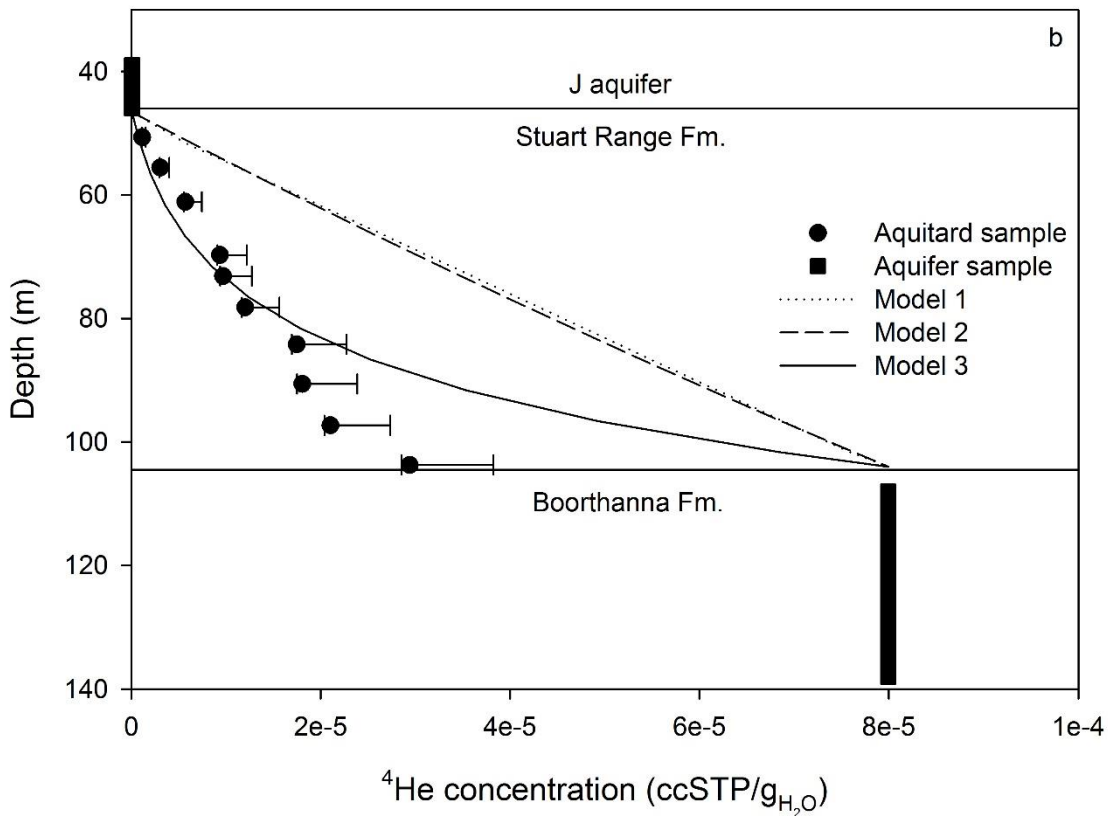
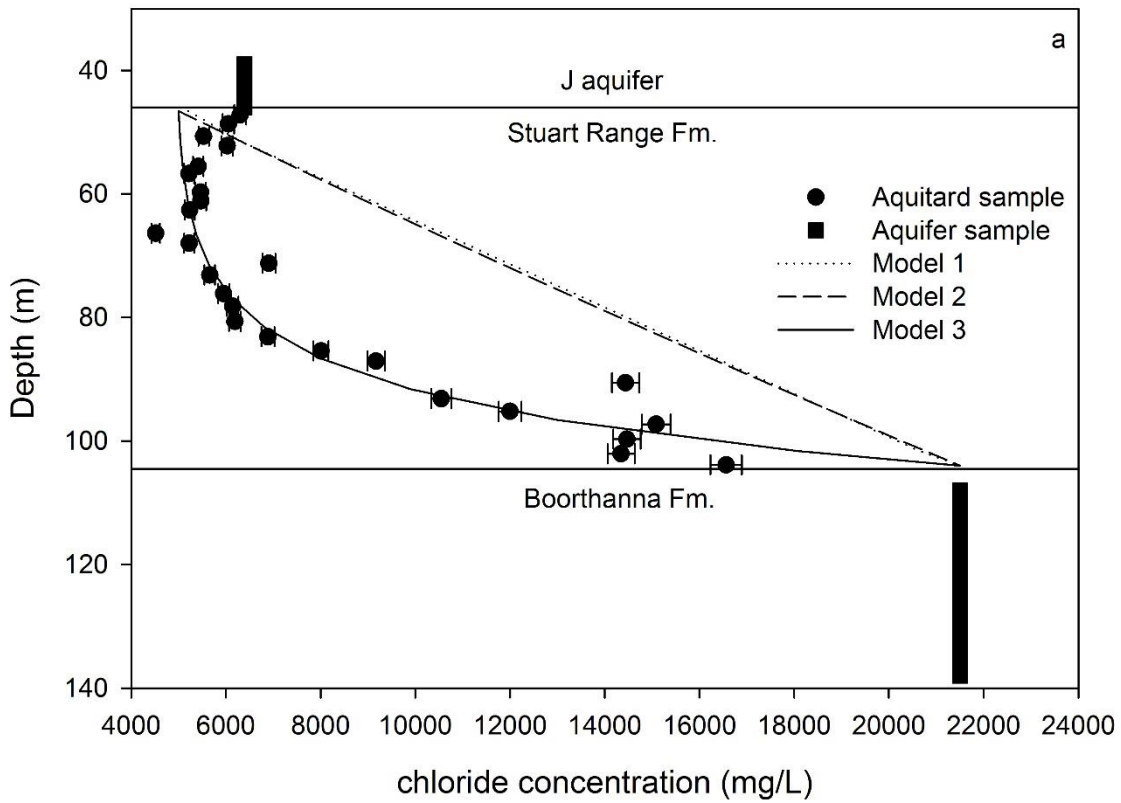


Figure 6.4 Profiles of (a) chloride and (b) ^4He concentrations. Circles indicate the pore water concentrations and the vertical bar represents the concentration in the aquifer, where the vertical length represents the screened interval. Error bars include total field and analytical errors and for ^4He the 30% degassing loss during vacuum extraction

(could be as high as 50% according to difference between measured and estimated Ne concentrations). Dotted line represents steady state solute transport analytical model 1 using estimated and calculated boundary conditions from our core measurements but diffusion only solute transport. Dashed line represents the steady state solute transport analytical model 2 using the estimated and calculated boundary conditions. Solid line represents the steady state solute transport analytical model 3 calibration of boundary conditions (v_z and D_e).

6.5.2 Model scenarios

The vertical hydraulic gradient through the aquitard (0.12) is three orders of magnitude greater than the horizontal hydraulic gradient in the aquifers (<0.0008 ; Figure 6.1) so one-dimensional vertical flow and transport simulations are considered appropriate for the solute profiles. Long groundwater flow paths in both aquifers and long-term stability in water chemistry associated with these may justify constant concentration boundary conditions. Therefore, the first conceptual models assumed constant concentration boundary conditions for both the upper and lower aquifers, as well as steady state solute transport (Table 6.2). The measured ^4He and chloride concentrations of the aquifer samples provided constraints at the top and bottom of the aquitard. This assumes that the concentrations at the well screens were representative for those at the aquitard boundaries (i.e. homogeneous aquifer concentrations), which will be reassessed later. In the first model realisation (model 1) transport was controlled by diffusion, with advection (vertical linear pore water velocity) being zero (Table 6.2). In model 2, the average calculated vertical linear pore water velocity based on Darcy's law was included, while in model 3 the estimated diffusion coefficients and vertical linear pore water velocity were adjusted to optimise the fit between the model and the measured solute profiles (Table 6.2).

A fourth model realisation was set up in order to assess the time required to reach steady state. As initial conditions in the aquitard are unknown it was necessary to assume that the initial chloride concentration in the aquitard pore water profile equaled the lower aquifer chloride concentration (Table 6.2). It is difficult to estimate the initial ^4He concentrations, but considering sediments recently deposited often release excess helium that built up in sediments prior to being weathered (Sheldon et al. 2003) we assumed ^4He concentrations equal to the lower aquifer concentration (Table 6.2). Identical transport parameters as model 3 were used, where initial pore water chloride concentration of 21,000 mg/L and helium concentration of 8.0×10^{-5} ccSTP/g_{H₂O} were assumed as the initial conditions (Table 6.2).

We hypothesise that the chloride increase visible in the upper 10 m of the profile is from reduced recharge and a subsequent increase in chloride concentration in the upper aquifer. As the flow path lag time and rate of climate change are unknown, an instantaneous concentration increase in the aquifer can estimate the minimum time since reduced recharge. This was tested in model 5 by increasing the chloride concentration in the upper boundary to the concentration measured in the upper aquifer once steady state solute transport was reached in model 4 (Table 6.2). Reduced recharge would also increase the ^4He concentration in the upper aquifer as the flow rates decrease, but since the concentrations in the aquifer are an order of magnitude lower than in the aquitard, this relative change is inconsequential.

In all of the above models, homogeneous solute concentrations throughout the aquifers are assumed. However, it is possible that the aquifers are chemically and isotopically stratified (Zhao et al. 1998; Park et al. 2002), such that the aquifer solute concentrations do not represent the top and bottom boundary conditions of the pore water profile. The helium concentration in the lower aquifer especially may not be representative because of upward diffusion from sediments below (Zhao et al. 1998). In order to test this, the lower boundary concentrations were reduced to those that fit the pore water profile in model 6 (Table 6.2). Model 7 tested subsequent perturbation of model 6 in the upper aquifer from reduced recharge and lower aquifer due to groundwater extraction (Table 6.2).

Comparison of different simulation results with measured data was undertaken using the scaled root mean squared error (SRMS) (Barnett et al. 2012):

$$SRMS = \frac{100}{\Delta C} \pi \sqrt{\frac{1}{n} \sum_{i=1}^n (z_{hi} - C_i)^2} \quad (6.10)$$

where z_{hi} are measurements of C_i at n locations and times and ΔC is the range of measured concentrations across the model domain.

Selection of the most appropriate model was based on both the SRMS errors, and whether it was justifiable from a hydrogeological perspective.

The helium accumulation rate ($G = 2.1 \times 10^{-6} \text{ ccSTP/m}^3_{\text{H}_2\text{O}}/\text{yr}$) and porosity ($n = 0.216$) determined from the core rock samples were kept constant in all the models. The diffusion coefficients, vertical linear pore water velocity estimated from current day hydraulic head measurements, or

initial solute boundary concentrations were varied in models 3–7 to provide the best fit for both chloride and helium with the smallest SRMS errors, as outlined in Table 6.2.

6.5.3 Model results

The diffusion-only transport scenario (model 1, $v_z = 0$) led to a linear concentration profile between the upper and lower aquifer (Figure 6.4), as expected. Model 2 differed only from model 1 in that it also included advection-driven solute transport ($v_z = 2.3 \times 10^{-5}$ m/yr; Table 6.2), but this resulted in only a slight adjustment in the simulated concentrations throughout the aquitard (Figure 6.4 a). However, in model 3 adjustment of transport parameters ($v_z = 3.5 \times 10^{-4}$ m/yr, $D_e = 1.2 \times 10^{-3}$ m²/yr for helium and $D_e = 7.8 \times 10^{-4}$ m²/yr for chloride; Table 6.1) provided a closer match not only for chloride, but also for the ⁴He concentration profile (Figure 6.4).

The characteristic timescales for diffusion and advection are 4×10^5 years (calculated using $t = z^2/(4D_e)$) and 3×10^5 years (calculated using $t = z/v_z$), respectively. This was further investigated in model 4 to simulate freshening of the aquifers. After an instantaneous reduction in the boundary concentrations, steady state solute transport is reached after 417,000 years for chloride and 369,000 years for helium (Figure 6.5 a and b). However, the assumption of a constant flow velocity, amongst other factors, over such a long time span is of course questionable. Once steady state conditions were reached in the numerical model, the chloride concentration at the upper boundary was increased to its present-day value measured in the upper aquifer in model 5 to infer the timing of the chloride concentration increase (Table 6.2). The simulated chloride concentration in the upper section of the profile best matched the measurements when it was assumed the increase occurred 3000 years ago (Figure 6.5 c and d).

Model 6 was used to determine if the chloride and ⁴He concentrations could be stratified in the lower aquifer, rather than homogeneous. The lower boundary concentrations were reduced to those at the lower section of the pore water profile (16,600 mg/L chloride and 3.0×10^{-5} ccSTP/g_{H2O} helium; Table 6.2). Except adjusting the vertical linear pore water velocity ($v_z = 7.0 \times 10^{-4}$ m/yr), all other transport parameters were the same as in model 2 (Table 6.2). The numerical model was then used for model 7, to increase the chloride concentration to that measured in the upper aquifer (6390 mg/L chloride; Table 6.2) and provides a match with the profile after 3000 years (Figure 6.6 c). The increase in the lower aquifer caused by pumping was considered by increasing the helium and chloride concentration in the lower aquifer to the measured concentrations in the lower aquifer, which still matches the profile after 10 years.

Model 7 provided the best fit for both chloride and helium with the smallest SRMS errors (Table 6.1; Figure 6.6 c and d).

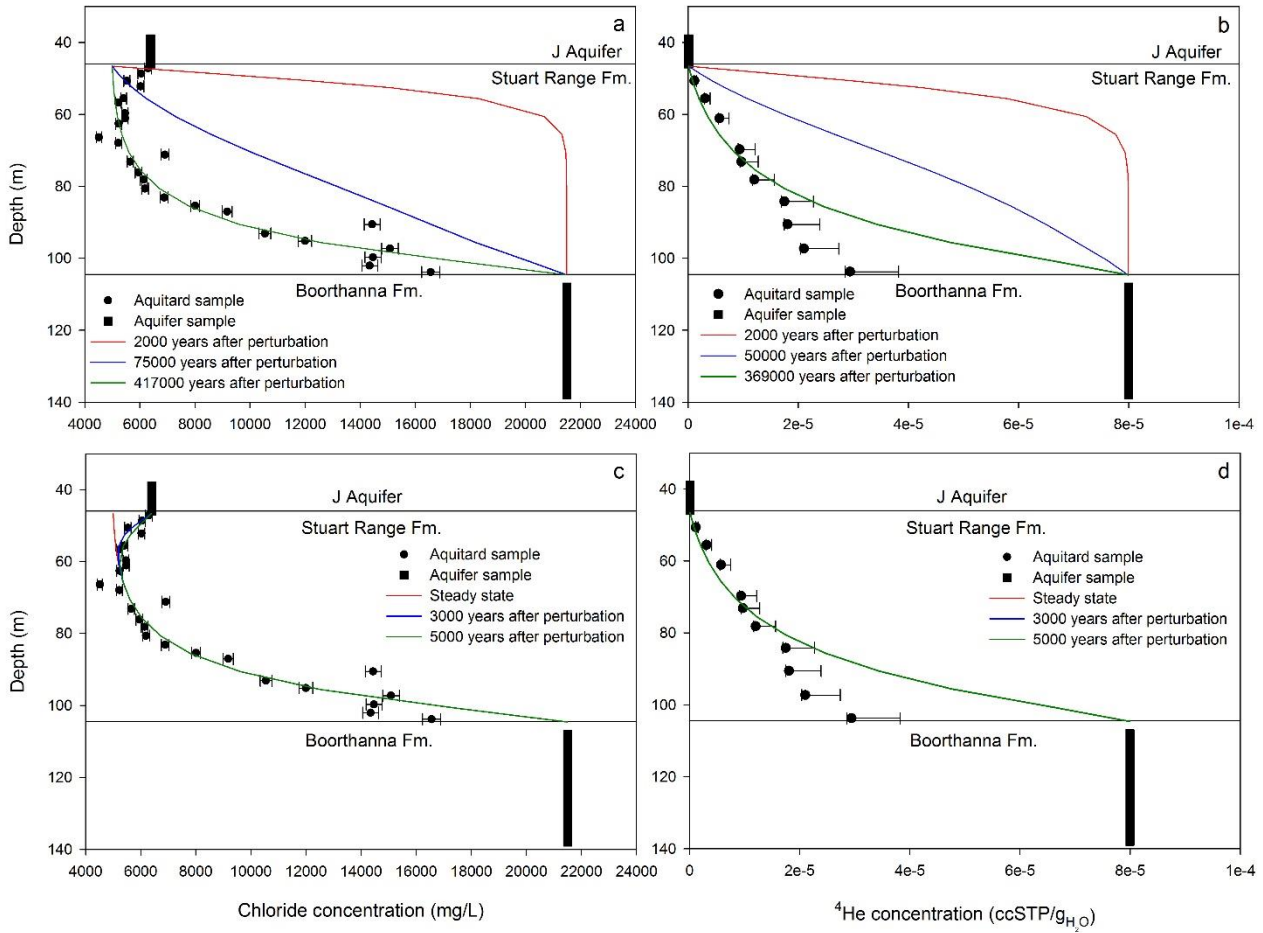


Figure 6.5 Time taken to reach steady state solute transport in model 4 from continuous high concentrations throughout the profile for (a) chloride and (b) ^4He concentration, the chloride concentration was then increased in the upper aquifer in model 5 giving the profiles for (c) chloride and (d) ^4He concentration.

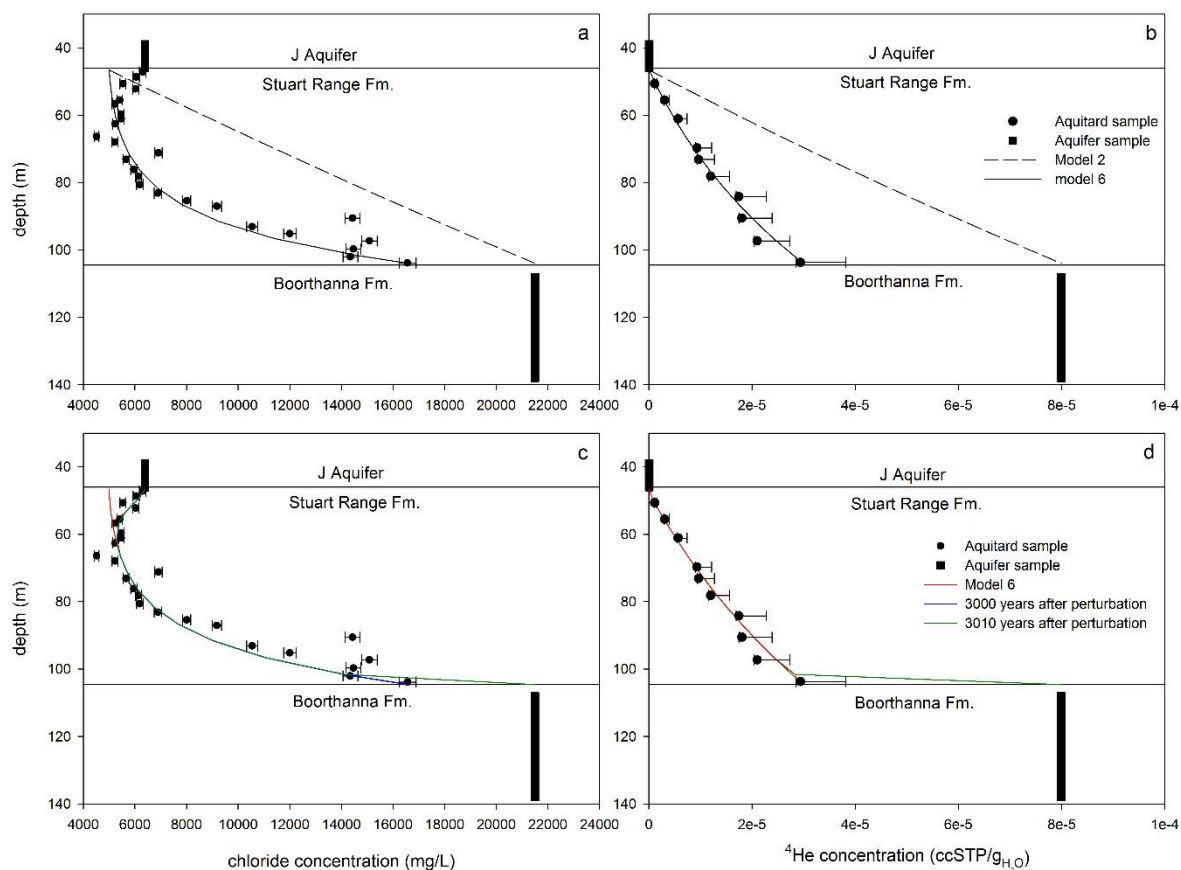


Figure 6.6 Steady state solute transport model 6 represented as a solid line compared to steady state solute transport analytical model 2 represented as a dashed line for (a) chloride and (b) ^4He concentration. The chloride concentration was then increased in the upper aquifer and then subsequently the helium and chloride concentrations were increased in the lower aquifer in model 7 giving the modelled profile for (c) chloride and (d) ^4He concentration.

6.6 Discussion

The recent pumping has only minimally affected the aquitard solute profiles, because with the estimated flow rate ($v_z = 6.0 \times 10^{-6} - 6.5 \times 10^{-3}$ m/year; Table 6.3) and 10 years of pumping, solute displacement will only have been up to 6 cm. Therefore, the solute transport profiles still reflect the changes brought about by processes operating over much longer timescales.

The modelled solute concentration profiles are sensitive to the inputs D_e and v_z as well as G . Both the field measurement-based and model-optimised values fall well within the range of values reported in the literature. D_e commonly ranges between 2×10^{-2} to 2×10^{-5} m^2/yr for chloride and between 2×10^{-2} to 2×10^{-5} m^2/yr , for helium (Rubel et al. 2002; Ali et al. 2011; Bensenouci et al. 2011; Mazurek et al. 2011; Gardner et al. 2012; Harrington et al. 2013). K_V and v_z values between

0.3×10^{-4} – 3×10^{-4} m/yr and 1×10^{-3} – 1×10^{-5} m/yr, respectively have been found in previous studies (Batlle-Aguilar et al. 2016). The radiogenic helium accumulation rate (G) of 2.1×10^{-6} ccSTP/m³_{H₂O}/yr ($G^* = 5.5 \times 10^{-7}$ ccSTP/m³_{aq}/yr) is similar to the production rates calculated for the aquifers and aquitards of the GAB, i.e. 1×10^{-5} – 4×10^{-6} ccSTP/m³_{H₂O}/yr, reported in other studies (Torgersen and Clarke 1985; Bethke et al. 1999; Beyerle et al. 1999; Lehmann et al. 2003; Gardner et al. 2012).

Steady state vertical flow conditions were assumed for all the models, although changes in recharge as well as topography over the timescales required to reach steady conditions may have resulted in variations of the vertical flux. However, given the uncertainty about the variability of hydrogeological conditions within the aquifers, it is not possible to justifiably include any transient flow conditions in the models. Moreover, good model fits are obtained based on the steady state assumption with minor perturbations to account for transience at the aquitard boundaries.

Models 1 and 2 were unable to explain the ⁴He and chloride solute pore water profiles (⁴He and Cl SRMS errors >30; Table 6.1; Figure 6.4). Through calibration of the model transport parameters v_z and D_e (i.e. model 3 and model 5) a close match for the chloride concentration profile (Figure 6.4 a and Figure 6.5 c) and a reasonable match for the ⁴He concentration data was obtained (Figure 6.4 b and Figure 6.5 d). Thus, model simulations suggest that the concentration profiles may largely reflect steady state conditions. Model 4 estimated that 417,000 years are needed to reach equilibrium (Figure 6.5 a and b). In models 3–5 the helium diffusion coefficient ($D_e = 1.2 \times 10^{-3}$ m²/yr) is an order of magnitude smaller than the value based on equation 5.5 and porosity ($D_e = 1.1 \times 10^{-2}$ m²/yr). These models provided a good match for chloride (Cl SRMS error = 10; Table 6.2), although the SRMS error in these model realisations was still deemed too high for helium (⁴He SRMS error = 20; Table 6.2).

Model 6 provided a good fit for the helium profile (Figure 6.6 b; ⁴He SRMS error = 18; Table 6.2). The match between the model and the measured chloride concentrations (Cl SRMS error = 12; Table 6.2) was good as well, except in the top part of the solute profile (Figure 6.6 a). The SRMS errors (Cl SRMS error = 10; ⁴He SRMS error = 6; Table 6.2) could be lowered by considering an increase of the chloride concentration since 3000 years for chloride at the top of the aquitard, and an increase of ⁴He and chloride at the bottom since 10 years. The model shows that the increase in concentrations in the lower aquifer has not changed the aquitard pore water profiles in the 10 year period that concentrations have increased (Figure 6.6 c and d).

The three times larger ^4He concentration in the lower aquifer compared to aquitard pore waters is likely because of additional ^4He production and upward diffusion from the basement (Zhao et al. 1998). The ^4He concentration in the lower aquifer and an estimated accumulation rate of 3×10^{-5} ccSTP/m³_{H₂O}/yr including upward diffusion from the basement as well as helium production (G) (Mahara et al. 2009) give a groundwater residence time of >1 Ma (calculated using $t = C/G$), highlighting that groundwater flow rates are slow at the site (Priestley et al. 2017). If the water flows very slowly, the horizontal flow will not smear out the vertical solute and isotope gradients (Walker and Cook 1991). The onset of groundwater pumping by the Prominent Hill mine in 2009 most likely extracted groundwater with higher helium, and chloride concentrations, from the basement below or a stagnant zone. Alternatively, there could be an offset due to the different sampling and measurement procedures between the aquitard and aquifer samples. The calibration of the mass spectrometers is unlikely to be the cause as the different measurement methods were undertaken with strict quality control measures. While there can be a sampling bias, it is not possible to directly compare the methods because aquifers have relatively high permeabilities, therefore water will drain out after sample collection and the gas signal will not be retained. Additionally, an aquifer core sample is likely to be contaminated by drilling fluids. However, the authors consider the sampling and measurement procedure unlikely to be the only cause of the offset because there is no offset between the upper aquifer and upper aquitard helium measurements (Figure 6.4).

The chloride concentration gradient at this location with higher salinity in the lower aquifer differs to the aquitard of Harrington et al. (2013) and Jones et al. (1994). The source of the dissolved salts in groundwater may be seawater, a result of evapotranspiration, a reflux brine below a discharge area, or a continental brine (Jones et al. 1994; Herczeg et al. 2001; Currell et al. 2015). The source of the salinity in the lower aquifer is unlikely to be seawater as the stable water isotope delta values are representative of meteoric water (Figure 6.2). Moreover, the concentrations are greater than that of seawater and the sea retreated 90 Ma ago. Thus, it seems highly unlikely that seawater would still be present in the pore waters. Evapotranspiration can concentrate salts up to 20 g/L (Allison and Hughes 1983) and could explain the chloride concentrations at this location (Priestley et al. 2017). The high salinity in the lower aquifer is also typical for those found in discharge environments elsewhere in Australia (Jones et al. 1994; Petrides et al. 2006), although discharge is clearly not occurring at this location at present. The origin of the high salinity can not

be established with certainty, but it must have formed under hydrogeological conditions much different from those today.

Gardner et al. (2012) and Harrington et al. (2013) modelled the chloride and helium profiles in the surficial aquitard (Bulldog Shale) confining the upper aquifer at two locations approximately 160 km from our site (Figure 6.1). Gardner et al. (2012) determined that helium transport through the aquitard is in steady state with an upward vertical linear pore water velocity between 5.7×10^{-3} to 3.8×10^{-6} m/yr. This magnitude is comparable with our modelled vertical linear pore water velocity of 7.0×10^{-4} m/yr, albeit that the direction is opposite. The chloride profiles in Harrington et al. (2013) reflect varying chloride inputs from the surface due to palaeoclimate changes. An increase in chloride concentration in the upper aquifer was interpreted to have occurred approximately 10,000 years ago as a response to climate change. At our site the chloride concentration increase in the upper aquifer was inferred to have occurred since 3000 years. The slightly different timing of chloride concentration increase in the upper aquifer is most likely because there is a time lag between the moment of recharge and the arrival of the more saline water at the bottom of the upper aquifer (Figure 6.1 b). Paleoclimate studies indicate drying of the climate over the last approximately 20,000 years, with current arid climatic conditions present for around 4000 years (Hesse et al. 2004; Magee et al. 2004; Cohen et al. 2011).

While there is still some uncertainty regarding the porosity that is accessible to anions in clays and initial transport parameters of helium are difficult to constrain using independent evidence (Mazurek et al. 2011), the use of both chloride and helium at this location in central Australia provided independent information about the hydrological conditions and helped constrain the models that fit the solute profiles. Helium being produced in-situ and influenced by groundwater residence time provided evidence of solute transport rates and processes, while chloride, besides providing evidence of solute transport, also provided insight into palaeohydrological conditions. This provides the natural background connectivity between the GAB and the Arckaringa Basin at the study site prior to further development of hydrocarbon resources mining or other changes.

6.7 Conclusions

This in-situ study examined solute transport processes in an aquitard separating the GAB and the Arckaringa Basin using chloride and helium. To determine if these tracers can be used in Australian case studies to examine vertical groundwater flow between these basins, and therefore to help understand the effects of groundwater abstraction for mining water supply. As well as, investigate

the potential use of these tracers in high level radioactive waste storage viability studies within central Australia.

The method worked at this location in central Australia with the use of chloride and helium. A match between a realistic model and both tracers is considered a valid representation of the site. The use of both chloride and helium concurrently limited the models that fit the data to the final model presented.

The final model that provided the best fit with both the chloride and helium profile was an initial steady state model that required a component of vertical groundwater flow through the aquitard. The vertical flow is very slow, only 0.7 mm/yr, but that controls the solute profile as well as diffusion. Therefore, solute transport is controlled by both diffusion and advection in this location. The upper section of the chloride profile requires an increase in chloride concentration since 3000 years ago in the upper aquifer. The chloride concentration increase at that time is almost certainly due to concentration of chloride in recharging groundwater due to the climate becoming more arid. The lower section of the profile is matched by an increase in both chloride and helium due to the onset of pumping in 2008 to provide groundwater to the Prominent Hill mine. Large volume groundwater extraction caused groundwater to be extracted from a stagnant zone and/or from the basement below with higher chloride and especially helium concentrations.

The hydraulic head profile shows that the drawdown response from pumping has already penetrated and moved through the aquitard. However, subsequent increase in chloride and helium concentration, from pumping in the lower aquifer, has not penetrated very far into the aquitard because the pressure response is much quicker than solute transport through the aquitard (against downward flow).

From this study, we find natural vertical groundwater flow velocity from the GAB to the Arckaringa Basin to be 0.7 mm/yr at the study site. Other studies of consolidated aquitards undertaken in cold or temperate climates also find solute transport controlled by diffusion with advective flow rates generally below 1 mm/yr (Remenda et al. 1996; Shaw and Hendry 1998; Harrington et al. 2001; Mazurek et al. 2011). The aquitard properties and hydraulic head measurements gave an instantaneous picture of vertical groundwater flow at the time of sampling and is an important element in the discussion. However, for a long-term perspective it is necessary to use environmental tracer profiles. Chloride and helium are useful tracers for understanding

groundwater flow conditions in arid zones and temperate climates. Chloride is also useful for understanding palaeohydrological conditions in arid zones because its concentration varies considerably due to high evapotranspiration compared to precipitation concentrating solutes in recharging groundwater. Therefore, both approaches are needed to investigate vertical groundwater flow and solute transport. In addition, it has been advantageous to look at both chloride and helium concentration in the study area.

Chapter 7 Conclusions

7.1 Summary of the findings

The three studies contained in this thesis investigated the connectivity between the GAB and the Arckaringa Basin in central Australia. A regional groundwater field investigation and aquitard coring program provided evidence of both diffuse inter-aquifer leakage and localised enhanced inter-aquifer leakage. The first regional-scale study investigated both diffuse and localised enhanced inter-aquifer leakage using geology, hydraulics and various environmental tracers. The second regional-scale study examined uranium isotope distributions and the complex processes controlling them in an attempt to understand inter-aquifer leakage. The third study specifically investigated diffuse inter-aquifer leakage through the aquitard using models of chloride and helium transport through the aquitard pore waters. The key findings from each of the three specific studies are as follows:

- i. Inter-aquifer leakage at a regional-scale between the GAB and underlying Arckaringa Basin was analysed with sparse observation points using geological, hydrological and tracer information at well couplets. Interpretation of aquitard hydraulic resistance provided evidence that diffuse inter-aquifer leakage rates are <1 mm/yr where the lower aquitard is thick and continuous; whereas this increases up to 7 m/yr where the lower aquitard is absent. Combined interpretation of hydrological and tracer information provided evidence for locations of enhanced inter-aquifer leakage where the lower aquitard is continuous. Decaying and accumulating tracers provided the clearest evidence of enhanced inter-aquifer leakage of groundwater of different residence times, especially radiogenic ^4He as it varied over five orders of magnitude, compared to just two orders of magnitude for ^{14}C and $^{36}\text{Cl}/\text{Cl}$. Radiogenic ^4He concentration and $^{87}\text{Sr}/^{86}\text{Sr}$ ratio mixing mass balance models highlighted that up to 80–95% of groundwater in the lower aquifer at one location could originate from the upper aquifer. The protocol of well couplet hydrochemistry sampling, as well as geological and hydrological data interpretation methods proposed could be applied elsewhere to investigate inter-aquifer leakage at a regional-scale.
- ii. The complex processes controlling uranium isotope distributions (^{238}U and ^{234}U) in groundwater in the GAB and underlying Arckaringa Basin have been examined using groundwater samples and a sequential extraction of aquifer sediment mineral phases. Rock weathering, the geochemical environment and α -recoil of daughter products control

^{238}U and ^{234}U isotope distributions. However, the importance of each of these processes is influenced by the groundwater processes occurring at the samples location. Generally, groundwater samples from the J aquifer have higher ^{238}U activity concentrations and $^{234}\text{U}/^{238}\text{U}$ activity ratios close to secular equilibrium. Recharge from ephemeral rivers pass through rocks that have already undergone extensive weathering and contain low ^{238}U activity concentrations. Other locations receiving no recharge contain high ^{238}U activity concentrations; probably due to leached uranium from uranium-rich aquifer sediments being kept in solution by complexation with carbonate. The deeper samples from the Boorthanna Fm. and basement aquifers have lower ^{238}U activity concentrations and higher $^{234}\text{U}/^{238}\text{U}$ activity ratios. The ^{238}U activity concentrations are lower because the uranium has been lost from solution as groundwater moves through the aquifer and α -recoil of ^{234}U results in elevated $^{234}\text{U}/^{238}\text{U}$ activity ratios. The aquifer sediment sequential extraction accessible to groundwater are lower than the groundwater $^{234}\text{U}/^{238}\text{U}$ activity ratios, therefore the groundwater $^{234}\text{U}/^{238}\text{U}$ activity ratios cannot be from dissolution and/or exchange with the groundwater accessible minerals in the aquifer. The magnitude of the $^{234}\text{U}/^{238}\text{U}$ activity ratio is dependent on the groundwater residence time or the rate of groundwater flow. Overall, the ^{238}U activity concentration and $^{234}\text{U}/^{238}\text{U}$ activity ratio variations have provided information on the major processes controlling them, and have given additional insight into recharge and groundwater flow processes; however, in this case they are not particularly sensitive to inter-aquifer leakage between the GAB and Arckaringa Basin.

- iii. One-dimensional analytical and numerical models of groundwater flow, and chloride and ^4He transport showed that both diffusion and slow downward advection through the aquitard pores control solute transport. The diffuse inter-aquifer leakage rate was determined to be 0.7 mm/yr, which agrees with the rate estimated in the regional groundwater study. The numerical simulations show that an increase in chloride concentration in the upper part of the profile is likely due to a reduction in recharge in the upper aquifer for at least 3000 years. Groundwater extraction since 2008 and resultant drawdown in the lower aquifer has penetrated and moved through the aquitard. However, the subsequent increase in chloride and helium concentration in the lower aquifer has not penetrated very far into the aquitard. The pressure response is much quicker than solute transport through the aquitard and there has been insufficient time for upward solute transport into the pore water profile by diffusion against downward

advection. The transport model of ^4He and chloride provides insight into how the two aquifers interact through the aquitard and indicate that climate change and pumping rates are being recorded in the aquitard profile. The combined use of chloride and helium provided independent information about the hydrological conditions and helped constrain the models that fit the solute profiles. Helium, being produced in-situ and influenced by groundwater residence time, provided evidence of solute transport rates and processes. Chloride, provided evidence not only of solute transport, but also provided insight into palaeohydrological conditions as its concentration varies considerably due to evapotranspiration in recharging groundwater. The aquitard properties and hydraulic head measurements gave an instantaneous picture of vertical groundwater flow at the time of sampling and is an important element in the discussion. However, environmental tracer profiles are required for a long-term perspective.

7.2 Future work

7.2.1 Site-specific investigations

The three studies contained in this thesis provided site-specific evidence of both diffuse inter-aquifer leakage rates and localised enhanced inter-aquifer leakage between the GAB and underlying Arckaringa Basin. It is possible that enhanced inter-aquifer leakage could occur at other locations across the basin, but the monitoring infrastructure lacks the resolution to establish this with certainty. Any future development of the GAB and underlying Arckaringa Basin should be accompanied by a local-scale assessment of the nature of any potential enhanced inter-aquifer leakage, supported by commensurate data, such as seismics to verify the continuity of layers. Additionally, these findings will have implications for the groundwater flow model of the GAB (Welsh 2006) especially as the GAB is losing water to the underlying Arckaringa Basin, and possibly other underlying basins, at a large spatial scale.

7.2.2 Generally applicable

This investigation of inter-aquifer connectivity links point-scale to whole-basin processes and is underpinned by field- and laboratory-focused research. An important extension of this work is to examine the general inclusion of these point-scale to whole-basin processes in analytical and numerical models. These processes have been examined in regionally specific models on a basin-by-basin approach (Castro et al. 1998a; Mazurek et al. 1998; Hart et al. 2006; Myers 2012). In

addition, the effect of heterogeneities on groundwater flow and solute transport processes have been investigated more generally in low permeability formations (Neuzil 1994; Harrington et al. 2007; Huysmans and Dassargues 2013). Nevertheless, it would be worthwhile to continue investigating if there is a generic way to incorporate inter-aquifer leakage processes in simple representative flow models. If possible, these simple models could then be used to determine if inter-aquifer connectivity is an important process within a basin, and this in turn would determine if a more focused study is required.

Increased permeability, and hence enhanced inter-aquifer leakage, is caused by heterogeneity (Neuzil 1994; Batlle-Aguilar et al. 2016); however, the exact location and effect of heterogeneity is site-specific, thus it may prove difficult to incorporate this in generic models without site-specific information. Therefore, clear methods for field-testing of potential mechanisms and pathways that groundwater can be contaminated are necessary to facilitate improved conceptual models and water balance models for groundwater management.

The multi-tracer approach along with groundwater hydraulics presented in Chapter 4 provides a tool-set to investigate enhanced inter-aquifer leakage in a regional-scale sedimentary basin even with a paucity of data. Well couplets are really useful, but rare in areas with sparse monitoring infrastructure. Therefore, when future drilling is considered, installation of well-designed multi-level observation wells is strongly recommended. While the usefulness of individual environmental tracers as tools to identify enhanced inter-aquifer leakage is dependent on study area conditions, the author strongly recommends the use of multiple environmental tracers, and especially multiple age tracers. However, uranium isotopes, while providing information on some groundwater flow processes, did not elucidate any further useful information in regards to inter-aquifer leakage. Uranium isotopes are only occasionally useful for investigating large-scale inter-aquifer leakage in groundwater basins with relatively simple uranium isotope variations between aquifers, such as in the Otway Basin, Australia (Herczeg et al. 1996) and the Continental Intercalaire aquifer, Tunisia (Dhaoui et al. 2016).

Once enhanced leakage has been identified, it is possible to use mixing mass balances to determine the proportion of leakage; however, what is necessary for regional groundwater models is the rate of enhanced inter-aquifer leakage, or volumetric flux. Another necessary extension of this project is the conversion of volume percentage calculations from mixing mass balances to a volumetric flux. Currently time intensive numerical models, often calibrated to

environmental tracers, are the only method available to estimate these enhanced inter-aquifer leakage fluxes (Gerber et al. 2001; Myers 2012).

The estimated diffuse leakage rates estimated from the regional hydraulics and geology agreed with the vertical advective flux through the aquitard pores provided by the one-dimensional numerical model. Therefore, considering that the cost of coring and sample analysis is prohibitive for general regional groundwater estimates, interpretation of the hydraulics and geology may be sufficient to include diffuse inter-aquifer leakage in regional groundwater models. For studies that require a more detailed understanding of solute transport, such as contaminant migration or waste repositories, the aquitard core profile should be investigated. An aquitard pore water study provides detailed results on diffuse inter-aquifer leakage, solute transport and often paleoclimate influences that have affected the study area. The solute of interest should be used where possible, such as the contaminant of interest or radionuclides in radioactive waste viability studies (Harte et al. 2006; Abdel Rahman et al. 2007; Shackelford and Moore 2013), or more generally multiple tracers can be used to help constrain the models that fit the solute profiles. Additionally, more studies should move toward 2D or even 3D aquitard pore water solute transport models that incorporate geological and chemical heterogeneity, although this then requires time intensive site-specific numerical models (Gerber et al. 2001; Harrington and Hendry 2005; Eaton et al. 2007).

Appendix A: Environmental tracers in groundwaters and pore waters to understand groundwater movement through an argillaceous aquitard

Published in *Procedia Earth and Planetary Science* and presented at the 15th Water-Rock Interaction International Symposium in Lisbon, Portugal: Stacey C. Priestley, Andrew J. Love, Vincent E. A. Post, Paul Shand, Daniel L. Wohling, Rolf Kipfer, Timothy E. Payne, Martin Stute, Lina Tyroller (2017) Environmental Tracers in Groundwaters and Pore waters to Understand Groundwater Movement Through an Argillaceous Aquitard, *Procedia Earth and Planetary Science*, 17, p. 420-423, doi:10.1016/j.proeps.2016.12.106

A.1 Abstract

Inter-aquifer leakage through an aquitard can be an important component of groundwater flow and can occur by diffuse leakage or via preferential pathways along secondary permeability features. In order to properly characterise inter-aquifer leakage it is desirable to use both pore water from the aquitard in conjunction with a regional investigation of groundwater in the aquifers. The aim of this study was to characterize inter-aquifer leakage through a regionally extensive aquitard between the Great Artesian Basin (GAB) and the deeper Arckaringa Basin of Australia. Chloride concentrations in the aquitard pore water profile indicates that transport through the aquitard is dominated by diffusion, but there is evidence at least at one location for increased inter-aquifer leakage due to secondary permeability features.

A.2 Introduction

Aquitards are very important, yet poorly understood components in groundwater flow systems (Back 1986). Regionally extensive aquitards confine and separate aquifers and play an important role in the physical and chemical evolution of groundwater, and can provide water from storage to pumped aquifers (Back 1986; Cherry and Parker 2004). Groundwater movement through an aquitard, here referred to as inter-aquifer leakage, can be an important component of groundwater flow, although it is orders of magnitude slower than through aquifers (Batlle-Aguilar et al. 2016). Quantification of inter-aquifer leakage is important for groundwater resource evaluation and extraction industries including unconventional gas and ore extraction.

Inter-aquifer leakage through a laterally-extensive aquitard can be severely limited but even in the tightest clay or shale aquitard there is always a small amount of diffuse leakage (Cherry and Parker 2004). The inter-aquifer leakage rate through the aquitard can increase if there are secondary permeability features through the aquitard (Neuzil 1986; Cherry and Parker 2004; Hendry and Wassenaar 2004; Hart et al. 2006).

To quantify inter-aquifer leakage different techniques are available. Chemical profiles through the aquitard can be used to investigate the transport mechanisms in the aquitard pore water (Desaulniers and Cherry 1989; Remenda et al. 1996; Hendry and Wassenaar 2004; Gimmi et al. 2007; Mazurek et al. 2009), whereas detection of inter-aquifer leakage through secondary permeability features requires a more regional-scale study. Inter-aquifer leakage through secondary permeability features has been identified in some regional groundwater investigations using hydraulic head measurements, environmental tracers and dating tracers in aquifers (Clark et al. 1997; Dogramaci and Herczeg 2002; Althaus et al. 2009; Mazurek et al. 2009; Gardner and Heilweil 2014).

Batlle-Aguilar et al. (2016) urged the use of and comparison of methods at different scales within the same formation. The aim of this study was to investigate inter-aquifer leakage through a regionally extensive aquitard between the Great Artesian Basin (GAB) and the Arckaringa Basin.

A.3 Study area

This study investigated inter-aquifer leakage between the GAB and Arckaringa Basin in the central to far north region of South Australia (Figure A.1, inset). The GAB comprises Jurassic to Cretaceous sediments that overly the Arckaringa Basin which is a Late Carboniferous to Early Permian sedimentary basin. The main aquifer unit in the GAB is the J aquifer and in the study area the main aquifer in the Arckaringa Basin is the Boorthanna Fm. (Figure A.1 a). The J aquifer and Boorthanna Fm. are separated by a mudstone, siltstone and shale aquitard, known as the Stuart Range Fm. (Figure A.1 b).

A.4 Methods

To investigate inter-aquifer leakage between the GAB and Arckaringa Basin regional groundwater samples as well as samples from the aquitard were collected. A core through the aquitard was drilled and aquitard samples collected for environmental tracer analysis (Mazurek et al. 2009).

Regional groundwater samples were analysed for various environmental tracers including major elements, stable isotopes of water, ^{14}C , ^{36}Cl , $^{87}\text{Sr}/^{86}\text{Sr}$, uranium isotopes, as well as noble gases.

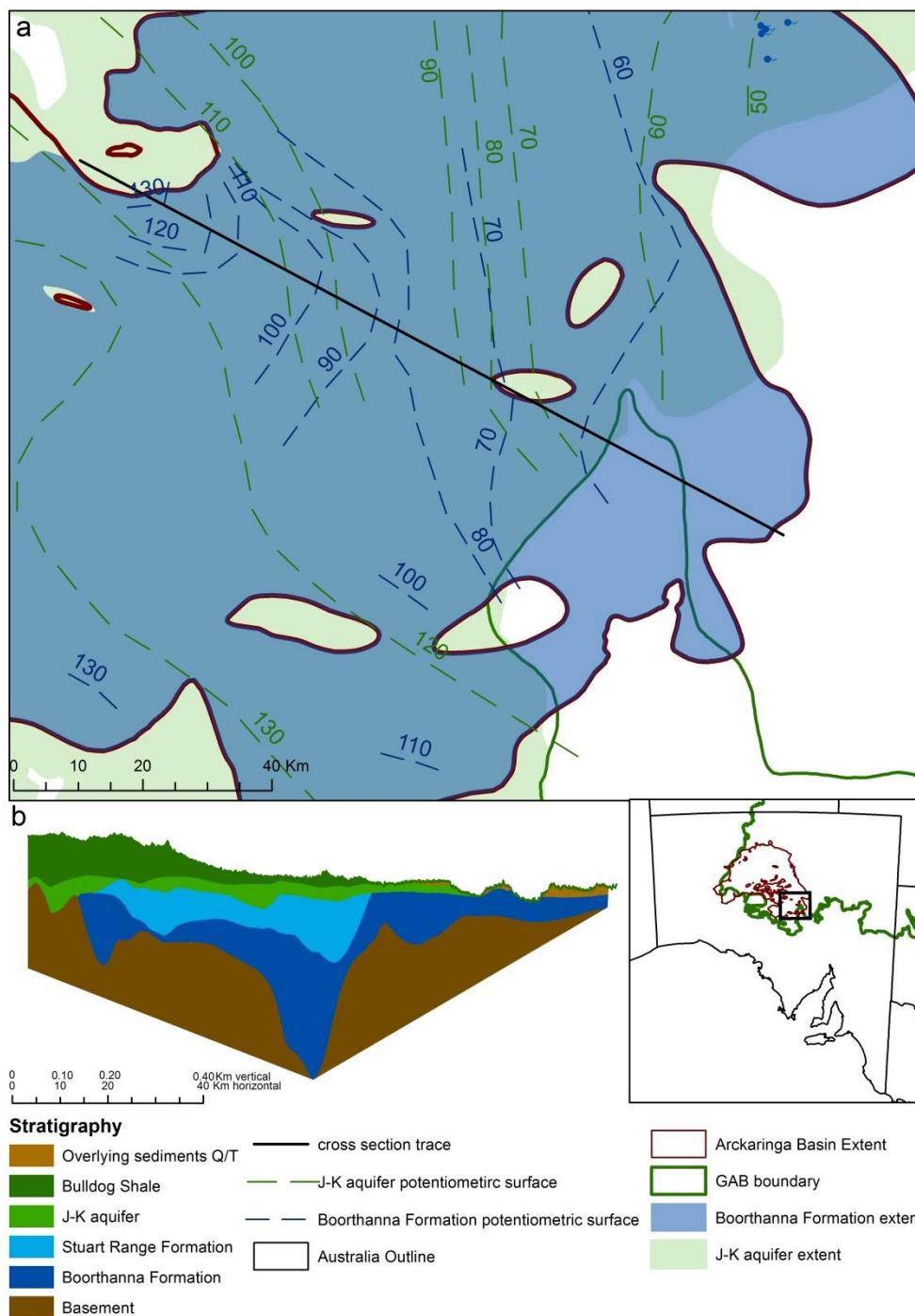


Figure A.1 (a) Map showing upper aquifer extent in green and the density corrected potentiometric surface in green dashed lines. The lower aquifer extent is shown in blue with the density corrected potentiometric surface in blue dashed lines. Cross-section through the study area is indicated with a solid black line and (b) stratigraphy of hydrogeological cross-section.

A.5 Results and discussion

The chloride concentrations in the aquitard pore water profile are shown in Figure A.2. Modelling the profile using the one-dimensional advection-dispersion equation showed that the dominant transport through the aquitard is diffusion. The regional groundwater samples show evidence of inter-aquifer leakage through secondary permeability features in the Stuart Range Fm. in the center of the basin. This inter-aquifer leakage has been identified by overlap in Sr and stable water isotope values, chloride concentrations as well as other hydrochemical evidence of mixing with shallower groundwater with shorter residence times. Further evidence is provided by hydraulic head data which showed a slight draw-down in the upper aquifer during pumping in the lower aquifer.

The results show that flow through the aquitard is dominated by diffusion; there is at least one location with increased inter-aquifer leakage due to secondary permeability features. These results are similar to other studies which have found inter-aquifer leakage through preferential pathways through aquitards (Love et al. 1996; Gardner and Heilweil 2014).

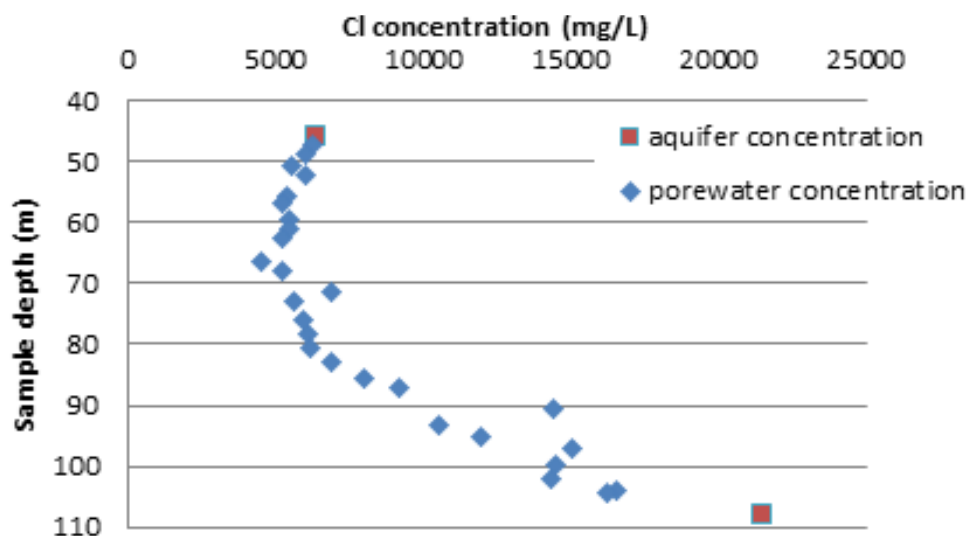


Figure A.2. Chloride concentration through the aquitard.

A.6 Conclusions

These results show that diffusion, although dominant is not the only flow mechanism through regional-scale aquitards, but secondary permeability features such as fractures and discontinuities can contribute to inter-aquifer leakage. Although cross formational flow is not regionally extensive, it may have a disproportionate impact on water flow and water quality.

Appendix B Detecting inter-aquifer leakage using multiple environmental tracers

Presented at the Analytical & Environmental Chemistry Division 2016 Division Meeting in Adelaide, Australia: Stacey C. Priestley, Andrew J. Love, Vincent E. A. Post, Paul Shand, Daniel L. Wohling, Timothy E. Payne, Rolf Kipfer. Detecting inter-aquifer leakage using multiple environmental tracers in Analytical & Environmental Chemistry Division 2016 Division Meeting, Adelaide, Australia, 18 July to 20 July 2016

Groundwater plays an important role in Australia's national water needs. It is essential for drinking water, agriculture, farming and mining, as well as groundwater dependent ecosystems. Informed management decisions regarding sustainable yields or potential exploitation require an understanding of the groundwater system (Neuman and Witherspoon 1972; Cherry and Parker 2004). Regionally-extensive aquitards (low permeability layers, such as clays) confine and separate aquifers and play an important role in the physical and chemical evolution of groundwater, and can provide water from storage to pumped aquifers (Back 1986; Cherry and Parker 2004). In most groundwater systems the quantity or location of inter-aquifer leakage, water movement through the aquitard, is unknown. In addition, the presence of secondary permeability features or preferential pathways through an aquitard can increase the rate of fluid movement through the aquitard at that location. Not taking into account leakage rates in the analysis of large-scale flow systems can lead to under or overestimation of groundwater flow rates in aquifers (Love et al. 1993; Tóth 2009). The aim of this study was to investigate inter-aquifer leakage through a regionally extensive aquitard between the Great Artesian Basin (GAB) and the deeper Arckaringa Basin in central Australia. Environmental tracer variations within the aquitard and aquifers were investigated in order to properly characterise inter-aquifer leakage. The environmental tracers in the aquitard pore water profile showed that transport through the aquitard pores is dominated by diffusion but there is at least one location with increased inter-aquifer leakage due to secondary permeability through the aquitard.

Appendix C Detecting inter-aquifer leakage and recharge using multiple environmental tracers

Presented at Goldschmidt in Yokohama, Japan: Stacey C. Priestley, Andrew J. Love, Vincent E. A. Post, Paul Shand, Rolf Kipfer, Timothy E. Payne, Martin Stute and Lina Tyroller. Detecting inter-aquifer leakage and recharge using multiple environmental tracers in Goldschmidt, Yokohama, Japan, 26 June to 1 July 2016

Inter-aquifer leakage can be an important component of groundwater flow with relevance to groundwater resource evaluation and extraction industries including ore extraction and unconventional gas. The presence of secondary permeability features or preferential pathways through an aquitard can increase the rate of fluid movement causing enhanced inter-aquifer leakage and can be identified by variations from expected environmental tracer behaviour.

Inter-aquifer leakage and recharge in a regional sedimentary basin were investigated in an arid environment using an integrated approach.

The methodology incorporated geological, hydrogeological and hydrochemical information in the basin to determine the likelihood and location of inter-aquifer leakage. The suite of environmental tracers and isotopes used included $\delta^{18}\text{O}$, $\delta^2\text{H}$, ^{14}C , ^{36}Cl , $^{87}\text{Sr}/^{86}\text{Sr}$, He isotopes and U isotopes. Of particular benefit was the analysis of hydraulic heads and environmental tracers at well couplets, comprising wells above and below an aquitard within a localised geographical area.

The methodology was successful in investigating inter-aquifer leakage and recharge in the western margin of the Great Artesian Basin, South Australia. There is evidence for inter-aquifer leakage in the centre of the basin ~40 km along a regional flow path. This was identified by a slight draw-down in the upper aquifer during pumping in the lower aquifer. By combining tracer based dating techniques (e.g. ^4He) with the analysis of reactive tracers (e.g. $^{87}\text{Sr}/^{86}\text{Sr}$) in well couplets, we were able to identify changes in groundwater residence time and isotopic signals in response to rapid water movement from one aquifer to another.

Appendix D A method to investigate inter-aquifer leakage using hydraulics and multiple environmental tracers

Poster presented at European Geosciences Union General Assembly 2016 in Vienna, Austria: Stacey C. Priestley, Andrew J. Love, Daniel L. Wohling, Vincent E. A. Post, Paul Shand, Rolf Kipfer, and Lina Tyroller. A method to investigate inter-aquifer leakage using hydraulics and multiple environmental tracers in European Geosciences Union General Assembly 2016, Vienna, Austria, 17 April to 22 April 2016

Informed aquifer management decisions regarding sustainable yields or potential exploitation require an understanding of the groundwater system (Alley et al. 2002; Cherry and Parker 2004). Recently, the increase in coal seam gas (CSG) or shale gas production has highlighted the need for a better understanding of inter-aquifer leakage and contaminant migration. In most groundwater systems, the quantity or location of inter-aquifer leakage is unknown. Not taking into account leakage rates in the analysis of large-scale flow systems can also lead to significant errors in the estimates of groundwater flow rates in aquifers (Love et al. 1993; Tóth 2009). There is an urgent need for robust methods to investigate inter-aquifer leakage at a regional-scale.

This study builds on previous groundwater flow and inter-aquifer leakage studies to provide a methodology to investigate inter-aquifer leakage in a regional sedimentary basin using hydraulics and a multi-tracer approach.

The methodology incorporates geological, hydrogeological and hydrochemical information in the basin to determine the likelihood and location of inter-aquifer leakage. Of particular benefit is the analysis of hydraulic heads and environmental tracers at nested piezometers, or where these are unavailable well couplets comprising wells above and below the aquitard of interest within a localised geographical area.

The proposed methodology has been successful in investigating inter-aquifer leakage in the Arckaringa Basin, South Australia. The suite of environmental tracers and isotopes used included the stable isotopes of water, radiocarbon, chloride-36, $^{87}\text{Sr}/^{86}\text{Sr}$ and helium isotopes. There is evidence for inter-aquifer leakage in the centre of the basin ~40 km along the regional flow path. This inter-aquifer leakage has been identified by a slight drawdown in the upper aquifer during pumping in the lower aquifer, overlap in Sr isotopes, $\delta^2\text{H}$, $\delta^{18}\text{O}$ and chloride concentrations as well as hydrochemical evidence of mixing with shallower groundwater with shorter residence times.

Appendix E Inter-aquifer leakage and groundwater flow inferred from environmental tracers especially noble gases

Presented at Australian Groundwater Conference 2015 in Canberra, Australia: Stacey C. Priestley, Andrew J. Love, Daniel L. Wohling, Vincent E. A. Post, Paul Shand, Rolf Kipfer, and Tim Payne. Inter-aquifer leakage and groundwater flow inferred from environmental tracers especially noble gases in Australian Groundwater Conference 2015 in Canberra, Australia, 3 November to 5 November 2015

Management decisions regarding sustainable yields or resource exploitation require an understanding of the groundwater system (Alley et al. 2002; Cherry and Parker 2004). There can be significant errors in the estimates of groundwater flow in large-scale flow systems by not taking into account inter-aquifer leakage rates (Love et al. 1993; Tóth 2009). In most groundwater systems, the quantity or location of inter-aquifer leakage is unknown. The increase in coal seam gas (CSG) production has provided further interest in inter-aquifer leakage and contaminant migration.

There are very few robust methods available to investigate inter-aquifer leakage on a regional-scale. This preliminary study investigated inter-aquifer leakage in arid-zone, regional-scale, sedimentary groundwater systems: the Great Artesian Basin (GAB) and the Arckaringa Basin.

Environmental tracers were used in conjunction with more traditional analysis of hydraulic head and geological data to determine groundwater flow paths, areas of groundwater mixing, and to characterise and quantify inter-aquifer leakage. The suite of environmental tracers and isotopes used includes the isotopes of water, radiocarbon, chloride-36, uranium isotopes and noble gases. The methodology was effective in identifying a lack of inter-aquifer connectivity at most locations and localised inter-aquifer leakage due to secondary permeability in the aquitard. Recharge from surface water features and around basement highs could also be inferred from the data.

Appendix F Inter-aquifer leakage and groundwater flow inferred from isotopes and noble gases

Presented at 13th Australasian Environmental Isotope Conference Australian Groundwater Conference 2015 in Sydney, Australia: Stacey C. Priestley, Andrew J. Love, Daniel L. Wohling, Vincent E. A. Post, Paul Shand, Rolf Kipfer, and Tim Payne. Inter-aquifer leakage and groundwater flow inferred from isotopes and noble gases in 13th Australasian Environmental Isotope Conference Australian Groundwater Conference 2015 in Sydney, Australia, 8 July to 10 July 2015

Informed aquifer management decisions regarding sustainable yields or potential exploitation require an understanding of the groundwater system (Alley et al. 2002; Cherry and Parker 2004). Recently, the increase in coal seam gas (CSG) or shale gas production has provided further interest in inter-aquifer leakage and contaminant migration. In most groundwater systems, the quantity or location of inter-aquifer leakage is unknown. Not taking into account leakage rates in the analysis of large-scale flow systems can lead to significant errors in the estimates of groundwater flow rates in aquifers (Love et al. 1993; Tóth 2009). There are very few robust methods that are available to investigate inter-aquifer leakage on a regional-scale.

This preliminary study investigated inter-aquifer leakage in an arid-zone, regional-scale, sedimentary groundwater system using environmental tracers, including isotopes and noble gases.

Environmental tracers are used in conjunction with more traditional analysis of hydraulic head and geological data to determine groundwater flow paths, areas of groundwater mixing, and to characterise and quantify inter-aquifer leakage. The suite of environmental tracers and isotopes used includes the isotopes of water, radiocarbon, chloride-36, uranium isotopes and noble gases from both groundwater and aquitard pore water.

References

- Abdel Rahman R.O., Zaki A.A. and El-Kamash A.M. (2007) Modeling the long-term leaching behavior of ^{137}Cs , ^{60}Co , and $^{152,154}\text{Eu}$ radionuclides from cement-clay matrices. *Journal of Hazardous Materials*. 145(3):372-380, doi 10.1016/j.jhazmat.2006.11.030
- Aggarwal P.K., Gat J.R. and Froehlich K. (2005) *Isotopes in the Water Cycle Past, Present and Future of a Developing Science*, The Netherlands: IAEA.
- Al T.A., Clark I.D., Kennell L., Jensen M. and Raven K.G. (2015) Geochemical evolution and residence time of porewater in low-permeability rocks of the Michigan Basin, Southwest Ontario. *Chem. Geol.* 404:1-17, doi 10.1016/j.chemgeo.2015.03.005
- Ali S., Stute M., Torgersen T., Winckler G. and Kennedy B.M. (2011) Helium measurements of pore fluids obtained from the San Andreas Fault Observatory at Depth (SAFOD, USA) drill cores. *Hydrogeology Journal*. 19(1):237-247, doi 10.2138/rmg.2002.47.13
- Allan R.J. (1990) Climate. In: Tyler MJ, Twidale CR, Davies M, et al. (eds) *Natural History of the North East Deserts*. Adelaide, S.A.: Royal Society of South Australia Inc., 107-118.
- Allchurch P. and Wopfner H. (1967) Cootanoorina No. 1 Well completion report. Report Book No. 65/104. Geological survey of South Australia.
- Alley W.M., Healy R.W., LaBaugh J.W. and Reilly T.E. (2002) Hydrology - Flow and storage in groundwater systems. *Science*. 296(5575):1985-1990, doi 10.1126/science.1067123
- Allison G.B. and Hughes M.W. (1983) The use of natural tracers as indicators of soil-water movement in a temperate semi-arid region. *J. Hydrol.* 60(1-4):157-173, doi 10.1016/0022-1694(83)90019-7
- Althaus R., Klump S., Onnis A., Kipfer R., Purtschert R., Stauffer F. and Kinzelbach W. (2009) Noble gas tracers for characterisation of flow dynamics and origin of groundwater: A case study in Switzerland. *J. Hydrol.* 370(1-4):64-72, doi 10.1016/j.jhydrol.2009.02.053
- Ambrose G.J. and Flint R.B. (1980) Billa Kalina, South Australia. Explanatory Notes. 1:250 000 geological series. geological sheet SH 53-7. Geological Survey of South Australia.
- Andrews J.N., Fontes J.C., Michelot J.L. and Elmore D. (1986) In-situ neutron flux, ^{36}Cl production and groundwater evolution in crystalline rocks at Stripa, Sweden. *Earth and Planetary Science Letters*. 77(1):49-58, doi 10.1016/0012-821X(86)90131-7
- Andrews J.N., Giles I.S., Kay R.L.F., Lee D.J., Osmond J.K., Cowart J.B., Fritz P., Barker J.F. and Gale J. (1982) Radioelements, radiogenic helium and age relationships for groundwaters from the granites at Stripa, Sweden. *Geochim. Cosmochim. Acta*. 46(9):1533-1543, doi 10.1016/0016-7037(82)90312-X
- Andrews J.N. and Kay R.L.F. (1982) $^{234}\text{U}/^{238}\text{U}$ activity ratios of dissolved uranium in groundwaters from a jurassic limestone aquifer in England. *Earth and Planetary Science Letters*. 57(1):139-151, doi 10.1016/0012-821X(82)90180-7
- Andrews J.N. and Kay R.L.F. (1983) The U contents and $^{234}\text{U}/^{238}\text{U}$ activity ratios of dissolved uranium in groundwaters from some Triassic sandstones in England. *Isotope Geoscience*. 1(2):101-117, doi 10.1016/S0009-2541(83)80011-4
- APHA (1998) *Standard Methods for the Examination of Water and Waste Water*, Washington DC: American Public Health Association.
- Appelo C.A.J. and Postma D. (2005) *Geochemistry, Groundwater and Pollution, Second Edition*, New York: CRC Press.
- Aquaterra. (2009) Prominent Hill Mine regional groundwater model. Prepared for OZ Minerals. Ref. No. A24C7-R001b.

- Aquaterra REM. (2005) Conceptual hydrogeological model of the Prominent Hill Mine Project. Prepared for Oxiana Ltd. Project No. (BJ)\02.
- Armstrong D. and Berry K.A. (1997) Olympic Dam Operations: Recalibration of GAB95 numerical flow model (renamed ODEX 1) and updated simulation of Borefield B operation. WMC Resources Ltd.
- Arslan S., Yazicigil H., Stute M., Schlosser P. and Smethie W.M., Jr. (2015) Analysis of groundwater dynamics in the complex aquifer system of Kazan Trona, Turkey, using environmental tracers and noble gases. *Hydrogeology Journal*. 23(1):175-194, doi 10.1007/s10040-014-1188-z
- Atkins M.L., Santos I.R., Perkins A. and Maher D.T. (2016) Dissolved radon and uranium in groundwater in a potential coal seam gas development region (Richmond River Catchment, Australia). *Journal of Environmental Radioactivity*. 154:83-92, doi 10.1016/j.jenvrad.2016.01.014
- Audibert M. (1976) Progress report on the Great Artesian Basin hydrogeological study, 1972-1974. Commonwealth of Australia: Bureau of Mineral Resources, 35.
- Bachu S. (1995) Flow of variable-density formation water in deep sloping aquifers: review of methods of representation with case studies. *J. Hydrol*. 164(1-4):19-38, doi 10.1016/0022-1694(94)02578-Y
- Back W. (1986) Role of aquitards in hydrogeochemical systems: a synopsis. *Appl. Geochem*. 1(3):427-437, doi 10.1016/0883-2927(86)90027-2
- Ballentine C.J., Burgess R. and Marty B. (2002) Tracing fluid origin, transport and interaction in the crust. In: Porcelli D, Ballentine CJ and Wieler R (eds) *Noble Gases in Geochemistry and Cosmochemistry*. 539-614.
- Barnett B., Townley L.R., Post V., Evans R.E., Hunt R.J., Peeters L., Richardson S., Werner A.D., Knapp A. and Boronkay A. (2012) Australian groundwater modelling guidelines. Waterlines report. Canberra: National Water Commission.
- Batlle-Aguilar J., Cook P.G. and Harrington G.A. (2016) Comparison of hydraulic and chemical methods for determining hydraulic conductivity and leakage rates in argillaceous aquitards. *J. Hydrol*. 532:102-121, doi 10.1016/j.jhydrol.2015.11.035
- Belperio A.P. (2005) Water in permian palaeochannels draining the Mount Woods Block. Adelaide: Minotaur Exploration Ltd.
- Bensenouci F., Michelot J.L., Matray J.M., Savoye S., Lavielle B., Thomas B. and Dick P. (2011) A profile of helium-4 concentration in pore-water for assessing the transport phenomena through an argillaceous formation (Tournemire, France). *Physics and Chemistry of the Earth*. 36(17-18):1521-1530, doi 10.1016/j.pce.2011.10.016
- Bensenouci F., Michelot J.L., Matray J.M., Savoye S., Tremosa J. and Gaboreau S. (2013) Profiles of chloride and stable isotopes in pore-water obtained from a 2000m-deep borehole through the Mesozoic sedimentary series in the eastern Paris Basin. *Physics and Chemistry of the Earth*. 65:1-10, doi 10.1016/j.pce.2011.10.024
- Bentley H.W., Phillips F.M. and Davis S.N. (1986) Chlorine-36 in the terrestrial environment. In: Fritz P and Fontes JC (eds) *Handbook of Environmental Isotope Geochemistry*. Amsterdam: Elsevier.
- Berry K.A. and Armstrong D. (1995) Hydrogeological investigation and numerical modelling Lake Eyre Region, Great Artesian Basin. Adelaide: WMC.
- Bethke C.M. and Johnson T.M. (2008) Groundwater age and groundwater age dating. *Annual Review of Earth and Planetary Sciences*. 36:121-152,
- Bethke C.M., Zhao X. and Torgersen T. (1999) Groundwater flow and the He-4 distribution in the Great Artesian Basin of Australia. *J Geophys Res-Sol Ea*. 104(B6):12999-13011, doi 10.1029/1999JB900085

- Beyerle U., Aeschbach-Hertig W., Imboden D.M., Baur H., Graf T. and Kipfer R. (2000) A mass spectrometric system for the analysis of noble gases and tritium from water samples. *Environmental Science & Technology*. 34(10):2042-2050, doi 10.1021/es990840h
- Beyerle U., Aeschbach-Hertig W., Peeters R., Kipfer R., Purtschert R., Lehmann B.E., Loosli H.H. and Love A. (1999) Noble gas data from the Great Artesian Basin provide a temperature record of Australia on time scales of 10^5 years. International symposium on isotope techniques in water resources development and management. Vienna.
- Brantley S.L., Yoxtheimer D., Arjmand S., Grieve P., Vidic R., Pollak J., Llewellyn G.T., Abad J. and Simon C. (2014) Water resource impacts during unconventional shale gas development: The Pennsylvania experience. *International Journal of Coal Geology*. 126:140-156, doi 10.1016/j.coal.2013.12.017
- Bredehoeft J.D., Neuzil C.E. and Milly P.C. (1983) Regional flow in the Dakota aquifer: a study of the role of confining layers. US Geological Survey Water-Supply Paper 2237. Reston, VA: U. S. G. P. O.
- Brenot A., Négrel P., Petelet-Giraud E., Millot R. and Malcuit E. (2015) Insights from the salinity origins and interconnections of aquifers in a regional scale sedimentary aquifer system (Adour-Garonne district, SW France): Contributions of $\delta^{34}\text{S}$ and $\delta^{18}\text{O}$ from dissolved sulfates and the $^{87}\text{Sr}/^{86}\text{Sr}$ ratio. *Appl. Geochem.* 53:27-41, doi 10.1016/j.apgeochem.2014.12.002
- Bunn S.E., Thoms M.C., Hamilton S.K. and Capon S.J. (2006) Flow variability in dryland rivers: Boom, bust and the bits in between. *River Research and Applications*. 22(2):179-186, doi 10.1002/rra.904
- Bureau of Meteorology. (2017) *Climate Data Online*. Available at: <http://www.bom.gov.au/climate/data/?ref=fr>.
- Candela L., Elorza F.J., Tamoh K., Jiménez-Martínez J. and Aureli A. (2014) Groundwater modelling with limited data sets: The Chari-Logone area (Lake Chad Basin, Chad). *Hydrological Processes*. 28(11):3714-3727, doi 10.1002/hyp.9901
- Cartwright I., Weaver T. and Petrides B. (2007) Controls on $^{87}\text{Sr}/^{86}\text{Sr}$ ratios of groundwater in silicate-dominated aquifers: SE Murray Basin, Australia. *Chem. Geol.* 246(1-2):107-123, doi 10.1016/j.chemgeo.2007.09.006
- Cartwright I., Weaver T.R., Cendón D.I., Fifield L.K., Tweed S.O., Petrides B. and Swane I. (2012) Constraining groundwater flow, residence times, inter-aquifer mixing, and aquifer properties using environmental isotopes in the southeast Murray Basin, Australia. *Appl. Geochem.* 27(9):1698-1709, doi 10.1016/j.apgeochem.2012.02.006
- Carvalho F.P. and Oliveira J.M. (2009) Performance of alpha spectrometry in the analysis of uranium isotopes in environmental and nuclear materials. *Journal of Radioanalytical and Nuclear Chemistry*. 281(3):591, doi 10.1007/s10967-009-0046-2
- Castro M.C., Goblet P., Ledoux E., Violette S. and De Marsily G. (1998a) Noble gases as natural tracers of water circulation in the Paris Basin. 2. Calibration of a groundwater flow model using noble gas isotope data. *Water Resour. Res.* 34(10):2467-2483, doi 10.1029/98WR01957
- Castro M.C., Jambon A., De Marsily G. and Schlosser P. (1998b) Noble gases as natural tracers of water circulation in the Paris Basin. 1. Measurements and discussion of their origin and mechanisms of vertical transport in the basin. *Water Resour. Res.* 34(10):2443-2466, doi 10.1029/98WR01956
- Cherdyntsev V., Chalov P. and Khasdarov G. (1955) On isotopic composition of radioelements in natural objects, and problems of geochronology. *Trans. 3rd session of the commission on determination of absolute age of geological formations*. Moscow: Izvestiya Akademii Nauk SSSR, 175-233.

- Cherry J.A. and Parker B.L. (2004) *Role of Aquitards in the Protection of Aquifers from Contamination: A "State of Science" Report*, Denver, USA: AWWA Research Foundation.
- Chkir N., Guendouz A., Zouari K., Hadj Ammar F. and Moulla A.S. (2009) Uranium isotopes in groundwater from the continental intercalaire aquifer in Algerian Tunisian Sahara (Northern Africa). *Journal of Environmental Radioactivity*. 100(8):649-656, doi 10.1016/j.jenvrad.2009.05.009
- Clark I.D., Al T., Jensen M., Kennell L., Mazurek M., Mohapatra R. and Raven K.G. (2013) Paleozoic-aged brine and authigenic helium preserved in an Ordovician shale aquiclude. *Geology*. 41(9):951-954, doi 10.1130/G34372.1
- Clark J.F., Stute M., Schlosser P. and Drenkard S. (1997) A tracer study of the Floridan aquifer in southeastern Georgia: Implications for groundwater flow and paleoclimate. *Water Resour. Res.* 33(2):281-289, doi 10.1029/96wr03017
- Coffey and Partners. (1983) Wintinna Coalfield Hydrogeological Study. Sydney: Meekatharra Minerals Ltd.
- Cohen T.J., Nanson G.C., Jansen J.D., Jones B.G., Jacobs Z., Treble P., Price D.M., May J.-H., Smith A.M., Ayliffe L.K. and Hellstrom J.C. (2011) Continental aridification and the vanishing of Australia's megalakes. *Geology*. 39(2):167-170, doi 10.1130/G31518.1
- Cook P.G. and Herczeg A.L. (2000) *Environmental Tracers in Subsurface Hydrology*. New York: Springer Science+Business Media
- Cowley V.M. and Martin A.R. (1991) Kingoonya, South Australia. Explanatory Notes. 1:250 000 geological series. geological sheet SH 53-11. Geological Survey of South Australia.
- CRAE. (1987) Arkeeta No. 1 Well completion report. CRAE Report No. 302889.
- Croisé J., Schlickerieder L., Marschall P., Boisson J.Y., Vogel P. and Yamamoto S. (2004) Hydrogeological investigations in a low permeability claystone formation: The Mont Terri Rock Laboratory. *Physics and Chemistry of the Earth*. 29(1):3-15, doi 10.1016/j.pce.2003.11.008
- Cudennec C., Leduc C. and Koutsoyiannis D. (2007) Dryland hydrology in Mediterranean regions - A review. *Hydrological Sciences Journal*. 52(6):1077-1087, doi 10.1623/hysj.52.6.1077
- Currell M. (2014) Mega-scale groundwater quality challenges and the need for an inter-disciplinary approach. *Hydrogeology Journal*. 22(4):745-748, doi 10.1007/s10040-014-1119-z
- Currell M.J., Dahlhaus P. and Li H. (2015) Stable isotopes as indicators of water and salinity sources in a southeast Australian coastal wetland: identifying relict marine water, and implications for future change. *Hydrogeology Journal*. 23(2):235-248, doi 10.1007/s10040-014-1199-9
- Dabous A.A. and Osmond J.K. (2001) Uranium isotopic study of artesian and pluvial contributions to the Nubian Aquifer, Western Desert, Egypt. *J. Hydrol.* 243(3-4):242-253, doi 10.1016/S0022-1694(00)00417-0
- Dabous A.A., Osmond J.K. and Dawood Y.H. (2002) Uranium/thorium isotope evidence for groundwater history in the Eastern Desert of Egypt. *Journal of Arid Environments*. 50(2):343-357, doi 10.1006/jare.2001.0861
- Deines P., Langmuir D. and Harmon R.S. (1974) Stable carbon isotope ratios and the existence of a gas phase in the evolution of carbonate ground waters. *Geochim. Cosmochim. Acta*. 38(7):1147-1164, doi 10.1016/0016-7037(74)90010-6
- Desaulniers D.E. and Cherry J.A. (1989) Origin and movement of groundwater and major ions in a thick deposit of Champlain sea clay near Montreal. *Canadian Geotechnical Journal*. 26(1):80-89, doi 10.1139/t89-009
- Desaulniers D.E., Cherry J.A. and Fritz P. (1981) Origin, age and movement of pore water in argillaceous quaternary deposits at 4 sites in southwestern Ontario. *J. Hydrol.* 50(1-3):231-257, doi 10.1016/0022-1694(81)90072-x

- Desaulniers D.E., Kaufmann R.S., Cherry J.A. and Bentley H.W. (1986) Cl-37-Cl-35 Variations in a diffusion-controlled groundwater system. *Geochim. Cosmochim. Acta.* 50(8):1757-1764, doi 10.1016/0016-7037(86)90137-7
- Dhaoui Z., Chkir N., Zouari K., Ammar F.H. and Agoune A. (2016) Investigation of uranium geochemistry along groundwater flow path in the Continental Intercalaire aquifer (Southern Tunisia). *Journal of Environmental Radioactivity.* 157:67-76, doi 10.1016/j.jenvrad.2016.03.005
- DMITRE. (2011) *Arckaringa Basin*. Available at: http://petroleum.statedevelopment.sa.gov.au/old-site/prospectivity/basin_and_province_information/prospectivity_arckaringa.
- Dogramaci S.S. and Herczeg A.L. (2002) Strontium and carbon isotope constraints on carbonate-solution interactions and inter-aquifer mixing in groundwaters of the semi-arid Murray Basin, Australia. *J. Hydrol.* 262(1-4):50-67, doi 10.1016/S0022-1694(02)00021-5
- Dogramaci S.S., Herczeg A.L., Schiff S.L. and Bone Y. (2001) Controls on $\delta^{34}\text{S}$ and $\delta^{18}\text{O}$ of dissolved sulfate in aquifers of the murray basin, Australia and their use as indicators of flow processes. *Appl. Geochem.* 16(4):475-488, doi 10.1016/S0883-2927(00)00052-4
- Drexel J.F. and Preiss W.V. (1995) *The Geology of South Australia Vol. 2, The Phanerozoic*. Adelaide: South Australia Geological Survey, Bulletin 54.
- Eaton T.T., Anderson M.P. and Bradbury K.R. (2007) Fracture control of ground water flow and water chemistry in a rock aquitard. *Ground Water.* 45(5):601-615, doi 10.1111/j.1745-6584.2007.00335.x
- Falck W.E., Bath A.H. and Hooker P.J. (1990) Long-Term Solute Migration Profiles in Clay Sequences. *Zeitschrift Der Deutschen Geologischen Gesellschaft.* 415 - 426.
- Faure G. (1986) *Principles of isotope geology*, New York: Wiley.
- Field R.A., Soltis J. and Murphy S. (2014) Air quality concerns of unconventional oil and natural gas production. *Environmental Sciences: Processes and Impacts.* 16(5):954-969, doi 10.1039/c4em00081a
- Fifield L.K., Tims S.G., Fujioka T., Hoo W.T. and Everett S.E. (2010) Accelerator mass spectrometry with the 14UD accelerator at the Australian National University. *Nuclear Instruments and Methods in Physics Research, Section B: Beam Interactions with Materials and Atoms.* 268(7-8):858-862, doi 10.1016/0168-583X(90)90412-N
- Fontes J.-C. (1992) Chemical and Isotopic Constraints on ^{14}C Dating of Groundwater. In: Taylor RE, Long A and Kra RS (eds) *Radiocarbon After Four Decades*. New York, NY: Springer New York, 242-261.
- Fontes J.C. and Garnier J.M. (1979) Determination of the initial ^{14}C Activity of the total dissolved carbon: A review of the existing model and a new approach. *Water Resour. Res.* 15(2):399-413, doi 10.1029/WR015i002p00399
- Fortin G., van der Kamp G. and Cherry J.A. (1991) Hydrogeology and hydrochemistry of an aquifer-aquitard system within glacial deposits, Saskatchewan, Canada. *J. Hydrol.* 126(3-4):265-292, doi 10.1016/0022-1694(91)90160-J
- Freeze R.A. and Witherspoon P.A. (1967) Theoretical analysis of regional groundwater flow: 2. Effect of water-table configuration and subsurface permeability variation. *Water Resour. Res.* 3(2):623-634, doi 10.1029/WR003i002p00623
- Freytag I.B. (1966) Proposed Rock Units for Marine Lower Cretaceous Sediments in the Oodnadatta Region of the Great Artesian Basin. *Quarterly Geological Notes.* 3-7.
- Gallagher K. and Lambeck K. (1989) Subsidence, sedimentation and sea-level changes in the Eromanga Basin, Australia. *Basin Research.* 2(2):115-131, doi 10.1111/j.1365-2117.1989.tb00030.x

- Gardner P.M. and Heilweil V.M. (2014) A multiple-tracer approach to understanding regional groundwater flow in the Snake Valley area of the eastern Great Basin, USA. *Appl. Geochem.* 45:33-49, doi 10.1016/j.apgeochem.2014.02.010
- Gardner W.P., Harrington G.A. and Smerdon B.D. (2012) Using excess He-4 to quantify variability in aquitard leakage. *J. Hydrol.* 468:63-75, doi 10.1016/j.jhydro1.2012.08.014
- Gascoyne M. (1992) Geochemistry of the actinides and their daughters. In: Ivanovich M and Harmon RS (eds) *Uranium Series Disequilibrium*. Oxford: Clarendon Press.
- Gat J.R., Mazar E. and Tzur Y. (1969) The stable isotope composition of mineral waters in the Jordan Rift Valley, Israel. *J. Hydrol.* 7(3):334-352, doi 10.1016/0022-1694(69)90108-5
- Gerber R.E., Boyce J.I. and Howard K.W.F. (2001) Evaluation of heterogeneity and field-scale groundwater flow regime in a leaky till aquitard. *Hydrogeology Journal.* 9(1):60-78, doi 10.1007/s100400000115
- Gibb R.J. (1970) Mechanisms Controlling World Water Chemistry. *Science.* 107:1088-1090, doi 10.1126/science.170.3962.1088
- Gimmi T., Waber H.N., Gautschi A. and Rubel A. (2007) Stable water isotopes in pore water of Jurassic argillaceous rocks as tracers for solute transport over large spatial and temporal scales. *Water Resour. Res.* 43(4), doi 10.1029/2005wr004774
- Gleeson T., Alley W.M., Allen D.M., Sophocleous M.A., Zhou Y., Taniguchi M. and Vandersteen J. (2012) Towards sustainable groundwater use: Setting long-term goals, backcasting, and managing adaptively. *Ground Water.* 50(1):19-26, doi 10.1111/j.1745-6584.2011.00825.x
- Glynn P.D. and Plummer L.N. (2005) Geochemistry and the understanding of ground-water systems. *Hydrogeology Journal.* 13(1):263-287, doi 10.1007/s10040-004-0429-y
- Godwin H. (1962) Half-life of radiocarbon. *Nature.* 195(4845):984, doi 10.1038/195984a0
- Goode D.J. (1996) Direct simulation of groundwater age. *Water Resour. Res.* 32(2):289-296, doi 10.1029/95WR03401
- Grathwohl P. (1958) *Diffusion in natural porous media: contaminant transport, sorption/desorption and dissolution kinetics*, New York: Springer Science+Business Media, LLC.
- Gumm L.P., Bense V.F., Dennis P.F., Hiscock K.M., Cremer N. and Simon S. (2016) Dissolved noble gases and stable isotopes as tracers of preferential fluid flow along faults in the Lower Rhine Embayment, Germany. *Hydrogeology Journal.* 24(1):99-108, doi 10.1007/s10040-015-1321-7
- Guttman J. and Kronfeld J. (1982) Tracing interaquifer connections in the Kefar Uriyya-Agur region (Israel), using natural uranium isotopes. *J. Hydrol.* 55(1-4):145-150, doi 10.1016/0022-1694(82)90125-1
- Habermehl M.A. (1980) The Great Artesian Basin, Australia. *BMR Journal of Australian Geology & Geophysics.* 9-38.
- Hamilton S.K., Bunn S.E., Thoms M.C. and Marshall J.C. (2005) Persistence of aquatic refugia between flow pulses in a dryland river system (Cooper Creek, Australia). *Limnology and Oceanography.* 50(3):743-754, doi 10.4319/lo.2005.50.3.0743
- Harrington G.A., Cook P.G. and Herczeg A.L. (2002) Spatial and temporal variability of ground water recharge in central Australia: A tracer approach. *Ground Water.* 40(5):518-527, doi 10.1111/j.1745-6584.2002.tb02536.x
- Harrington G.A., Gardner W.P., Smerdon B.D. and Hendry M.J. (2013) Palaeohydrological insights from natural tracer profiles in aquitard porewater, Great Artesian Basin, Australia. *Water Resour. Res.* 49:4054 - 4069, doi 10.1002/wrcr.20327
- Harrington G.A. and Hendry M.J. (2005) Chemical heterogeneity in diffusion-dominated aquitards. *Water Resour. Res.* 41(12), doi 10.1029/2004wr003928

- Harrington G.A., Hendry M.J. and Robinson N.I. (2007) Impact of permeable conduits on solute transport in aquitards: Mathematical models and their application. *Water Resour. Res.* 43(5), doi 10.1029/2005wr004144
- Harrington G.A., Love A.J. and Herczeg A.L. (2001) *Relative importance of physical and geochemical processes affecting solute distributions in a clay aquitard*, Leiden: A. A. Balkema Publishers.
- Harrison J.J., Zawadzki A., Chisari R. and Wong H.K.Y. (2011) Separation and measurement of thorium, plutonium, americium, uranium and strontium in environmental matrices. *Journal of Environmental Radioactivity*. 102(10):896-900, doi 10.1016/j.jenvrad.2010.05.010
- Hart D.J., Bradbury K.R. and Feinstein D.T. (2006) The vertical hydraulic conductivity of an aquitard at two spatial scales. *Ground Water*. 44(2):201-211, doi 10.1111/j.1745-6584.2005.00125.x
- Harte P.T., Konikow L.F. and Hornberger G.Z. (2006) Simulation of solute transport across low-permeability barrier walls. *J. Contam. Hydrol.* 85(3-4):247-270, doi 10.1016/j.jconhyd.2006.02.012
- Hasegawa T., Nakata K., Mahara Y., Habermehl M.A., Oyama T. and Higashihara T. (2016) Characterization of a diffusion-dominant system using chloride and chlorine isotopes (^{36}Cl , ^{37}Cl) for the confining layer of the Great Artesian Basin, Australia. *Geochim. Cosmochim. Acta*. 192:279-294, doi 10.1016/j.gca.2016.08.002
- Henderson G.M., Slowey N.C. and Haddad G.A. (1999) Fluid flow through carbonate platforms: Constraints from $^{234}\text{U}/^{238}\text{U}$ and Cl^- in Bahamas pore-waters. *Earth and Planetary Science Letters*. 169(1-2):99-111, doi 10.1016/j.margeo.2016.06.011
- Hendry M.J., Barbour S.L., Novakowski K. and Wassenaar L.I. (2013) Paleohydrogeology of the Cretaceous sediments of the Williston Basin using stable isotopes of water. *Water Resour. Res.* 49, doi 10.1002/wrcr.20321
- Hendry M.J., Barbour S.L., Zettl J., Chostner V. and Wassenaar L.I. (2011) Controls on the long-term downward transport of $\delta^2\text{H}$ of water in a regionally extensive, two-layered aquitard system. *Water Resour. Res.* 47, doi 10.1029/2010wr010044
- Hendry M.J. and Harrington G.A. (2014) Comparing vertical profiles of natural tracers in the Williston Basin to estimate the onset of deep aquifer activation. *Water Resour. Res.* 50(8):6496-6506, doi 10.1002/2014wr015652
- Hendry M.J., Kelln C.J., Wassenaar L.I. and Shaw J. (2004) Characterizing the hydrogeology of a complex clay-rich aquitard system using detailed vertical profiles of the stable isotopes of water. *J. Hydrol.* 293(1-4):47-56, doi 10.1016/j.jhydrol.2004.01.010
- Hendry M.J., Schmeling E., Wassenaar L.I., Barbour S.L. and Pratt D. (2015a) Determining the stable isotope composition of pore water from saturated and unsaturated zone core: Improvements to the direct vapour equilibration laser spectrometry method. *Hydrology and Earth System Sciences*. 19(11):4427-4440, doi 10.5194/hess-19-4427-2015
- Hendry M.J., Solomon D.K., Person M., Wassenaar L.I., Gardner W.P., Clark I.D., Mayer K.U., Kunimaru T., Nakata K. and Hasegawa T. (2015b) Can argillaceous formations isolate nuclear waste? Insights from isotopic, noble gas, and geochemical profiles. *Geofluids*. 15(3):7, doi 10.1111/gfl.12132
- Hendry M.J. and Wassenaar L.I. (1999) Implications of the distribution of δD in pore waters for groundwater flow and the timing of geologic events in a thick aquitard system. *Water Resour. Res.* 35(6):1751-1760, doi 10.1029/1999wr900046
- Hendry M.J. and Wassenaar L.I. (2000) Controls on the distribution of major ions in pore waters of a thick surficial aquitard. *Water Resour. Res.* 36(2):503-513, doi 10.1029/1999wr900310
- Hendry M.J. and Wassenaar L.I. (2004) Transport and geochemical controls on the distribution of solutes and stable isotopes in a thick clay-rich till aquitard, Canada. *Isot. Environ. Health Stud.* 40(1):3-19, doi 10.1080/10256010310001644942

- Hendry M.J., Wassenaar L.I. and Kotzer T. (2000) Chloride and chlorine isotopes (^{36}Cl and $\delta^{37}\text{Cl}$) as tracers of solute migration in a thick, clay-rich aquitard system. *Water Resour. Res.* 36(1):285-296, doi 10.1029/1999wr900278
- Herczeg A.L., Dogramaci S.S. and Leaney F.W.J. (2001) Origin of dissolved salts in a large, semi-arid groundwater system: Murray Basin, Australia. *Marine and Freshwater Research.* 52(1):41-52, doi 10.1071/MF00040
- Herczeg A.L., James Simpson H., Robert F. and Anderson R. (1988) Uranium and radium mobility in groundwaters and brines within the Delaware basin, Southeastern New Mexico, U.S.A. *Chemical Geology: Isotope Geoscience Section.* 72(2):181-196, doi 10.1016/0168-9622(88)90066-8
- Herczeg A.L. and Leaney F.W. (2011) Review: Environmental tracers in arid-zone hydrology. *Hydrogeology Journal.* 19(1):17-29, doi 10.1007/s10040-010-0652-7
- Herczeg A.L., Love A.J., Allan G., Fifield L.K. and Int Atom Energy A. (1996) Uranium-234/238 and chlorine-36 as tracers of inter-aquifer mixing: Otway Basin, South Australia. *Isotopes in Water Resources Management, Vol 2.* 123-133.
- Herczeg A.L., Torgersen T., Chivas A.R. and Habermehl M.A. (1991) Geochemistry of ground waters from the Great Artesian Basin, Australia. *J. Hydrol.* 126(3-4):225-245, doi 10.1016/0022-1694(91)90158-E
- Hesse I.P., Magee J.W. and Kaars S.v.d. (2004) Late Quaternary climates of the Australian arid zone: a review *Quaternary International.* 118-119:87-102, doi 10.1016/S1040-6182(03)00132-0
- Hiscock K.M., Rivett M.O. and Davison R.M. (2002) Sustainable groundwater development. Geological Society Special Publication. 193:1-14,
- Hooker P.J., Bertrami R., Lombardi S., Onions R.K. and Oxburgh E.R. (1985a) He-3 anomalies and crust-mantle interaction in Italy. *Geochim. Cosmochim. Acta.* 49(12):2505-2513, doi 10.1016/0016-7037(85)90118-8
- Hooker P.J., Onions R.K. and Oxburgh E.R. (1985b) Helium-isotopes in North-sea gas-fields and the Rhine rift. *Nature.* 318(6043):273-275, doi 10.1038/318273a0
- Horseman S.T., Higgo J.J.W., Alexander J. and Harrington J.F. (1996) Water, gas and solute movement through argillaceous media. Paris: Nuclear Energy Agency REP.
- Howe P.E., Baird D.J. and Lyons D.J. (2008) Hydrogeology of the Southeast Portion of the Arckaringa Basin and Southwest Portion of the Eromanga Basin, South Australia. *Water Down Under.* Adelaide, 13.
- Huysmans M. and Dassargues A. (2005) Review of the use of Péclet numbers to determine the relative importance of advection and diffusion in low permeability environments. *Hydrogeology Journal.* 13(5-6):895-904, doi 10.1007/s10040-004-0387-4
- Huysmans M. and Dassargues A. (2013) The effect of heterogeneity of diffusion parameters on chloride transport in low-permeability argillites. *Environmental Earth Sciences.* 68(7):1835-1848, doi 10.1007/s12665-012-1871-0
- IAEA. (2009) A Procedure for the Rapid Determination of Pu Isotopes and Am-241 in Soil and Sediment Samples by Alpha Spectrometry. Analytical Quality in Nuclear Applications No. IAEA/AQ/11. Vienna: International Atomic Energy Agency.
- IESC. (2014) Aquifer connectivity within the Great Artesian Basin, and the Surat, Bowen and Galilee Basins, Background review, Commonwealth of Australia. Australia.
- Ingerson E. and Pearson F.J., Jr. (1964) Estimation of age and rate of motion of ground-water by the ^{14}C method In: Miyake Y and Koyama T (eds) *Recent Research in the Field of Hydrosphere, Atmosphere, and Nuclear Geochemistry.* Tokyo: Maruzen, 263-283.

- Ivanovich M., Fröhlich K. and Hendry M.J. (1991) Uranium-series radionuclides in fluids and solids, Milk River aquifer, Alberta, Canada. *Appl. Geochem.* 6(4):405-418, doi 10.1016/0883-2927(91)90040-V
- Jackson R.E., Gorody A.W., Mayer B., Roy J.W., Ryan M.C. and Van Stempvoort D.R. (2013) Groundwater protection and unconventional gas extraction: The critical need for field-based hydrogeological research. *Groundwater.* 51(4):488-510, doi 10.1111/gwat.12074
- Jähne B., Heinz G. and Dietrich W. (1987) Measurement of the diffusion coefficients of sparingly soluble gases in water. *Journal of Geophysical Research: Oceans.* 92(C10):10767-10776, doi 10.1029/JC092iC10p10767
- Johnson T.M. and DePaolo D.J. (1997) Rapid exchange effects on isotope ratios in groundwater systems 2. Flow investigation using Sr isotope ratios. *Water Resour. Res.* 33(1):197-209, doi
- Jones B.F., Hanor J.S. and Evans W.R. (1994) Sources of dissolved salts in the central Murray Basin, Australia. *Chem. Geol.* 111(1-4):135-154, doi 10.1016/0009-2541(94)90087-6
- Jurgens B.C., Fram M.S., Belitz K., Burow K.R. and Landon M.K. (2010) Effects of Groundwater Development on Uranium: Central Valley, California, USA. *Ground Water.* 48(6):913-928, doi 10.1111/j.1745-6584.2009.00635.x
- Keller C.K. and van der Kamp G. (1988) Hydrogeology of two Saskatchewan tills, II. Occurrence of sulfate and implications for soil salinity. *J. Hydrol.* 101(1-4):123-144, doi 10.1016/0022-1694(88)90031-5
- Keller C.K., Van Der Kamp G. and Cherry J.A. (1986) Fracture permeability and groundwater flow in clayey till near Saskatoon, Saskatchewan (Canada). *Canadian Geotechnical Journal.* 23(2):229-240, doi 10.1139/t86-032
- Keller C.K., van der Kamp G. and Cherry J.A. (1987) Permeability of a thick clayey till deposit near Warman, Saskatchewan. *Canadian Geotechnical Conference.*
- Keller C.K., Van Der Kamp G. and Cherry J.A. (1988) Hydrogeology of two Saskatchewan tills, I. Fractures, bulk permeability, and spatial variability of downward flow. *J. Hydrol.* 101(1-4):97-121, doi 10.1016/0022-1694(88)90030-3
- Kellett J.R., Veitch S., McNaught I. and van der Voort A. (1999) Hydrogeological Assessment of a Region In Central Northern South Australia. Canberra: Bureau of Rural Sciences Australia.
- Kelln C.J., Wassenaar L.I. and Hendry M.J. (2001) Stable isotopes ($\delta^{18}\text{O}$, $\delta^2\text{H}$) of pore waters in clay-rich aquitards: A comparison and evaluation of measurement techniques. *Ground Water Monitoring and Remediation.* 21(2):108-116, doi 10.1111/j.1745-6592.2001.tb00306.x
- Keppel M., Jensen-Schmidt B., Wohling D. and Sampson L. (2015) A hydrogeological characterisation of the Arckaringa Basin. Adelaide: Government of South Australia, through Department of Environment, Water and Natural Resources.
- Keppel M., Karlstrom K.E., Love A.J., Priestley S.C., Wohling D. and De Ritter S. (2013) Allocating Water and Maintaining Springs in the Great Artesian Basin, Volume I: Hydrogeological Framework of the Western Great Artesian Basin. Canberra: National Water Commission.
- Kinhill Stearns. (1984) Olympic Dam Project Supplementary Environmental Studies: Mound Springs. Adelaide, SA: Kinhill Stearns.
- Kipfer R., Aeschbach-Hertig W., Peeters F. and Stute M. (2002) Noble gases in lakes and ground waters. In: Porcelli D, Ballentine CJ and Wieler R (eds) *Noble Gases in Geochemistry and Cosmochemistry.* Chantilly: Mineralogical Soc Amer, 615-700.
- Kleinig T., Priestley S.C., Wohling D. and Robinson N.I. (2015) Arckaringa Basin aquifer connectivity. Adelaide: Government of South Australia, through Department of Environment, Water and Natural Resources.
- Konikow L.F. and Arevalo J.R. (1993) Advection and diffusion in a variable-salinity confining layer. *Water Resour. Res.* 29(8):2747-2761, doi 10.1029/93wr00965

- Konikow L.F. and Neuzil C.E. (2007) A method to estimate groundwater depletion from confining layers. *Water Resour. Res.* 43(7), doi 10.1029/2006wr005597
- Koroleva M., Alt-Epping P. and Mazurek M. (2011) Large-scale tracer profiles in a deep claystone formation (Opalinus Clay at Mont Russelin, Switzerland): Implications for solute transport processes and transport properties of the rock. *Chem. Geol.* 280(3-4):284-296, doi 10.1016/j.chemgeo.2010.11.016
- Kretschmer P. and Wohling D. (2014) Groundwater recharge in the eastern Anangu Pitjantjatjara Yankunytjatjara Lands. Adelaide: Government of South Australia, through the Department of Environment, Water and Natural Resources.
- Krieg G.W., Callen R.A., D.I.Gravestock and Gatehouse C.G. (1990) Geology. In: Tyler MJ, Twidale CR, Davies M, et al. (eds) *Natural History of the North East Deserts*. Adelaide, S.A.: Royal Society of South Australia Inc., 1-26.
- Kronfeld J., Godfrey-Smith D.I., Johannessen D. and Zentilli M. (2004) Uranium series isotopes in the Avon Valley, Nova Scotia. *Journal of Environmental Radioactivity.* 73(3):335-352, doi 10.1016/j.jenvrad.2003.11.002
- Kronfeld J., Gradsztajn E., Müller H.W., Radin J., Yaniv A. and Zach R. (1975) Excess ^{234}U : An aging effect in confined waters. *Earth and Planetary Science Letters.* 27(2):342-345, doi 10.1016/0012-821X(75)90046-1
- Kronfeld J. and Rosenthal E. (1981) Uranium isotopes as a natural tracer in the waters of the Bet Shean-Harod Valleys, Israel. *J. Hydrol.* 50(C):179-190, doi 10.1016/0022-1694(81)90068-8
- Langmuir D. (1978) Uranium solution-mineral equilibria at low temperatures with applications to sedimentary ore deposits. *Geochim. Cosmochim. Acta.* 42(6 PART A):547-569, doi 10.1016/0016-7037(78)90001-7
- Larroque F., Cabaret O., Atteia O., Dupuy A. and Franceschi M. (2013) Vertical heterogeneities of hydraulic aquitard parameters: preliminary results from laboratory and in situ monitoring. *Hydrological Sciences Journal-Journal Des Sciences Hydrologiques.* 58(4):912-929, doi 10.1080/02626667.2013.783215
- Larsen D., Gentry R.W. and Solomon D.K. (2003) The geochemistry and mixing of leakage in a semi-confined aquifer at a municipal well field, Memphis, Tennessee, USA. *Appl. Geochem.* 18(7):1043-1063, doi 10.1016/S0883-2927(02)00204-4
- Law K.T. and Lee C.F. (1981) Initial Gradient in a Dense Glacial Till. *Proceedings of the International Conference on Soil Mechanics and Foundation Engineering.* 441-446.
- Lehmann B.E., Love A., Purtschert R., Collon P., Loosli H.H., Kutschera W., Beyerle U., Aeschbach-Hertig W., Kipfer R., Frapet S.K., Herczeg A., Moran J., Tolstikhin I.N. and Groning M. (2003) A comparison of groundwater dating with Kr-81, Cl-36 and He-4 in four wells of the Great Artesian Basin, Australia. *Earth and Planetary Science Letters.* 211(3-4):237-250, doi 10.1016/S0012-821X(03)00206-1
- Linc Energy. (2010a) PEL 117 Combined well completion report, Albany-1 and Albany-1A, Arckaringa Basin.
- Linc Energy. (2010b) PEL 121 Well completion report Magilia-1, Arckaringa Basin.
- Love A.J., Herczeg A.L., Armstrong D., Stadter F. and Mazar E. (1993) Groundwater-flow regime within the Gambier Embayment of the Otway basin, Australia - evidence from hydraulics and hydrochemistry. *J. Hydrol.* 143(3-4):297-338, doi 10.1016/0022-1694(93)90197-h
- Love A.J., Herczeg A.L., Sampson L., Cresswell R.G. and Fifield L.K. (2000) Sources of chloride and implications for Cl-36 dating of old groundwater, southwestern Great Artesian Basin, Australia. *Water Resour. Res.* 36(6):1561-1574, doi 10.1029/2000WR900019
- Love A.J., Herczeg A.L. and Walker G. (1996) Transport of water and solutes across a regional aquitard inferred from deuterium and chloride profiles Otway Basin, Australia. *Isotopes in Water Resources Management (Proc. Symp. Vienna, 1995).* IAEA (1995), 273-286.

- Love A.J., Wohling D., Fulton S., Rousseau-Gueutin P. and De Ritter S. (2013) Allocating Water and Maintaining Springs in the Great Artesian Basin, Volume II: Groundwater Recharge, Hydrodynamics and Hydrochemistry of the Western Great Artesian Basin. Canberra: National Water Commission.
- Lyons D. and Hulmes K. (2010) Hydrogeology of the south-eastern Arckaringa Basin and overlying south-western Eromanga Basin, and the implications for sustainable water supply development in central South Australia. National Groundwater Conference. Canberra.
- Macfarlane P.A., Doveton J.H., Feldman H.R., Butler J.J., Combes J.M. and Collins D.R. (1994) Aquifer/aquitard units of the Dakota aquifer system in Kansas - methods of delineation and sedimentary architecture effects on groundwater-flow and flow properties. *Journal of Sedimentary Research Section B-Stratigraphy and Global Studies*. 464-480.
- Magee J.W., Miller G.H., Spooner N.A. and Questiaux D. (2004) Continuous 150 ky monsoon record from Lake Eyre, Australia: Insolation-forcing implications and unexpected Holocene failure. *Geology*. 32(10):885-888, doi 10.1130/G20672.1
- Mahara Y., Habermehl M.A., Hasegawa T., Nakata K., Ransley T.R., Hatano T., Mizuochi Y., Kobayashi H., Ninomiya A., Senior B.R., Yasuda H. and Ohta T. (2009) Groundwater dating by estimation of groundwater flow velocity and dissolved ^4He accumulation rate calibrated by ^{36}Cl in the Great Artesian Basin, Australia. *Earth and Planetary Science Letters*. 287:43-56, doi 10.1016/j.epsl.2009.07.034
- Marschall P., Croisé J., Schlickenrieder L., Boisson J.Y., Vogel P. and Yamamoto S. (2004) Synthesis of Hydrogeological Investigations at the Mont Terri Site (Phases 1 to 5). In: Heitzmann P (ed) Mont Terri Project – Hydrogeological Synthesis, Osmotic Flow. Reports of the Federal Office for Water and Geology (FOWG), Geology Series No. 6. Bern.
- Martel D.J., Deak J., Dovenyi P., Horvath F., O'Nions R.K., Oxburgh E.R., Stegena L. and Stute M. (1989) Leakage of helium from the Pannonian basin. *Nature*. 342(6252):908-912, doi 10.1038/342908a0
- Marty B., Dewonck S. and France-Lanord C. (2003) Geochemical evidence for efficient aquifer isolation over geological timeframes. *Nature*. 425(6953):55-58, doi 10.1038/nature01966
- Masoud M., Schumann S. and Mogheeth S.A. (2013) Estimation of groundwater recharge in arid, data scarce regions; an approach as applied in the El Hawashya basin and Ghazala sub-basin (Gulf of Suez, Egypt). *Environmental Earth Sciences*. 69(1):103-117, doi 10.1007/s12665-012-1938-y
- Mazor E. and Bosch A. (1987) Noble gases in formation fluids from deep sedimentary basins: a review. *Appl. Geochem.* 2(5-6):621-627, doi 10.1016/0883-2927(87)90014-X
- Mazurek M., Alt-Epping P., Bath A., Gimmi T., Niklaus Waber H., Buschaert S., Cannière P.D., Craen M.D., Gautschi A., Savoye S., Vinsot A., Wemaere I. and Wouters L. (2011) Natural tracer profiles across argillaceous formations. *Appl. Geochem.* 26(7):1035-1064, doi 10.1016/j.apgeochem.2011.03.124
- Mazurek M., Alt-Epping P., Bath A., Gimmi T. and Waber H.N. (2009) *Natural Tracer Profiles Across Argillaceous Formations: The CLAYTRAC Project*: OECD Publishing.
- Mazurek M., Alt-Epping P., Gimmi I., Waber H.N., Bath A., Buschaert S. and Gautschi A. (2007) *Tracer profiles across argillaceous formations: A tool to constrain transport processes: Water-Rock Interaction, Vols 1 and 2, Proceedings*.
- Mazurek M., Lanyon G.W., Vomvoris S. and Gautschi A. (1998) Derivation and application of a geologic dataset for flow modelling by discrete fracture networks in low-permeability argillaceous rocks. *J. Contam. Hydrol.* 35(1-3):1-17, doi 10.1016/S0169-7722(98)00111-9
- McCallum J.L., Cook P.G., Dogramaci S., Purtschert R., Simmons C.T. and Burk L. (2017) Identifying modern and historic recharge events from tracer-derived groundwater age distributions. *Water Resour. Res.* 53(2):1039–1056, doi 10.1002/2016WR019839.

- McCutcheon S.C., Martin J.L. and Barnwell Jr T.O. (1993) Water Quality. In: Maidment DR (ed) *Handbook of Hydrology*. New York: McGraw-Hill.
- McMahon T., Murphy R., Little P., Costelloe J., Peel M., Chiew F., Hayes S., Nathan R. and Kandel D. (2005) Hydrology of Lake Eyre Basin. Armadale: Sinclair Knight Merz.
- Méjean P., Pinti D.L., Larocque M., Ghaleb B., Meyzonnat G. and Gagné S. (2016) Processes controlling ^{234}U and ^{238}U isotope fractionation and helium in the groundwater of the St. Lawrence Lowlands, Quebec: The potential role of natural rock fracturing. *Appl. Geochem.* 66:198-209, doi 10.1016/j.apgeochem.2015.12.015
- Melloul A.J. (1995) Use Of Principal Components Analysis For Studying Deep Aquifers With Scarce Data-Application To The Nubian Sandstone Aquifer, Egypt And Israel. *Hydrogeology Journal.* 3(2):19-39, doi 10.1007/s100400050056
- Miles C., Keppel M., Osti A. and Foulkes J. (2015) Context statement for the Arckaringa subregion. Product 1.1 for the Arckaringa subregion from the Lake Eyre Basin Bioregional Assessment. . Australia: Department of the Environment, Bureau of Meteorology, CSIRO, Geoscience Australia and Government of South Australia.
- Moya C.E., Raiber M., Taulis M. and Cox M.E. (2015) Hydrochemical evolution and groundwater flow processes in the Galilee and Eromanga basins, Great Artesian Basin, Australia: A multivariate statistical approach. *Science of the Total Environment.* 508:411-426, doi 10.1016/j.scitotenv.2014.11.099
- Münnich K.-O. (1957) Messung des ^{14}C -Gehaltes von hartem Grundwasser. *Naturwissenschaften.* 34:32-33, doi 10.1007/BF01146093
- Myers T. (2012) Potential Contaminant Pathways from Hydraulically Fractured Shale to Aquifers. *Ground Water.* 50(6):872-882, doi 10.1111/j.1745-6584.2012.00933.x
- Neuman S.P. and Witherspoon P.A. (1972) Field determination of hydraulic properties of leaky multiple aquifer systems. *Water Resour. Res.* 8(5):1284-1298, doi 10.1029/WR008i005p01284
- Neuzil C.E. (1986) Groundwater-flow in low-permeability environments. *Water Resour. Res.* 22(8):1163-1195, doi 10.1029/WR022i008p01163
- Neuzil C.E. (1994) How Permeable are Clays and Shales. *Water Resour. Res.* 30(2):145-150, doi 10.1029/93wr02930
- Neuzil C.E. and Bredehoeft J.D. (1980) Measurement of in-situ hydraulic conductivity in the cretaceous Pierre Shale. 3rd Invitational Well-Testing Symposium: Well Testing in Low Permeability Environments. Berkeley, California, USA, 96-102.
- NHMRC and NRMCC. (2011) Australian Drinking Water Guidelines Paper 6 National Water Quality Management Strategy. Canberra: National Health and Medical Research Council, National Resource Management Ministerial Council, Commonwealth of Australia.
- Norman D.I. and Musgrave J.A. (1994) N_2 -Ar-He compositions in fluid inclusions - indicators of fluid source. *Geochim. Cosmochim. Acta.* 58(3):1119-1131, doi 10.1016/0016-7037(94)90576-2
- Ortega-Guerrero A. (2003) Origin and geochemical evolution of groundwater in a closed-basin clayey aquitard, Northern Mexico. *J. Hydrol.* 284(1-4):26-44, doi 10.1016/S0022-1694(03)00239-7
- Osenbrück K., Lippmann J. and Sonntag C. (1998) Dating very old pore waters in impermeable rocks by noble gas isotopes. *Geochim. Cosmochim. Acta.* 62(18):3041-3045, doi 10.1016/S0016-7037(98)00198-7
- Osmond J.K. and Cowart J.B. (1976) The theory and uses of natural uranium isotopic variations in hydrology. *Atomic Energy Review.* 621-679.
- Osmond J.K. and Cowart J.B. (1992) Ground water. In: Ivanovich M and Harmon RS (eds) *Uranium Series Disequilibrium*. Oxford: Clarendon Press.

- Osmond J.K. and Ivanovich M. (1992) *Uranium-series mobilization and surface hydrology*, Oxford: Clarendon Press.
- Osmond J.K., Kaufman M.I. and Cowart J.B. (1974) Mixing volume calculations, sources and aging trends of Floridan aquifer water by uranium isotopic methods. *Geochim. Cosmochim. Acta.* 38(7):1083-1100, doi 10.1016/0016-7037(74)90006-4
- Oz Minerals. (2013) Sustainability Report 2013. Melbourne, Australia.
- Paces J.B., Ludwig K.R., Peterman Z.E. and Neymark L.A. (2002) $^{234}\text{U}/^{238}\text{U}$ evidence for local recharge and patterns of groundwater flow in the vicinity of Yucca Mountain, Nevada, USA. *Appl. Geochem.* 17(6):751-779, doi 10.1016/S0883-2927(02)00037-9
- Paces J.B. and Wurster F.C. (2014) Natural uranium and strontium isotope tracers of water sources and surface water-groundwater interactions in arid wetlands - Pahrnagat Valley, Nevada, USA. *J. Hydrol.* 517:213-225, doi 10.1016/j.jhydrol.2014.05.011
- Park J., Bethke C.M., Torgersen T. and Johnson T.M. (2002) Transport modeling applied to the interpretation of groundwater ^{36}Cl age. *Water Resour. Res.* 38(5):11-115, doi 10.1029/2001WR000399
- Patriarche D., Ledoux E., Michelot J.L., Simon-Coinçon R. and Savoye S. (2004a) Diffusion as the main process for mass transport in very low water content argillites: 2. Fluid flow and mass transport modeling. *Water Resour. Res.* 40(1):W015171-W0151715, doi 10.1029/2003WR002700
- Patriarche D., Michelot J.L., Ledoux E. and Savoye S. (2004b) Diffusion as the main process for mass transport in very low water content argillites: 1. Chloride as a natural tracer for mass transport - Diffusion coefficient and concentration measurements in interstitial water. *Water Resour. Res.* 40(1):W015161-W0151619, doi 10.1029/2003WR002600
- Payne T.E. and Airey P.L. (2006) Radionuclide migration at the Koongarra uranium deposit, Northern Australia - Lessons from the Alligator Rivers analogue project. *Physics and Chemistry of the Earth.* 31(10-14):572-586, doi 10.1016/j.pce.2006.04.008
- Pearson F.J. (1999) What is the porosity of a mudrock? Geological Society Special Publication. 158:9-21,
- Petrides B., Cartwright I. and Weaver T.R. (2006) The evolution of groundwater in the Tyrrell catchment, south-central Murray Basin, Victoria, Australia. *Hydrogeology Journal.* 14(8):1522-1543, doi 10.1007/s10040-006-0057-9
- Phillips F.M. (2013) Chloride-36 dating of old groundwater. In: IAEA (ed) *Isotope Methods for Dating Old Groundwater*. Vienna: International Atomic Energy Agency.
- Plummer L.N. and Glynn P.D. (2013) Radiocarbon dating in groundwater systems. In: IAEA (ed) *Isotope Methods for Dating Old Groundwater*. Vienna: International Atomic Energy Agency.
- Porcelli D. (2008) Investigating Groundwater Processes Using U- and Th-Series Nuclides. *Radioactivity in the Environment.* 13:105-153, doi 10.1016/S1569-4860(07)00004-6
- Porcelli D. and Swarzenski P.W. (2003) The behavior of U- and Th-series nuclides in groundwater. *Reviews in Mineralogy and Geochemistry.* 52(1):317-361, doi 10.2113/0520317
- Post V., Kooi H. and Simmons C. (2007) Using hydraulic head measurements in variable-density ground water flow analyses. *Ground Water.* 45(6):664-671, doi 10.1111/j.1745-6584.2007.00339.x
- Post V.E.A., Vassolo S.I., Tiberghien C., Baranyikwa D. and Miburo D. (2017) Weathering and evaporation controls on dissolved uranium concentrations in groundwater – A case study from northern Burundi. *Science of The Total Environment.* 607–608:281-293, doi 10.1016/j.scitotenv.2017.07.006
- Priestley S.C., Wohling D.L., Keppel M.N., Post V.E.A., Love A.J., Shand P., Tyroller L. and Kipfer R. (2017) Detecting inter-aquifer leakage in areas with limited data using hydraulics and

- multiple environmental tracers, including ^4He , $^{36}\text{Cl}/\text{Cl}$, ^{14}C and $^{87}\text{Sr}/^{86}\text{Sr}$. *Hydrogeology Journal*. 25(7):2031-2047, doi 10.1007/s10040-017-1609-x
- Pucci A.A. (1998) Hydrogeochemical processes and facies in confining units of the Atlantic Coastal Plain in New Jersey. *Ground Water*. 36(4):635-644, doi 10.1111/j.1745-6584.1998.tb02838.x
- Rahm B.G. and Riha S.J. (2014) Evolving shale gas management: Water resource risks, impacts, and lessons learned. *Environmental Sciences: Processes and Impacts*. 16(6):1400-1412, doi 10.1039/C4EM00018H
- Remenda V.H., van der Kamp G. and Cherry J.A. (1996) Use of vertical profiles of $\delta^{18}\text{O}$ to constrain estimates of hydraulic conductivity in a thick, unfractured aquitard. *Water Resour. Res.* 32(10):2979-2987, doi 10.1029/96wr01778
- Richards J. (2013) 2012 Groundwater annual environmental review and assessment of effects. Oz Mineral.
- Rosenthal A. and Kronfeld J. (1982) $^{234}\text{U}/^{238}\text{U}$ disequilibria as an aid to the hydrological study of the Judea Group aquifer in eastern Judea and Samaria, Israel. *J. Hydrol.* 58(1-2):149-158, doi 10.1016/0022-1694(82)90075-0
- Rosholt J.N. (1983) Isotopic composition of uranium and thorium in crystalline rocks. *Journal of Geophysical Research*. 88(B9):7315-7330, doi 10.1029/JB088iB09p07315
- Rubel A.P., Sonntag C., Lippmann J., Pearson F.J. and Gautschi A.A. (2002) Solute transport in formations of very low permeability: Profiles of stable isotope and dissolved noble gas contents of pore water in the Opalinus Clay, Mont Terri, Switzerland. *Geochim. Cosmochim. Acta*. 66(8):1311-1321, doi 10.1016/s0016-7037(01)00859-6
- Rudolph D.L., Cherry J.A. and Farvolden R.N. (1991) Groundwater-flow and solute transport in fractured lacustrine clay near Mexico-city. *Water Resour. Res.* 27(9):2187-2201, doi 10.1029/91wr01306
- RUST PPK Consultants. (1994) Regional simulation of cumulative impacts arising from groundwater abstractions in the Great Artesian Basin. NSW: RUST PPK Consultants.
- Sacchi E., Michelot J.L., Pitsch H., Lalieux P. and Aranyossy J.F. (2001) Extraction of water and solutes from argillaceous rocks for geochemical characterisation: Methods, processes, and current understanding. *Hydrogeology Journal*. 9(1):17-33, doi 10.1007/s100400000113
- Sampson L., Wohling D., Jensen-Schmidt B. and Fulton S. (2012a) South Australia and Northern Territory Great Artesian Basin (Eromanga Basin) Hydrogeological Map – Part 1. Department of Environment, Water and Natural Resources, South Australian Government.
- Sampson L., Wohling D., Jensen-Schmidt B. and Fulton S. (2012b) South Australia and Northern Territory Great Artesian Basin (Eromanga Basin) Hydrogeological Map – Part 2. Department of Environment, Water and Natural Resources, South Australian Government.
- Sampson L., Wohling D., Keppel M. and Jensen-Schmidt B. (2015) South Australia Arckaringa Basin Hydrogeological Map – Part 2. Adelaide: Department of Environment, Water and Natural Resources, South Australian Government.
- Sanford W.E. (1997) Correcting for diffusion in carbon-14 dating of ground water. *Ground Water*. 35(2):357-361, doi 10.1111/j.1745-6584.1997.tb00093.x
- Sanford W.E., Aeschbach-Hertig W. and Herczeg A.L. (2011) Preface: Insights from environmental tracers in groundwater systems. *Hydrogeology Journal*. 19(1):1-3, doi 10.1007/s10040-010-0687-9
- Sanford W.E., Doughten M.W., Coplen T.B., Hunt A.G. and Bullen T.D. (2013) Evidence for high salinity of Early Cretaceous sea water from the Chesapeake Bay crater. *Nature*. 503(7475):252-256, doi 10.1038/nature12714

- Savoie S., Michelot J.L., Bensenouci F., Matray J.M. and Cabrera J. (2008) Transfers through argillaceous rocks over large space and time scales: Insights given by water stable isotopes. *Physics and Chemistry of the Earth*. 33(SUPPL. 1):S67-S74, doi 10.1016/j.pce.2008.10.049
- Schaffhauser T., Chabaux F., Ambroise B., Lucas Y., Stille P., Reuschlé T., Perrone T. and Fritz B. (2014) Geochemical and isotopic (U, Sr) tracing of water pathways in the granitic Ringelbach catchment (Vosges Mountains, France). *Chem. Geol.* 374-375:117-127, doi 10.1016/j.chemgeo.2014.02.028
- Senior B.R., Mond A. and Harrison P.L. (1978) Geology of the Eromanga Basin. Canberra: Bureau of Mineral Resources, Geology and Geophysics.
- Shackelford C.D. and Moore S.M. (2013) Fickian diffusion of radionuclides for engineered containment barriers: Diffusion coefficients, Porosities, And complicating issues. *Engineering Geology*. 152:133-147, doi 10.1016/j.enggeo.2012.10.014
- Shand P., Darbyshire D.P.F., Love A.J. and Edmunds W.M. (2009) Sr isotopes in natural waters: Applications to source characterisation and water–rock interaction in contrasting landscapes. *Appl. Geochem.* 24(4):574-586, doi 10.1016/j.apgeochem.2008.12.011
- Shaw R.J. and Hendry M.J. (1998) Hydrogeology of a thick clay till and Cretaceous clay sequence, Saskatchewan, Canada. *Canadian Geotechnical Journal*. 35(6):1041-1052, doi 10.1139/cgj-35-6-1041
- Sheldon A.L., Solomon D.K., Poreda R.J. and Hunt A. (2003) Radiogenic helium in shallow groundwater within a clay till, southwestern Ontario. *Water Resour. Res.* 39(12), doi 10.1029/2002wr001797
- Sheng Z.Z. and Kuroda P.K. (1984) The α -recoil effects of uranium in the Oklo reactor. *Nature*. 312(5994):535-536, doi 10.1038/312535a0
- Sheppard S.C., Sheppard M.I., Gallerand M.-O. and Sanipelli B. (2005) Derivation of ecotoxicity thresholds for uranium. *Journal of Environmental Radioactivity*. 79(1):55-83, doi 10.1016/j.jenvrad.2004.05.015
- Sidele W.C. and Lee P.Y. (1996) Uranium Contamination in the Great Miami Aquifer at the Fernald Environmental Management Project, Fernald, Ohio. *Ground Water*. 34(5):876-882, doi 10.1111/j.1745-6584.1996.tb02082.x
- SKM. (2009a) Aries Borefield production drilling, well construction and aquifer testing completion report. Prepared for OZ Minerals Limited. Sinclair Knight Merz Pty Limited.
- SKM. (2009b) Prominent Hill Regional Conceptual Hydrogeological Model. Prepared for OZ Minerals. Sinclair Knight Merz Pty Limited. Project Number VE23235.
- SKM. (2010) Prominent Hill Mine Groundwater Model Update (PH5). Prepared for OZ Minerals. Project Number VE23146.600.
- Smerdon B.D., Ransley T.R., Radke B.M. and Kellett J.R. (2012) Water resource assessment for the Great Artesian Basin. A report to the Australian Government from the CSIRO Great Artesian Basin Water Resource Assessment. Australia: CSIRO Water for a Healthy Country Flagship.
- Smerdon B.D., Smith L.A., Harrington G.A., Gardner W.P., Plane C.D. and Sarout J. (2014) Estimating the hydraulic properties of an aquitard from in situ pore pressure measurements. *Hydrogeology Journal*. doi 10.1007/s10040-014-1161-x
- Solomon D.K., Hunt A. and Poreda R.J. (1996) Source of radiogenic helium 4 in shallow aquifers: Implications for dating young groundwater. *Water Resour. Res.* 32(6):1805-1813, doi 10.1029/96wr00600
- Standards Australia. (1999) Method of testing soils for engineering purposes. AS 1289.0—1999. New South Wales: Council of Standards Australia.
- Standards Australia. (2000) Method of testing soils for engineering purposes. AS 1289.0—2000. New South Wales: Council of Standards Australia.

- Stuiver M. and Polach H.A. (1977) Reporting of ^{14}C data. *Radiocarbon*. 19(3):355-363, doi 10.1017/S0033822200003672
- Stute M., Forster M., Frischkorn H., Serejo A., Clark J.F., Schlosser P., Broecker W.S. and Bonani G. (1995) Cooling of Tropical Brazil (5-Degrees-C) During the Last Glacial Maximum. *Science*. 269(5222):379-383, doi 10.1126/science.269.5222.379
- Suckow A. (2013) System analysis using multitracer approaches. In: IAEA (ed) *Isotope Methods for Dating Old Groundwater*. Vienna: International Atomic Energy Agency, 217-244.
- Suckow A., Taylor A., Davies P. and Leaney F. (2016) Geochemical baseline monitoring. Australia: CSIRO.
- Suksi J., Rasilainen K. and Marcos N. (2006) U isotopic fractionation - A process characterising groundwater systems. Uranium in the Environment: Mining Impact and Consequences. 683-690.
- Tamers M.A. (1967) Surface-water infiltration and groundwater movement in arid zones in Venezuela. *Isotopes in Hydrology*. Vienna: International Atomic Energy Agency (IAEA).
- Tavenas F., Jean P., Leblond P. and Leroueil S. (1983) The permeability of natural soft clays. Part II: permeability characteristics. *Canadian Geotechnical Journal*. 20(4):645-660, doi 10.1139/t83-073
- Torgersen T. (1980) Controls on pore-fluid concentration of ^4He and ^{222}Rn and the calculation of $^4\text{He}/^{222}\text{Rn}$ ages. *Journal of Geochemical Exploration*. 13(1):57-75, doi 10.1016/0375-6742(80)90021-7
- Torgersen T. and Clarke W.B. (1985) Helium accumulation in groundwater, I: An evaluation of sources and the continental flux of crustal ^4He in the Great Artesian Basin, Australia. *Geochim. Cosmochim. Acta*. 49(5):1211-1218, doi 10.1016/0016-7037(85)90011-0
- Torgersen T. and Stute M. (2013) Helium (and other noble gases) as a tool for understanding long timescale groundwater transport. In: IAEA (ed) *Isotope Methods for Dating Old Groundwater*. Vienna: International Atomic Energy Agency.
- Tóth J. (2009) *Gravitational Systems of Groundwater Flow: Theory, Evaluation, Utilization*: Cambridge University Press.
- Toupin D., Eadington P.J., Person M., Morin P., Wieck J. and Warner D. (1997) Petroleum hydrogeology of the Cooper and Eromanga basins, Australia: Some insights from mathematical modeling and fluid inclusion data. *AAPG Bulletin*. 577-603.
- Townsend T.J. and Ludbrook N.H. (1975) Revision of Permian and Devonian nomenclature of four formations in and below the Arckaringa Basin. *Quarterly Geological Notes*. Geological Survey South Australia, 2-5.
- Trabelsi R., Kacem A., Zouari K. and Rozanski K. (2009) Quantifying regional groundwater flow between Continental Intercalaire and Djefara aquifers in southern Tunisia using isotope methods. *Environmental Geology*. 58(1):171-183, doi 10.1007/s00254-008-1503-x
- Tricca A., Wasserburg G.J., Porcelli D. and Baskaran M. (2001) The transport of U- and Th-series nuclides in a sandy unconfined aquifer. *Geochim. Cosmochim. Acta*. 65(8):1187-1210, doi 10.1016/S0016-7037(00)00617-7
- Trincheró P., Delos A., Molinero J., Dentz M. and Pitkänen P. (2014) Understanding and modelling dissolved gas transport in the bedrock of three Fennoscandian sites. *J. Hydrol.* 512:506-517, doi 10.1016/j.jhydrol.2014.03.011
- Tucker L. (1997) Correlation of Permian sandstones in the Officer, Arckaringa and Pedirka Basins. Report No. DME 493/96. Adelaide Department of Mines and Energy Resources South Australia.
- van der Kamp G. (2001) Methods for determining the in situ hydraulic conductivity of shallow aquitards - an overview. *Hydrogeology Journal*. 9(1):5-16, doi 10.1007/s100400000118

- Van Loon L.R., Glaus M.A. and Müller W. (2007) Anion exclusion effects in compacted bentonites: Towards a better understanding of anion diffusion. *Appl. Geochem.* 22(11):2536-2552, doi 10.1016/j.apgeochem.2007.07.008
- Vesterbacka P., Mäkeläinen I. and Arvela H. (2005) Natural radioactivity in drinking water in private wells in Finland. *Radiation Protection Dosimetry.* 113(2):223-232, doi 10.1093/rpd/nch446
- Vidic R.D., Brantley S.L., Vandenbossche J.M., Yoxtheimer D. and Abad J.D. (2013) Impact of shale gas development on regional water quality. *Science.* 340(6134), doi 10.1126/science.1235009
- Vogel J.C. (1967) Investigation of groundwater flow with radiocarbon. *Isotopes in Hydrology.* Vienna: International Atomic Energy Agency (IAEA), 355-369.
- Vogel J.C. (1970) ¹⁴C-dating of groundwater. *Isotope Hydrology.* Vienna: International Atomic Energy Agency (IAEA).
- Vogel J.C. and Ehhalt D. (1963) The Use of the Carbon Isotopes in Groundwater Studies. *Radioisotopes in Hydrology.* Vienna: International Atomic Energy Agency (IAEA).
- Waber H.N., Frapce S.K. and Gautschi A. (2001) *Cl-isotopes as indicator for a complex paleohydrogeology in Jurassic argillaceous rocks, Switzerland*, Leiden: A a Balkema Publishers.
- Waber H.N. and Smellie J.A.T. (2008) Characterisation of pore water in crystalline rocks. *Appl. Geochem.* 23(7):1834-1861, doi 10.1016/j.apgeochem.2008.02.007
- Walker G.R. and Cook P.G. (1991) The importance of considering diffusion when using carbon-14 to estimate groundwater recharge to an unconfined aquifer. *J. Hydrol.* 128(1):41-48, doi 10.1016/0022-1694(91)90130-A
- Wang Y., Jiao J.J., Cherry J.A. and Lee C.M. (2013) Contribution of the aquitard to the regional groundwater hydrochemistry of the underlying confined aquifer in the Pearl River Delta, China. *Science of the Total Environment.* 461-462:663-671, doi 10.1016/j.scitotenv.2013.05.046
- Warrier R.B., Castro M.C., Hall C.M. and Lohmann K.C. (2013) Large atmospheric noble gas excesses in a shallow aquifer in the Michigan Basin as indicators of a past mantle thermal event. *Earth and Planetary Science Letters.* 375:372-382, doi 10.1016/j.epsl.2013.06.001
- Wassenaar L.I., Hendry M.J., Chostner V.L. and Lis G.P. (2008) High Resolution Pore Water $\delta^2\text{H}$ and $\delta^{18}\text{O}$ Measurements by $\text{H}_2\text{O}_{(\text{liquid})}$ - $\text{H}_2\text{O}_{(\text{vapor})}$ Equilibration Laser Spectroscopy. *Environmental Science & Technology.* 42(24):9262-9267, doi 10.1021/es802065s
- Weiss R.F. (1968) Piggyback sampler for dissolved gas studies on sealed water samples. *Deep-Sea Research and Oceanographic Abstracts.* 15(6):695-699, doi 10.1016/0011-7471(68)90082-X
- Welch A.H. and Lico M.S. (1998) Factors controlling As and U in shallow ground water, southern Carson Desert, Nevada. *Appl. Geochem.* 13(4):521-539, doi 10.1016/S0883-2927(97)00083-8
- Welsh W.D. (2006) Great Artesian Basin transient groundwater model. Canberra: Bureau of Rural Sciences.
- Welsh W.D. (2007) Groundwater balance modelling with Darcy's Law. Canberra: The Australian National University.
- WHO. (2004) Uranium in Drinking-water. World Health Organization.
- Wohling D., Keppel M., Fulton S., Costar A., Sampson L. and Berens V. (2013) Australian Initiative on Coal Seam Gas and Large Coal Mining - Arckaringa Basin and Pedirka Basin Groundwater Assessment Projects. Adelaide: Government of South Australia, through Department of Environment, Water and Natural Resources.

- Wopfner H., Freytag I.B. and Heath G.R. (1970) Basal Jurassic-Cretaceous rocks of the western Great Artesian Basin, South Australia: Stratigraphy and environment. *AAPG Bulletin*. 54(3):381-416,
- Wopfner H. and Twidale C.R. (1967) Geomorphological history of the Lake Eyre basin. In: Jennings JN and Mabbutt JA (eds) *Landform studies from Australia and New Guinea*. Canberra, 119-143.
- Yanase N., Nightingale T., Payne T. and Duerden P. (1991) Uranium Distribution in Mineral Phases of Rock by Sequential Extraction Procedure. *Radiochimica Acta*. 387.
- Yanase N., Payne T.E. and Sekine K. (1995) Groundwater geochemistry in the Koongarra ore deposit, Australia (II) : activity ratios and migration mechanisms of uranium series radionuclides. *Geochemical Journal*. 29(1):31-54, doi 10.2343/geochemj.29.31
- Yuan-Hui L. and Gregory S. (1974) Diffusion of ions in sea water and in deep-sea sediments. *Geochim. Cosmochim. Acta*. 38(5):703-714, doi 10.1016/0016-7037(74)90145-8
- Zhao X., Fritzel T.L.B., Quinodoz H.A.M., Bethke C.M. and Torgersen T. (1998) Controls on the distribution and isotopic composition of helium in deep ground-water flows. *Geology*. 26(4):291-294, doi 10.1130/0091-7613(1998)026<0291:COTDAI>2.3.CO;2
- Zheng C. and Wang P.P. (1999) MT3DMS: A Modular Three-Dimensional Multispecies Transport Model for Simulation of Advection, Dispersion, and Chemical Reactions of Contaminants in Groundwater Systems; Documentation and User's Guide. Strategic Environmental Research and Development Program. Washington: U.S. Army Corps of Engineers, 221.
- Zilberbrand M., Rosenthal E. and Weinberger G. (2014) Natural tracers in Senonian-Eocene formations for detecting interconnection between aquifers. *Appl. Geochem*. 47:157-169, doi 10.1016/j.apgeochem.2014.05.022